ASSESSMENT OF TENSEGRITY STRUCTURES

Static, Dynamic, and Dynamic Stability Analysis
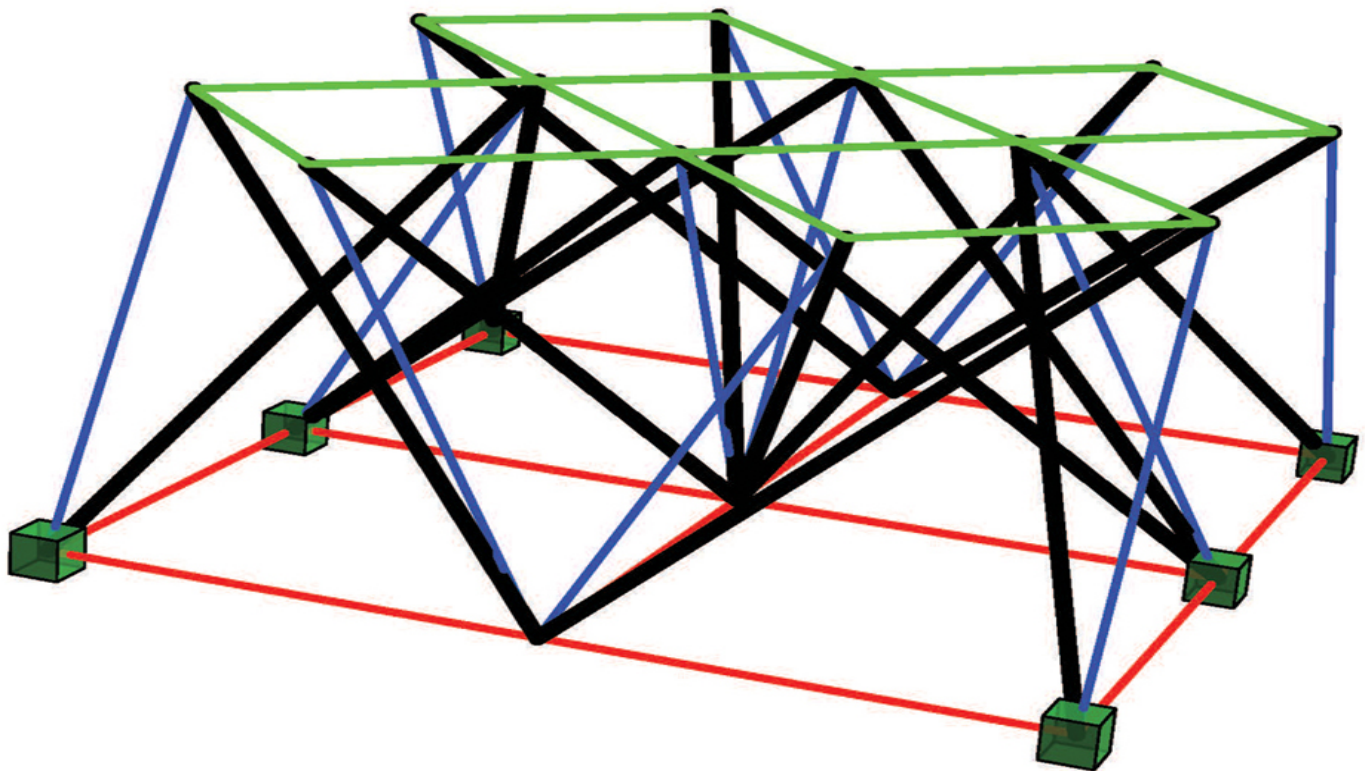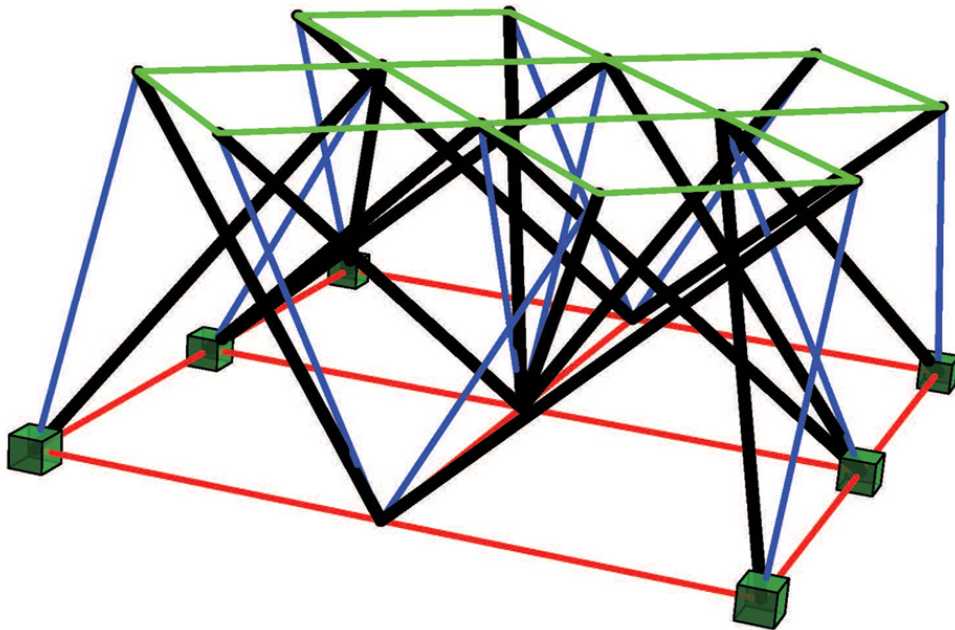
PAULINA OBARA

CRC Press
Taylor & Francis Group

ASSESSMENT OF TENSEGRITY STRUCTURES

Static, Dynamic, and Dynamic Stability Analysis

PAULINA OBARA

Assessment of Tensegrity Structures

This book provides a comprehensive understanding of tensegrity structures. It contains both theoretical background and examples. First, a geometrically non-linear model and the methods used to evaluate the behavior of tensegrity structures are explained. Next, a broad spectrum of different planar and spatial design solutions it considers.

Assessment of Tensegrity Structures is very logically organized, reflecting its practical subject matter, beginning with the simplest two-dimensional structure, for which solutions can be presented in explicit form, and ending with more complex tensegrity structures used in civil engineering such as domes, towers, and plates.

This book is intended for anyone interested in tensegrity systems, from beginners to those who want to deepen their knowledge of them.

Paulina Obara is professor at the Kielce University of Technology, Faculty of Civil Engineering and Architecture, Poland. Her specialization is civil engineering, with a particular focus on the mechanics of structural engineering. Her expertise encompasses dynamic and stability analysis of rod structures. For a decade, she has been engaged in tensegrity systems from a mechanical point of view.

Assessment of Tensegrity Structures

Static, Dynamic, and Dynamic Stability Analysis

Paulina Obara

In memory of my beloved daughter Isabell

This book has happened because of you and is dedicated to you.

My love to you is eternal

Contents

Preface

Applications of the tensegrity concept in civil engineering are still quite innovative. However, the interest of architects and engineers in its practical application has recently been growing. Consequently, it seems to be important. This book is a compact and coherent contribution that enables an understanding of the behavior of these unusual systems under constant and time-varying external loads. In addition, in tensegrity structures, periodical changing of loads over time can cause unstable vibrations.

This book enables a proper understanding of the tensegrity structures. It contains both theoretical background and examples. First, a geometrically non-linear model and the methods used to evaluate the behavior of tensegrity structures are explained. Next, a broad spectrum of different planar and spatial design solutions is considered. The book is very logically organized, in line with its down-to-earth subject, beginning with the simplest two-dimensional structure, for which solutions can be presented in explicit form, and ending with more complex tensegrity structures used in civil engineering such as domes, towers, and plates.

Chapter 1, the 'Introduction', provides an overview of the fundamental concepts associated with tensegrity systems. The text begins with an overview of the concept's inception and progresses to its implementation in civil engineering. It provides comprehensive explanations of the standard applications, including the use of tensegrity principles in the construction of domes, towers/booms, and double-layer

grids. Additionally, it presents a concise overview of existing research in this field, highlighting the types of problems that will be addressed in greater detail in subsequent chapters. It should be noted that this chapter does not include any mathematical descriptions, which will be discussed in more detail in the subsequent chapters.

Chapter 2, 'Mathematical Model of Tensegrity Element', presents a geometrically non-linear model of the tensegrity element. The mathematical description is presented step by step for the benefit of the reader, who is less familiar with the solid mechanics. Above all, this section is primarily intended to familiarize the reader with the notation adopted throughout this book. The majority of developments have been carried out using the simple matrix-vector notation. Only an introduction needs tensor notation to explain the non-linear theory of elasticity. The mathematical model proposed in this chapter is sufficient for qualitative and quantitative analysis of both planar and spatial lattice structures, including tensegrity structures, in in a geometrically nonlinear and physically linear context. It is thus possible to design tensegrity structures using their unique properties, which allow the control of static and dynamic parameters. The defined matrices of initially prestressed tensegrity elements were used in the calculation procedure based on the finite element method. The calculation module was developed in Mathematica environment, which simplified operations through its built-in functions and commands.

Chapter 3, 'Assessment of Tensegrity Structures – Theory', presents the basic assumptions adopted in consideration and a mathematical description of the methods used to evaluate the behavior of tensegrity structures. It is divided into four sections, i.e., qualitative analysis, static analysis, dynamic analysis, and dynamic stability analysis. The analyses are explained in detail and their flowcharts are presented. The equations were used to

build the calculation procedure written in the Mathematica environment. The program makes it possible to freely define the geometry of the structure, material parameters and loads, and then identification of the self-stress state and track the behavior of selected static, geometric, and dynamic parameters in the function of initial prestress. The calculation procedure includes the analysis of geometrically non-linear truss systems and allows for the full analysis at any initial prestress level. The algebraic system of non-linear equations was solved by implementing the Newton-Raphson method. This is the mathematical background for the fourth chapter, which contains examples.

Chapter 4, 'Assessment of Tensegrity Structures – Examples', presents a comprehensive approach that includes a complete qualitative and quantitative static and dynamic assessment of tensegrity structures. The considerations are organized, consistent with its practical focus. First, to illustrate the behavior of structures characterized by self-stress states and infinitesimal mechanisms, the simplest truss consisting of two elements is considered. Although this structure is neither an ideal nor a pure tensegrity, its behavior fully reflects the behavior of tensegrity structures and makes it possible to determine the impact of the initial prestress level on the static and dynamic parameters in the explicit form contained in this study. Next, the basic two-dimensional (2D) models and the most popular three-dimensional (3D) tensegrity modules are considered, i.e., Simplex and Quartex modules. The presented 2D models can be used to create tensegrity domes. In turn, the 3D models can be used to create towers and double-layered tensegrity grids. The most common two qualitatively different tensegrity domes, i.e., Geiger dome and Levy dome are analyzed. Finally, the behavior of towers and double-layered grids built with Simplex and Quartex modules is compared.

The model proposed in the book is sufficient for qualitative and quantitative analysis of both planar and spatial tensegrity structures. It is thus possible to design these structures and use their unique properties to control static and dynamic parameters. Moreover, understanding the behavior of tensegrity structures enables unconventional applications. The tensegrity concept can be used in the design of complex and intelligent structures with self-control, self-diagnosis, self-repair, and active control. New and future potential applications can make use of tensegrity-inspired metamaterials with their exceptional mechanical properties. The book offers a comprehensive approach that includes a complete qualitative and quantitative static and dynamic evaluation, including an assessment of the effect of initial prestress on the distribution of unstable areas.

This book is structured step by step and is designed for everyone interested in tensegrity systems, from beginners to those who want to deepen their knowledge of the parametric analysis of tensegrity structures.

Acknowledgments

I would like to express my gratitude to a few people, thanks to whom I am where I am. Firstly, I am deeply grateful to my mentor, Professor Andrzej Gomuliński. The professor's personality and passion had a huge impact on my life and scientific development. I chose to work at the university instead of a professional practice because it allowed me to satisfy my curiosity and develop my interests. In this book, I mention the work of Professor Wojciech Gilewski, who got me interested in the tensegrity structures, and my doctoral students: Joanna Kłosowska, Katarzyna Nowak, Wojciech Mochocki, Justyna Tomasik, and Maryna Solovei.

I would especially like to thank Professor Urszula Radoń and my other friends. I finished this book only because of your support.

1 Introduction

> **NOTE**
>
> Names introduced by the author are italicized.

1.1 FROM ART TO STRUCTURAL ENGINEERING

Tensegrity is a term derived from the English language as a compound of two words: 'tension' and 'integrity'. The term describes systems composed only of compressed (struts, rods, bars) and tensed elements (cables). These components are assembled in a self-balanced way, which means that there is an equilibrium stress state among struts and cables under zero external loads (the initial prestress). That configuration of internal forces is called a 'self-stress state'. This feature is independent of the structure's geometrical and mechanical characteristics. It only depends on the configuration of the structural elements.

The idea of tensegrity is a relatively new structural concept, whose first patents date back to the 1960s of the 20th century. It is an interesting example of an idea that has penetrated from the world of art to the world of science. The concept of tensegrity originated in the trend of Constructivism, an artistic direction that emerged in Russia in 1913. In opposition to other avant-garde directions, in Constructivism the form of the work was limited to the use of simple geometric elements, i.e., the circle, the rectangle,

and the straight line. The first tensegrity systems were found in arts (Snelson, 2013). Currently, due to their universality and simplicity of the elements, it is possible to use tensegrity ideas in many fields, from micro- to macroscale. Tensegrity models can be used to describe the mechanical behavior of living cells subjected to environmental changes (Khunsaraki et al., 2021; Voloshin, 2020), in biomedicine (biotensegrity) (Brandao Mendes, 2021; Chai Lian et al., 2020; Jung et al., 2021), in mechanical engineering (Dong et al., 2021; Wang and Post, 2021), or as a new material called metamaterial (Al Sabouni-Zawadzka, 2020, 2022; Al Sabouni-Zawadzka and Gilewski, 2018, 2019; Hrazmi et al., 2021; Intrigila et al., 2022; Micheletti et al., 2023; Vangelatos et al., 2020).

An application of the tensegrity concept in civil engineering is still quite innovative, and the interest of architects and engineers in the practical application of this solution is recently growing: 'Tensegrity: from Art to Structural Engineering' (Motro, 2012). In the last years, numerous projects and implementations of the tensegrity idea have been created. The attractiveness of tensegrity structures arises from the designers' striving for originality and innovation. Despite these systems being made from the simplest possible elements, this idea produces structures that are very atypical yet visually appealing. It should also be noted that the geometric form of tensegrity is closely related to the achievement of a suitable arrangement of forces in the structure, allowing these systems to maintain stability with the lowest possible number of elements used. Therefore, they are considered one of the most optimal systems. Additionally, the unique nature of tensegrity characterized by specific mechanical and mathematical properties distinguishes them from conventional systems. From a mechanical point of view, the most interesting for all are tensegrity structures characterized by the occurrence of infinitesimal mechanisms. This is the second immanent

feature of tensegrity structures. In the absence of initial prestress, such systems are unstable, i.e., geometrically variable. The stabilization occurs only after the introduction of initial prestress. The stiffness of structures depends on the initial prestress level, and its modification allows for controlling the static and dynamic parameters. These tensegrity systems offer many advantages over conventional structural systems. They have higher load-bearing capacity than conventional structures with the same mass and occupy less space, and it is easy to change their geometrical configuration due to the presence of the mechanisms. Additionally, the possibility of controlling the behavior of the structure throughout the adjustment of the initial prestress-level forces of the structure is very promising. The tensegrity concept can be used in the design of deployable and intelligent structures with self-control, self-diagnosis, self-repair, and active control (Adam and Smith, 2006, 2007, 2008; Djouadi et al., 1998; Gilewski and Al Sabouni-Zawadzka, 2015; Hrazmi et al., 2021; Masic and Skelton, 2002; Skelton and de Oliviera, 2009, 2010; Veuve et al., 2015, 2017; Zhang L.Y. et al., 2022).

These applications take advantage of the unique mechanical and mathematical properties of tensegrity systems. Unfortunately, it should be noted that in the literature, the word 'tensegrity' is often used inaccurately. This term is often used to describe structures that do not contain tensegrity features. Lack of understanding of what tensegrity systems are makes it impossible to distinguish them from conventional cable–strut systems. For this reason, the identification of the self-stress states and infinitesimal mechanisms is a key problem in the design process of tensegrity structures, especially in the case of civil engineering.

1.2 BEGINNING OF TENSEGRITY IDEA

The precursor of the tensegrity idea was Latvian constructivist artist Karl Ioganson (1890–1929). In 1921 during an exhibition held in Moscow, Ioganson presented a sculpture named 'Gleichgewichtkonstruktion' (gleichgewicht – equilibrium, konstruktion – construction) (Burkhardt, 2008; Gengnagel, 2002; Gough, 1998, 2005; Wroldsen, 2007). This structure was fully deformable and consisted of three struts (thick line), seven tensioned cables (thin line), and one freely hanging cable serving to change the configuration of the system while maintaining its equilibrium (Figure 1.1a). This sculpture is considered to be the first proto-tensegrity structure (Emmerich, 1988). Emmerich added that this configuration was very similar to the proto-system invented by him in 1964 with three struts and nine cables. However, the absence of prestress, which is one of the characteristics of tensegrity systems, does not allow Ioganson's 'sculpture-structure' to be considered the first of this type of structure. Another of Ioganson's artworks of special interest is a structure made of three wooden struts (thick line) forming a right-angled spatial construction cross-interconnected with nine cables (thin line) (Figure 1.1b). A detailed description of constructivism and Ioganson's works can be found in Gough (2005).
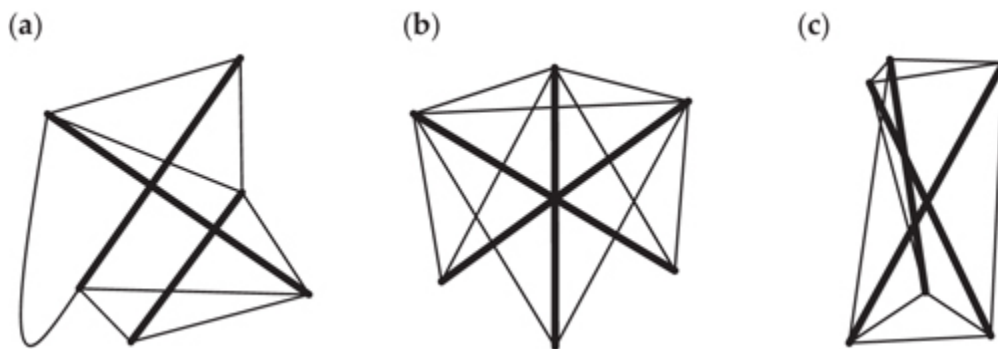
FIGURE 1.1 Reconstruction of sculptures of Karl Ioganson: (**a**) Gleichgewichtkonstruktion; based on (Gengnagel, 2002), (**b**) spatial

construction 1920–21; based on (Gough, 1998), and (**c**) spatial construction 1920–21; based on (Gough, 1998).↵
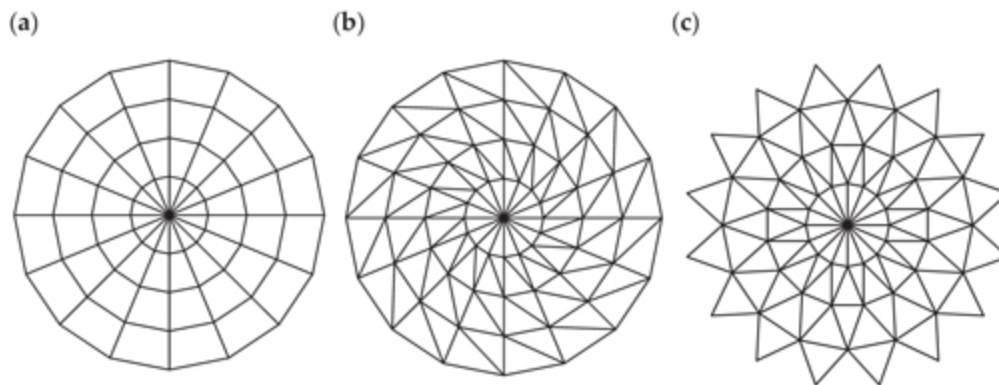
FIGURE 1.2 Dome patterns: (**a**) Ribbed dome, (**b**) Schwedler dome, and (**c**) Lamella-Kiewitt dome.

Ioganson's work consisted of searching for new construction forms. Although he did not develop his ideas in the field of engineering structures, he predicted these possibilities: 'From painting to sculpture, from sculpture to construction, from construction to technology and invention – this is my chosen path, and will surely be the ultimate goal of every revolutionary artist'. His sculptures are not tensegrity; however, Gough presented a tensegrity prism (Figure 1.1c) made of three struts (thick line) and nine cables (thin line). He claimed that the prism was a modern reconstruction of Ioganson's sculpture (Gough, 1998, 2005). This structure looks like the simplest early tensegrity module, which was independently patented by the aforementioned French architect David Georges Emmerich (1925–1996) (Emmerich, 1964) and two Americans – architect Richard Buckminster Fuller (1895–1983) (Fuller, 1962) and sculptor Kenneth Snelson (1927–2016) (Snelson,

1965), who was Fuller's student. These three authors are considered the creators of tensegrity systems.

The term tensegrity was coined by Fuller in 1955, and he first patented the definition of tensegrity (Fuller, 1962). Fuller described tensegrity systems as 'islands of compression in a sea of tension'. Three years later, Snelson patented the system, which he called 'Continuous Tension, Discontinuous Compression Structures' (Snelson, 1965). The more precise definition was patented by Emmerich (1964). He added the condition of self-stress state: tensegrity structures consist of rods mounted in such a way that the struts remain physically isolated in a continuous set of cables. All these elements must be in close proximity to one another and interconnected by tensional prestress. No external supports or anchors are required. It makes the structure as strong as a self-supporting structure, hence the name self-stress state. In the following years, all three authors continued to work on tensegrity systems. Fuller and Emmerich developed their ideas in architecture, while Snelson (1996, 2013) focused on his artistic work. A detailed description of the work of Fuller, Emmerich, and Snelson can be found among others in the works of Motro (1992, 2003, 2011) and Gomez-Jauregui (2004, 2009). In turn, compilations and overviews of the applications of tensegrity structures in all fields (architecture, engineering, construction, robotics, space, etc.) from 1921 to the present day are presented in the paper (Gomez-Jauregui et al., 2023).

1.3 DEFINITIONS OF TENSEGRITY SYSTEMS

The idea of tensegrity was first described about 60 years ago, but no precise and general definition has been agreed upon so far. This thereby paves the way for confusion and

misuse of the term in technical applications. The term is often used for trusses that have little to do with the tensegrity principle as defined by the creators of this idea.

The first patented definitions by creators of tensegrity systems are very general. In the 60 years since the first tensegrity structures were patented, there have been attempts to modify and refine the first definitions. The most widely accepted definition of tensegrity is formulated by Pugh (1976), in which he combines the two previous statements: '*A tensegrity system is established when a set of discontinuous compression components interacts with a set of continuous tensile components to define a stable volume in space*'. This definition was narrowed by Motro (1992, 2003). Motro distinguished two different concepts – 'patent based' and the 'extended' definition. The first definition is:

> *Tensegrity systems are spatial reticulate systems in a state of self-stress. All their elements have a straight middle fibre and are of equivalent size. Tensioned elements have no rigidity in compression and constitute a continuous set. Compressed elements constitute a discontinuous set. Each node receives one and only one compressed element.*

In turn, the 'extended' definition has some common points with Pugh's definition but has additional factors: '*the compressed elements are included inside the continuous set in tension, and the system has self-equilibrium stability*'. Hanaor (1994) describes tensegrity structures as '*internally prestressed, free-standing pin-jointed networks, in which the cables or tendons are tensioned against a system of bars or struts*'. A broader interpretation is proposed by Miura and Pellegrino (Tibert, 2002; Tibert and Pellegrino, 2003) who

classify tensegrity as '*any structure realized from cables and struts, to which a state of prestress is imposed that imparts tension to all cables*'. A narrower interpretation, also by Miura and Pellegrino, adds to the above definition of the notion that '*as well as imparting tension to all cables, the state of prestress serves the purpose of stabilizing the structure, thus providing first-order stiffness to its infinitesimal mechanisms*'. Wang (1998) defines tensegrity structures as '*Self-stressed equilibrium cable networks in which a continuous system of cables (tendons) are stressed against a discontinuous system of struts; or structures composed of tensegrity simplexes*'. Zhang and Ohsaki (2015), based on existing definitions, describe characteristics of a tensegrity structure as follows:

(1) The structure is free-standing, without any support. (2) The structural members are straight. (3) There are only two different types of structural members: struts carrying compression and cables carrying tension. (4) The struts do not contact with each other at their ends.

Skelton et al. (Masic and Skelton, 2002, 2004; Skelton et al., 2001a, 2001b, 2002a, 2002b; Skelton and de Oliviera, 2009; Williamson et al., 2003a, 2003b) take a different approach. They introduce the concept of tensegrity configuration: '*Configuration forms a tensegrity configuration if the given configuration can be stabilized by some set of internal tensile members, i.e., connected between the rigid bodies*'. Additionally, they defined the classes of structural systems: 'A tensegrity configuration that has no contacts between its right bodies is a class 1 tensegrity system, and a tensegrity system with as many as k right bodies contact is a class k tensegrity system'.

Corresponding to Skelton's Class-*k* tensegrity structure, Bieniek (2009a, 2009b, 2011, 2012, 2015a, 2015b, 2016, 2017) and Bieniek et al. (2019) suggested assuming new Class-Theta (Θ) tensegrity systems. Each of the proposed tensegrity systems possesses an exterior and interior set of tension elements (cables), which are never connected to each other. The compressive elements (struts) always lie between these two sets of cables. Bieniek distinguished two subclasses within Class-Theta tensegrity systems. The first subclass includes tensegrity module with a single interior tendon. Alternatively, the second subclass includes tensegrity module comprising a disconnected set of compressed elements that are joined with an exterior and interior set of tension components simultaneously.

Moored and Bart-Smith (2009) subsequently proposed the term 'clustered tensegrity' to denote a particular class of tensegrity structures having sliding or continuous cables. A clustered tensegrity is defined to '*be a tensegrity structure where at least two cable elements are grouped together to become a single element. Each group of individual cables that are combined into one continuous cable is then called a cable-element cluster*'.

The different approach to definition is based on the characteristic features of tensegrity structures closely related to their benefits, which distinguish them from conventional cable–strut structures:

- the tensegrity structure is a truss (*TT*);
- there is a self-stress state understood as the system of self-equilibrated normal forces, which satisfies homogeneous equations of equilibrium; this feature is independent of the structure's geometrical and mechanical characteristics, and it only relies on the configuration of the elements of structures (*SS*);
- tensile elements have no stiffness in compression, which means they are cables (*TC*);
- there is an infinitesimal mechanism or mechanisms stiffened by the self-stress state (*IM*);

- the set of compressed components (struts) is contained within the continuous net of cables (*IN*);
- the struts do not touch each other and form a discontinuous set (*DS*).

The first definition based on the characteristic features of tensegrity structures was proposed by Gilewski et al. (2016a, 2016b) and Obara et al. (2019). The characteristics mentioned earlier are used to classify structures as 'pure tensegrity' or 'structures with tensegrity features'. 'Pure tensegrity' is represented by a structure that has all of the six features. It means a pure tensegrity structure is a truss in which there is an infinitesimal mechanism stiffened by a self-stress state. Additionally, components in compression create a discontinuous system inside a continuous system of components in tension, which have no compressive rigidity. In turn, 'structures with tensegrity features' include a wider range of systems in which some properties of tensegrity can be ignored. Structures assigned to this group fulfill three obligatory criteria, such as *TT*, *SS*, and *TC*, and have at least one of the features: *IM*, *DS*, or *IN.* That classification was revised by Obara (2019a) and extended to four classes. For a detailed description, see Section 3.3.2 of Chapter 3.

1.4 ADVANTAGES AND DISADVANTAGES OF TENSEGRITY STRUCTURES

Tensegrity structures have many advantages that distinguish them from typical cable–strut structures (Skelton et al., 2001b):

- tensegrity structures are efficient – by increasing the use of tensile elements, maximum strength can be achieved with minimum weight;
- tensegrity structures are collapsible and economical – compressed elements are not connected or connected by hinges; this solution allows

them to be moved, disassembled, and folded into a compact volume, which in turn saves on transportation and crew costs of assembly;

- tensegrity structures are more reliable – greater structural reliability can be expected by using axially tensed or compressed elements; the modeling is more precise than with elements that deform in two or three directions; the tensed elements form a continuous network, while compression elements do not connect, so their work is local, which means that the stays are not subjected to large buckling loads;
- tensegrity structures can be easily tuned and repaired – the infinitesimal mechanisms make it possible to control the stiffness, which depends on the state of self-tension stabilizing the structure;
- tensegrity structures enable control and improvement of static and dynamic properties of structures.

In addition to these undeniable advantages, the disadvantages should also be noted. They are related to the problems that occur in both the design and construction processes. At the design stage, the problem is:

- modeling of structural behavior should take into account aspects such as effects of geometric nonlinearity, friction at nodes, execution tolerances, operation of the structure at the erection stage, etc;
- complicated analysis of structures due to large displacement gradients, susceptibility to the effects of dynamic loads, and the need to analyze the various phases of assembly;
- design of connections, which are a key element of all spatial structures, plays a special role in the case of tensegrity structures; connections must be lightweight and made with high accuracy, since tensegrity structures are very sensitive to any inaccuracies and changes in geometry.

In turn, during the construction process, the problem is:

- complicated, multi-phase assembly;
- costly and tedious in construction details;
- difficult prestressing program (cable tension programming);
- execution of connections;
- anchoring of tendons;
- adherence to the designed geometry of the structure.

These disadvantages limit the applicability of tensegrity structures as load-bearing structures for engineering

structures, but in recent years, interest in this type of construction has grown tremendously.

1.5 TENSEGRITY STRUCTURES IN CIVIL ENGINEERING

Attempts to apply tensegrity structures in civil engineering go back to the origins of the idea itself. In recent years, there has been a growing interest in these applications. This includes both standard (domes, towers, booms, bridges, footbridges, and double-layer grids) and non-standard (deployable and intelligent structures) solutions. This growth is due to an increase in both design and execution capabilities. This is related to the development of advanced computational techniques and the development of construction technologies and materials (Wang et al., 2024).

In this book, the standard application is described in detail, i.e., the use of tensegrity ideas for the construction of domes, towers, booms, and double-layer grids. The detailed description of the mechanics of tensegrity systems allows for understanding the behavior of these unusual structures. It should be mentioned that tensegrity structures can be used in the construction of bridges and footbridges (Bel Hadj Ali et al., 2010; Feron et al., 2019; Kasprzak, 2014; Korkmaz et al., 2010, 2011a, 2011b; Metodieva, 2014; Micheletti, 2005, 2012; Pleşcan et al., 2018; Rhode-Barbarigos et al., 2009; Rhode-Barbarigos, Bel Hadj Ali et al., 2010; Rhode-Barbarigos, Jain et al., 2010, 2012; Veuve et al., 2015, 2017).

1.5.1 Cable–Strut Domes

Domes are one of the oldest covers used in civil engineering. These structures have been known since 27 BCE, i.e., since the Romans used stone blows to cover their palaces. In modern times, concrete or steel is used to build

domes. The most popular ones are steel domes, which are lighter than other conventional forms. These kinds of structures are the best solution for long-span roofs. Steel domes can be divided into standard (traditional domes) and non-standard ones (conventional cable–strut domes and tensegrity cable–strut domes).

The standard domes are built with rods assembled in single-layer or double-layer grids. Depending on the arrangement of the rods, the structures can be divided into several groups (dome patterns). The most common are four of them, i.e., Ribbed dome (Figure 1.2a) (Alpatov et al., 2016; Jeleniewicz et al., 2024; Zabojszcza et al., 2021); Schwedler dome - devised by Schwedler in 1863 (Figure 1.2b) (Radoń et al., 2020, 2023; Manguri et al., 2024; Xiaoyang et al., 2010) Lamella-Kiewitt dome devised by Zollinger in 1908 and adapted by Kiewitt (Figure 1.2c) (Dudzik and Potrzeszcz-Sut, 2021; Potrzeszcz-Sut, 2020; Potrzeszcz-Sut and Dudzik, 2022; Xiaoyang et al., 2010; Zabojszcza and Radoń, 2019, 2020; Zhang et al., 2019). It should be noted that Kiewitt adapted the Lamella system to be used in larger, circular dome structures, and he patented this design in 1959 (Kiewitt, 1959). This system was used, among others, to create non-standard solutions (tensegrity cable–strut domes), namely the cable–strut Kiewitt domes (Chen et al., 2023; Ma et al., 2018; Mottahedin and Keyvani, 2023; Yuan et al., 2007; Zhang and Feng, 2017). The tensegrity cable–strut domes are structurally effective in long-span roofs. They are made by uniformly distributed load-bearing structures, which are fixed by the circumference-clamping ring. Although these systems are rod-like structures, some specific mechanical and mathematical properties distinguish them from conventional cable–strut domes. These structures are characterized by a system of internal forces, which holds the struts and cables in stable equilibrium under zero external loads.

The first tensegrity cable–strut dome was proposed and patented in 1988 by Geiger (1988); The main principle behind Geiger's dome is that all tension is achieved through the roof structure by means of tensed cables and discontinuous compressed struts. The original structure consisted of radial trusses with tensed and compressed elements. This type of roof has low-profile configurations that reduce wind lift, uneven snow settling, and use less material to cover the roof. One of the main advantages of this structure is that its weight per square meter does not change with increasing span. This solution was used on the roof of the Olympic Gymnastics Hall in Seoul. The roof with a 120-m span consists of radially arranged flat girders (Rastorfer, 1988).

From the beginning of the idea to the present day, new topologies based on the original patent have been created. There are four different design solutions called 'Geiger domes':

- *regular Geiger dome type B* (Figure 1.3a) – dome according to Geiger patent; load-bearing girders are connected by a ring (Albertin et al., 2012; Biondini et al., 2011; Chen et al., 2022, 2023; Ding et al., 2018; Fu, 2006; Jiang et al., 2019; Kłosowska, 2018; Malerba et al., 2012; Mottahedin and Keyvani, 2023; Qin et al., 2023; Yuan et al., 2007; Zhang and Feng, 2017);
- *regular Geiger dome type A* (Figure 1.3b) – load-bearing girders are connected by a strut (Ma et al., 2018; Wu et al., 2018, 2020);
- *modified Geiger dome type B* (Figure 1.3c) – the modification of the Geiger patent by adding additional cables connecting the top nodes; load-bearing girders are connected by a ring (Zhang and Feng, 2017);
- *modified Geiger dome type A* (Figure 1.3d) – modified Geiger patent with load-bearing girders connected by a strut (Atig et al., 2017; Kim and Sin, 2014; Kim et al., 2001).
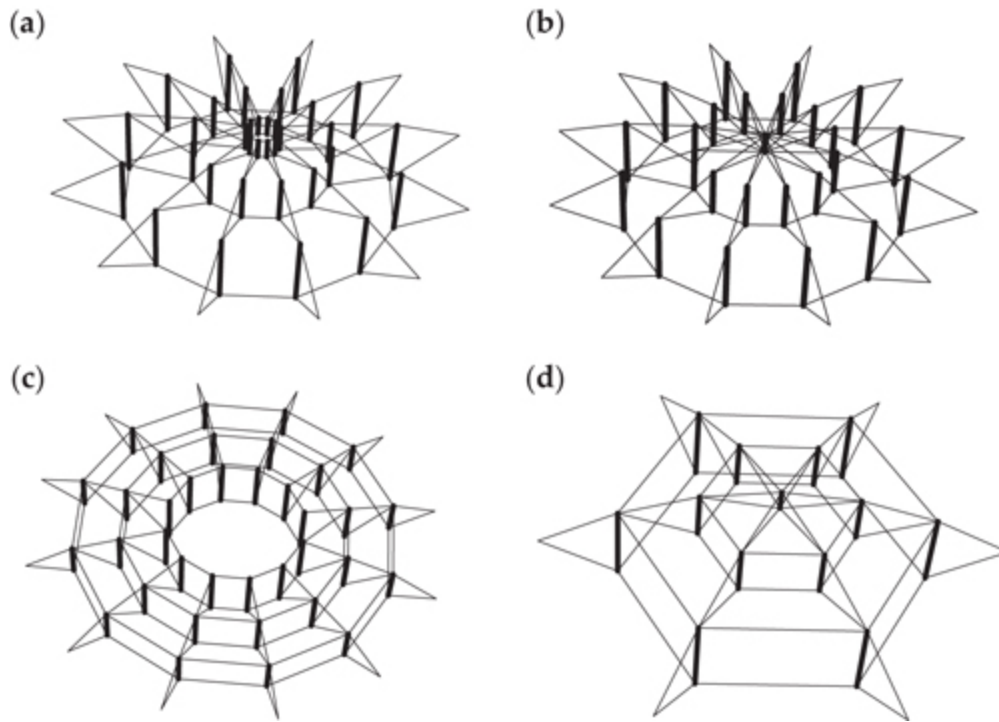
FIGURE 1.3 Variants of the *Geiger domes*: (a) *regular Geiger dome type B; based on* (Yuan et al., 2007), (b) *regular Geiger dome type A; based on* (Ma et al., 2018), (c) *modified Geiger dome type B; based on* (Zhang and Feng, 2017), and (d) *modified Geiger dome type A; based on* (Atig et al., 2017).↵

After the appearance of the Geiger dome, many researchers presented their ideas of cable structures, i.e., Terry (1996), Wang (1998), Rębielak (2000), Kawaguchi et al. (1999), and Levy (1989). The last idea is the second, after the Geiger dome, most common tensegrity dome. The Levy dome, unlike the Geiger dome, is a triangular structure where cables and struts are not in the same plane. Levy's idea was used to build a stadium cover in Atlanta (Georgia Dome) in the United States in 1992 (Gerardo and Levy, 1992). This is an example of one of the largest dome in the world. The dome was built on an elliptical plan, with

dimensions of 227 × 185 m and an area of 37,200 m². The Georgia Dome was referred to as the first Hypar-tensegrity dome

Two different design solutions called 'Levy domes' can be found in the literature:

- *Levy dome type B* (Figure 1.4a) – load-bearing girders are connected by a ring (Chen and Feng, 2012a; Ding et al., 2021; Ma et al., 2020; Yuan et al., 2007; Zhang et al., 2007);
- *Levy dome type A* (Figure 1.4b) – load-bearing girders are connected by a strut (Chen et al., 2020; Kmet and Mojdis, 2014; Ma et al., 2018; Yuan et al., 2007; Sun and Xiao, 2021; Zhang et al., 2018; Zhang et al., 2023).
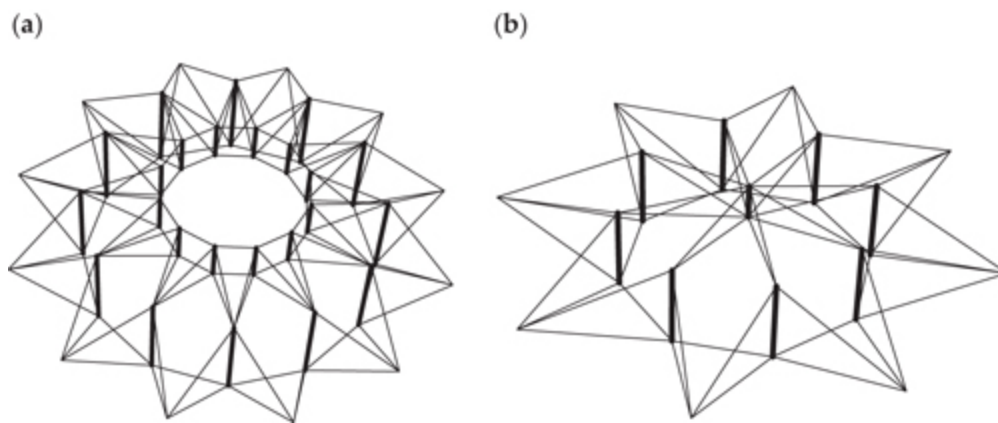
FIGURE 1.4 Variants of the *Levy domes*: (a) *Levy dome type B; based on* (Ma et al., 2020), (b) *Levy dome type A; based on* (Chen et al., 2020).

Practical application of tensegrity domes requires a thorough examination of static and dynamic properties, as well as the overall behavior of the structure. Most of the research to date focuses on layout design (Rębielak, 2000; Yuan et al., 2007) or shape optimization (Chen et al., 2023; Kawaguchi et al., 1999; Mottahedin and Keyvani, 2023; Zhang and Feng, 2017). A smaller number of studies focused on the static parameters of tensegrity structures.

Due to the unconventional shape and unique features of tensegrity domes, parametric analysis considering the effect of initial prestress on behavior is very important. The effect of initial prestress on the mechanical properties, i.e., displacements and stiffness, was investigated (Ding et al., 2018; Chen et al., 2022; Fu, 2006; Kmet and Mojdis, 2014; Obara, 2019a; Shen et al., 2021; Sun and Xiao, 2021; Wu et al., 2018, 2020; Yan et al., 2019). Moreover, the dynamic response to changes in initial prestress was presented (Atig et al., 2017; Chen and Feng, 2012a; Kim and Sin, 2014; Ma et al., 2020; Obara, 2019a; Qin et al., 2023; Sun and Xiao, 2021; Volokh et al., 2003). A detailed description and parametric analysis of tensegrity *Geiger and Levy domes* were presented (Obara and Solovei, 2023, 2024; Obara et al., 2023a, 2023b, 2024).

Some other interesting unusual tensegrity domes are membrane roofs supported by two tensegrity modules called White Rhino (Gilewski et al., 2017; Gomez-Jauregui et al., 2023; Kawaguchi et al., 2011) and prototypes of knit tensegrity shells composed of an elastic membrane and bamboo struts (Gupta et al., 2020).

1.5.2 TOWERS AND BOOMS

Tensegrity towers and booms (beam-like structures) are built by linearly connecting the basic three-dimensional tensegrity modules (units). The units can be connected node-to-node (Ashwear et al., 2016; Bel Hadj Ali et al., 2021; Kan et al., 2018; Safaei et al., 2013; Schlaich, 2004; Skelton and de Oliveira, 2010; Snelson, 2013) or strut-to-cable (Lee and Choong, 2018; Masic and Skelton, 2004; Mochocki, 2022; Snelson, 2013; Safaei et al., 2013; Xu and Luo, 2011). Dozens of tensegrity modules can be found in the literature. These range from the simplest, patented in 1960 (see Section 1.2) to complex forms, the search for which is the subject of many works. The simplest modules are regular

prisms with a triangular base, constructed from three struts. Tensegrity structures can also be based on other regular prisms with any number of struts. It is also possible to create modules inscribed in a truncated cone. Such structures are classified as so-called cylindrical systems. The construction of tensegrity modules can also be based on truncated Platonic solids (regular polyhedra) or Archimedean solids (semi-formal polyhedra) – spherical systems. It should be noted that the geometry of tensegrity is not always identical to the corresponding solids, since they would not then be in a stable configuration if they were identical, the structure would not be in a stable configuration The first catalog of tensegrity systems was created by Pugh (1976). He described three basic patterns of structural configurations: rhombic (diamond-pattern systems), circumferential, and zigzag (oblique). In the rhombic pattern, each strut is on the longer diagonal axis of a rhombus composed of cables. A circumferential tensegrity system is characterized by circuits formed by the struts. A zigzag tensegrity system, on the other hand, is one in which a total of three noncollinear cables lie between the two ends of each strut (Bieniek, 2012; Gomez-Jauregui, 2004). A description of the simplest spatial tensegrity structures, their mathematical models, and methods for designing complex structures is presented in Burkhardt (2008).

The simplest modules (basic 3D modules) are diamond-pattern systems consisting of:

- twelve elements, i.e., three struts (thick line) and nine cables (thin line) (Figure 1.5a, b), known as: elementary equilibrium, three-bar unit/module, three-strut T-prism, T-3 unit, three-strut simplex, triplex, triangular prism tensegrity structures, trigonal tensegrity prism, *Simplex module* (Aloui et al., 2019; Ashwear et al., 2016; Chen and Feng, 2012a; Chen and Qin, 2024; Emmerich, 1964; Estrada et al., 2006; Fuller, 1962; Gilewski and Al Sabouni-Zawadzka, 2020; Gilewski et al., 2015, 2017; Intrigila et al., 2022; Małyszko, 2016, 2017; Małyszko and Rutkiewicz, 2019, 2020; Małyszko et

al., 2018; Mochocki, 2022; Rutkiewicz, 2023; Safaei et al., 2013; Skelton and de Oliveira, 2010; Snelson, 1965; Zhang L.Y. et al., 2014, 2018);

- sixteen elements, i.e., 4 struts (thick line) and 12 cables (thin line) (Figure 1.5c, d), known as: quadrangular prismatic tensegrity, quadrangular cylindrical tensegrity structure, basic Quadruplex module, quadruplex, 4-strut Simplex, four-bar module, *Quartex module* (Al Sabouni-Zawadzka et al., 2024; Estrada et al., 2006; Faroughi and Lee, 2014; Gilewski and Al Sabouni-Zawadzka, 2021; Intrigila et al., 2022; Kebiche et al., 1999; Liu and Paulino, 2019; Mochocki, 2022; Oliveto and Sivaselvan, 2011; Safaei et al., 2013; Shekastehband et al., 2012; Tran and Lee, 2010a; Zhang L.Y. et al., 2018, 2022).
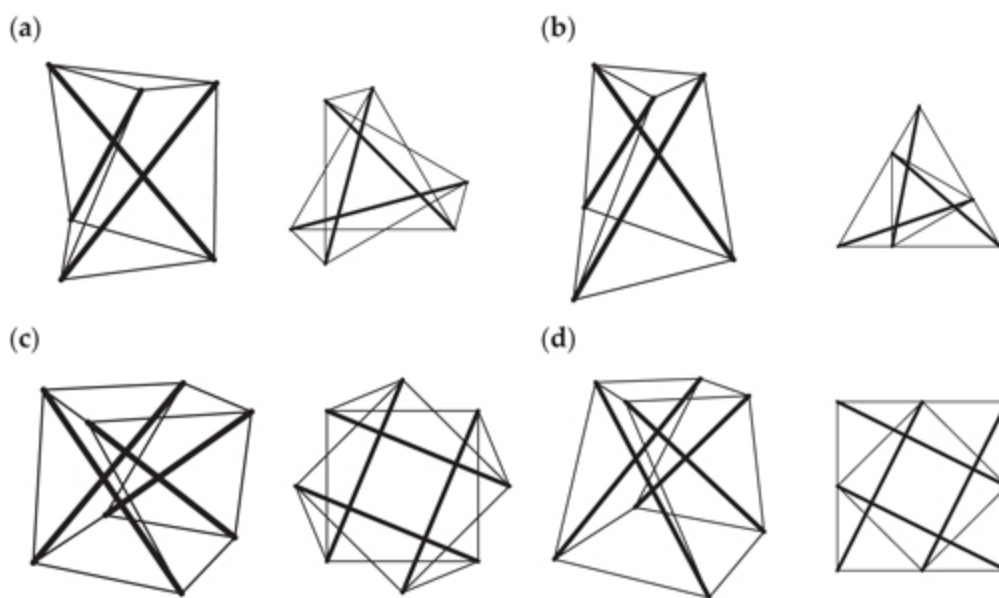
FIGURE 1.5 Simplest tensegrity modules: (a) *regular Simplex module*, (b) *modified Simplex module*, (c) *regular Quartex module*, and (d) *modified Quartex module*.⏎

There are two versions of the basic 3D modules mentioned earlier, i.e., *regular* and *modified*. In the first case, the top surface is like the bottom one (Figure 1.5a, c), whereas in the second, the top surface is inscribed into the bottom one (Figure 1.5b, d). The modification makes it easy to combine single module into multi-module structures.

The most popular in use are towers/booms built with units connected node-to-node built with:

regular Simplex modules (Figure 1.6a, b) (Al Sabouni-Zawadzka, 2016; Ashwear et al., 2016; Cao et al., 2024; Gilewski, Kłosowska et al., 2019; Kłosowska, 2018; Małyszko and Rutkiewicz, 2019; Mochocki, 2022; Pinaud et al., 2004; Rutkiewicz, 2023, 2024; Safaei et al., 2013; Schlaich, 2004; Skelton and de Oliveira, 2009, 2010; Snelson, 2013; Wang and Senatore, 2020; Yildiz and Lesieutre, 2022; Zawadzki and Al Sabouni-Zawadzka, 2020);
modified Simplex modules (Figure 1.6b) (Obara and Tomasik, 2023c, 2023d);
regular Quartex modules (Figure 1.6c) (Mochocki, 2022);
modified Quartex modules (Figure 1.6d) (Bel Hadj Ali et al., 2021; Kan et al., 2018; Safaei et al., 2013).

A detailed description and parametric analysis of towers built with *Simplex* and/or *Quartex modules* were presented (Mochocki, 2022; Mochocki and Obara, 2021; Obara and Tomasik, 2023c, 2023d).
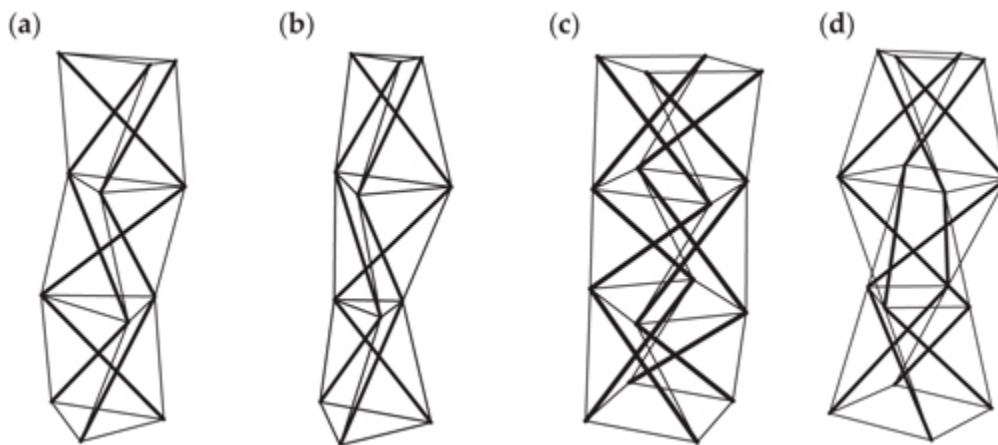
FIGURE 1.6 Models of tensegrity towers built with three: (a) *regularSimplex modules* (b) *modified Simplex modules* (c) *regular Quartex modules*, (d) *modified Quartex modules.*

Examples of existing towers are the Zig-Zag Tower (Snelson, 2013), the Warnow Tower (Kłosowska et al., 2018;

Kłosowska, 2018; Schlaich, 2004), and the Needle Tower (Snelson, 2013). They are built with *Simplex modules.* The first tower is, in truth, a Snelson's model built in 1997 with a height of 1.16 m; however, the second tower measured 49.2 m high. The Warnow Tower was built in 2003 for the opening of the International Garden Exhibition in Rostock, Germany. The tower was designed by Mike Schlaich. The structure consists of six modules, each 8.3 m in height. A module was composed of three steel-tube compression members, three heavy-duty diagonal cables, and three thin horizontal cables. Each stacked prism, in turn, was rotated by 30°. To increase the height further, architects added a stainless steel needle suspended from the top prism, extending the tower by 12.5 m. The tower was founded on a concrete base and foundation piles with a diameter of 8 m. In turn, the third tower was built in 1969 in the Kröller-Müller Museum in Otterlo, the Netherlands. The tower measures 30 m high and modules were connected strut-to-cable, which results in an unusual pattern of twisted stars when looking at the tower from below.

1.5.3 DOUBLE-LAYER GRIDS

One of the applications of the tensegrity principle in civil engineering is double-layer grids. Double-layer tensegrity grids are built by planar connection of the basic three-dimensional tensegrity modules. Adjacent modules can be connected in a contiguous configuration (struts are connected to each other) or a non-contiguous configuration (maintaining a discontinuous arrangement of compressed elements). Modules can be connected edge-to-edge, node-to-node, or strut-to-cable. Generally, the elements of a double-layer grid are organized into two parallel planes, which are connected by vertical and diagonal elements. In the horizontal projection, the elements are arranged in a regular pattern. In view of the double-layer grid

construction, they are called 'tensegrity plate-like structures', 'tensegrity plates', and 'tensegrity plate strips'. Due to this, tensegrity double-layer grids can be analyzed using a discrete model or continuum model (Al Sabouni-Zawadzka, 2016; Al Sabouni-Zawadzka and Gilewski, 2016; Al Sabouni-Zawadzka et al., 2016; Gilewski, Obara et al., 2019; Obara, 2019b, 2019c; Obara and Tomasik, 2023b).

The first double-layer tensegrity grids were constructed by Emmerich. In the patent (Emmerich, 1964), Emmerich proposed a structure consisting of *modified Simplex modules* with node-to-node connections. In turn, the first experimental model was created by Kono and Kunieda (1996, 1997a, 1997b) and Kono et al. (1997). It was built with 33 *modified Simplex modules*. The span of the structure was 9 m, and its area was 80 m^2. The research conducted by the Japanese team finally resulted in the granting of a patent in 2001 (Kono and Kunieda, 2001). An analysis of double-layer tensegrity grids composed of *regular Simplex modules* was carried out by Olejnikova (Olejnikova, 2012) and others (Gilewski and Al Sabouni-Zawadzka, 2015; Gomez-Jauregui et al., 2011, 2012, 2013; Wang, 1998, 1999, 2004, 2012; Wang and Li, 2003a, 2003b, 2005; Wang and Liu, 1996). For example, a model of double-layer tensegrity grids built with 24 *modified Simplex modules* is shown in Figure 1.7. A detailed description and parametric analysis of double-layer tensegrity grids built with *regular* and/or *modified Simplex modules* were presented (Obara and Tomasik, 2021; Tomasik, 2023; Tomasik and Obara, 2021, 2023).
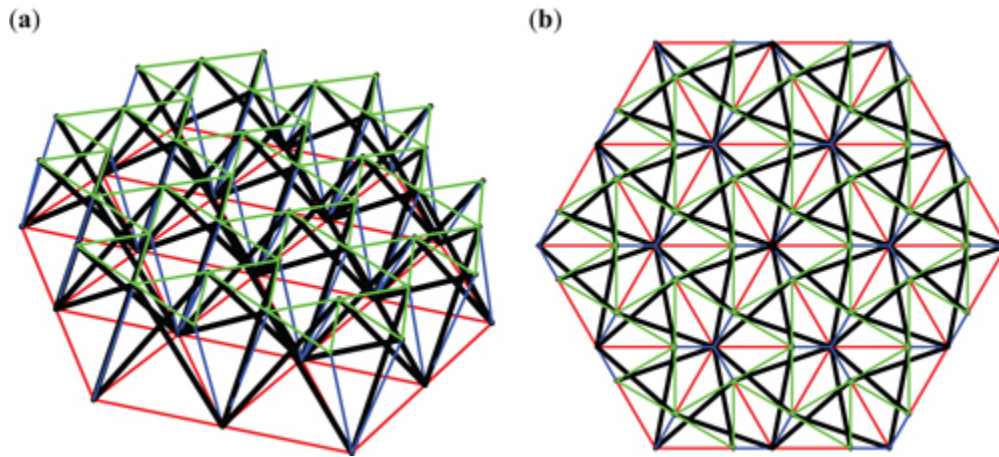
FIGURE 1.7 Model of double-layer tensegrity grids built with 24 *modified Simplex modules*: (**a**) 3D view, (**b**) plan view.↵

The second most popular module used to build double-layer tensegrity grids is the *Quartex module.* Square bases, due to their perpendicular arrangement, allow relatively easy construction of structures. The connection of the modules does not require additional components, and the cables of the lower bases are common to adjacent modules. The first structure built with connected edge-to-edge *modified Quartex modules* was proposed by Emmerich (Emmerich, 1964). An analysis of double-layer tensegrity grids composed of *modified Quartex modules* was carried out Olejnikova (Olejnikova, 2012), Al Sabouni-Zawadzka and Gilewski (Al Sabouni-Zawadzka and Gilewski, 2016), and others (Averseng, 2005; Faroughi and Lee, 2014, 2015; Faroughi et al., 2015; Gilewski et al., 2019; Gomez-Jauregui et al., 2012, 2013; Kan et al., 2018; Kono et al., 1999; Metrouni et al., 2024; Oliveto and Sivaselvan, 2011; Quirant et al., 2003; Shekastehband et al., 2011, 2012; Tran and Lee, 2010b; Wang, 1998). For example, a model of double-layer tensegrity grids built with 25 *modified Quartex modules* is shown in Figure 1.8. A detailed description and parametric analysis of double-layer tensegrity grids built

with *regular* and/or *modified Quartex modules* were presented (Gilewski, Kłosowska et al., 2019; Obara, 2019a; Obara and Tomasik, 2020, 2021a, 2023a, 2023b).
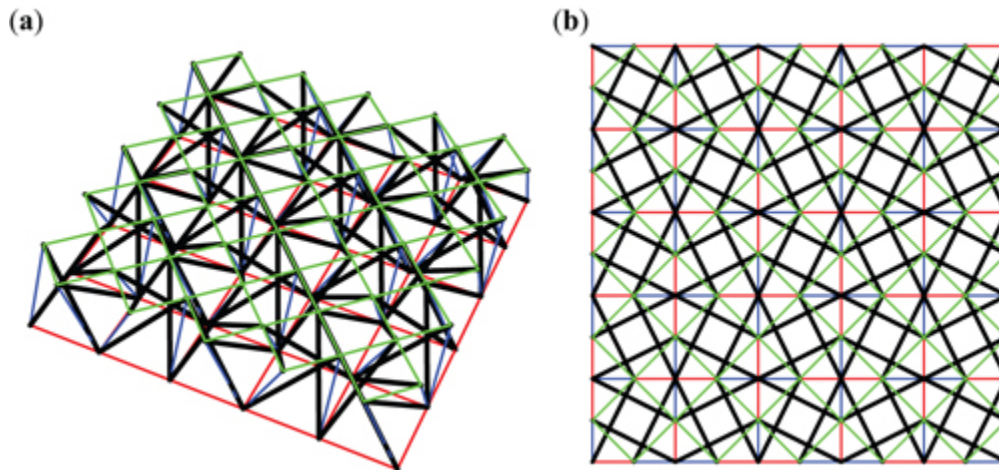
FIGURE 1.8 Model of double-layer tensegrity grids built with 25 *modified Quartex modules*: (**a**) 3D view, (**b**) plan view.

The most famous and the most spectacular example of a double-layer tensegrity grid was the Blur Building pavilion (Crawfordt, 2015; Gilewski et al., 2016b; Kłosowska, 2018), created as a temporary structure for Expo 2012 in Switzerland. The form is based on the work of Buckminster Fuller. Elizabeth Diller and Ricardo Scofidio were the creators of the architectural project. The structure measured 300 ft in width, 200 ft deep, and 75 ft high. The double-layer tensegrity grid was also used as the roofing of a bank annex patio in Athens (Liapi and Kim, 2009). A similar construction is used as the roofing of the exhibition pavilion in Patras, Greece (Liapi and Kim, 2009).

Other suggestions for the application of tensegrity double-layer grids in real engineering constructions can be found, for example, as a curved tensegrity vault (Liapi and Kim, 2003; Falk, 2006), a tensegrity platform (Hrazmi et al.,

2021), and as a tensegrity building facade (Kabošová et al., 2019; Miranda et al., 2020).

1.6 BRIEF REVIEW OF THE LITERATURE

The subject of tensegrity systems is very popular and continues explored. It is impossible to review all of the papers. However, based on the known literature (including our own chapters), six main subject areas are identified:

- form-finding methods;
- optimization algorithms;
- shape control methods;
- impulse loads;
- parametric analysis;
- dynamic stability analysis.

The first area is concerned with the search for geometrical stable self-balancing configuration. It means looking for a configuration of elements at which there is a stable self-stress state in the structure. The form-finding methods will be described in Section 3.2.1.

The second area focuses on the optimization of tensegrity structures. The optimization focuses on looking for the new topologies to achieve desired performance criteria, such as the level of stiffness. The algorithms that change the shape of the structures are proposed (Albertin et al., 2012; Ashwear et al., 2016; Bel Hadj Ali et al., 2010; Biondini et al., 2011; Caluwaerts and Carbajal, 2015; Dong et al., 2021; Feron et al., 2019; Lee S. and Lee J., 2014; Lu et al., 2010; Liu and Paulino, 2019; Masic and Skelton, 2004, 2006; Mottahedin and Keyvani, 2023; Sultan et al., 2002; Xiaoyang et al., 2010; Yildiz and Lesieutre, 2022; Zhang and Feng, 2017).

The most important research on the analysis of tensegrity structures focuses mainly on the third area, i.e., on the control of the shape of the structure under the influence of external forces. The search for the force–displacement relationship can be carried out by examining the damping and frequency of vibrations and by examining the change in geometry. Control methods are divided into passive and active (Ashwear et al., 2016; Averseng et al., 2005; Bel Hadj Ali and Smith, 2010; Domer et al., 2003; Faroughi and Lee, 2015; Faroughi et al., 2015; Fraternali et al., 2012; Kan et al., 2018; Manguri et al., 2024; Oliveto and Sivaselvan, 2011; Skelton, 2005, 2006; Skelton et al., 2001a; Wroldsen, 2007; Veuve et al., 2017; Zhang et al., 2023).

The fourth area is concerned with the impact of impulsive loading on the behavior of the structure. It is a very important subject. The purpose of the analysis was to determine critical dynamic loads in order to compare them with critical static loads. Parameters such as impulsive load duration, prestress level, damping coefficients, and support conditions were considered. The analysis was performed with and without the initial prestress (Atig et al., 2017; Fabbrocino and Carpentieri, 2017; Małyszko et al., 2018; Nagase and Skelton, 2014; Rimoli, 2018; Shekastehband and Ayoubi, 2019).

The fifth area focuses on the influence of the initial prestress level on the static and dynamic properties of structures (Angellier et al., 2013; Ashwear et al., 2016; Bel Hadj Ali and Smith, 2010; Chen and Feng, 2012b; Fu, 2006; Gilewski and Al Sabouni-Zawadzka, 2015; Gilewski et al., 2017; Gilewski Kłosowska et al., 2019; Hanaor, 1991; Hanaor and Liao, 1991; Kasprzak, 2014; Kłosowska, 2018; Kłosowska et al., 2018; Małyszko and Rutkiewicz, 2019, 2020; Małyszko, 2016; Małyszko et al., 2018; Mochocki and Obara, 2021; Murakami, 2001a, 2001b; Ashwear and Eriksson, 2014, 2015; Murakami and Nishimura, 2001a, 2001b, 2001c; Obara, 2019a, 2019b, 2019c; Obara and

Solovei, 2023, 2024; Obara and Tomasik, 2021a, 2021b, 2023a, 2023b, 2023c; Obara et al., 2023a, 2024; Oppenheim and Williams, 2001).

The sixth area is concerned with the influence of the initial prestress level on the unstable regions. In comparison to the abundant literature on the abovementioned areas, the dynamic stability analysis has been developed slightly (Obara, 2019a; Obara and Solovei, 2024; Obara and Tomasik, 2023d).

1.7 CHAPTER SUMMARY

The literature analysis shows that the majority of studies focus on tensegrity design, the search for stable forms, optimization algorithms, methods for controlling the shape of tensegrity structures under external loads, and their practical applications. However, parametric analysis, including the influence of the initial prestress on the static, stability, and dynamic properties of tensegrity structures, is the subject of much less work. In addition, these works relate to specific solutions. There is a lack of monographic studies that concisely describe the behavior of the full spectrum of tensegrity structures. The studies known to the author lack the analysis of dynamic stability understood in terms of the Bolotin approach (Bolotin, 1956), except three works (Obara, 2019a; Obara and Solovei, 2024; Obara and Tomasik, 2023d). This problem is often confused with the issues of impulse loads.

Dynamic stability analysis leads to the determination of parametric resonance areas (unstable regions), which risk a structure's durability. From the point of view of the physical interpretation of the phenomenon of dynamic instability, if the load parameters are within the defined limits of unstable regions, the structure experiences vibrations with increasing amplitude. There is abundant literature on parametric vibrations that essentially defines all the basic issues (see Section 3.5). Nevertheless, tensegrities are a special example of structures. Unlike conventional cable–strut frameworks, tensegrity structures are characterized by a system of internal forces that hold the elements in stable equilibrium (the initial prestress). The main purpose of this book is to explore the extent to which initial prestress affects the distribution of unstable regions in tensegrity structures.

The book contains both theoretical background and examples. First, a geometrically non-linear model and methods used to evaluate the behavior of tensegrity structures are explained. Next, a broad spectrum of different planar and spatial design solutions is considered. The book combines theoretical background with practical examples. It begins with a simple two-dimensional structure, whose solutions can be explicitly presented, and progresses to more complex three-dimensional tensegrity structures used in civil engineering, such as domes, towers, and plates.

REFERENCES

Adam, B., Smith, I.F.C. (2006). Learning, self-diagnosis and multi-objective control of an active tensegrity structure, *Advances in Engineering Structures, Mechanics & Construction* 140, 439–448.

Adam, B., Smith, I.F.C. (2007). Self-diagnosis and self-repair of an active tensegrity structure, *Journal of Structural Engineering* 133(12), 1752–1761.

Adam, B., Smith, I.F.C. (2008). Active tensegrity: A control framework for an adaptive civil – engineering structure, *Computers & Structures* 86, 2215–2223.

Albertin, A., Malerba, P.G., Pollini, N., Quagliaroli, M. (2012). *Genetic algorithms in the optimization of cable systems, Newsletter EnginSoft* 9(1), 30–33.

Aloui, O., Flores, J., Orden, D., Rhode-Barbarigos, L. (2019). Cellular morphogenesis of three-dimensional tensegrity structures, *Computer Methods in Applied Mechanics and Engineering* 346, 85–108, doi: 10.1016/j.cma.2018.10.048.

Alpatov, V.Y., Veremeenko, O.Y., Sakharov, A.A., Shirokov, V.S. (2016). Trial design of a dome roof for an church, *MATEC Web Conference* 86, 02015, doi: 10.1051/matecconf/20168602015.

Al Sabouni-Zawadzka, A. (2016). *A study of the feasibility of using the smart structures in bridge construction (in Polish)*, Ph. D. Thesis, Publishing House of the Warsaw University of Technology, Warsaw, Poland.

Al Sabouni-Zawadzka, A. (2020). Extreme mechanical properties of regular tensegrity unit cells in 3D lattice metamaterials, *Materials* 13(21), 4845, doi: org/10.3390/ma13214845.

Al Sabouni-Zawadzka, A. (2022). *High performance tensegrity-inspired metamaterials and structures* (1st Edition), CRC Press, Taylor & Francis Group, Boca Raton, London, New York, doi: 10.1201/9781003343202.

Al Sabouni-Zawadzka, A., Gilewski, W. (2016). On orthotropic properties of tensegrity structures, *Procedia Engineering* 153, 887–894.

Al Sabouni-Zawadzka, A., Gilewski, W. (2018). Smart metamaterial based on the simplex tensegrity pattern, *Materials* 11(5), 673, doi: 10.3390/ma11050673.

Al Sabouni-Zawadzka, A., Gilewski, W. (2019). Soft and stiff simplex tensegrity lattices as extreme smart metamaterials, *Materials* 12(1), 187, doi: 10.3390/ma12010187.

Al Sabouni-Zawadzka, A., Gilewski, W. Charandabi, R.N., Zawadzki, A. (2024). Stability of tensegrity-inspired structures fabricated through additive manufacturing, *Composite Structures*, 118377, doi: 10.1016/j.compstruct.2024.118377.

Al Sabouni-Zawadzka, A., Kłosowska, J., Obara, P., Gilewski, W. (2016). Continuum model of orthotropic tensegrity plate-like structures with self-stress included, *Engineering Transactions* 64(4), 501–508.

Angellier, N., Dubé, J.F., Quirant, J., Crosnier, B. (2013). Behavior of a double-layer tensegrity grid under static loading: Identification of self-stress level, *Journal of Structural Engineering* 139(6), 1075–1081, doi: 10.1061/(ASCE)ST.1943-541X.0000710.

Ashwear, N., Eriksson, A. (2014). Natural frequencies describe the pre-stress in tensegrity structures, *Computer and Structur* 138(1), 162–171.

Ashwear, N., Eriksson, A. (2015). Influence of temperature on the vibration properties of tensegrity structures, *International Journal of Mechanical Sciences* 99, 237–250.

Ashwear, N., Tamadapu, G., Eriksson, A. (2016). Optimization of modular tensegrity structures for high stiffness and frequency separation requirements, *International Journal of Solids and Structures* 80, 297–309, doi: 10.1016/j.ijsolstr.2015.11.017.

Atig, M., El Ouni, M.H., Kahla, N.B. (2017). Dynamic stability analysis of tensegrity systems, *European Journal of Environmental and Civil Engineering* 23(6), 675–692.

Averseng, J., Dube, J.F., Crosnier, B., Motro, R. (2005). *Active control of a tensegrity plane grid*, Proceedings of the 44th IEEE Conference on Decision and Control, and the European Control Conference 2005, Seville, Spain, 12–15 December, 6830–6834.

Bel Hadj Ali, N., Kan, Z., Peng, H., Rhode-Barbarigos, L. (2021). On static analysis of tensile structures with sliding cables: The frictional sliding case, *Engineering with Computers* 37, 1429–1442, doi: 10.1007/s00366-019-00893-z.

Bel Hadj Ali, N., Rhode-Barbarigos, L., Pascual, A.A., Smith, I.F.C. (2010). Design optimization and dynamic analysis of a tensegrity-based footbridge, *Engineering Structures* 32(11), 3650–3659, doi: 10.1016/j.engstruct.2010.08.009.

Bel Hadj Ali, N., Smith, I.F.C. (2010). Dynamic behavior and vibration control of a tensegrity structure, *International Journal of Solids and Structures* 47(9), 1285–1296, doi: 10.1016/j.ijsolstr.2010.01.012.

Bieniek, Z. (2009a). *A review of the tensegrity systems, symmetry: Art and science*, The Journal of the International Society for the Interdisciplinary Study of Symmetry, Special Issue for the Conference of ISIS Symmetry Wrocław and Cracow, Poland, Lugosi G., Nagy D. (Eds.), 14–19 September 2009, 1–4, 48–51.

Bieniek, Z. (2009b). *Space-filling tetrahedra, symmetry: Art and science*, The Journal of the International Society for the Interdisciplinary Study of Symmetry, Special Issue for the Conference of ISIS Symmetry Wrocław – Kraków, Poland, Lugosi G., Nagy D. (Eds.), 14–19 September 2009, 1–4, 44–47.

Bieniek, Z. (2011). *Chosen ideas of geometrical shaping of modular tensegrity structures*, Structural Engineers World Congress: Como, Italy, Congress paper on CD.

Bieniek, Z. (2012). *Tensegrity – integrating tension in architectural systems (in Polish)*, Publishing House of the Rzeszów University of Technology, Rzeszów, Poland.

Bieniek, Z. (2015a). *A mathematical model of the Class Theta tetrahedral tensegrity module*, Proceedings of Lightweight Structures in Civil Engineering – Contemporary Problems, XXI LSCE, Local Seminar of IASS Polish Chapter, Tarczewski R., Bieniek Z. (Eds.), Rzeszów University of Technology, 9–16.

Bieniek, Z. (2015b). Examples of cable-bar modular structures based on the Class-Theta tensegrity systems, *Journal of Civil Engineering and Architecture* 9, 1452–1462.

Bieniek, Z. (2016). Self-equilibrium geometry of the class-theta tetrahedral tensegrity module, *Engineering Transactions* 64(4), 441–448.

Bieniek, Z. (2017). The self-equilibrium problem of the Class-Theta tetrahedral tensegrity module, *Composites Part B: Engineering* 115, 21–29, doi: 10.1016/j.compositesb.2016.10.054.

Bieniek, Z., Mascolo, I., Amendola, A., Micheletti, A., Luciano, R., Fraternali, F. (2019). *Computational prediction of the stability of tensegrity structures*, Proceedings of the COMPDYN 2019 – 7th ECCOMAS Thematic Conference on Computational Methods in Structural Dynamics and Earthquake Engineering, Crete, Greece, 24–26 June 2019, doi: 10.7712/120119.7065.18375.

Biondini, F., Malerba, P.G., Quagliaroli, M. (2011). *Structural optimization of cable systems by genetic algorithms*, Proceedings of the 2011 World Congress on Advances in Structural Engineering and Mechanics (ASEM'11+), Seoul, Korea, 18–22 September.

Blur Building, https://dsrny.com/project/blur-building (accessed 05 September 2020).

Bolotin, V.V. (1956). *Dynamic stability of elastic systems (in Russian)*, Gostekhizdat, Moscow, Russia.

Brandao Mendes, A.N. (2021). *Nonlinear mechanics of bioinspired tensegrity systems*, Ph. D. Thesis, Rio de Janeiro, Brazil.

Burkhardt, R.W. Jr. (2008). *A practical guide to tensegrity design*, http://bobwb.Tripod.com (accessed 05 September 2020).

Caluwaerts, K., Carbajal, J.P. (2015). Energy conserving constant shape optimization of tensegrity structures, *International Journal of Solids and Structures* 58, 117–127.

Cao, Z., Luo, A., Liu, H., Feng, Y. (2024). A novel torque application method for tensegrity structures, *Mechanics Based Design of Structures and Machines*, 1–22, doi: 10.1080/15397734.2024.2309531.

Chai Lian, O., Kok Keong, C., Nishimura, T., Jae-Yeol, K. (2020). Form-finding of spine inspired biotensegrity model, *Applied, Sciences* 10(18), 6344, doi: 10.3390/app10186344.

Chen, L., Huang, K., Liu, Y., Zeng, Y., Li, Z., Zhou, Y., Dong, S. (2023). Optimisation of cable dome structure design for progressive collapse resistance, *Applied, Sciences* 13(4), 2086, doi: 10.3390/app13042086.

Chen, L., Li, Z., Liu, Y., Huang, K., Zeng, Y., Zhou, Y., Dong, S. (2022). Analysis and evaluation of the progressive collapse behaviour of a cable dome structure, *Buildings* 12, 1700, doi: 10.3390/buildings12101700.

Chen, M., Qin, J. (2024). *Form-finding and physical property predictions of tensegrity structures using deep neural networks*, doi: 10.13140/RG.2.2.31645.32480.

Chen, Y., Feng, J. (2012a). Generalized eigenvalue analysis of symmetric prestressed structures using group theory, *Journal of Computing in Civil Engineering* 26(4), 488–497.

Chen, Y., Feng, J. (2012b). Initial prestress distribution and natural vibration analysis of tensegrity structures based on group theory, *International Journal of Structural Stability and Dynamics* 12(2), 213–231.

Chen, Y., Yan, J., Feng, J., Sereh, P. (2020). A hybrid symmetry–PSO approach to finding the self-equilibrium configurations of prestressable pin-jointed assemblies, *Acta Mechanica* 231(4), 1485–1501, doi: 10.1007/s00707-019-02586-6.

Crawfordt, L. (2015). *Transgender architectonics: The shape of change in modernist space*, Routledge, London, UK.

Ding, M., Luo, B., Ding, S., Shen, Y., Huang, L. (2021). Experimental investigation and numerical simulation of a levy hinged-beam cable dome, *Buildings* 11(3), 110, doi: 10.3390/buildings11030110.

Ding, M., Luo, B., Pan, J., Guo, Z. (2018). Experimental study and comparative analysis of a geiger-type ridge-beam cable dome structure, *International Journal of Civil Engineering* 16, 1739–1755, doi: 10.1007/s40999-018-0331-y.

Djouadi, S., Motro, R., Pons, J.C., Crosnier, B. (1998). Active control of tensegrity systems, *Journal of Aerospace Engineering* 11(2), 37–44.

Domer, B., Raphael, B., Shea, K., Smith, I.F.C. (2003). A study of two stochastic search methods for structural control, *Journal of Computing in Civil Engineering* 17(3), 132–141, doi: 10.1061/(ASCE)0887-3801(2003)17:3(132).

Dong, Y., Ding, J., Wang, C., Liu, X. (2021). Kinematics analysis and optimization of a 3-DOF planar tensegrity manipulator under workspace constraint, *Machines* 9(11), 256, doi: 10.3390/machines9110256.

Dudzik, A., Potrzeszcz-Sut, B. (2021). Hybrid approach to the first order reliability method in the reliability analysis of a spatial structure, *Applied, Sciences* 11(2), 648, doi: org/10.3390/app11020648

Emmerich, D.G. (1964). *Construction de reseaux autotendants*, Paris, French Patent No 1.377.290.

Emmerich, D.G. (1988). *Structures tendues et autotendante*, Paris, France.

Estrada, G.G., Bungartz, H.J., Mohrdieck, C. (2006). Numerical form-finding of tensegrity structures, *International Journal of Solids and Structures* 43, 6855–6868.

Fabbrocino, F., Carpentieri, G. (2017). Three-dimensional modeling of wave dynamics of tensegrity lattices, *Composite Structures* 173, 9–16, doi: 10.1016/j.compstruct.2017.03.102.

Falk, A. (2006). *Architectural and structural development of plate tensegrity*, Proceedings of the International Association for Shell and Spatial Structures 2006 Symposium, Beijing, China, 16–19 October.

Faroughi, S., Lee, J. (2014). Geometrical nonlinear analysis of tensegrity based on a co-rotational method, *Advances in Structural Engineering* 17(1), 41–51.

Faroughi, S., Lee, J. (2015). Analysis of tensegrity structures subject to dynamic loading using a Newmark approach, *Journal of Building Engineering* 2, 1–8, doi: 10.1016/j.jobe.2015.03.005.

Faroughi, S., Khodaparast, H.H., Friswell, M.I. (2015). Non-linear dynamic analysis of tensegrity structures using a co-rotational method, *International Journal of Non-Linear Mechanics* 69, 55–65.

Feron, J., Boucher, L., Denoël, V., Latteur, P. (2019). Optimization of footbridges composed of prismatic tensegrity modules, *Journal of Bridge Engineering* 24(12), doi: 10.1061/(ASCE)BE.1943-‐5592.00014

Fraternali, F., Senatore, L., Daraio, C. (2012). Solitary waves on tensegrity lattices, *Journal of the Mechanics and Physics of Solids* 60(6), 1137–1144.

Fu, F. (2006). Non-linear static analysis and design of Tensegrity domes, *Steel and Composite Structures* 6(5), 417–433.

Fuller, R.B. (1962). *Tensile-integrity structures*, New York, United States Patent No 3.063.521.

Geiger, D.H. (1988). *Roof structure*, New York, United States Patent No 4.736.553.

Gengnagel, C. (2002). *Arbeitsblätter "tensegrity"* Fakultät für Architektur, Technische Universität München, Munich.

Gerardo, C., Levy, M.P. (1992). *Analysis of the Georgia dome cable roof*, Proceedings of Eighth Conference of Computing in Civil Engineering and Georgraphic Information Systems Symp., ASCE, Reston, VA.

Gilewski, W., Al Sabouni-Zawadzka, A. (2015). *On possible applications of smart structures controlled by self-stress,Archives of Civil and Mechanical Engineering* 15(2), 469–478, doi: 10.1016/j.acme.2014.08.006.

Gilewski, W., Al Sabouni-Zawadzka, A. (2020). Equivalent mechanical properties of tensegrity truss structures with self-stress included, *European Journal of Mechanics*

- A/Solids 83, 103998, doi: 10.1016/j.euromechsol.2020.103998.

Gilewski, W., Al Sabouni-Zawadzka, A. (2021). *Towards recognition of scale effects in a solid model of lattices with tensegrity-inspired microstructure*, *Solids* 2, 50–59, doi: 10.3390/solids2010002.

Gilewski, W., Kłosowska, J., Obara, P. (2015). Application of singular value decomposition to qualitative analysis of trusses and tensegrity structures (in Polish), *ACTA Scientarum Polonarum, Serie Architectura* 14(3), 3–20.

Gilewski, W., Kłosowska, J., Obara, P. (2016a). Form finding of tensegrity structures via singular value decomposition of compatibility matrix, *Advances in Mechanics: Theoretical, Computational and Interdisciplinary Issues*, 191–195.

Gilewski, W., Kłosowska, J., Obara, P. (2016b). Verification of tensegrity properties of kono structure and blur building, *Procedia Engineering* 153, 173–179, doi: 10.1016/j.proeng.2016.08.099.

Gilewski, W., Kłosowska, J., Obara, P. (2017). *The influence of self-stress on the behaviour of a tensegrity-like real structure*, Proceedings of MATEC Web of Conferences 117, 00079, XXVI R-S-P Seminar 2017, Theoretical Foundation of Civil Engineering, doi: 10.1051/matecconf/20171170007.

Gilewski, W., Kłosowska, J., Obara, P. (2019). Parametric analysis of some tensegrity structures, *MATEC Web of Conferences* 262, 10003, doi: 10.1051/matecconf/201926210003.

Gilewski, W., Obara, P., Al Sabouni-Zawadzka, A. (2019). 2D Theory of shell-like tensegrity structures, *Recent Developments in the Theory of Shells, part of the book series: Advanced Structured Materials* 110, 271–283, Springer.

Gomez-Jauregui, V. (2004). *Tensegrity structures and their application to architecture*, Master Thesis, School of

Architecture Queen's University Belfast, Belfast, Ireland.

Gomez-Jauregui, V. (2009). *Controversial origins of tensegrity*, Proceedings of the International Association for Shell and Spatial Structures (IASS) Symposium 2009, Valencia, A. Domingo, C. Lazaro (eds), Evolution and Trends in Design, Analysis and Construction of Shell and Spatial Structures, 28 September – 2 October 2009, Universidad Politechnica de Valencia, 1642–1652.

Gómez-Jáuregui, V., Arias, R., Otero, C., Manchado, C. (2012). Novel technique for obtaining double-layer tensegrity grids, *International Journal of Space Structures* 27 (2–3), 155–166, doi: 10.1260/0266-3511.27.2-3.155.

Gomez-Jauregui, V., Carrillo-Rodriguez, A., Manchado, C., Lastra-Gonzalez, P. (2023). Tensegrity applications to architecture, engineering and robotics: A review, *Applied, Sciences* 13(15), 8669, doi: 10.3390/app13158669.

Gomez-Jauregui, V., Manchado, C., Otero, C. (2013). *Comparison between new families of double-layer tensegrity, grids*, Proceedings of the First Conference Transformables 2013, In the Honor of Emilio Perez Piñero 18th–20th September 2013, School of Architecture Seville, Spain, EDITORIAL STARBOOKS, Felix Escrig and Jose Sanchez (eds.), 201–206.

Gómez-Jáuregui, V., Otero, C., Arias, R., Manchado, C. (2011). *New configurations for double-layer tensegrity grids*, Proceeding of Conference: Structural Engineers World Congress.

Gough, M. (1998). In the laboratory of constructivism: Karl Ioganson's cold structures, *Journal STORage* 84, 90–117.

Gough, M. (2005). *T*, University of California Press, Berkeley.

Gupta, S.S., Tan, Y.Y., Chia, Z.P., Pambudi, C.P., Quek, H., Yogiaman, C., Tracy, K.J. (2020). Prototyping knit

tensegrity shells: A design-to-fabrication workflow, *SN Applied Science* 2, 1062.

Hanaor, A. (1991). Double-layer tensegrity grids: Static load response. Part II: Experimental study, *Journal of Structural Engineering* 117(6), 1675–1684, doi: 10.1061/(ASCE)0733-9445(1991)117:6(1675).

Hanaor, A. (1994). Geometrically rigid double-layer tensegrity grids, *International Journal of Space Structures* 9(4), 227–238.

Hanaor, A., Liao, M.-K. (1991). Double-layer tensegrity grids: Static load response. Part I: Analytical study, *Journal of Structural Engineering* 117(6), 1660–1674, doi: 10.1061/(ASCE)0733-9445(1991)117:6(1660).

Hrazmi, I., Averseng, J., Quirant, J., Jamin, F. (2021). Deployable double layer tensegrity grid platforms for sea accessibility, *Engineering Structures* 231, 111706.

Intrigila, C., Micheletti, A., Nodargi, N.A., Artioli, E., Bisegna, P. (2022). Fabrication and experimental characterisation of a bistable tensegrity-like unit for lattice metamaterials, *Additive Manufacturing* 57, 102946, doi: 10.1016/j.addma.2022.102946.

Jeleniewicz, K., Jaworski, J., Żółtowski, M. , Uziębło, I., Stefańska, A., Dixit, S. (2024). Steel ribbed dome structural performance with different node connections and bracing system, *Scientific Reports* 14, 14013, doi: 10.1038/s41598-024-64811-0.

Jiang, Z., Liu, X., Shi, K., Zhang, Z. (2019). Catenary equation-based approach for force finding of cable domes, *International Journal of Steel Research* 19(1), 283–292, doi: 10.1007/s13296-018-0117-8.

Jung, E., Ly, V., Cheney, C., Cessna, N., Ngo, M.L., Castro, D., Teodorescu, M. (2021). Design, construction and validation of a proof of concept flexible–rigid mechanism emulating human leg behavior, *Applied, Sciences* 11(19), 9351, doi: 10.3390/app11199351.

Kabošová, L., Kormaníková, E., Kmet, S., Katunský, D. (2019). *Shape-changing tensegrity-membrane building skin*, Proceedings of the 4th International Scientific Conference Structural and Physical Aspects of Construction Engineering (SPACE 2019), Strbske Pleso, Slovakia, 13–15 November.

Kan, Z., Peng, H., Chen, B., Zhong, W. (2018). Nonlinear dynamic and deployment analysis of clustered tensegrity structures using a positional formulation FEM, *Composite Structures* 187, 241–258.

Kasprzak, A. (2014). *Assessing the feasibility of using tensegrity structures in bridge construction (in Polish)*, Ph. D. Thesis, Publishing House of the Warsaw University of Technology, Warsaw, Poland.

Kawaguchi, K., Ohya, S., Vormus, S. (2011). *Long-term monitoring of white Rhino, building with tensegrity skeletons*, Proceedings of 35th Annual Symposium of IABSE / 52nd Annual Symposium of IASS / 6th International Conference on Space Structures: Taller, Longer, Lighter – Meeting growing demand with limited resources, London, United Kingdom, September.

Kawaguchi, M., Tatemichi I., Chen, P.S. (1999). Optimum shapes of a cable dome structure, *Engineering Structures* 21(8), 719–725, doi: 10.1016/S0141-0296(98)00026-1.

Kebiche, K., Kazi-Aoual, M.N., Motro, R. (1999). Geometrical non-linear analysis of tensegrity systems, *Engineering Structures* 21(9), 864–876.

Khunsaraki, G.M., Oscuii, H.N., Voloshin, A. (2021). Study of the mechanical behavior of subcellular organelles using a 3D finite element model of the tensegrity structure, *Applied, Sciences* 11(1), 249, doi: 10.3390/app11010249.

Kiewitt, G. (1959). *Roof structure*, United States Patent No 2.908.236.

https://patentimages.storage.googleapis.com/bc/c9/cc/3b4b42bf32a7ea/US2908236.pdf

Kim, S.-D., Kim, H.S., Baek, I.S. (2001). Effects by bracing reinforcement on the instability phenomenon of cable domes, *Journal of the Korean Association for Spatial Structures* 1(2), 75–83.

Kim, S.-D., Sin, I.-A. (2014). A comparative analysis of dynamic instability characteristic of Geiger-typed cable dome structures by load condition, *Journal of the Korean Association for Spatial Structures, Korean Association for Spatial Structures* 14(1), 85–91, doi: 10.9712/KASS.2014.14.1.085.

Kłosowska, J. (2018). *Assessing the feasibility of using tensegrity construction in cubic construction (in Polish)*, PhD Thesis, Publishing House of the Kielce University of Technology, Kielce, Poland.

Kłosowska, J., Obara, P., Gilewski, W. (2018). Self-stress control of real civil engineering tensegrity structures, *AIP Conference Proceedings*, 150004, doi: 10.1063/1.5019157.

Kmet, S., Mojdis, M. (2014). Adaptive cable dome, *Journal of Structural Engineering* 14(9), 04014225.

Kono, Y., Choong, K.K., Shimada, T., Kunieda, H. (1999). An experimental investigation of a type of double-layer tensegrity grids, J*ournal of the International Association for Shell and Spatial Structures* 40(130), 103–111.

Kono, Y., Kunieda, H. (1996). *Tensegrity grids transformed from double-layer space grids*, Proceedings of Conceptual Design of Structures, IASS, Stuttgart, 293–300.

Kono, Y., Kunieda, H. (1997a). *A class of double-layer tensegrity grid domes*, Singapore, 455–463.

Kono, Y., Kunieda, H. (1997b). Experimental study on static load responses of double layer tensegrity grids, *Journal of Structural and Construction Engineering AIJ* 502, 93–97.

Kono, Y., Kunieda, H. (2001). *Frame structure and method for forming the same*, United States Patent No 6.192.644.B1. https://doi.org/10.3130/aijs.62.73_3

Kono, Y., Kunieda, H., Shimada, T. (1997). Form-finding of double-layer tensegrity grids with multiple states of self-stress, *Journal of Structural and Construction Engineering AIJ* 62(501), 73–76.

Korkmaz, S., Bel Hadj Ali, N., Smith, I.F.C. (2010). *Self-repair of a tensegrity pedestrian bridge through grouped actuation*, Proceedings of the International Conference on Computing in Civil and Building Engineering.

Korkmaz, S., Bel Hadj Ali, N., Smith, I.F.C. (2011a). Configuration of control system for damage tolerance of a tensegrity bridge, *Advanced Engineering Informatics* 26, 145–155.

Korkmaz, S., Bel Hadj Ali, N., Smith, I.F.C. (2011b). Determining control strategies for damage tolerance of an active tensegrity structure, *Engineering Structures* 33, 1930–1939.

Lee, S.W., Choong, K.K. (2018). Form-finding of four-stage tensegrity mast, *International Journal of Civil Engineering and Technology* 9(7), 1425–1434.

Lee, S.W., Lee, J. (2014). Optimum self-stress design of cable–strut structures using frequency constraints, *International Journal of Mechanical Sciences* 89, 462–469.

Levy, M.P. (1989). *Hypar-tensegrity dome*, *Proceedings of International Symposium on Sports Architecture*, Beijing, China: 157–162.

Liapi, K., Kim, J. (2003). *A parametric approach to the design of a tensegrity vaulted dome for an ephemeral structure for the 2004 olympics* Proceedings of the the 2003 Annual Conference of the Association for Computer Aided Design in Architecture, Indianapolis, USA, 24–27 October, 301–309.

Liapi, K., Kim, J. (2009). *Tensegrity structures of helical shape: A parametric approach*, Proceedings of the Conference on Computation: The New Realm of Architectural Design, Istanbul, Turkey, 16–19 September, 53–58.

Liu, K., Paulino, G.H. (2019). Tensegrity topology optimization by force maximization on arbitraryground structures, *Structural and Multidisciplinary Optimization* 59, 2041–2062, doi: 0.1007/s00158-018-2172-3.

Lu, X., Chen, S., Zhao, X., Lu, X. (2010). *Lectotype optimization Of single-layer steel reticulated dome based On BP neural network method*, Proceedings of 2010 Seventh International Conference on Fuzzy Systems and Knowledge Discovery 5, 2100–2104.

Malerba, P.G., Patelli, M., Quagliaroli, M. (2012). An extended force density method for the form finding of cable systems with new forms, *Structural Engineering and Mechanics* 42(2), 191–210.

Małyszko, L. (2016). Static response of axially loaded tensegrity prism—example of using proprietary programming language, in Małyszko, L., Tarczewski, R., eds., *Lightweight structures in civil engineering: Contemporary problems XXII*, University of Warmia and Mazur, Olsztyn, Poland, 43–48.

Małyszko, L. (2017). Design of tensegrity modules with UHMWPE cables based on experiments and nonlinear behaviour, in Gołębiowska, I., Dutkiewicz, M., eds., *Lightweight structures in civil engineering: Contemporary problems XXIII*, UTP University of Science and Technology: Bydgoszcz, Poland, 25–30.

Ma, Q., Ohsaki, M., Chen, Z., Yan, X. (2018). Step-by-step unbalanced force iteration method for cable-strut structure with irregular shape, *Engineering Structures* 177, 331–344, doi: 10.1016/j.engstruct.2018.09.081.

Ma, S., Chen, M., Yuan, X., Skelton, R.E. (2020). *Design and analysis of deployable clustered tensegrity cable*

domes, Proceedings of the IASS Annual Symposium 2020/21 and the 7th International Conference on Spatial Structures.

Małyszko, L., Rutkiewicz, A. (2019). The concept of use tensegrity modules in steel tower constructions (in Polish), *Inżynieria i Budownictwo* 75(7–8), 331–334.

Małyszko, L., Rutkiewicz, A. (2020). Response of a tensegrity simplex in experimental tests of a modal hammer at different self-stress levels, *Applied, Sciences* 10(23), 8733, doi: 10.3390/app10238733.

Małyszko, L., Rutkiewicz, A., Bilko, P. (2018). Dynamic response of a tensegrity simplex in impact hammer tests, in Kamiński, M., Szafran, J., eds., *Lightweight structures in civil engineering: Contemporary problems XXIV*, Łódź University of Technology, Łódź, Poland, 69–75.

Manguri, A., Saeed, N, Kazemi, F., Asgarkhani, N., Jankowski, R. (2024). The effect of minimum actuation limit in shape control of a single-layer dome frame, *Eurasian Journal of Science and Engineering* 10(1), 77–88.

Masic, M., Skelton, R.E. (2002). *Deployable plates made from stable-element class 1 tensegrity*, A.M.R. McGowan, ed., Proceedings of SPIE 4698, 220–230.

Masic, M., Skelton, R.E. (2004). *Optimization of class 2 tensegrity towers*, Proceedings of SPIE's 11th Annual International Symposium on Smart Structures and Materials, San Diego, CA.

Masic, M., Skelton, R.E. (2006). Selection of prestress for optimal dynamic/control performance of tensegrity structures, *International Journal of Solids and Structures* 43, 2110–2125.

Metodieva, I.Y. (2014). *Potential applications of tensegrity structures to bridge construction*, Proceedings of Second International Conference on Traffic and Transport Engineering, Belgrade, 583–589.

Metrouni, T., Khellaf, N., Kebiche, (2024). K. Non-linear behavior of double-layered grids, *Slovak Journal of Civil Engineering* 32(1), 10–17, doi: 0.2478/sjce-2024-0002.

Micheletti, A. (2005). *Modular tensegrity structures: The Tor Vergata footbridge* Proceedings of the 2nd International Conference on Footbridges, Venice, Italy.

Micheletti, A. (2012). Modular tensegrity structures: The Tor Vergata footbridge, *Mechanics, Models and Methods in Civil Engineering LNACM* 61, 375–384.

Micheletti, A., Santos, F. A., Guest, S. (2023). Prestrain-induced bistability in the design of tensegrity unitsfor mechanical metamaterials, *Applied, Physics Letters* 123, 121702, doi: 10.1063/5.0160023.

Miranda, R., Babilio, E., Peña, D., Santos, F., Fraternali, F. (2020). *Mechanics of energy harvesters based on tensegrity solar facades,*; IOP Publishing, Bristol.

Mochocki, W. (2022). *Static-strength analysis of lattice towers in a probabilistic approach (in Polish)*, Ph. D. Thesis, Publishing House of the Kielce University of Technology, Kielce, Poland.

Mochocki, W., Obara, P. (2021). *Reliability analysis of tensegrity towers in a system approach*, Modern Trends in Research on Steel, Aluminium and Composite Structures, Routledge, ISBN: 978-0-367-67637-7.

Moored, K.W., Bart–Smith, H. (2009). Investigation of clustered actuation in tensegrity structures, *International Journal of Solids and Structures* 46(17), 3272–3281, doi: 10.1016/j.ijsolstr.2009.04.026.

Motro, R. (1992). Tensegrity systems: the state of the art, *International Journal of Space Structures* 7(2), 75–83, doi: 10.1177/026635119200700201.

Motro, R. (2003). *Tensegrity: Structural systems for the future*, Kogan Page, London, UK.

Motro, R. (2011). *Tension structures in fifty years of progress for shell and spatial structures*, IASS Jubilee Book, Multi-Sciences 14.

Motro, R. (2012). *Tensegrity: From art to structural engineering*, Proceedings of IASS-APCS Symposium, May, Seoul, Sout Korea.

Mottahedin, A., Keyvani, J. (2023). Optimum design of cable domes using enhanced colliding bodies optimization algorithm with the substructuring method, *Iranian Journal of Science and Technology, Transactions of Civil Engineering* 47, 2571–2580, doi: 10.1007/s40996-022-01030-5.

Murakami, H. (2001a). Static and dynamic analyses of tensegrity structures. Part 1. Nonlinear equations of motion, *International Journal of Solids and Structures* 38(20), 3599–3613, doi: 10.1016/S0020-7683(00)00232-8.

Murakami, H. (2001b). Static and dynamic analyses of tensegrity structures. Part 2. Quasi-static analysis, *International Journal of Solids and Structures* 38(20), 3615–3629, doi: 10.1016/S0020-7683(00)00233-X.

Murakami, H., Nishimura, Y. (2001a). Static and dynamic characterization of regular truncated icosahedral and dodecahedral tensegrity modules, *International Journal of Solids and Structures* 38(50–51), 9359–9381, doi: 10.1016/S0020-7683(01)00030-0.

Murakami, H., Nishimura, Y. (2001b). Initial shape finding and modal analyses of cyclic right-cylindrical tensegrity modules, *Computers & Structures* 79(9), 891–917, doi: 10.1016/S0045-7949(00)00196-6.

Murakami, H., Nishimura, Y. (2001c). Static and dynamic characterization of some tensegrity modules, *Journal of Applied Mechanics* 68(1), 19–27, doi: 10.1115/1.1331058.

Nagase, K., Skelton, R.E. (2014). Network and vector forms of tensegrity system dynamics, *Mechanics Research Communications* 59, 14–25, doi: 10.1016/j.mechrescom.2014.03.007.

Obara, P. (2019a). *Dynamic and dynamic stability of tensegrity structures (in Polish)*, Publishing House of the Kielce University of Technology, Kielce, Poland.

Obara, P. (2019b). Analysis of orthotropic tensegrity plate strips using a continuum two-dimensional model, *MATEC Web of Conferences* 262, 10010, doi: 10.1051/matecconf/201926210010.

Obara, P. (2019c). Application of linear six-parameter shell theory to the analysis of orthotropic tensegrity plate-like structures, *Journal of Theoretical and Applied Mechanics* 57(1), 167–178, doi: 10.15632/jtam-pl.57.1.167.

Obara, P., Kłosowska, J., Gilewski, W. (2019). Truth and myths about 2D tensegrity trusses, *Applied Sciences* 9(1), 179, doi: 10.3390/app9010179.

Obara, P., Solovei, M. (2023). Assessment of the impact of the number of girders on the dynamic behaviour of Geiger dome, *Archives of Civil Engineering* 69(3), 597–611, doi: 10.24425/ace.2023.146100.

Obara, P., Solovei, M. (2024). Influence of the initial prestress level on the distribution of regions of dynamic instability of geiger domes, *Applied Sciences* 14(17): 7512, doi: 10.3390/app14177512.

Obara, P., Solovei, M., Tomasik, J. (2023a). Qualitative and quantitative analysis of tensegrity steel domes, *Bulletin of Polish Academy of Sciences* 71(1), 1–8, doi: 10.24425/bpasts.2023.144574.

Obara, P., Solovei, M., Tomasik, J. (2023b). Genetic algorithm via other methods for determination self-stress states of tensegrity domes, *Applied Sciences* 13(9), 5267, doi: 10.3390/app13095267.

Obara, P., Tomasik, J. (2020). Parametric analysis of tensegrity plate-like structures: Part 1—qualitative analysis, *Applied Sciences* 10(20), 7042, doi: 10.3390/app10207042.

Obara, P., Tomasik, J. (2021a). Parametric analysis of tensegrity plate-like structures: Part 2—quantitative analysis, *Applied Sciences* 11(2), 602, doi: 10.3390/app11020602.

Obara, P., Tomasik, J. (2021b). Active control of stiffness of tensegrity plate-like structures built with simplex modules, *Materials* 14(24), 7888, doi: 10.3390/ma14247888.

Obara, P., Tomasik, J. (2023a). Influence of the support conditions on dynamic response of tensegrity grids built with Quartex modules, *Archives of Civil Engineering* 69(3), 629–644, doi: 10.24425/ace.2023.146102.

Obara, P., Tomasik, J. (2023b). Validation of the continuum orthotropic model of tensegrity beam-like and plate-like structures, *Archives of Mechanics* 75(3), 249–269, doi: 10.24423/aom.4182.

Obara, P., Tomasik, J. (2023c). Dynamic stability of tensegrity structures – Part I: The time-independent external load, *Materials* 16(2), 580, doi: 10.3390/ma16020580.

Obara, P., Tomasik, J. (2023d). Dynamic stability of tensegrity structures – Part II: The periodic external load, *Materials* 16(13), 4564, doi: 10.3390/ma16134564.

Obara, P., Tomasik, J., Solovei, M. (2024). Parametric dynamic analysis of tensegrity cable-strut domes, *Journal of Theoretical and Applied Mechanics* 62(2), 253–267 doi: 10.15632/jtam-pl/183833.

Olejnikova, T. (2012). Double layer tensegrity grids, *Acta Polytechnica Hungarica* 9(5), 95–106.

Oliveto, N.D., Sivaselvan, M.V. (2011). Dynamic analysis of tensegrity structures using a complementary framework, *Computers and Structures* 89(23), 2471–2483, doi: 10.1016/j.compstruc.2011.06.003.

Oppenheim, I.J., Williams, W.O. (2001). Vibration of an elastic tensegrity structure, *European Journal of*

Mechanics and Solids 20(6), 1023–1031, doi: 10.1016/S0997-7538(01)01181-0.

Pinaud, J.-P., Solari, S., Skelton, R.E. (2004). *Deployment of a class 2 tensegrity boom*, Proceedings of SPIE – The International Society for Optical Engineering.

Pleşcan, C., Conţiu, M., Dósa, A. (2018). A study of a tensegrity structure for a footbridge, *IOP Conference Series: Materials Science and Engineering* 399, 012044, doi: 10.1088/1757-899X/399/1/012044.

Potrzeszcz-Sut, B. (2020). Reliability analysis of shell truss structure by hybrid Monte Carlo method, *Journal of Theoretical and Applied Mechanics* 58(2), 469–482, doi: 10.15632/Jtam-Pl/118886.

Potrzeszcz-Sut, B., Dudzik, A. (2022). Three methods in reliability assessment of engineering structure, *International Journal of Engineering and Advanced Technology* 11(3), 114–118.

Pugh, A. (1976). *An introduction to tensegrity*, University of California Press: Berkeley, USA.

Qin, W., Gao, H., Xi, Z., Feng, P., Li, Y. (2023). Shaking table experimental investigations on dynamic characteristics of CFRP cable dome, *Engineering Structures* 281, 115748, doi: 10.1016/j.engstruct.2023.115748.

Quirant, J., Kazi-Aoual, M.N., Motro, R. (2003). Designing tensegrity systems: The case of a double layer grid, *Engineering Structures* 25(9), 1121–1130.

Radoń, U., Zabójszcza, P., Opatowicz, D. (2020). Assesment of the effect of wind load on the load capacity of a single-layer bar dome, *Buildings* 10(179), 1–27, doi: 10.3390/buildings10100179.

Radoń, U., Zabojszcza, P., Sokol, M. (2023). The influence of dome geometry on the results of modal and buckling analysis, *Applied Sciences* 13(4), 2729, doi: 10.3390/app13042729.

Rastorfer, D. (1988). *Structural gymnastic for the olympics*, *Architectural Record,* September.

Rębielak, J. (2000). *Special forms of structural system proposed for cable domes* III, C.A. Brebbia & F.P. Escrig (Editors), WIT Press, www.witpress.com, ISBN 1-85312-817-1.

Rhode-Barbarigos, L., Bel Hadj Ali, N., Motro, R., Smith, I.F.C. (2009). *Tensegrity modules for pedestrian bridges*, Proceedings of the International Association for Shell and Spatial Structures (IASS) Symposium 2009: Evolution and Trends in Design, Analysis and Construction of Shell and Spatial Structures, 28 September–2 October 2009, Universidad Politecnica Valencia, Spain, Domingo A., Lazaro C. (eds.).

Rhode-Barbarigos, L., Bel Hadj Ali, N., Motro, R., Smith, I.F.C. (2010). Designing tensegrity modules for pedestrian bridges, *Engineering Structures* 32(4), 1158–1167, doi: 10.1016/j.engstruct.2009.12.042.

Rhode-Barbarigos, L., Jain, H., Kripakaran, P., Smith, I.F.C. (2010). Design of tensegrity structures using parametric analysis and stochastic search, *Engineering with Computers* 26(2), 193–203.

Rhode-Barbarigos, L., Motro, R., Smith, I.F.C. (2012). *A transformable tensegrity-ring footbridge*, Proceedings of IASS-APCS Symposium, Seoul, Korea.

Rimoli, J.J. (2018). A reduced-order model for the dynamic and post-buckling behavior of tensegrity structures, *Mechanics of Materials* 116, 146–157, doi: 10.1016/j.mechmat.2017.01.009.

Rutkiewicz, A. (2023). *Experimental and numerical studies of tensegrity structures in tower design (in Polish)*, PhD Thesis, Publishing House of the Warsaw University of Technology, Warsaw, Poland.

Rutkiewicz, A. (2024). Tensegrity simplex column analysis with different support conditions, *Engineering Structures* 317, 118655, doi: /10.1016/j.engstruct.2024.118655.

Safaei, S.D., Eriksson, A., Micheletti, A., Tibert, G. (2013). Study of various tensegrity modules as building blocks for slender booms, *International Journal of Space Structures* 28(1), 41–52, doi: 10.1260/0266-3511.28.1.41.

Schlaich, M. (2004). The messeturm in rostock: A tensegrity tower, *Journal of the International Association for Shell and Spatial Structures IASS* 45(145), 93–98.

Shekastehband, B., Abedi, K., Chenaghlou, M.R. (2011). Sensitivity analysis of tensegrity systems die to member loss, *Journal of Constructional Steel Research* 67(9), 1325–1340.

Shekastehband, B., Abedi, K., Dianat, N., Chenaghlou, M.R. (2012). Experimental and numerical studies on the collapse behavior of tensegrity systems considering cable rupture and strut collapse with snap-through, *International Journal of Non-Linear Mechanics* 47(7), 751–768.

Shekastehband, B., Ayoubi, M. (2019). Nonlinear dynamic instability behavior of tensegrity grids subjected to impulsive loads, *Thin-Walled Structures* 136, 1–15.

Shen, X., Zhang, Q., Lee, D.S.H., Cai, J., Feng, J. (2021). Static behavior of a retractable suspen-dome structure, *Symmetry* 13(7), 1105.

Skelton, R.E. (2005). *Dynamics and control of tensegrity systems*, Proceedings of IUTAM Symposium on Vibration Control of Nonlinear Mechanisms and Structures, Springer, 309–318.

Skelton, R.E. (2006). *Dynamics of tensegrity systems: Compact forms*, Proceedings of 45th IEEE Conference on Decision and Control, 2276–2281.

Skelton, R.E., Adhikari, R., Pinaud, J.P., Chan, W., Helton, J.W. (2001b). *An introduction to the mechanics of tensegrity structures*, Proceedings of the 40th IEEE

Conference on Decision and Control, Orlando, FL, December, 4254–4258.

Skelton, R.E., de Oliveira, M.C. (2009). *Tensegrity systems*, Springer: London, UK.

Skelton, R.E., Helton, J.W., Adhikari, R., Pinaud, J.P., Chan, W. (2002a). An introduction to the mechanics of tensegrity structures, in *Handbook of mechanical systems design* (Chapter 17), CRC Press, Boca Raton.

Skelton, R.E., de Oliveira, M.C. (2010). Optimal complexity of deployable compressive structures, *Journal of the Franklin Institute* 347, 228–256.

Skelton, R.E., Pinaud, J.P., Mingori, D.L. (2001a). Dynamics of the shell class of tensegrity structures, *Journal of the Franklin Institute* 338, 255–320.

Skelton, R.E., Williamson, D., Han, J.H. (2002b). Equilibrium conditions of a class 1 tensegrity structures, *Advances in the Astronautical Sciences Spaceflight Mechanics* 112, 02–177, 927–950.

Snelson, K. (1965). *Continuous tension, discontinuous compression structures*, New York, United States Patent No 3.169.611.

Snelson, K. (1996). Snelson on the tensegrity invention, *International Journal of Space Structures* 11(1–2), 43–48, doi: 10.1177/026635119601-2.

Snelson, K. (2013). *Art and ideas*, New York, US.

Sultan, C., Corless, M., Skelton, R. (2002). Linear dynamics of tensegrity structures, *Engineering Structures* 24(6), 671–685, doi: 10.1016/S0141-0296(01)00130-4.

Sun, G., Xiao, S. (2021). Test and numerical investigation mechanical behavior of cable dome, *International Journal of Steel Structures* 21(4), 1502–1514.

Terry, W.L. (1996). *Tension braced* , United States Patent No 5.502.928.

Tibert, A.G. (2002). *Deployable tensegrity structures for space applications*, PhD Thesis, Royal Institute of Technology, Stockholm, Sweden.

Tibert, A.G., Pellegrino, S. (2003). *Deployable tensegrity masts*, Proceedings of 44th AIAA/ASME/ASCE/AHS/ASC Structures, Structural Dynamics and Materials Conference and Exhibit, Norfolk, VA, US.

Tomasik, J. (2023*). Parametric analysis of double-layer tensegrity girds – discrete and continual model (in Polish)*, PhD Thesis, Publishing House of the Kielce University of Technology, Kielce, Poland.

Tomasik, J., Obara, P. (2021). *Impact of the self-stress state on the static properties of double-layered tensegrity grids*, Modern Trends in Research on Steel, Aluminium and Composite Structures, Routledge, ISBN: 978-0-367-67637-7.

Tomasik, J., Obara, P. (2023). The application of the immanent tensegrity properties to control the behavior of double-layered grids, *Archives of Civil Engineering* 69(1), 131–145, doi: 10.24425/ace.2023.144164.

Tran, H.C., Lee, J. (2010a). Initial self-stress design of tensegrity grid structures, *Computers & Structures* 88(9–10), 558–566, doi: 10.1016/j.compstruc.2010.01.011.

Tran, H.C., Lee, J. (2010b). Self-stress design of tensegrity gird structures with exostresses, *International Journal of Solids and Structures* 47(20), 2660–2671, doi: 10.1016/j.ijsolstr.2010.05.020.

Vangelatos, Z., Micheletti, A., Grigoropoulos, C.P., Fraternali, F. (2020). Design and testing of bistable lattices with tensegrity architecture and nanoscale features fabricated by multiphoton lithography, *Nanomaterials* 10(4), 652, doi: 10.3390/nano10040652.

Veuve, N., Dalil Safaei, S., Smith, I.F.C. (2015). Deployment of a tensegrity footbridge, *Journal of Structural Engineering* 141(11), 04015021.

Veuve, N., Sychterz, A.C., Smith, I.F.C. (2017). Adaptive control of a deployable tensegrity structure, *Engineering Structures* 152(1), 14–23.

Volokh, K.Y., Vilnay, O., Averbuh, I. (2003). Dynamics of cable structures, *Journal of Engineering Mechanics* 129(2), 175–180, doi: 10.1061/(ASCE)0733-9399(2003)129:2(175).

Voloshin, A. (2020). Migration of the 3T3 cell with a lamellipodium on various stiffness substrates—tensegrity model, *Applied Sciences* 10(19), 6644, doi: 10.3390/app10196644.

Wang, B.B. (1998). Cable-strut systems: Part I – tensegrity, *Journal of Constructional Steel Research* 45(3), 281–289, doi: 10.1016/S0143-974X(97)00075-8.

Wang, B.B. (1999). Simplexes in tensegrity systems, *Journal of the International Association for Shell and Spatial Structures* 40(129), 57–64.

Wang, B.B. (2004). *Free-standing tension structures: From tensegrity systems to cable-strut systems*, CRC Press, New York.

Wang, B.B. (2012). Realizing cable-strut systems, *International Journal of Architectural Technology* 42(1), 42–53.

Wang, B.B., Li, Y. (2003a). Novel cable-strut grids made of prisms: Part I. Basic theory and design, *Journal of the International Association for Shell and Spatial Structures* 44(142), 93–108.

Wang, B.B., Li, Y. (2003b). Novel cable-strut grids made of prisms: Part II. Deployable and architectural studies, *Journal of the International Association for Shell and Spatial Structures* 44(142), 109–125.

Wang, B.B., Li, Y. (2005). Cable-strut systems of non-contiguous strut configurations - Morphological study, *Journal of the International Association for Shell and Spatial Structures* 46(147), 23–39.

Wang, B.B., Liu, X.L. (1996). Integral-tension research in double-layer tensegrity grids, *International Journal of Space Structures* 11(4), 349–355.

Wang, T., Post, M.A. (2021). A symmetric three degree of freedom tensegrity mechanism with dual operation modes for robot actuation, *Biomimetics* 6(2), 30, doi: 10.3390/biomimetics6020030.

Wang, W., Guo, Q., Li, J. (2024). Characterization, applications and new technologies of civil engineering materials and structures, *Materials* 17, 2058, doi: 10.3390/ma17092058

Wang, Y., Senatore, G. (2020). Extended integrated force method for the analysis of prestress-stable statically and kinematically indeterminate structures, *International Journal of Solids and Structures* 202, 798–815, doi: 10.1016/j.ijsolstr.2020.05.029.

Williamson, D., Skelton, R.E., Han, J.H. (2003a). Equilibrium conditions of a tensegrity structure, *International Journal of Solids and Structures* 40(23), 6347–6367, doi: 10.1016/S0020-7683(03)00400-1.

Williamson, D., Skelton, R.E., Han, J.H. (2003b). Equilibrium conditions of class 1 tensegrity structures, *Revue Francaise de Genie* 7, 291–310.

Wroldsen, A.S. (2007). *Modelling and control of tensegrity structures*, Ph.D. Thesis, Department of Marine Technology, Norwegian University of Science and Technology, Trondheim, Norway.

Wu, X., Deng, H., Zhu, D. (2018). Determination of target modes for monitoring the stiffness of cable domes considering random pretension deviations, *Journal of Engineering Mechanics* 144(2), 04017178, doi: 10.1016/j.jcsr.2018.10.022.

Wu, X., Xu, S., Ma, J., Miao, F. (2020). Measuring full static displacements of cable domes based only on limited tested locations, *Applied Mathematical Modeling* 77(2), 1054–1064, doi: 10.1016/j.apm.2019.08.018.

Xiaoyang, L., Chen, S., Lu, X. (2010). *Lectotype optimization of single-layer steel reticulated dome based on BP neural network method*, Seventh

International Conference on Fuzzy Systems and Knowledge Discovery 5, 2100–2104.

Xu, X., Luo, Y. (2011). Multistable tensegrity structures, *Journal of Structural Engineering* 137(1), 117–123, doi: 10.1061/(ASCE)ST.1943-541X.0000281.

Yan, X., Yang, Y., Chen, Z., Ma, Q. (2019). Mechanical properties of a hybrid cable dome under non-uniform snow distribution, *Journal of Constructional Steel Research* 153, 519–532, doi: 10.1016/j.jcsr.2018.10.022.

Yildiz, K., Lesieutre, G.A. (2022). Sizing and prestress optimization of Class–2 tensegrity structures for space boom applications, *Engineering with Computers* 38, 1451–1464, doi: 10.1007/s00366-020-01111-x.

Yuan, X., Chen, L., Dong, S. (2007). Prestress design of cable domes with new forms, *International Journal of Solids and Structures* 44(9), 2773–2782, doi: 10.1016/j.ijsolstr.2006.08.026.

Zabojszcza, P., Radoń, U. (2019). The impact of node location imperfections on the reliability of single-layer steel domes, *Applied Sciences* 9(13), 2742, doi: 10.3390/app9132742.

Zabojszcza, P., Radoń, U. (2020). Stability analysis of the single-layer dome in probabilistic description by the Monte Carlo method, *Journal of Theoretical and Applied Mechanics* 58(2), 425–436, doi: 10.15632/jtam-pl/118950.

Zabojszcza, P., Radoń, U., Szaniec, W. (2021). Probabilistic approach to limit states of a steel dome, *Materials* 14(19), 5528, doi: 10.3390/ma14195528.

Zawadzki, A., Al Sabouni-Zawadzka, A. (2020). In search of lightweight deployable tensegrity columns, *Applied Sciences* 10(23), 8676, doi: 10.3390/app10238676.

Zhang, P., Feng, J. (2017). Initial prestress design and optimization of tensegrity systems based on symmetry and stiffness, *International Journal of Solids and*

Structures 106–107, 68–90, doi:
10.1016/j.ijsolstr.2016.11.030.

Zhang, H., Lu, J., Lu, M., Li, N. (2023). Active control
experiments on a Levy cable dome, *Engineering
Structures* 278, 115450, doi:
10.1016/j.engstruct.2022.115450.

Zhang, J.Y., Ohsaki, M. (2015). *Tensegrity structures: Form,
stability, and symmetry*, Springer, Japan.

Zhang, L., Chen, W., Dong, S. (2007). Initial pre-stress
finding procedure and structural performance research
for Levy cable dome based on linear adjustment theory,
Journal of Zhejiang University SCIENCE A 8(9): 1366–
1372.

Zhang, L.Y., Li, Y., Cao, Y.-P., Feng, X.Q. (2014). Stiffness
matrix based form-finding method of tensegrity
structures, *Engineering Structures* 58, 36–48, doi:
10.1016/j.engstruct.2013.10.014.

Zhang, L.Y., Zhu, S.-X., Li, S.-X., Xu, G.-K. (2018). Analytical
form-finding of tensegrities using determinant of force-
density matrix, *Composite Structures* 189, 87–98, doi:
10.1016/j.compstruct.2018.01.054.

Zhang, L.Y. Zheng, Y.,Yin, X., Zhang, S., Li, H.-Q., Xu, G.-K.
(2022). A tensegrity-based morphing module for
assembling various deployable structures, *Mechanism
and Machine Theory* 173, 104870, doi:
10.1016/j.mechmachtheory.2022.104870.

Zhang, M., Liu, Y.-P., Yu, Z.-X., Parke, G. (2019). Study of
seismic resistance of Kiewit-8 dome considering key
structural design parameters, *Advanced Steel
Construction* 15(4), 386–397, doi:
10.18057/IJASC.2019.15.4.9.

2 Mathematical Model of Tensegrity Element

NOTE

In mathematical description, the following are assumed: $i, j, k, l = 1, 2, 3$.

2.1 INTRODUCTION

Tensegrity structures are spatial trusses that consist of tensed cables (which do not have compression rigidity) and struts. These elements are assembled in a self-balanced way, which means that there is an equilibrium stress state among struts and cables (the initial prestress) under zero external loads. The second important feature of these systems is the occurrence of infinitesimal mechanism (or mechanisms), which describes local geometric variability in the range of small displacements. Note, in contrast, a finite mechanism (rigid body motion) refers to motions that do not change the distance between any pair of nodes. The specificity of tensegrity systems lies in the fact that the initial prestress stabilizes the existing infinitesimal mechanisms. Another specific property of these systems is the size of the displacements, which can be large even with small deformations.

To describe the behavior of tensegrity structures, a geometrically non-linear model of elements, in which there are large gradients of displacements but small strain gradients, is adopted (Bathe, 1996; Crisfield, 1991; de Borst, 1999; de Borst et al., 2012; Fung, 1969; Timoshenko and Goodier, 1962). Owing to the specificity of these systems, additionally, the condition of initial stresses (Argyris and Scharpf, 1972), related to the introduction of the self-stress state, is taken into account (Faroughi and Lee, 2014; Kebiche et al., 1999; Motro, 1984; Obara, 2019; Pagitz and Tur, 2009; Tran and Lee, 2011).

A solid elastic body covering an area B_0 in the initial configuration ${}^0C$ (the undeformed configuration) is considered. The area is a subset of the three-dimensional Euclidean space R^2 (Figure 2.1). The following designations are adopted in the description of the initial configuration: B_0 – inside area, ∂B_0 – boundary area (∂B_{0u}– with known displacements, ∂B_{0p} – with known loads), ρ_0 – density, f_0 – mass forces, $\rho_0 f_0$ – volume forces, and p_0 – surface forces. The actual configuration ${}^1C$ (the deformed configuration) is described without subscript, respectively.
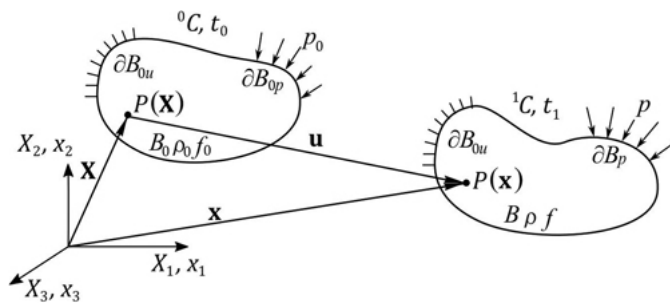
FIGURE 2.1 Initial and actual configurations of an elastic body.

As a basis for formulating the equations, the partially non-linear theory of elasticity in the Total Lagrangian – TL (Lagrange's stationary description) approach is adopted. The spatial coordinates x in the actual configuration at the moment t_1 $\left({}^1C\right)$ are expressed by the material coordinates X in the initial configuration at the moment t_0 $\left({}^0C\right)$:

$$x = x(X, t) \Rightarrow x_i = x_i(X_j, t)$$

The Cartesian coordinate system $x_i \equiv X_i$ is assumed. The displacement of any point (2.1) $P(x)$ of the deformed body is described as

$$u = x - X \Rightarrow u_i(X) = x_i - X_i$$

2.1.1 LOCAL FORMULATION OF THE BOUNDARY PROBLEM (2.2)

The state of deformation in the actual configuration, related to the initial configuration, is described by the symmetric ($E_{ij} = E_{ji}$ for $i \neq j$) Green–Lagrange strain tensor

$$E_{ij}(X) = \frac{1}{2}\left[\frac{\partial u_i}{\partial X_j} + \frac{\partial u_j}{\partial X_i} + \frac{\partial u_k}{\partial X_i}\frac{\partial u_k}{\partial X_j}\right]; X \in B_0.$$

Assuming large displacement gradients, the actual configuration ${}^1C$ is fundamentally (2.3) different from the initial configuration ${}^0C$. The elementary area ∂A_0 in the ${}^0C$ configuration changes when moving to the ${}^1C$ configuration. The stress state is determined on the unknown configuration of the deformed body. The quantity describing the stress state is the first or the second Pioli–Kirchhoff stress tensor. A consequence of adopting Lagrange's stationary description (TL) is the use of the second, symmetric, Pioli–Kirchhoff tensor

$$S_{kl} = J\frac{\partial X_k}{\partial x_i}\frac{\partial X_l}{\partial x_j}\sigma_{ij}; \qquad J = \det\left(\frac{\partial x_i}{\partial X_j}\right),$$

where σ_{ij} is the Cauchy stress tensor describing the measure of internal interactions (2.4) in the actual configuration and J is the Jacobian transformation. In turn, assuming the material is linear and elastic, the constitutive relationships between deformations (2.3) and stresses (2.4) are described as

$$S_{kl} = C_{klij}E_{ij},$$

where C_{klij} is the material constants tensor. Taking into account the equality of the (2.5) resultant volumetric forces in the initial and actual configurations

$$\int\limits_{B_0} (\rho_0 f_{0i})dB_0 = \int\limits_{B} (\rho f_i)dB,$$

the equilibrium equations in Lagrange's stationary description are as follows: (2.6)

$$\frac{\partial}{\partial X_k}\left[S_{kl}\left(\delta_{il} + \frac{\partial u_i}{\partial X_l}\right)\right] + \rho_0 f_{0i} = 0; \quad \delta_{il} = \begin{cases} \delta_{il} = 0 & if \quad i \neq l \\ \delta_{il} = 1 & if \quad i = l \end{cases},$$

where δ_{il} is the Kronecker delta. (2.7)

In solving the boundary problem, the equilibrium equations (2.7) need to be supplemented with static and/or geometric boundary conditions. Assuming the conservative nature of the loads

$$\int_{\partial B_{0p}} p_{0i} d(\partial B_0) = \int_{\partial B_p} p_i d(\partial B),$$

the static boundary conditions take the following form: (2.8)

$$p_{0i} - S_{jl}\left(\delta_{il} + \frac{\partial u_i}{\partial X_l}\right)v_{0j} = 0,$$

where v_{0j} is the normal vector of the boundary area ∂B_{0p}. On the other hand, the (2.9) geometrical boundary conditions are known in the boundary area ∂B_{0u}:

$$u_i(X) = \widehat{u}_i; X \in \partial B_{0u},$$

where $\widehat{u}_i$ is the known displacement. (2.10)

2.1.2 GLOBAL FORMULATION OF THE BOUNDARY PROBLEM

The global boundary problem can be formulated using the principle of virtual work or the principle of stationary total potential energy. In the first approach, the forces p_{0i} distributed on the area ∂B_{0p} and the volumetric forces $\rho_0 f_{0i}$ in the area B_0, make on the virtual displacements δu_i work equals to the internal energy (work of the stress S_{ij} on the virtual strain δE_{ij}):

$$\int_{B_0} [\delta E_{ij} S_{ij}] dB_0 = \int_{\partial B_{0p}} [\delta u_i p_{0i}] d(\partial B_{0p}) + \int_{B_0} [\delta u_i (\rho_0 f_{0i})] dB_0.$$

In the second approach, a conservative system is in a state equilibrium if the first (2.11) variation of the potential energy is zero and the second variation of the potential energy is positively defined:

$$\delta E_p = 0 \text{ and } \delta^2 E_p > 0.$$

Equation $(2.12)_1$ is the principle of stationary total potential energy and leads to the (2.12) determination of the equilibrium equations, in which there is a secant stiffness matrix. On the other hand, calculating the second variation of potential energy, we obtain a tangent stiffness matrix, with condition $(2.12)_2$ implying its positive determinacy (the matrix is symmetric and its leading principal minors are positive).

The total potential energy

$$E_p = E_s - L_p$$

(2.13)

consists of the elastic strain potential energy E_s and the external load potential L_p, respectively:

$$E_s = \frac{1}{2} \int_{B_0} [E_{ij}S_{ij}]dB_0,$$

$$L_p = \int_{\partial B_{0p}} [u_i p_{0i}]d(\partial B_{0\mathrm{p}}) + \int_{B_0} [u_i(\rho_0 f_{0i})]dB_0.$$

(2.14)

2.2 GEOMETRICAL NON-LINEAR MODEL OF FINITE TENSEGRITY ELEMENT

The finite tensegrity element is a modified truss element. The modification refers to the inclusion of the initial stress σ_0 in the initial configuration. Assuming the axial load, both the strain and stress tensors reduce to only one component. The strain state tensor (2.3) is described by the elongation of the element

$$\varepsilon = E_{11}; \qquad E_{11} = \frac{\partial u_1}{\partial X_1} + \frac{1}{2}\left[\left(\frac{\partial u_1}{\partial X_1}\right)^2 + \left(\frac{\partial u_2}{\partial X_1}\right)^2 + \left(\frac{\partial u_3}{\partial X_1}\right)^2\right],$$

whereas the stress state tensor (2.4) is described by normal stress with part of an initial stress σ_0:

(2.15)

$$\sigma = S_{11}; \quad S_{11} = E\varepsilon + \sigma_0$$

where E is the Young modulus.

(2.16)

Taking into account the dimensionless variable $\xi = X_1/l_0$, the strain field (2.15) can be expressed as

$$\varepsilon = Lu + \frac{1}{2}g^T g,$$

where

(2.17)

$$L = \frac{1}{l_0}\begin{bmatrix} \frac{d}{d\xi} & 0 & 0 \end{bmatrix}$$

is the differential operator matrix,

(2.18)

$$u = [u_i]^T$$

is the displacement field, and

(2.19)

$$g = \frac{1}{l_0}\left[\frac{du_i}{d\xi}\right]^T$$

is the vector of displacement field gradients. (2.20)

In the following sections, the static and dynamic equilibrium equations will be derived for a space finite tensegrity element. An undeformed configuration (initial) ^0C and two deformed configurations (actual) ^tC and $^{t+\Delta t}C$ (Figure 2.2) are considered. In the initial configuration, the cross-sectional area and the length are relatively A_0 and l_0, whereas in the actual configurations they are A and l, respectively. It should be noted that the inclusion of the initial stress σ_0 in the initial configuration results in an axial force in the tensegrity element
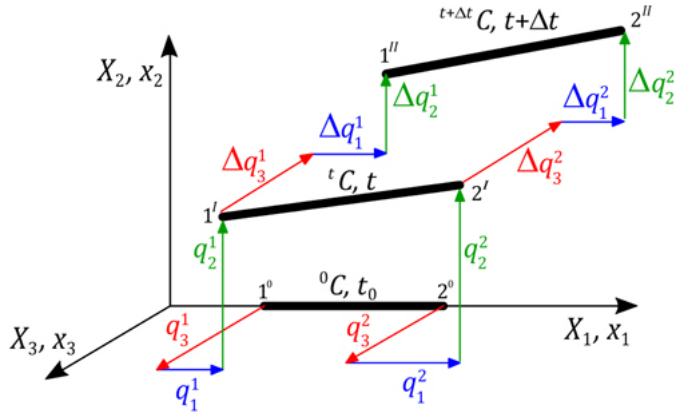
FIGURE 2.2 Space finite tensegrity element.

$$S = A_0\sigma_0$$

To build the static equilibrium equation, the non-incremental and incremental (2.21) versions of the equations will be formulated. The principle of stationary total potential energy (2.12) and the principle of virtual work (2.11) will be used, respectively. In turn, to formulate the dynamic equilibrium equation, the principle of virtual work (2.11) will be used, in which gravity forces are included.

2.2.1 SECANT STIFFNESS MATRIX

The static equilibrium equation in the non-incremental version is formulated in the actual configuration at the moment $\left(^tC\right)$. The finite tensegrity element is described by the vector of nodal coordinates $^tq^e$ and corresponding to it the vector of nodal forces $^tQ^e$:

$$^tq^e = \begin{bmatrix} q_i^1 & q_i^2 \end{bmatrix}^T, \quad ^tQ^e = \begin{bmatrix} Q_i^1 & Q_i^2 \end{bmatrix}^T$$

The displacement field (2.19) at the moment t (2.22)

$$^tu^e = N^e(\xi)\,^tq^e$$

is approximated by the linear shape functions (2.23)

$$N^e(\xi) = \begin{bmatrix} 1-\xi & 0 & 0 & \xi & 0 & 0 \\ 0 & 1-\xi & 0 & 0 & \xi & 0 \\ 0 & 0 & 1-\xi & 0 & 0 & \xi \end{bmatrix}.$$

(2.24)

The approximation (2.23) leads to obtaining the vector of displacement field gradients (2.20) at the moment t

$$^tg_e = \Gamma^{et}q^e,$$

where (2.25)

$$\Gamma^e = \frac{1}{l_0}\begin{bmatrix} -1 & 0 & 0 & 1 & 0 & 0 \\ 0 & -1 & 0 & 0 & 1 & 0 \\ 0 & 0 & -1 & 0 & 0 & 1 \end{bmatrix}.$$

Introducing an elongation matrix (2.26)

$$B_0^e = LN^e(\xi) \xrightarrow{(2.18)\text{and}(2.24)} B_0^e = \frac{1}{l_0}\begin{bmatrix} -1 & 0 & 0 & 1 & 0 & 0 \end{bmatrix},$$

and a linear displacement-dependent matrix (2.27)

$$B_1^e = \left({}^tq^e\right)^T (\Gamma^e)^T \Gamma^e \xrightarrow{(2.22)_1 and(2.26)} B_1^e = \frac{1}{l_0^2}\begin{bmatrix} -\Delta_{u_1} & -\Delta_{u_2} & -\Delta_{u_3} & \Delta_{u_1} & \Delta_{u_2} & \Delta_{u_3} \end{bmatrix}$$

where $\Delta_{u_i} = q_i^2 - q_i^1$, the strain field (2.17) at the moment t can be expressed as (2.28)

$$^t\varepsilon_e = \left[\mathrm{B}_0^e + \frac{1}{2}\mathrm{B}_1^e \right] {}^tq^e.$$

In turn, the constitutive relationship (2.16) is as follows: (2.29)

$$^t\sigma_e = E^t\varepsilon_e + \sigma_0^e$$

The total potential energy (2.13) in the actual configuration at the moment t $\left({}^tC\right)$ is (2.30) given by

$$E_p = \frac{1}{2}\int\limits_{V_0} \left[\left({}^t\varepsilon_e\right)\left({}^t\sigma_e\right) \right] \mathrm{d}V_0 - \left({}^tq^e\right)^T \left({}^tQ^e\right).$$

Taking into account the geometrical (2.29) and constitutive (2.30) relationships, the (2.31) potential energy (2.31) can be expressed as

$$E_p = \left({}^tq^e\right)^T \left[\frac{1}{2}K_L^e + \frac{1}{2}K_G^e(S) + \frac{1}{4}K_{u1}^e + \frac{1}{8}K_{u2}^e \right] {}^tq^e + \left({}^tq^e\right)^T \left(F_0^e - {}^tQ^e\right),$$

where (2.32)

$$K_L^e = EA_0 l_0 (B_0^e)^T B_0^e \xrightarrow{(2.27)} K_L^e = \frac{EA_0}{l_0} \begin{bmatrix} I_0 & -I_0 \\ -I_0 & I_0 \end{bmatrix}$$

is the linear stiffness matrix, (2.33)

$$K_G^e(S) = S l_0 (\Gamma^e)^T \Gamma^e \xrightarrow{(2.26)} K_G^e(S) = \frac{S}{l_0} \begin{bmatrix} I & -I \\ -I & I \end{bmatrix}$$

is the geometrical stiffness matrix (the initial stress matrix), (2.34)

$$K_{u1}^e = EA_0 l_0 \left[(B_0^e)^T B_1^e + (B_1^e)^T B_0^e \right] \xrightarrow{(2.27) \text{ and } (2.28)} K_{u1}^e = \frac{EA_0}{l_0^2} \begin{bmatrix} I_1 & -I_1 \\ -I_1 & I_1 \end{bmatrix}$$

is the first part of the non-linear stiffness matrix, (2.35)

$$K_{u2}^e = EA_0 l_0 (B_1^e)^T B_1^e \xrightarrow{(2.28)} K_{u2}^e = \frac{EA_0}{l_0^3} \begin{bmatrix} I_2 & -I_2 \\ -I_2 & I_2 \end{bmatrix}$$

is the second part of the non-linear stiffness matrix, (2.36)

$$F_0^e = S l_0 B_0^e \xrightarrow{(2.27)} F_0^e = S \begin{bmatrix} -I_{F0} \\ I_{F0} \end{bmatrix}$$

is the vector of internal forces arising from the initial stresses. In formulas (2.33)–(2.37) (2.37), the following matrices are included:

$$I_{F0} = \begin{bmatrix} 1 \\ 0 \\ 0 \end{bmatrix}, I = \begin{bmatrix} 1 & 0 & 0 \\ 0 & 1 & 0 \\ 0 & 0 & 1 \end{bmatrix}, I_0 = \begin{bmatrix} 1 & 0 & 0 \\ 0 & 0 & 0 \\ 0 & 0 & 0 \end{bmatrix},$$

$$I_1 = \begin{bmatrix} 2\Delta_{u_1} & \Delta_{u_2} & \Delta_{u_3} \\ \Delta_{u_2} & 0 & 0 \\ \Delta_{u_3} & 0 & 0 \end{bmatrix}, \qquad I_2 = \begin{bmatrix} (\Delta_{u_1})^2 & \Delta_{u_1}\Delta_{u_2} & \Delta_{u_1}\Delta_{u_3} \\ \Delta_{u_1}\Delta_{u_2} & (\Delta_{u_2})^2 & \Delta_{u_2}\Delta_{u_3} \\ \Delta_{u_1}\Delta_{u_3} & \Delta_{u_2}\Delta_{u_3} & (\Delta_{u_3})^2 \end{bmatrix}$$

The principle of stationary total potential energy (2.12) results in the non-incremental (2.38) static equilibrium equation of the tensegrity element

$$K_S^e \left({}^t q^e \right) {}^t q^e = {}^t Q^e - F_0^e$$

where (2.39)

$$K_S^e(q) = K_L^e + K_G^e(S) + K_{N,NL}^e(q)$$

is the secant matrix consisting of the linear part K_L^e (2.33), quasi-linear parts caused (2.40) by the initial stress $K_G^e(S)$ (2.34), and of the non-linear stiffness matrix

$$K^e_{N,NL}(q) = \frac{1}{2}\left(K^e_{u2} + K^e_{N,u1}\right)$$

with the matrix (2.36) and the non-symmetric part (2.41)

$$K^e_{N,u1} = \frac{EA_0}{l_0^2}\begin{bmatrix} I_{N1} & -I_{N1} \\ -I_{N1} & I_{N1} \end{bmatrix}; \qquad I_{N1} = \begin{bmatrix} 3\Delta_{u_1} & \Delta_{u_2} & \Delta_{u_3} \\ 2\Delta_{u_2} & 0 & 0 \\ 2\Delta_{u_3} & 0 & 0 \end{bmatrix}.$$

The equilibrium equation (2.39) takes into account the axial force S (2.21) caused by (2.42) the initial stress, σ_0, which is the most important feature of tensegrity structures.

2.2.2 Tangent Stiffness Matrix

The static equilibrium equation in the incremental version is formulated in the actual configuration at the moment $t + \Delta t$ $\left({}^{t+\Delta t}C\right)$. The finite tensegrity element is described by the vector of nodal coordinates ${}^{t+\Delta t}q_e$ and corresponding to it the vector of nodal forces ${}^{t+\Delta t}Q_e$:

$$ {}^{t+\Delta t}q_e = {}^{t}q_e + \Delta q^e, \qquad {}^{t+\Delta t}Q_e = {}^{t}Q_e + \Delta Q^e$$

where $\Delta q^e = \begin{bmatrix} \Delta q_i^1 & \Delta q_i^2 \end{bmatrix}^T$ and $\Delta Q^e = \begin{bmatrix} \Delta Q_i^1 & \Delta Q_i^2 \end{bmatrix}^T$ are the vectors of (2.43) displacement increments and nodal force increments, respectively. The displacement field (2.19) at the moment $t + \Delta t$

$$ {}^{t+\Delta t}u_e = {}^{t}u_e + \Delta u^e$$

is expressed by the displacement field increments (2.44)

$$\Delta u^e = N^e \Delta q^e$$

approximated by the linear shape functions (2.24). The strain field (2.17) at the (2.45) moment $t + \Delta t$ can be expressed as

$$ {}^{t+\Delta t}\varepsilon_e = LN^e\left({}^{t+\Delta t}q_e\right) + \frac{1}{2}\left({}^{t+\Delta t}g_e\right)^T\left({}^{t+\Delta t}g_e\right),$$

where ${}^{t+\Delta t}g_e = {}^{t}g_e + \Delta g_e$ is the vector of displacement field gradients (2.20) at the (2.46) moment $t + \Delta t$, while $\Delta g_e = \Gamma^e \Delta q_e$ is the vector of displacement field gradient increments. It should be noted that the strain fields can also be described as

$$ {}^{t+\Delta t}\varepsilon_e = {}^{t}\varepsilon_e + \Delta\varepsilon^e$$

which leads to obtain the strain field increment (2.47)

$$\Delta\varepsilon^e = {}^{t+\Delta t}\varepsilon_e - {}^t\varepsilon_e$$

Using the formulas (2.29) and (2.46), the strain field increments (2.48) take the form: (2.48)

$$\Delta\varepsilon^e = \left[B_0^e + B_1^e + \frac{1}{2}B_2^e\right]\Delta q^e,$$

where (2.49)

$$B_2^e = (\Delta q^e)^T (\Gamma^e)^T \Gamma^e$$

$$\downarrow (2.26)$$

$$B_2^e = \frac{1}{l_0^2}\left[-\frac{d\Delta u_1}{d\xi} \quad -\frac{d\Delta u_2}{d\xi} \quad -\frac{d\Delta u_3}{d\xi} \quad \frac{d\Delta u_1}{d\xi} \quad \frac{d\Delta u_2}{d\xi} \quad \frac{d\Delta u_3}{d\xi}\right],$$

where $\Delta u_i = \Delta q_i^2 - \Delta q_i^1$. In turn, the constitutive relationship (2.16) is as follows: (2.50)

$$^{t+\Delta t}\sigma_e = {}^t\sigma_e + \Delta\sigma^e$$

where $\Delta\sigma^e = E\Delta\varepsilon_e$ is the stress field increment. (2.51)

The principle of virtual work (2.11) in the actual configuration at the moment $t + \Delta t$ $\left(^{t+\Delta t}C\right)$ is given by

$$\int_{V_0}\left[\delta\left(^{t+\Delta t}\varepsilon_e\right)\left(^{t+\Delta t}\sigma_e\right)\right]\mathrm{d}V_0 = \left[\delta\left(^{t+\Delta t}q_e\right)\right]^T\left(^{t+\Delta t}Q_e\right).$$

At the moment t, both displacement and strain are constant, so the variation of these (2.52) quantities is zero:

$$\delta\left(^tq_e\right) = 0, \delta\left(^t\varepsilon_e\right) = 0$$

while the variation of strain increments (2.48) from the moment t to $t + \Delta t$ equals (2.53)

$$\delta\Delta\varepsilon^e = [B_0^e + B_1^e + B_2^e]\delta\Delta q^e$$

By substituting variations (2.53) and (2.54) into Equation (2.52), taking into account (2.54) relations (2.43) and (2.51), the incremental static equilibrium equation of the finite tensegrity element is obtained:

$$A_0 l_0 [B_0^e + B_1^e + B_2^e]^T\left[^t\sigma_e + E\left(B_0^e + B_1^e + \frac{1}{2}B_2^e\right)\Delta q^e\right] = {}^tQ_e + \Delta Q^e.$$

After neglecting the non-linear parts due to the displacement increment Δq^e, (2.55) Equation (2.55) can be written in the form:

$$K_T^e(q)\Delta q^e = R^e + \Delta Q^e$$

where (2.56)

$$K_T^e(q) = K_L^e + K_G^e(S) + K_{GN}^e(N) + K_{NL}^e(q)$$

is the tangential stiffness matrix composed of the linear part K_L^e (2.33), two quasi-(2.57) linear parts, i.e., the part caused by the initial prestress $K_G^e(S)$ (2.34) and the part caused by axial forces N, which results from external loads

$$K_{GN}^e(N) = \frac{N}{l_0}\begin{bmatrix} I & -I \\ -I & I \end{bmatrix}; N = EA_0\left({}^t\varepsilon_e\right),$$

and on the non-linear part (2.58)

$$K_{NL}^e(q) = K_{u1}^e + K_{u2}^e$$

which is the symmetric displacement stiffness matrix consisting of the matrices(2.59) (2.35) and (2.36).

In turn, R^e in (2.56) is the residual force vector

$$R^e = {}^tQ_e - F^e$$

depends on the vector of nodal forces ${}^tQ_e$ and on the inertial force vector (2.60)

$$F^e = (S+N)l_0[B_0^e + B_1^e]^T \Rightarrow F^e = (S+N)\begin{bmatrix} -I_{F1} \\ I_{F1} \end{bmatrix}; I_{F1} = \begin{bmatrix} 1 + \frac{\Delta_{u_1}}{l_0} \\ \frac{\Delta_{u_2}}{l_0} \\ \frac{\Delta_{u_3}}{l_0} \end{bmatrix}.$$

Because the initial configuration is not deformed, the axial force N (2.58)$_2$ is not a(2.61) real force. It is the component of the second symmetric Piola–Kirchhoff stress tensor, whereas` the real force is defined on the basis of the Cauchy tensor as

$$N' = N\frac{l}{l_0}.$$

2.2.3 CONSISTENT MASS MATRIX (2.62)

In static equilibrium equations, the assumption was made that the finite tensegrity element is weightless. Taking into account the motion of an element, the forces of gravity and the causes of motion are considered, i.e., mass forces and resistance to motion as time variables. The dynamic equilibrium equation can be described using the principle of virtual work (2.11) supplemented by the forces of inertia $\rho_0\ddot{u}_i$ (damping forces are omitted)

$$\int\limits_{B_0} [\delta E_{ij} S_{ij}] dB_0 = \int\limits_{\partial B_{0p}} [\delta u_i (p_{0i})] d(\partial B_{0p}) + \int\limits_{B_0} [\delta u_i (\rho_0 f_{0i} - \rho_0 \ddot{u}_i)] dB_0.$$

Equation (2.63) in the actual configuration at the moment t $\left({}^t C\right)$ is expressed as   (2.63)

$$\int\limits_{V_0} \delta \left({}^t \varepsilon_e\right) \left({}^t \sigma_e\right) dV_0 = \int\limits_{A} \left[\delta \left({}^t u^{e|}(\xi, t)\right)\right]^T p(\xi, t) dA +$$

$$+ \int\limits_{V_0} \left[\delta \left({}^t u^{e|}(\xi, t)\right)\right]^T \rho_0 \left[f_0(\xi, t) - {}^t \ddot{u}^{e|}(\xi, t)\right] dV_0,$$

where $p(\xi, t)$ is the load vector and $f_0(\xi, t)$ is the mass forces vector. In the actual (2.64) configuration at the moment $\left({}^t C\right)$, the finite tensegrity element is described by the vector of nodal coordinates and corresponding the vector of nodal forces (2.22), depending on time: ${}^t q^e = {}^t q^e(t)$ and ${}^t Q^e = {}^t Q^e(t)$. It leads to the displacement field (2.19) being a function of two variables and approximated by the linear shape functions (2.24):

$$ {}^t u^e(\xi, t) = N^e(\xi) {}^t q^e(t).$$

Due to this, the acceleration field is expressed as   (2.65)

$$ {}^t \ddot{u}^e(\xi, t) = N^e(\xi) {}^t \ddot{q}^e(t)$$

Substituting the geometrical (2.29) and constitutive (2.30) relationships into Equation (2.66) (2.64), taking into account the approximations (2.65) and (2.66), and relation (2.53), the equation of undamped motion of the finite tensegrity element is obtained:

$$ M^e {}^t \ddot{q}^e(t) + K_S^e {}^t q^e(t) = P^e(t) - F_0^e$$

where   (2.67)

$$ M^e = \int\limits_{V_0} \rho_0 [N^e(\xi)]^T N^e(\xi) dV_0 \quad \xrightarrow{\text{(2.24)}} \quad M^e = \frac{\rho_0 A_0 l_0}{6} \begin{bmatrix} 2I & I \\ I & 2I \end{bmatrix}$$

is the consistent mass matrix, and   (2.68)

$$ P^e(t) = \int\limits_{V_0} \rho_0 [N^e(\xi)]^T f_0(\xi, t) dV_0 + {}^t Q^e(t)$$

is the load vector.   (2.69)

It should be noted that the equation of motion (2.67) can also be derived using Hamilton's principle (Fung, 1969), Lagrange's equation (Langer, 1980; Gomuliński and Witkowski, 1993), or directly from d'Alembert's principle (Langer, 1980). The choice of the

principle of virtual work was dictated by the consequence of the description used in the book.

2.2.4 TRANSFORMATION TO GLOBAL COORDINATE SYSTEM

The matrices described above relate to the local coordinate system (X_1, X_2, X_3) associated with the initial configuration of the element. Analysis of a structure as a set of elements and nodes requires relating them to the global coordinate system (x, y, z). The transformation of geometric $q^e = q^e(X_1, X_2, X_3)$ and static $Q^e = Q^e(X_1, X_2, X_3)$ parameters from the local to the global system, i.e., $\overline{q}^e = \overline{q}^e(x, y, z)$, $\overline{Q}^e = \overline{Q}^e(x, y, z)$, is done according to Figure 2.3 and is expressed as
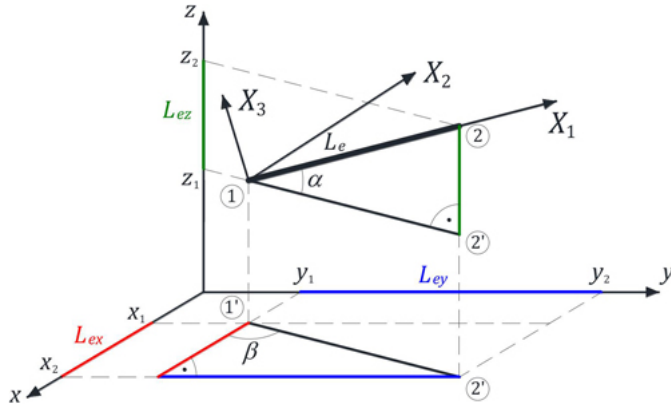
FIGURE 2.3 Transformation from the local (X_1, X_2, X_3) to global (x, y, z) coordinate system.

$$q^e = T^e \overline{q}^e, Q^e = T^e \overline{Q}^e$$

with   (2.70)

$$T^e = \begin{bmatrix} T_1 & 0 \\ 0 & T_1 \end{bmatrix}; T_1 = \begin{bmatrix} \cos\alpha\cos\beta & \cos\alpha\sin\beta & \sin\alpha \\ -\sin\beta & \cos\beta & 0 \\ -\sin\alpha\cos\beta & -\sin\alpha\sin\beta & \cos\alpha \end{bmatrix}$$

where   (2.71)

$$\cos\alpha = \frac{\sqrt{L_{ex}^2 + L_{ey}^2}}{L_e}, \quad \sin\alpha = \frac{L_{ez}}{L_e}, \quad \cos\beta = \frac{L_{ex}}{\sqrt{L_{ex}^2 + L_{ey}^2}}, \quad \sin\beta = \frac{L_{ey}}{\sqrt{L_{ex}^2 + L_{ey}^2}},$$

$L_{ex} = x_2 - x_1$, $L_{ey} = y_2 - y_1$, $L_{ez} = z_2 - z_1$.

Knowledge of the transformation laws of geometric and static parameters (2.70) allows us to determine the transformations of the stiffness matrix K^e and vectors F^e of an element from the local to the global coordinate system, respectively:

$$\overline{K}^e = (T^e)^T K^e T^e,$$

$$\overline{F}^e = (T^e)^T F^e \qquad (2.72)$$

It should be noted that the mass matrix does not depend on the coordinate system, (2.73) i.e., $\overline{M}^e = M^e$. In turn, the row dimensionless elongation matrix

$$B^e = l_0 B_0^e$$

where the matrix B_0^e is defined by formula (2.27), is transformed according to the (2.74) formula

$$\overline{B}^e = B^e T^e$$

and finally is expressed as (2.75)

$$\overline{B}^e = \begin{bmatrix} -c_x & -c_y & -c_z & c_x & c_y & c_z \end{bmatrix} \in \mathbb{R}^{1 \times 6},$$

where (2.76)

$$c_x = \frac{L_{ex}}{L_e}, c_y = \frac{L_{ey}}{L_e}, c_z = \frac{L_{ez}}{L_e}$$

are the directional cosines.

2.3 CHAPTER SUMMARY

The mathematical model proposed in this chapter is sufficient for qualitative and quantitative analyses of both planar and spatial lattice structures, including tensegrity structures, in the geometrically non-linear and physically linear domains. It is thus possible to design tensegrity structures using their unique properties, which allow the control of static and dynamic parameters.

The defined matrices of initially prestressed tensegrity elements were used in the calculation procedure based on the finite element method. The calculation module was written in the Mathematica environment, owing to which operations were simplified by using functions and commands implemented there.

REFERENCES

Argyris, J.H., Scharpf, D.W. (1972). Large deflection analysis of prestressed networks, *Journal of the Structural Division* 98(3), 633–654.

Bathe, K.J. (1996). *Finite element procedures in engineering analysis*, Prentice Hall, New York.

Crisfield, M.A. (1991), *Non-linear finite element analysis of solid and structures: Essentials*, John Wiley & Sons, New York.

De Borst, R. (1999). *Computational methods in non-linear solid mechanics* TU Delft, Netherlands.

De Borst, R., Crisfield, M.A., Remmers, J.J.C., Verhoosel, C.V. (2012). *Non-linear finite element analysis of solid and structures*, John Wiley & Sons, The Atrium, Southern Gate.

Faroughi, S., Lee, J. (2014). Geometrical nonlinear analysis of tensegrity based on a co-rotational method, *Advances in Structural Engineering* 17(1), 41–51.

Fung, Y.C. (1969). *Foundations of solid mechanics*, Prentice Hall, New York.

Gomuliński, A., Witkowski, M. (1993). *Mechanics of structures (advanced course) (in Polish)*, Publishing House of the Warsaw University of Technology, Warsaw, Poland.

Kebiche, K., Kazi-Aoual, M.N., Motro, R. (1999). Geometrical non-linear analysis of tensegrity systems, *Engineering Structures* 21(9), 864–876.

Langer, J. (1980), *Dynamic of structure (in Polish)*, Publishing House of the Wroclaw University of Technology, Wroclaw, Poland.

Motro, R. (1984), *Forms and forces in tensegrity systems*, H. Nooshin (ed.), Proceedings of Third International Conference on Space Structures, Elsevier, 180–185.

Obara, P. (2019). *Dynamic and dynamic stability of tensegrity structures (in Polish)*, Publishing House of the Kielce University of Technology, Kielce, Poland.

Pagitz, M., Tur, J.M. (2009). Finite element based form finding algorithm, *International Journal of Solids and Structures* 46(17), 3235–3240.

Timoshenko, S., Goodier, J.N. (1962). *Theory of elasticity*, McGraw-Hill Book Company, New York.

Tran, H.C., Lee, J. (2011). Geometrical and material nonlinear analysis of tensegrity structures, *Acta Mechanical Science* 27(6), 938–949.

3 Assessment of Tensegrity Structures – Theory

3.1 INTRODUCTION

The complete analysis of tensegrity structures is a two-stage process. The first stage involves identifying self-stress states and infinitesimal mechanisms (qualitative analysis). The qualitative analysis is is crucial for understanding the unique properties of tensegrity systems, which, in certaincases, allow for the control of both, in certaincases, allow for the control of both static and dynamic parameters. The second stage focuses on the behavior of tensegritiy structures under external loads (quantitative analysis), which includes static, dynamic, and dynamic stability analysis. In classical lattice structures, quantitative analysis is typically conducted under the assumption of small displacements, employing a linear geometric model. However, this approach is unsuitable for tensegrity structures. The quasi-linear model (second-order theory) is also inadequate. Both approaches fail to account for a critical feature of the tensegrity structure – stiffening under the influence of external load. In tensegrity structures, external loads cause displacements in accordance with the form of the infinitesimal mechanism, causes additional prestress of the structure – tensile forces increase in the cables, and compressive forces increase in the struts. In such cases, the initial response is insufficient to predict the behavior of the structure. Therefore, a more appropriate approach is needed, one that assumes large displacements, as described by third-order theory.

3.2 MODEL OF TENSEGRITY STRUCTURE

The tensegrity structure is modeled using the finite element formalism (Bathe, 1996; Szmelter, 1980; Zienkiewicz and Taylor, 2000). This structure is an n-element spatial truss ($e = 1, 2, \ldots, n$) with m degrees of freedom described by a displacement vector as described in the global coordinate system (x, y, z)

$$q = \begin{bmatrix} q_1 & q_2 & \ldots & q_m \end{bmatrix}^T \in \mathbb{R}^{m \times 1}$$

and loaded by forces applied at the nodes $\hspace{8cm}$ (3.1)

$$P = \begin{bmatrix} P_1 & P_2 & \ldots & P_m \end{bmatrix}^T \in \mathbb{R}^{m \times 1}$$

The components of the structure are modeled as the space finite tensegrity elements(3.2) e of Young's modulus E_e, density ρ_e, cross-sectional area A_e, and length L_e (Figure 3.1). The elements are described by the matrices defined in Section 2.2, i.e.:
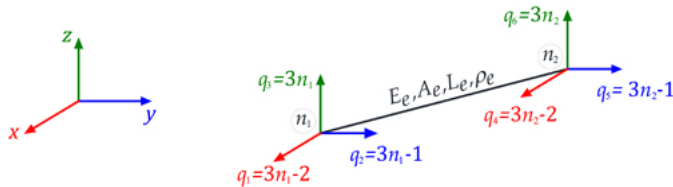
FIGURE 3.1 Global degrees of freedom of a space finite tensegrity element.⏎

- elongation matrix B^e (2.74);
- stiffness matrices K^e:

  - linear stiffness matrix K_L^e (2.33);
  - geometrical stiffness matrices: $K_G^e(S)$ (2.34), $K_{GN}^e(N)$ (2.58);
  - non-linear stiffness matrices: K_{u1}^e (2.35), K_{u2}^e (2.36), $K_{N,u1}^e$ (2.42);

- consistent mass matrix M^e (2.68).

After transformations of (2.72), (2.73), and (2.75) to the global coordinate system (x, y, z) and aggregation, the structural matrices are determined. The aggregation is made by using the Boolean matrix (the connectivity matrix) $C^e \in \mathbb{R}^{6 \times m}$. It is assumed that the number of global degrees of freedom of each element $q_i (i = 1 \div 6)$ corresponds to the number of global nodes of elements n_1, n_2, as shown in Figure 3.1. Consequently, the non-zero elements of C^e can be expressed as $C^{iq_i} = 1$. Transformation and aggregation of element matrices lead to the elongation matrix B, stiffness matrices K (including all forms mentioned above, i.e., linear, geometric, and non-linear), and mass matrix M, respectively:

$$B = \begin{bmatrix} B^1 C^1 & B^2 C^2 & \ldots & B^n C^n \end{bmatrix}^T \in \mathbb{R}^{n \times m},$$

(3.3)

$$K = \sum_{i=1}^{n} (C^e)^T K^e C^e \quad \in \mathbb{R}^{m \times m},$$

(3.4)

$$M = \sum_{i=1}^{n} (C^e)^T M^e C^e \quad \in \mathbb{R}^{m \times m},$$

where B^e, K^e are the transformed matrices (the mass matrix does not depend on the (3.5) coordinate system, i.e., $M^e = M^e$). In turn, the elasticity of the structure is described by a matrix

$$E = diag \begin{bmatrix} \dfrac{E_1 A_1}{L_1} & \dfrac{E_2 A_2}{L_2} & \ldots & \dfrac{E_n A_n}{L_n} \end{bmatrix} \in \mathbb{R}^{n \times n}.$$

In the qualitative and quantitative analyses, the following assumptions are made: (3.6)

- tensegrity structures are prestressed; this means that no cable is loose (the effect of overhang on the effective modulus of elasticity has been neglected);
- tensegrity members are straight and connected by nodes, which are pin-joints;
- there are two types of elements in a prestressed structure, i.e., struts, which are responsible for carrying compressive prestress and cables, which are responsible for carrying tensile prestress;
- there are two types of nodes, i.e., fixed (supported) nodes, which cannot have any displacements even when subjected to external loads, and free nodes, the displacements of which are not constrained;
- support is established and scleronomic;
- external loads are conservative and are applied at the nodes;
- member failure, such as yielding or buckling, is not considered;
- self-weight is transferred to nodes as point loads; hence, non-axial stresses in the tensegrity members are neglected;
- material is assumed to be linear, elastic, continuous, homogeneous, and isotropic;
- large displacement gradients are possible;

- in all design situations, the initial prestress level is high enough that only tension occurs in the cables – the problem is considered physically linear;
- in static considerations, elements are assumed to be weightless;
- in dynamic considerations the effect of damping is ignored.

The analyses of the behavior of tensegrity structures are divided into four sections:

- qualitative analysis – identification of self-stress states and infinitesimal mechanisms, and correct classifications of structure;
- static analysis – quantitative assessment of the static behavior of structures under time-independent external loads;
- dynamic analysis – parametric analysis determining the influence of initial prestress on dynamic properties, including the frequency and forms of vibrations;
- dynamic stability analysis – determination of the resonance frequency of periodic loads and unstable regions as a function of initial prestress.

3.3 QUALITATIVE ANALYSIS

Qualitative analysis is required to determine the immanent features such as infinitesimal mechanisms and self-equilibrated systems of longitudinal forces (self-stress states) that stabilize mechanisms. Self-stress states may also occur in geometrically invariable structures. Tensegrity features are independent of external loads as well as the geometrical and mechanical characteristics of the structure. In the absence of externally applied loads, tensegrity as a type of form-active structure requires a self-balancing configuration which is determined through a process called 'form-finding'.

Over the past decades, many research efforts have been devoted to searching for effective form-finding methods. A literature review has revealed a wide variety of form-finding methods, which are continuously being refined and improved.

3.3.1 THE MOST POPULAR FORM-FINDING METHODS

Most methods require the initial topology of the structure to search for the correct form of tensegrity, whereas information about the initial configuration is unnecessary. A comprehensive review of presented existing methods for tensegrity structures is included (Harichandran and Yamini Sreevalli, 2016; Juan and Tur, 2008; Kasprzak, 2014; Sultan, 2009; Tibert and Pellegrino, 2003; Veenendaal and Block, 2012). Generally, the form-finding methods can be divided into three groups:

1. *kinematical methods* – methods involving minimizing the length of cables while maintaining a constant length, or maximizing the length of struts until a maximum is reached, or maximizing the length of the struts at a constant length of the cables:

   - *analytical solution* – consists of parameterizing the functions that determine the pre-assumed coordinates of the nodes, and then minimizing or maximizing the length of the selected elements (Connelly and Terrel, 1995; Gilewski and Kasprzak, 2013; Kener, 1976; Pellegrino and Calladine, 1986);
   - *nonlinear programing* – consists of solving a multi-parameter minimization problem, with imposed constraints, using computer techniques (Pellegrino, 1986);
   - *dynamic relaxation* – consists of searching for a stable configuration of tensegrity using the kinetic energy (Baudriller et al., 2006; Barnes, 1999; Motro, 1984; Skelton and de Oliveira, 2009).

2. *static methods* – methods consist of finding the configuration of elements with equilibrium forces at each unloaded node:

   - *analytical solutions* (Connelly and Terrel, 1995; Kenner, 1976; Zhang Q. et al., 2020);
   - *force density method* – the most widely used and modified method; the main assumption is the linearization of the equilibrium equations at the node; the biggest difficulty is the need to assume the value of the force density at the beginning of the process (Cai et al., 2018; Cao et al., 2024; Linkwitz, 1999; Luo and Lu, 2006;

Masic et al., 2005; Schek, 1974; Wang Y. et al., 2021; Xu et al., 2018; Zhang and Ohsaki, 2015; Zhang L.Y. et al., 2018);

- ○ *energy optimization* – consists of searching for the minimum of the potential energy of a prestressed structure (Connelly, 1993; Connelly and Back, 1998, Skelton et al., 2002);
- ○ *reduced coordinates method* – consists of defining the geometry of the structure and determining the equilibrium matrix in a symbolic way (Sultan et al., 1999; Skelton et al., 2001).

3. methods combining kinematic and static approaches (Masic et al., 2005; Zhang and Oshaki, 2006).

A specific approach to form-finding in tensegrity structures involves *numerical methods*. These methods automate the process of finding the right form based on selected approaches presented above. These procedures employ a variety of optimization techniques (Estrada et al., 2006; Koohestani, 2013; Koohestani and Guest, 2013; Michelleti and Wiliams, 2007; Pagitz and Tur, 2009; Tran and Lee, 2007, 2010a, 2010b, 2011; Wang K. et al., 2021; Zang and Ohsaki, 2006; Zhang P. et al., 2021). An interesting form-finding method was proposed by Li et al., who used a stochastic approach based on the Monte Carlo method (Li et al., 2010).

In recent years, in the process of searching for a stable configuration of tensegrity structures, evolutionary optimization techniques have been increasingly used. These methods look for better solutions, modeling their operation on mechanisms occurring during natural evolution. One of the optimization techniques is the *genetic algorithm*. This algorithm, inspired by the process of natural selection and genetics, was first presented by Holland (Holland, 1975). In the case of tensegrity, the genetic algorithm is mostly used as a form-finding method for regular (Jo et al., 2004; Koohestani, 2012; Lee et al., 2017; Obara et al., 2023; Paul et al., 2005; Yamamoto et al., 2011) and irregular (Ma et al., 2019; Uzun, 2016; Xu and Luo, 2010) structures. To predict the geometric configurations and physical properties (nodal coordinates, member forces, and natural frequencies) of any tensegrity structures in equilibrium states, a neural network can also be used (Chen and Qin, 2024; Sun et al., 2022).

Among the methods mentioned, some have been adapted from other fields to civil engineering, as well as those developed specifically for the mechanics of tensegrity. These methods are usually complex and time-consuming but often fail to address all the distinctive characteristics of tensegrity structures. These methods are employed to determine the initial equilibrium configuration and to shape the overall structural geometry. In turn, when the geometry is known, a spectral analysis of truss matrices is the simplest approach to identifying the distinctive characteristics of tensegrity structures. There are two kinds of methods:

- *spectral analysis of the stiffness matrix with the effect of self-equilibrated forces* – this method leads to determine the self-stress states and mechanisms and allows determination of what kind of mechanisms they are – finite or infinitesimal (Obara, 2019; Obara and Tomasik, 2021);
- *singular value decomposition of the elongation matrix or the equilibrium matrix* – this method leads to determine the self-stress states and mechanisms but does not allow determination of what kind of mechanisms they are (Calladine, 1982; Gilewski, et al., 2015; Kłosowska, 2018; Kłosowska et al., 2018; Murakami, 2001b; Murakami and Nishimura, 2001a; Obara, 2019; Obara and Tomasik, 2020; Pellegrino, 1990, 1993; Pellegrino and Calladine, 1986; Rahami et al., 2013; Tomasik, 2023; Tran and Lee, 2010b; Zhang Q. et al., 2021).

3.3.2 DISTINCTIVE CHARACTERISTICS OF TENSEGRITY STRUCTURES

The distinctive characteristics of tensegrity structures are intimately associated with the advantages that set them apart from conventional cable–strut structures. There are six features, which can be enumerated as follows:

- *TT* – tensegrity is a truss;
- *SS* – there is a self-stress state (self-equilibrated system of internal forces);
- *TC* – tensile elements are cables;
- *IM* – there is an infinitesimal mechanism;

- *IN* – the set of struts is contained within the continuous net of cables;
- *DS* – the struts form a discontinuous set.

In accordance with the mentioned features, four distinct classes are distinguished (Table 3.1):

TABLE 3.1 Tensegrity Classification⏎

Characteristic features/Tensegrity classes	TT	TC	SS		IM	IN	DS
ideal tensegrity	+	+	+	+	+	+	+
pure tensegrity	+	+	+	+	+	+	–
structures with tensegrity features of class 1	+	+	+	–	+	–/+	–
structures with tensegrity features of class 2	+	+	+	–/+	–	+	–
						–	+

- *ideal tensegrity* – structures that meet all features (*TT*, *SS*, *IM*, *TC*, *DS*, *IN*) and all self-stress states (including the superposed one) must identify the appropriate normal forces in the structural elements (cables must be in tension and struts must be in compression) and ensure the stability of the structure;
- *pure tensegrity* – structures satisfy the first five requirements, i.e., *TT*, *SS*, *IM*, *TC*, *DS*, and all self-stress states identify the appropriate normal forces in the structural elements and ensure the stability of the structure;
- *structure with tensegrity features of class 1* – structures meet the conditions of the first four features (*TT*, *SS*, *IM*, *TC*) and at least one self-stress state identifies the appropriate normal forces in the structural elements and ensures the stability of the structure;
- *structure with tensegrity features of class 2* – structures meet only the three requirements, i.e., *TT*, *SS*, and *TC*, and either feature *IN* or *DS*; additionally, at least one self-stress state identifies the appropriate normal forces in the structural elements and ensures the stability of the structure.

Ideal tensegrity and *pure tensegrity* practically do not exist in civil engineering. However, they serve as the basis for creating *structures with tensegrity features*. The classification of *structures with tensegrity features* into two classes is based on the significance of the influence of infinitesimal mechanisms' influence on structural behavior. The distinctiveness of tensegrity structures lies in the self-stress state stabilizing existing infinitesimal mechanisms. For structures with mechanisms, adjusting the level of prestress allows for controlling both static and dynamic properties.

The proposed classification systematizes and precisely defines tensegrity structures, minimizing the misuse of the term to refer to structures that are not them. Moreover, such systematization in engineering practice facilitates the analysis and design of tensegritiy structures. This approach accounts for the distinct behavior of tensegrity structures under external loads. In the case of deployable structures, the ability to control their behavior is particularly critical. From the point of view of structural mechanics, one of the most important tensegrity features is the mechanism. Self-stress states play a crucial role in stabilizing infinitesimal mechanisms, highlighting the distinctiveness of tensegrity structures.

3.3.3 Identification of Distinctive Characteristics of Tensegrity Structures

Identifying immanent features, such as self-stress states and mechanisms, relies on analyzing the properties of the elongation matrix. Singular value decomposition (SVD) is employed (Golub and Kahan, 1965; Klema, 1980; Long, 1983; Stewart, 1998; Strang, 1993). This decomposition expresses a matrix as the product of a square unitary matrix, a rectangular diagonal matrix with real non-negative coefficients, and the Hermitian conjugate of the unitary matrix. The coefficients of the diagonal matrix are known as the singular values (also referred to as principal or special values) of the decomposed matrix. When a given matrix has real coefficients, the unitary matrices become orthonormal, and Hermite coupling becomes transpose.

Applying the singular value decomposition, the elongation matrix **B** (3.3) can be represented as a product of three matrices

$$B = YZX^T$$

with certain properties described below. (3.7)

NOTE

Due to the fact that all calculations are made using the procedure written in the Mathematica environment, with functions and commands implemented there, it should be noted that decomposition (3.7) can be done using the following command:

$$\{Y, Z, X\} = \mathrm{N[SingularValueDecomposition}[B]]$$

(3.a)

- The matrix $Y \in \mathbb{R}^{n \times n}$ in (3.7) is orthogonal, and the columns are the eigenvectors of the eigenproblem

$$\left(BB^T - \mu I\right)y = 0$$

which solutions can be expressed as (3.8)

$$BB^T = \left[YHY^T\right] \in \mathbb{R}^{n \times n},$$

where (3.9)

$$H = diag[\mu_1 \quad \mu_2 \quad \dots \quad \mu_n] \in \mathbb{R}^{n \times n}$$

$$Y = [y_1 \quad y_1 \quad \dots \quad y_n] \in \mathbb{R}^{n \times n}$$
(3.10)

are matrices of eigenvalues and eigenvectors, respectively. The solution of the eigenproblem (3.8) leads to the identification of the self-stress state or states. There is no self-equilibrated system of internal forces if all eigenvalues (3.10) are positive. Zero eigenvalues $(\mu_i = 0)$ are related to the non-zero solutions of homogeneous equations called self-stress states, or more precisely, self-equilibrated normal forces that satisfy homogeneous equations of equilibrium. The self-stress states can be considered as the eigenvectors in (3.11) related to zero eigenvalues $y_i(\mu_i = 0)$. (3.11)

- The matrix $X \in \mathbb{R}^{m \times m}$ in (3.7) is also orthogonal, and the columns are the eigenvectors of the following eigenproblem:

$$\left(B^T B - \gamma I\right)x = 0,$$

which solutions can be expressed as (3.12)

$$B^T B = \left[XLX^T\right] \in \mathbb{R}^{m \times m},$$

where (3.13)

$$L = diag[\gamma_1 \quad \gamma_2 \quad \dots \quad \gamma_m] \in \mathbb{R}^{m \times m},$$

$$X = [x_1 \quad x_2 \quad \dots \quad x_m] \in \mathbb{R}^{m \times m}$$
(3.14)

are matrices of eigenvalues and eigenvectors, respectively. The solution of the eigenproblem (3.12) leads to the identification of the mechanism of geometric variation of the structure. The eigenvalues (3.14) describe the energy states of the structure, while the eigenvectors (3.15) describe the nature of deformation. There is no motion when all eigenvalues are positively defined in the structure. However, zero eigenvalues $\left(\gamma_i = 0\right)$ are related to the mechanisms, which can be considered as the eigenvectors in (3.15) related to zero eigenvalues $x_i(\gamma_i = 0)$. (3.15)

The matrix $Z \in \mathbb{R}^{n \times m}$ in (3.7) is a rectangular diagonal matrix. The elements of this matrix are the square roots of the eigenvalues of both eigenproblem (3.8) and (3.12). It should be noted that the eigenvalue matrices (3.10) and (3.14) are dependent on the matrix Z as follows:

$$H = ZZ^T \in \mathbb{R}^{n \times n} \mathrm{and} L = Z^T Z \in \mathbb{R}^{m \times m}$$

The abovementioned considerations prove that knowledge of the dimensionless(3.16) elongation matrix **B** (3.3) is sufficient to identify the self-stress states and mechanisms. However, this information is not complete from a mechanical point of view. First, the vectors $y_i(\mu_i = 0)$ identified from the eigenproblem (3.8) do not always identify the

appropriate normal forces in the structural elements (cables must be in tension and struts must be in compression). Second, the vectors $x_i(\gamma_i = 0)$ identified from the eigenproblem (3.12) do not identify whether the mechanisms are infinitesimal or finite. Third, the SVD decomposition (3.7) does not check the stability of the structure. These three problems are solved by the spectral analysis of the stiffness matrix with the effect of self-equilibrated forces:

$$[K_L + K_G(S) - oI]z = 0$$

where K_L is the linear stiffness matrix and $K_G(S)$ is the geometric stiffness matrix (prestress matrix), depending on the self-equilibrated forces in elements (3.17)

$$S = y_S S \in \mathbb{R}^{n \times 1},$$

where y_S is the vector of the self-stress state $y_S = y_i(\mu_i = 0)$, identified by solving the eigenproblem (3.8), and S is the initial prestress level. The vector y_S is dimensionless and independent of the structure's geometrical and mechanical characteristics. It only relies on the configuration of the elements. In turn, the initial prestress level S is unique for each system and depends on the geometrical and mechanical characteristics of the structure and external loads. However, in order to perform the spectral analysis (3.17), the initial prestress level can be assumed as $S = 1$. (3.18)

Full solutions to the eigenproblem (3.17) can be expressed in the condensed form

$$K_L + K_G(S) = \left[\Lambda O \Lambda^T \right] \in \mathbb{R}^{m \times m}$$

where   (3.19)

$$O = diag \begin{bmatrix} o_1 & o_2 & \ldots & o_n \end{bmatrix} \in \mathbb{R}^{m \times m},$$

$$\Lambda = \begin{bmatrix} z_1 & z_2 & \ldots & z_n \end{bmatrix} \in \mathbb{R}^{m \times m}$$ (3.20)

are matrices of eigenvalues and eigenvectors, respectively. There are three possibilities of obtained eigenvalues (3.20):   (3.21)

- if all eigenvalues are positive numbers, the structure is stable; this means the self-stress states identify the appropriate normal forces in the structural elements and stabilize mechanisms, i.e., the mechanisms are infinitesimal;
- zero eigenvalues are related to finite mechanisms;
- if there are any negative eigenvalues the structure is unstable.

NOTE

1. In the case of complex structures used in civil engineering, solutions to the eigenproblem (3.8) lead to obtaining more than one self-stress state. These self-equilibrated normal forces satisfy the homogeneous equations of equilibrium, but they do not always identify the type of element correctly. Usually, only the superposition of all the self-stress states gives the expected results. Such is the case with tensegrity domes. In turn, in the case of tensegrity structures built by connecting the basic three-dimensional tensegrity modules, i.e., towers/booms and double-layer girds,

the superposition of all self-stress states leads to obtaining the self-stress states for the single module, including common elements.

2. The linear stiffness matrix K_L can be built according to aggregation (3.4) or directly by using the elongation matrix B (3.3) and the elasticity matrix E (3.6):

$$K_L = B^T E B$$

3. It can be noted, if the unit elasticity matrix $E \equiv I$ is considered, the linear stiffness matrix (3.b) will be of the form   (3.b)

$$K_L = B^T B$$

This means that the identification of the mechanism can be carried out   (3.c) this spectral analysis of matrix (3.c) – see Equation (3.12).

4. The spectral analysis of the stiffness matrix (3.17) can be performed using the matrix (3.c). However, this is not always appropriate. Inclusion of material and geometrical characteristics is recommended in this analysis.

Qualitative analysis of tensegrity truss (*TT*) identifies self-stress states (*SS*) and infinitesimal mechanisms (*IM*). In turn, the identified self-stress state defines the other distinctive characteristics of the tensegrity structure, i.e., *TC* (tensile elements are cables), *IN* (the set of struts is contained within the continuous net of cables), and *DS* (the struts form a discontinuous set). Thus, this analysis ensures accurate classification. The qualitative analysis process is summarized in the flowchart shown in Figure 3.2. If multiple self-stress states are identified, spectral analysis of the stiffness matrix must be performed for each. For *ideal tensegrity* and *pure tensegrity,* all self-stress states must be appropriate – ensuring correct identification of normal forces in structural elements and guaranteeing structural stability. Conversely, for *structures with tensegrity features*, at least one self-stress state must be appropriate and provide structural stability. The flowchart of classification summary is shown in Figure 3.3.
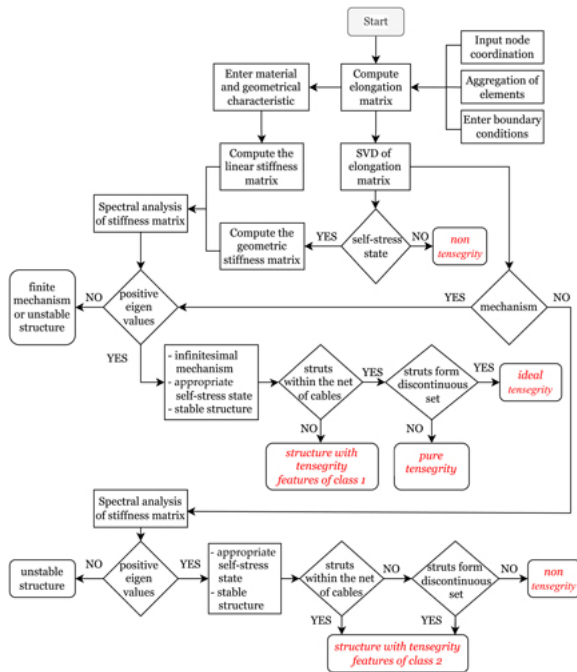
FIGURE 3.2 Flowchart of qualitative analysis.
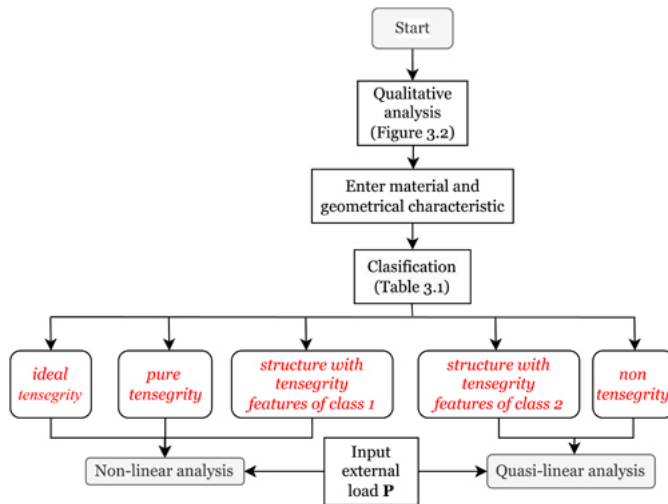
FIGURE 3.3 Flowchart of classification summary.

Qualitative assessment is the first step in the analysis of tensegrity structures. Next, the quantitative assessment can be carried out. It includes static, dynamic, and stability-dynamic analysis. However, independent of this kind of analysis, a very important aspect is the determination of the prestress range, i.e., the minimum and maximum levels of the initial prestress. The initial prestress level in each structure is unique and depends on design assumptions and external loads:

- **the minimum prestress level** S_{min} is related to the appropriate distribution of normal forces in the elements of the structure; i.e., the cables must be tensioned and the struts must be compressed. The external load can cause a different distribution of normal forces, and this can be corrected by the introduction of the proper initial prestress level;

- **the maximum prestress level** S_{max} is related to the load-bearing capacity of the most stressed elements, i.e., on the effort of the structure

$$W_{\max} = \frac{N_{max}}{N_{Rd}},$$

where $N_{\max}$ is a maximum normal force and N_{Rd} is a load-bearing capacity. The flowchart for the determination of the prestress range is shown in Figure 3.4. (3.22)
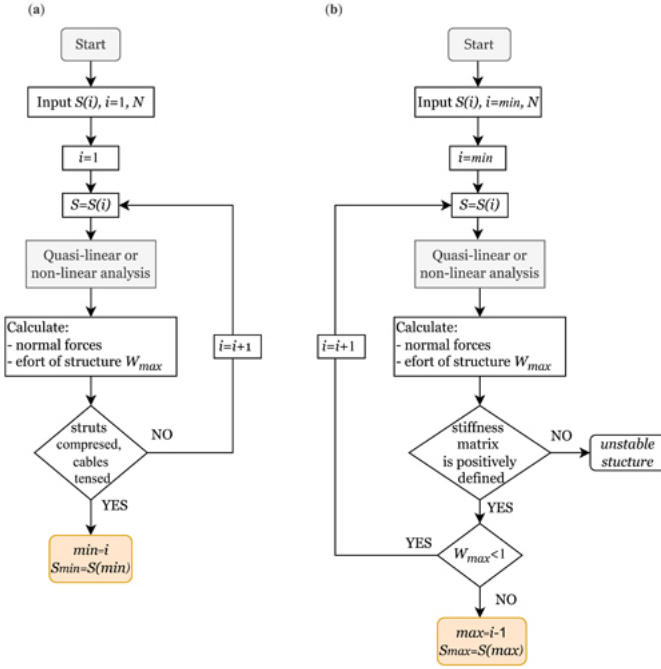
FIGURE 3.4 Flowchart for the determination of the prestress range: (a) the minimum prestress level $S_{\min}$ and (b) the maximum prestress level $S_{\max}$.

3.4 STATIC ANALYSIS

Static analysis involves studying the behavior of a structure under time-independent external loads $P = P(t = 0)$. The equilibrium equation can be formulated in non-incremental and incremental versions, as in the case of a single finite tensegrity element (see Sections 2.2.1 and 2.2.2). The principle of stationary total potential energy (2.12) and the principle of virtual work (2.11) are used, respectively.

The static equilibrium equation in the non-incremental version is formulated in the actual configuration at the moment $\left({}^{t}C\right)$. The principle of stationary total potential energy (2.12) results in the equation

$$K_S q = P,$$

where (3.23)

$$K_S = [K_L + K_G(S) + K_{N,NL}(q)]$$

is the secant matrix, while $\hspace{10cm}$ (3.24)

$$K_{N,NL}(q) = \left[\frac{1}{2} \left(K_{N,u1} + K_{u2} \right) \right]$$

is the non-linear displacement stiffness matrix with the non-symmetric part $K_{N,u1}$. $\quad$ (3.25)

In turn, the equilibrium equation in the incremental version is formulated in the actual configuration at the moment $t + \Delta t \left({}^{t+\Delta t}C \right)$. The principle of virtual work (2.11) leads to the obtained equation.

$$K_T \Delta q = \Delta P + R$$

where $\Delta q \in \mathbb{R}^{m \times 1}$ is the vector of displacement increments, $\Delta P \in \mathbb{R}^{m \times 1}$ is the (3.26) vector of load increments, $R \in \mathbb{R}^{m \times 1}$ is the residual force vector, and

$$K_T = [K_L + K_G(S) + K_{GN}(P) + K_{NL}(q)]$$

is the tangential stiffness matrix. The matrix (3.27) consists of the linear and (3.27) geometric stiffness matrices, as in the secant stiffness matrix (3.24); however, the non-linear part consists of the symmetric displacement stiffness matrix

$$K_{NL}(q) = [K_{u1} + K_{u2}]$$

and the geometric stiffness matrix $K_{GN}(P)$ depending on the longitudinal forces, (3.28) which results from external loads. The calculations of this matrix are carried out in four steps:

- **Step 1** – determination of the displacements from the non-linear system of equilibrium equations (3.23).
- **Step 2** – determination of the deformation of the element in the actual configuration:

$$\varepsilon = \frac{1}{2} \frac{\left(L_e^a \right)^2 - \left(L_e \right)^2}{\left(L_e \right)^2},$$

where L_e^a is the length of the element in the actual configuration: $\hspace{4cm}$ (3.29)

$$L_e^a = \sqrt{\left(\Delta_{u_2} \right)^2 + \left(\Delta_{u_3} \right)^2 + \left(L_e + \Delta_{u_1} \right)^2},$$

where $\Delta_{u_i} = q_i^2 - q_i^1 (i = 1, 2, 3)$ are the displacement increments between nodes of (3.30) elements.

- **Step 3** – determination of the real normal force in the element on the basis of the Cauchy tensor (2.62):

$$N_e = E_e A_e \varepsilon \sqrt{1 + 2\varepsilon}.$$

- **Step 4** – determination of the geometric stiffness matrix $K_{GN}(P)$ depending on the longitudinal forces N_e, (3.31) which results from external load P.

NOTE

Longitudinal forces N depend only on the external loads $\rightarrow N \equiv N(P)$; however, the total longitudinal forces depend on the external loads P and the initial prestress level $S \rightarrow N \equiv N(P+S)$.

It should be noted that the residual force vector **R** in (3.26) results from the aggregation. In equilibrium, it is equal to zero $(R = 0)$, whereas in a process of iteration, a norm **R** is the 'distance' from the equilibrium state. The iterative process converges if $R \rightarrow 0$.

To solve the system of non-linear equations (3.23) and (3.26), numerical iterative or incremental-iterative techniques should be used (Bathe, 1996; Crisfield, 1991; de Borst, 1999; de Borst et al., 2012; Rakowski and Kasprzyk, 2005; Szmelter, 1980). In this book, the Newton–Raphson method is applied (Rakowski and Kasprzyk, 2005).

NOTE

In the quasi-linear analysis, the secant matrix (3.24) equals the tangential stiffness matrix (3.27):

$$K_S(q) \equiv K_T(q) = K_L + K_G(S),$$

and the static equilibrium equations (3.23) and (3.26) take the following form: (3.d)

$$[K_L + K_G(S)]q = P$$

To solve the system of quasi-linear equations (3.e), the Gaussian elimination method (3.e) is applied. In this case, the stiffness depends only on the linear part K_L and on the initial prestress $K_G(S)$. Omitting the initial prestress leads to a linear equation

$$K_L q = P$$

(3.f)

In the case of tensegrity structures, the static assessment is a parametric assessment of the influence of the initial prestress level S on static parameters, i.e., the displacements, normal forces, and effort of the structure. To illustrate the influence of external loads on stiffening, two approaches are taken into consideration, i.e., the quasi-linear approach (second-order theory) (3.d) and the non-linear approach (third-order theory) (3.23) or (3.26). Additionally, to measure stiffening, a *global stiffness parameter* (*GSP*) is proposed. This dimensionless parameter measures the influence of the initial prestress level on the total stiffness of the structure at a given load. It represents the ratio of two strain energies measured at the minimum and i-th levels of initial prestress:

$$GSP = \frac{[q(S_{min})]^T K_S(S_{min})q(S_{min})}{[q(S_i)]^T K_S(S_i)q(S_i)},$$

where $K_S(S_{min})$ and $q(S_{min})$ are a secant stiffness matrix and a displacement (3.32) vector at a minimum initial prestress level, and $K_S(S_i)$ and $q(S_i)$ at the i-th prestress level, respectively. Each time the initial prestress level changes, the stability of the structure is verified using the spectral analysis of the secant matrix (3.24):

$$[K_S - oI]z = 0.$$

If all eigenvalues are positive numbers $(o_i > 0)$, the secant stiffness matrix is (3.33) positively defined, which means the structure is stable. The static analysis process is summarized in the flowchart shown in Figure 3.5.
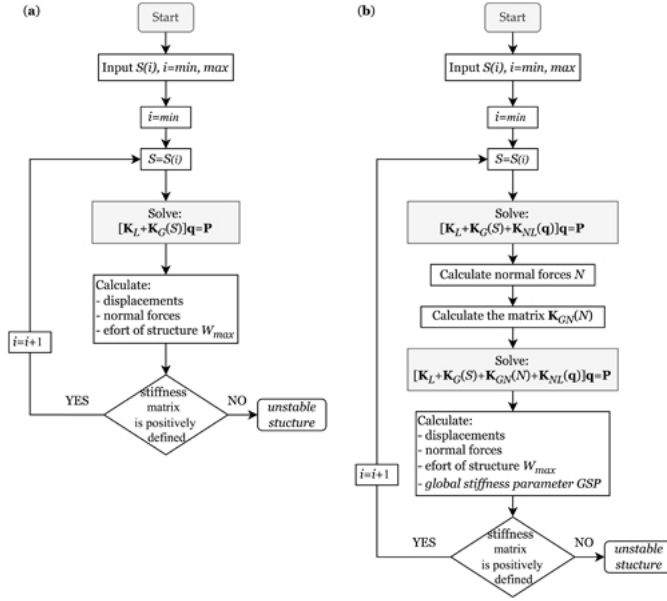
FIGURE 3.5 Flowchart of static analysis: (a) quasi-linear analysis and (b) non-linear analysis.⏎

3.5 DYNAMIC ANALYSIS

Dynamic analysis, considered in this book, involves studying the influence of the initial prestress level on the frequency and forms of vibrations. The dynamic response is studied by modal analysis (Ashwear and Eriksson, 2014; Ashwear et al., 2016; Bel Hadj Ali and Smith, 2010; Bel Hadj Ali et al., 2010; Chen and Feng, 2012a, 2012b; Faroughi et al., 2015; Gilewski and Kasprzak, 2013; Gilewski et al., 2019; Kan et al., 2018; Murakami, 2001a; Murakami and Nishimura, 2001a, 2001b; Rimoli, 2018; Safaei et al., 2013).

The quasi-linear dynamic model can be effectively employed instead of a complete non-linear model. The principle of virtual work (2.64) in the actual configuration at the moment $\left({}^{t}C\right)$, with off load, leads to the equation of undamped natural motion of the tensegrity structure:

$$M\ddot{q}(t) + [K_L + K_G(S)]q(t) = O$$

where $\ddot{q} \in \mathbb{R}^{m \times 1}$ is the acceleration vector. Taking into account the harmonic motion, (3.34)

$$q(t) = a\sin(\omega t),$$

where $a \in \mathbb{R}^{m \times 1}$ is the amplitude vector and ω is the circular frequency of vibrations, (3.35) Equation (3.34) is written as:

$$\left[K_L + K_G(S) - \omega^2 M\right]a = 0.$$

(3.36)

Modal analysis (3.36) leads to the determination of the natural circular frequency of vibration. It should be noted that for a tensegrity structure characterized by mechanisms, the omission of the influence of initial prestress (**S** = 0) in (3.36) leads to zero frequencies. These zero values correspond to the vibration patterns that implement the mechanisms. In such cases, taking into account the influence of prestress forces **S,** there are three possibilities:

- if eigenvalues of the spectral analysis (3.36) are positive numbers, the prestress forces **S** stabilize the structure, it means the mechanisms are infinitesimal;
- if the eigenvalues still remain zero, then the related mechanisms are finite;
- if the eigenvalues are negative numbers, the structure is unstable.

Due to the fact that modal analysis allows for the identification of mechanisms, it can also be used as a form-finding method (Gilewski and Kasprzak, 2013).

Taking into account that the external loads stiffen the tensegrity structure, the influence of the time-independent external load *P* on the frequencies is considered. The load is treated as the initial disturbance of the equilibrium state, i.e., as the imposition of the initial conditions. Hence, the frequencies are called free, and they are determined by modal analysis, taking into account the geometric stiffness matrix depending on longitudinal forces, which results from external loads $K_{GN}(P)$:

$$\left[K_L + K_G(S) + K_{GN}(P) - \Omega^2 M\right]a = 0$$

Modal analyses (3.36) and (3.37) lead to the determination of the natural frequency (3.37) $f_i(0)$, and the free frequency $f_i(P)$, respectively, corresponding to the circular frequency of vibration $\omega_i = \omega_i(0)$ or $\Omega_i = \Omega_i(P)$:

$$f_i(0) = \frac{\omega_i}{2\pi}, f_i(P) = \frac{\Omega_i}{2\pi}.$$

The dynamic analysis process is summarized in the flowchart shown in Figure 3.6.　　(3.38)

FIGURE 3.6 Flowchart of dynamic analysis: (a) natural frequency and (b) free frequency.
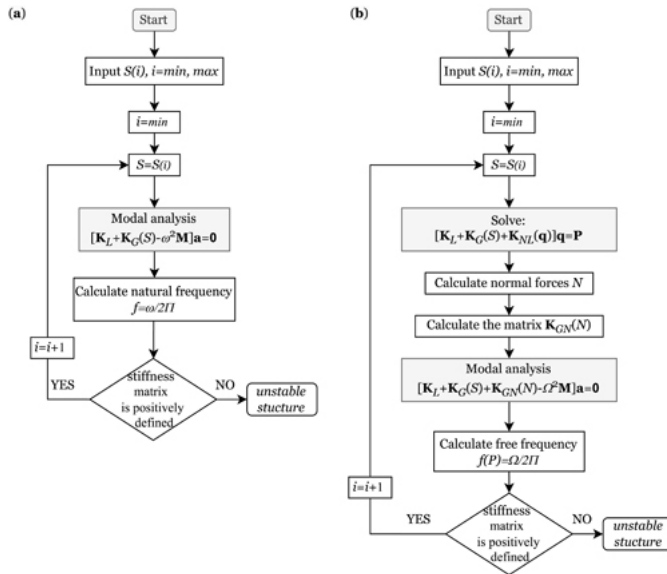
3.6 DYNAMIC STABILITY ANALYSIS

Stability is the ability of a system to remain in the configuration formed under a given load. This is directly related to the type of equilibrium. The equilibrium of a deformed configuration can be stable or unstable. When equilibrium is considered as a special type of motion, studying stability becomes equivalent to studying motion stability. In other words, if a system is tilted out of equilibrium and the cause that caused this tilting is removed, then motion in this system will be initiated. If this motion occurs around the equilibrium with limited (non-increasing) amplitudes, the equilibrium is considered stable. If, on the other hand, when tilted and left to itself, the system shows an increase in displacement (monotonic or fluctuating), that is, its motion will be unstable, then the equilibrium is unstable. The study and assessment of the stability of system motion caused by various types of excitation is called dynamic stability.

The criterion of dynamic stability, in its most general form, was formulated by Lyapunov (Lyapunov stability) (La Salle et al., 1962; Lefschetz and La Salle, 1966; Lyapunov, 1892) and in a slightly different form by Lagrange (Cunningham, 1958; Gomuliński and Witkowski, 1993). The differences in the two formulations mentioned are, in fact, of little importance. In both cases, the stability of the system is equated with the study of the stability of motion. Stable motion – characterized by non-increasing amplitudes over time – indicates the stability of the preceding equilibrium and, consequently, the system's stability. For the study of stability under static loads, the motion must be initiated by the introduction of small perturbations of the displacement state. In such cases, the dynamic criterion yields results consistent with energy and static criteria, making its application optional.

The situation is different if stability refers to a system subjected to periodic dynamic loads. In such cases, the system is not in static equilibrium but exhibits motion. Assuming a system has scleronomic constraints, its motion is an oscillation around the static equilibrium. If a small perturbation induces a new motion with limited solutions, the original motion is static. The instability of the induced motion means the instability of the original motion. This scenario exemplifies dynamic instability or parametric resonance. Unstable motions pose a risk to the structural durability.

Dynamic stability, or, to put it in Bolotin's terms, 'dynamic instability' (Bolotin, 1999), leads to the determination of resonance frequencies of periodic excitations and to the determination of Ince–Strutt maps with stable and unstable regions (parametric resonance regions). From the point of view of the physical interpretation of the phenomenon of dynamic instability, if the load parameters are within the defined limits of instability, the structure experiences vibrations with increasing amplitude. The most widespread and applicable to technical issues is the analysis of parametric resonance regions at a force

$$P(t) = P + P_t \Phi(t),$$

where P is the constant value of the periodic force, P_t is the amplitude of the periodic (3.39) force, and $\Phi(t)$ is a periodic function. The unstable regions are on frequency

$$\Omega = \frac{\Omega_i}{k} \ \text{ or } \ \Omega = \frac{\Omega_i \pm \Omega_j}{2k}; \ \ k = 1, 2, \ldots; \ i \neq j,$$

where Ω_i and Ω_j are free frequencies of structures loaded with a constant part of the (3.40) load P. In the first case, there are periodic resonances, while in the second, combined resonances. From a technical point of view, the most important are the main unstable regions, i.e., first-order periodic resonances (at $k = 1$). The Ince–Strutt maps are obtained by solving the non-linear parametric equations of motion (Mathieu equations) (Mathieu, 1868). Stable regions correspond to finite solutions of the equations, while unstable regions correspond to solutions that increase indefinitely in time (Cunningham, 1958).

The stability charts of the Mathieu equations published in the literature are usually calculated using various methods, i.e., the harmonic balance method (Bolotin, 1956, 1999; Bolotin et al., 1965; Briseghella et al., 1998; Gomuliński and Witkowski, 1993; Jani and Chakraborty, 2021; Kruszewski, 1959; Langer, 1980; Misiak and Stachura, 2010; Obara and Gilewski, 2016; Pomaro and Majorana, 2021; Volmir, 1963; Ziemba, 1959), perturbation method (small parameter method, Poincaré method) (Awrejcewicz and Andrianov, 2000; Chau, 2018; Cunningham, 1958; Garus et al., 2023; Obara and Gilewski, 2016), Galerkin method (Pomaro and Majorana, 2021; Yang et al., 2010; Zhang Q.C et al., 2021), multiscale methods (Lee et al., 1998), averaging method (Yang et al., 2010), discrete singular convolution (Song et al., 2016), homotopy perturbation method (Ghomeshi Bozorg and Keshmiri, 2013; Liao, 2013), and adomian decomposition method (Keskin, 2019).

There is abundant literature on parametric vibrations, which essentially defines all the basic issues (Bigoni and Kirillov, 2019; Bolotin, 1956, 1999; Bolotin et al., 1965; Chmielewski and Zębaty, 1998; Cunningham, 1958; Gomuliński and Witkowski, 1993; Kruszewski, 1959; Langer, 1980; Simitses, 1990; Volmir, 1963; Wei-Chau, 2006; Ziemba, 1959; Życzkowski, 1988). Dynamic instability in elastic structures remains a compelling area of analytical, numerical, and experimental research, with many unresolved challenges. A survey of selected topics of current research interest concerning the dynamic instability of elastic structures is presented (Mascolo, 2019). Mascolo has compiled the most important recent developments and international trends and described any possible future challenges with the most popular methods.

This book serves as a supplementary resource to contemporary monographs on the dynamic stability of structures. The study investigates the behavior of tensegrity systems. These structures feature an additional parameter – initial prestress level S, which affects the shape and range of unstable regions. Multiple unstable regions exist, with the first (main) region being the most significant. The study specifically examines how the initial prestress level influences this primary unstable region.

Structural instability problems typically involve nonlinear challenges, addressed through iterative or incremental-iterative analysis of large displacement gradients. However, in the case of dynamic instability analysis, the nature of motion is studied. A quasi-linear approach is sufficient to determine the conditions under which the motion is of an unsteady nature, with solutions that increase indefinitely with time. Admittedly, the determination of the magnitude of the amplitudes of these oscillations can only be obtained from non-linear vibration equations. However, without knowing the magnitude of the amplitudes, the quasi-linear theory gives a sufficiently complete and accurate view of the issue of instability. Due to this, the boundaries of the stable and unstable regions (Ince–Strutt maps) are determined by the periodic solutions of the equation of motion with the geometrical stiffness matrices $K_G(S)$ and $K_{GN}(P)$ and the periodic load $P(t)$ (3.39):

$$M\ddot{q}(t) + [K_L + K_G(S) + P(t)K_{GN}(P)]q(t) = 0.$$

The differential equation with time-varying coefficients (3.41) is called a Hill equation(3.41) (Bolotin, 1956, 1999; Bolotin et al., 1965; Briseghella et al., 1998; Langer, 1980; Gomuliński and Witkowski, 1993; Misiak and Stachura, 2010; Obara and Gilewski, 2016). Taking the special case in which the periodic function is harmonic with frequency θ

$$\Phi(t) = \cos(\theta t); \quad \theta = \frac{2\pi}{T},$$

Equation (3.41) takes a Mathieu equation form: (3.42)

$$M\ddot{q}(t) + \Big[K + K_{GN}(P)\Big]q(t) + v\cos(\theta t)K_{GN}(P)q(t) = 0,$$

where (3.43)

$$K = K_L + K_G(S), \qquad v = \frac{P_t}{P},$$

and the matrix $K_{GN}(P)$ depends on the longitudinal forces that result from the(3.44) constant value P of the periodic force. This matrix is calculated using the algorithm presented in Section 3.4. In turn, the matrix K includes stiffening by the initial prestress forces **S.**

The problem of dynamic instability analysis leads to determining the conditions under which the motion equation (3.43) has non-zero solutions. To solve these non-linear equations, the most common approximate methods are used, i.e., the harmonic balance method and the small parameter method. Both of these methods are based on the analysis of the solution of a particular system of differential equations arising from Floquet's theory (Bolotin, 1956; Gomulinski and Witkowski, 1993).

3.6.1 HARMONIC BALANCE METHOD

The harmonic balance method (HBM) can be used to obtain first, second, third, etc., resonance regions. Using this method, it is assumed that Equation (3.43) is solved as a Fourier series with period $2T$ to obtain odd regions and with period T to obtain even regions. Because the first region is the subject of consideration, the Fourier series with period $2T$ is used:

$$q(t) = \sum_{k=1,3,5}^{\infty} \left(a_k \sin\frac{k\theta t}{2} + b_k \cos\frac{k\theta t}{2} \right),$$

where a_k and b_k are constant coefficients. Substituting the Fourier series (3.45) and(3.45) the acceleration of the displacement (3.45)

$$\ddot{q}(t) = -\sum_{k=1,3,5}^{\infty} \frac{k^2\theta^2}{4} \left(a_k \sin\frac{k\theta t}{2} + b_k \cos\frac{k\theta t}{2} \right)$$

into (3.43), and using trigonometric formulas: (3.46)

$$\cos(\theta t)\sin\frac{k\theta t}{2} = \frac{1}{2}\sin\frac{(2+k)\theta t}{2} - \frac{1}{2}\sin\frac{(2-k)\theta t}{2},$$

$$\cos(\theta t)\cos\frac{k\theta t}{2} = \frac{1}{2}\cos\frac{(2+k)\theta t}{2} + \frac{1}{2}\cos\frac{(2-k)\theta t}{2},$$

an infinite linear combination of trigonometric functions is obtained (3.47)

$$A_1\sin\frac{\theta t}{2} + B_1\cos\frac{\theta t}{2} + A_3\sin\frac{3\theta t}{2} + B_3\cos\frac{3\theta t}{2} + A_5\sin\frac{5\theta t}{2} + \cdots = 0,$$

where A_i and B_i are coefficients arising after balancing the terms with appropriate(3.48) harmonics:

$$A_1 = C_1 a_1 - D a_1 + D a_3, B_1 = C_1 b_1 + D b_1 + D b_3,$$

$$A_3 = Da_1 + C_3a_3 + Da_5, B_3 = Db_1 + C_3b_3 + Db_5,$$

$$A_5 = Da_3 + C_5a_5 + Da_7, B_5 = Db_3 + C_5b_5 + Db_7$$

where (3.49)

$$D = \frac{1}{2}\upsilon K_{GN}(P), C_k = K + K_{GN}(P) - \frac{k^2\theta^2}{4}M; k = 1, 3, 5, \ldots.$$

(3.50)

NOTE

The dependencies (3.47) are formulated by knowing trigonometric formulas:

$$2\cos\frac{\alpha+\beta}{2}\sin\frac{\alpha-\beta}{2} = \sin\alpha - \sin\beta$$

$$2\cos\frac{\alpha+\beta}{2}\cos\frac{\alpha-\beta}{2} = \cos\alpha + \cos\beta$$

where (3.g)

$$\alpha = \frac{(2+k)\theta t}{2}, \qquad \beta = \frac{(2-k)\theta t}{2}.$$

The fulfillment of Equation (3.48) for each t leads to the following condition:

$$A_1 = B_1 = A_3 = B_3 = A_5 = \cdots = 0.$$

Equation (3.51) results in the linear separated homogeneous systems with infinite (3.51) equations and unknown coefficients a_k and b_k. Non-zero solutions of the obtained homogeneous systems consequently lead to obtain conditional equation for a solution with period $2T$

$$\det \begin{matrix} K + K_{GN}(P) \mp \frac{1}{2}\upsilon K_{GN}(P) - \frac{\theta^2}{4}M & & \frac{1}{2}\upsilon K_{GN}(P) \\ \frac{1}{2}\upsilon K_{GN}(P) & & K + K_{GN}(P) - \frac{9\theta^2}{4}M \\ 0 & & \frac{1}{2}\upsilon K_{GN}(P) \\ \ldots & & \ldots \end{matrix}$$

(3.52)
Equation (3.52) leads to obtaining the first, third, fifth, etc., resonance regions. Considering the determinant of the first degree of (3.52),

$$\det\left\{K_L + K_G(S) + \left(1 \mp \frac{1}{2}\upsilon\right)K_{GN}(P) - \pi^2\eta^2M\right\} = 0; \quad \eta = \frac{\theta}{2\pi},$$

the boundaries of the first (main) resonance regions with the first approximation in (3.53) the plane of parameters η (the resonance frequency (Hz)) and υ (the pulsatility index (-))

are obtained.

3.6.2 SMALL PARAMETER METHOD

Using the small parameter method (SPM), a modal transformation is used. The displacement vector $\mathbf{q}(t)$ is expressed in terms of the principal (modal) coordinates $r(t) \in \mathbb{R}^{m \times 1}$:

$$q(t) = Vr(t),$$

where (3.54)

$$V = \begin{bmatrix} \alpha_1 a_1 & \alpha_2 a_2 & \cdots & \alpha_m a_m \end{bmatrix} \in \mathbb{R}^{m \times m}$$

is the modal transformation matrix composed of M-orthonormal eigenvectors $\alpha_k a_k$.(3.55) Eigenvectors are multiplied by a parameter

$$\alpha_k = \sqrt{\frac{m_0}{m_a}}; \quad m_a = a_k^T M a_k; \quad k = 1, 2, \ldots,$$

where $m_0 = 1$ is the parameter expressed in unit mass and $\mathbf{a}_k$ is the eigenvector(3.56) related to the frequency Ω_k. A modal transformation matrix fulfills the following conditions:

$$V^T M V = m_0 I,$$

$$V^T \Big[K + K_{GN}(P) \Big] V = m_0 \Omega^2$$

where $\Omega^2 = \mathrm{diag} \begin{bmatrix} \Omega_1^2 & \Omega_2^2 & \cdots & \Omega_m^2 \end{bmatrix} \in \mathbb{R}^{m \times m}$ is the diagonal matrix of the(3.57) squared frequencies determined from Equation (3.37). The modal transformation matrix (3.55) is needed to obtain the M-orthonormal geometric stiffness matrix

$$\overset{*}{K}_{GN}(P) = V^T K_{GN}(P) V.$$

It should be noted that, due to the fact that $\overset{*}{K}_{GN}$ is not a diagonal matrix, the modal(3.58) transformation of the equation of motion (3.43) did not cause a separation of equations. Nevertheless, the properties of the transformation matrix (3.57) make the expressions outside the diagonal of the matrix small relative to those located on the diagonal. The approximate nature of the considerations authorizes the treatment of the matrix (3.58) as the matrix with dominant diagonal terms

$$\overset{*}{K}_{GN}(P) = \mathrm{diag} \begin{bmatrix} \overset{*}{K}_{GN1} & \overset{*}{K}_{GN2} & \cdots & \overset{*}{K}_{GNm} \end{bmatrix}.$$

The equation of motion (3.43) in modal coordinates (3.54) takes the following form: (3.59)

$$\ddot{r}(t) + \left[\Omega^2 + \frac{\upsilon}{m_0} \overset{*}{K}_{GN}(P) \cos(\theta t) \right] r(t) = 0.$$

The modal coordinate transformation, including the dependence (3.58), decouples(3.60) the coupled set of equations of motion so they can be solved using the single Mathieu differential equation

$$\ddot{r}_k(t) + \Omega_k^2[1 + 2v_{Gk}\cos(\theta t)]r_k(t) = 0; \qquad k = 1, 2, \ldots$$

where (3.61)

$$v_{Gk} = \frac{vK_{GNk}^*(P)}{2m_0\Omega_k^2}$$

is the pulsatility index. Equation (3.61) is true for any form of vibrations, so the (3.62) parameter k can be omitted in the next consideration. Due to this, the pulsatility index (3.62) can be written as

$$v_G = \frac{vK_{GN1}^*}{2m_0\Omega_0^2},$$

where K_{GN1}^* is the first part of the M-orthonormal geometric stiffness matrix (3.59) (3.63) and Ω_0 is the first free frequency, including the static component P of the periodic force.

In the following considerations, the pulsatility index (3.63) is treated as small. Therefore, the solutions of Equation (3.61) and the square of the frequency Ω^2 are represented as power series with respect to this small parameter:

$$r(t) = r_0(t) + v_G r_1(t) + v_G^2 r_2(t) + \ldots$$

$$\Omega^2(v_G) = \Omega_0^2(v_G) + v_G\Omega_1^2(v_G) + v_G^2\Omega_2^2(v_G) + \ldots \tag{3.64}$$

Substituting (3.64) and (3.65) into (3.61) and omitting higher-order terms gives the (3.65) infinite recursive sequence of differential equations with constant coefficients:

$$v_G^0 : \ddot{r}_0 + \Omega_0^2 r_0 = 0,$$
$$v_G^1 : \ddot{r}_1 + \Omega_0^2 r_1 = -\Omega_1^2 r_0 - 2\Omega_0^2 r_0\cos(\theta t),$$

$$v_G^2 : \ddot{r}_2 + \Omega_0^2 r_2 = -\Omega_2^2 r_0 - \Omega_1^2 r_1 - 2[\Omega_1^2 r_0 + \Omega_0^2 r_1]\cos(\theta t)$$

Taking into account the solution of the homogeneous differential equation $(3.66)_1$: (3.66)

$$r_0 = A_0\cos(\Omega_0 t) + B_0\sin(\Omega_0 t)$$

assuming that the frequency of the periodic force is twice the frequency of oscillation (3.67) $\theta = 2\Omega_0$ and using known trigonometric formulas:

$$2\cos(\Omega_0 t)\cos(2\Omega_0 t) = \cos(3\Omega_0 t) + \cos(\Omega_0 t),$$

$$2\sin(\Omega_0 t)\cos(2\Omega_0 t) = \sin(3\Omega_0 t) - \sin(\Omega_0 t),$$

the first-order approximation $(3.66)_2$ is obtained (3.68)

$$\ddot{r}_1 + \Omega_0^2 r_1 = -A_0(\Omega_0^2 + \Omega_1^2)\cos(\Omega_0 t) + B_0(\Omega_0^2 - \Omega_1^2)\sin(\Omega_0 t)$$
$$-\Omega_0^2[A_0\cos(3\Omega_0 t) + B_0\sin(3\Omega_0 t)].$$

Solution of (3.69) is the function (3.69)

$$r_1 = A_1\cos(\Omega_0 t) + B_1\sin(\Omega_0 t) + r_{1S}$$

where (3.70)

$$
\begin{aligned}
r_{1S} = {} & -\frac{A_0\left(\Omega_0^2 + \Omega_1^2\right)}{2\Omega_0} t\sin(\Omega_0 t) + \frac{B_0\left(\Omega_0^2 - \Omega_1^2\right)}{2\Omega_0} t\cos(\Omega_0 t) \\
& + \frac{A_0}{8}\cos(3\Omega_0 t) + \frac{B_0}{8}\sin(3\Omega_0 t)
\end{aligned}
$$

is the particular integral. The first two terms of (3.71) are secular terms that (3.71) determine the unstable nature of the solution. If we eliminate one of them, the classic border solution, consisting of periodic functions and one secular term, is obtained. This elimination is realized by assuming

$$\Omega_0^2 \pm \Omega_1^2 = 0 \rightarrow \Omega_1^2 = \pm\Omega_0^2$$

Including the condition (3.72), the square of the frequency (3.65) is represented as (3.72)

$$\Omega^2 = \Omega_0^2 \pm \upsilon_G \Omega_0^2.$$

Assuming $\theta = 2\Omega$ results in the following formula for the first resonance frequency: (3.73)

$$\eta = \frac{\Omega_0}{\pi}\sqrt{1 \pm \upsilon_G}.$$

Based on (3.74), the first (main) unstable regions with the first approximation in the (3.74) plane of parameters η and υ_G can be determined.

In summary, the boundaries of the main unstable regions can be obtained based on Equation (3.53) obtained using the harmonic balance method (HBM) or on the simple formula (3.74) obtained using the small parameter method (SPM). The main purpose is to determine the influence of the initial prestress level S on the shape and range of unstable regions $A_\eta(S_i)$. For quantitative assessment, a nondimensional parameter is introduced

$$\lambda = \frac{A_\eta(S_i)}{A_\eta(S_{min})},$$

which expresses the ratio of the area of the unstable region at the i-th level of initial (3.75) prestress $A_\eta(S_i)$ to the area of the unstable region at the minimum initial prestress level $A_\eta(S_{min})$. This parameter measures the changes in areas of unstable regions as the initial prestress level increases. The range of the parameter λ is defined as a value between 1 and 0. In the case of $\lambda = 1$, there is potential for the excitation of unstable motion, whereas in the case of $\lambda = 0$, such a risk is absent. Additionally, from the perspective of structural durability, the character of change in the parameter with growth the initial prestress level is important. The best solution is when the parameter λ decreases exponentially as the initial prestress level increases.

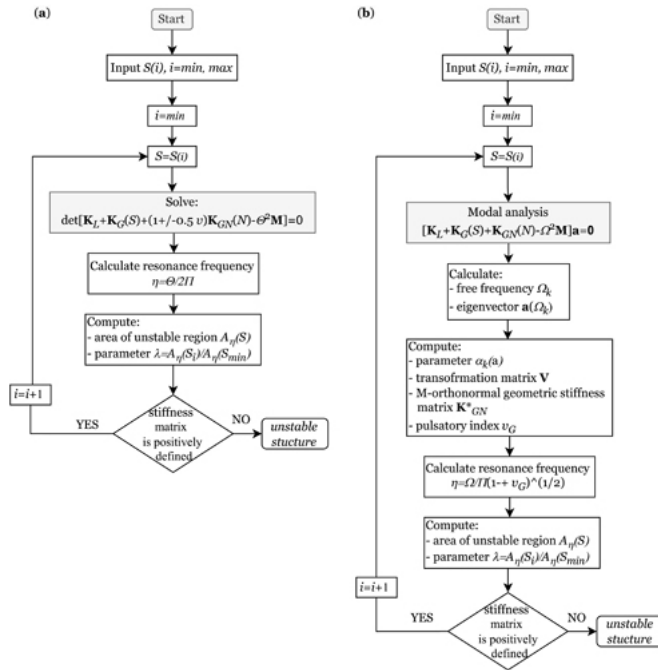The dynamic stability analysis process is summarized in the flowchart shown in Figure 3.7.

FIGURE 3.7 Flowchart of dynamic stability analysis: (a) harmonic balance method and (b) small parameter method.

3.7 CHAPTER SUMMARY

This chapter provides the theoretical foundation for the final chapter. The qualitative, static, dynamic, and dynamic stability analyses are explained in detail. The presented equations were used to build the calculation procedure written in the Mathematica environment. The nonlinear algebraic system was solved using the Newton–Raphson method. The process begins by calculating the nodal displacement using second-order theory. At this point, only the linear system of equations needs to be solved (in this case, the existing Mathematica toolbox was used). Next, the obtained vector of nodal displacements is used in the first iteration in order to find the results according to the third-order theory. The program continues to iterate until the specified precision is achieved or the maximum number of iterations is exceeded. If the solution is not found, the user must increase the number of iterations or change the initial vector of displacements, for example, by changing the initial prestress level.

The calculation procedure includes the analysis of geometrically non-linear truss systems and allows for the full analysis at any initial prestress level. The program allows flexible definition of structural geometry, material parameters, and loads. It also identifies the self-stress state and tracks the behavior of selected static, geometric, and dynamic parameters in relation to initial prestress levels.

REFERENCES

Ashwear, N., Eriksson, A. (2014). Natural frequencies describe the pre-stress in tensegrity structures, *Computer and Structures* 138(1), 162–171.

Ashwear, N., Tamadapu, G., Eriksson, A. (2016). Optymization of modular tensegrity structures for high stiffness and frequency separation requirements, *International Journal of Solids and Structures* 80, 297–309.

Awrejcewicz, J., Andrianov, I. (2000). *Asymptotic methods and their application in shell theory (in Polish),* WNT, Warsaw, Poland.

Barnes, M.R. (1999). Form-finding analysis of tension structures by dynamic relaxation, *International Journal of Space Structures* 14(2), doi: 10.1260/0266351991494722.

Bathe, K.J. (1996). *Finite element procedures in engineering analysis*, Prentice Hall, New York, USA.

Baudriller, H., Bernard, M., Cañadasa, P., Montcourrier, P., Parmeggiani, A., Bettache, N., (2006). Form-finding of complex tensegrity structures: Application to cell cytoskeleton modeling, *Comptes Rendus Mecanique* 334(11), 662–668.

Bel Hadj Ali, N., Rhode-Barbarigos, L., Pascual, A. A., Smith, I.F.C. (2010). Design optimization and dynamic analysis of a tensegrity-based footbridge, *Engineering Structures* 32(11), 3650–3659, doi: 10.1016/j.engstruct.2010.08.009.

Bel Hadj Ali, N., Smith, I.F.C. (2010). Dynamic behavior and vibration control of a tensegrity structure, *International Journal of Solids and Structures* 47(9), 1285–1296, doi: 10.1016/j.ijsolstr.2010.01.012.

Bigoni, D., Kirillov, O. (2019). *Dynamic* 586, Switzerland, Springer, ISBN: 978-3-319-93721–2.

Bolotin, V.V. (1956). *Dynamic stability of elastic systems (in Russian)*, Gostekhizdat, Moscow, Russia.

Bolotin, V.V. (1999). Dynamic instabilities in mechanics of structures, *Applied Mechanics Reviews*, 52, R1–R9, doi:10.1115/1.3098924.

Bolotin, V.V., Weingarten, V., Greszczuk, L.B., Trigoroff, K.N., Gallegos, K.D., Cranch, E.T. (1965). Dynamic stability of elastic systems, *Journal of Applied Mechanics*, 32, 718–718, doi: 10.1115/1.3627306.

Briseghella, L., Majorana, C.E. Pellegrino, C. (1998). Dynamic stability of elastic structures: a finite element approach, *Computers & Structures* 69, 11–25.

Cai, J., Wang, X., Deng, X., Feng, J. (2018). Form-finding method for multi-mode tensegrity structures using extended force density method by grouping elements, *Composite Structures* 187, 1–9.

Cao, Z., Luo, A., Feng, Y., Liu, H. (2024). Form-finding for tensegrity structures based on the equilibrium equation, *Mechanics Research Communications*, 136, 104256, doi.org/10.1016/j.mechrescom.2024.104256.

Calladine, C.R. (1982). Modal stiffnesses of a pretensioned cable net, *International Journal of Solids and Structures* 18(10), 829–846.

Chau, K.T. (2018). *Applications of differential equations in engineering and mechanics*, CRC Press, Taylor & Francis Group, Boca Raton, London, New York.

Chen, M., Qin, J. (2024). *Form-finding and physical property predictions of tensegrity structures using deep neural networks*, doi: 10.13140/RG.2.2.31645.32480.

Chen, Y., Feng, J. (2012a). Generalized eigenvalue analysis of symmetric prestressed structures using group theory, *Journal of Computing in Civil Engineering* 26(4), 488–497.

Chen, Y., Feng, J. (2012b). Initial prestress distribution and natural vibration analysis of tensegrity structures based on group theory, *International Journal of Structural Stability and* 12(2), 213–231.

Chmielewski, T., Zębaty, Z. (1998). *Fundamentals of building dynamics (in Polish)*, Arkady, Warsaw, Poland.

Connelly, R. (1993). *Rigidity*, Wills, J.M., eds., Handbook of convex geometry, Amsterdam, The Netherlands, Elsevier Publishers Ltd, 223–271.

Connelly, R., Back, A. (1998). Mathematics and tensegrity, *American Sciences* 86, 142–151.

Connelly, R., Terrell, M. (1995). Globally rigid symmetric tensegrities, *Structural Topology* 21, 59–78.

Crisfield, M.A. (1991). *Non-linear finite element analysis of solid and structures: Essentials* John Wiley & Sons, New York, NY.

Cunningham, W.J. (1958). *Introduction to nonlinear analysis*, Mc Graw-Hill Book Company, New York, Toronto, London.

De Borst, R. (1999). *Computational methods in non-linear solid mechanics* TU Delft, Netherlands.

De Borst, R., Crisfield, M.A., Remmers, J.J.C., Verhoosel, C.V. (2012). *Non-linear finite element analysis of solid and structures*, John Wiley & Sons, The Atrium, Southern Gate,

Estrada, G., Bungartz, H.J., Mohrdieck, C. (2006). Numerical form-finding of tensegrity structures, *International Journal of Solids and Structures* 43, 6855–6868.

Faroughi, S., Khodaparast, H.H., Friswell, M.I. (2015). Non-linear dynamic analysis of tensegrity structures using a co-rotational method, *International Journal of Non-Linear Mechanics* 69, 55–65.

Garus, S., Garus, J., Sochacki, W., Nabiałek, M., Petru, J., Borek, W., Šofer, M., Kwiatoń, P. (2023). Influence of material distribution and damping on the dynamic stability of Bernoulli-Euler beams, *Bulletin of Polish Academy of Sciences*, 71(4), e145567, doi:10.24425/bpasts.2023.145567.

Ghomeshi Bozorg, M., Keshmiri, M. (2013). Stability analysis of nonlinear time varying system of beam-moving mass considering friction interaction, *Indian Journal of Science and Technology* 6(11), 5459–5468.

Gilewski, W., Kasprzak, A. (2013). *Tensegrity form-finding via modal analysis*, T. Łodygowski, 20th International Conference on Computer Methods in Mechanics, Short Papers, Poznan, Poland.

Gilewski, W., Kłosowska, J., Obara, P. (2015). Application of singular value decomposition to qualitative analysis of trusses and tensegrity structures (in Polish), *ACTA Scientarum*

Polonarum, Serie Architectura 14(3), 3–20.

Gilewski, W., Kłosowska, J., Obara, P. (2019). Parametric analysis of some tensegrity structures, *MATEC Web of Conferences* 262, 10003.

Golub, G., Kahan, W. (1965). Calculating the singular values and pseudo-inverse of a matrix, *Journal of the Society for Industrial and Applied Mathematics, Series B: Numerical Analysis* 2(2), 205–224.

Gomuliński, A., Witkowsk,i M. (1993). *Mechanics of structures (advanced course) (in Polish)*, Oficyna Wydawnicza Politechniki Warszawskiej, Warsaw, Poland.

Harichandran, A., Yamini Sreevalli, I. (2016). Form-finding of tensegrity structures based on force density method, *Journal of Science and Technology* 9(24), 1–6.

Holland, J.H. (1975). *Adaptation in natural and artificial systems: An introductory analysis with application to biology, control, and artificial intelligence*, MIT Press, Michigan.

Jani, N., Chakraborty, G. (2021)**.** Parametric resonance in cantilever beam with feedback-induced base excitation, *Journal of Vibration Engineering & Technologies* 9, 291–301, doi: 10.1007/s42417-020-00226–1.

Jo, N.C., Choi, S.Y., Han, S.E. (2004). *Shape optimization of the cable dome system* Proceeding of the Computational Structural Engineering Institut Shape optimization of the Conference, Computational Structural Engineering Institute of Korea, 151–160.

Juan, S.H., Tur, J.M.M. (2008). Tensegrity frameworks: Static analysis review, *Mechanism and Machine Theory* 43(7), 859–881.

Kan, Z., Peng, H., Chen, B., Zhong, W. (2018). Nonlinear dynamic and deployment analysis of clustered tensegrity structures using a positional formulation FEM, *Composite Structures* 187, 241–258.

Kasprzak, A. (2014). *Assessing the feasibility of using tensegrity structures in bridge construction (in Polish)*, Ph. D. Thesis, Publishing House of the Warsaw University of Technology, Warsaw, Poland.

Kenner, H. (1976), *Geodesic math and how to use it*, Berkeley and Los Angeles, University of California Press.

Keskin, AÜ. (2019). Adomian decomposition method (ADM), in *Boundary value problems for engineers*, Springer International Publishing, Basel, 311–359, doi: 10.1007/978-3-030-21080-9_7.

Klema, V.C. (1980). The singular value decomposition: It's computation and some applications, *IEEE Transaction on Automatic Control* 25(2), 164–176, doi: 10.1109/TAC.1980.1102314.

Kłosowska, J. (2018). *Assessing the feasibility of using tensegrity construction in cubic construction (in Polish),* Ph. D. Thesis, Publishing House of the Kielce University of Technology, Kielce, Poland.

Kłosowska, J., Obara, P., Gilewski, W. (2018). Self-stress control of real civil engineering tensegrity structures, *AIP Conference ProceedingsteAIP Conference Proceedings*, 150004, doi: 10.1063/1.5019157.

Koohestani, K. (2012). Form-finding of tensegrity structures via genetic algorithm, *International Journal of Solids and Structures* 49(5), 739–747.

Koohestani, K. (2013). A computational framework for the form-finding and design of tensegrity structures, *Mechanics Research Communications* 54, 41–49.

Koohestani, K., Guest, S.D. (2013). A new approach to the analytical and numerical form-finding of tensegrity structures, *International Journal of Solids and Structures* 50(19), 2995–3007.

Kruszewski, J. (1959). *Finite element method in structural dynamics (in Polish)*, Arkady, Warsaw, Poland.

La Salle, J., Lefschetz, S., Alverson, R.C. (1962). Stability by liapunov's direct method with applications, *citehysics Today* 15tehysics Today 15#x2013;59, doi:10.1063/1.3057800.

Langer, J. (1980). *Structure dynamics (in Polish)*, Wroclaw University of Technology, Wroclaw, Poland.

Liao, S. (2013). Chapter 1: Chance and challenge: A brief review of the homotopy analysis method, in *Advanced homotopy analysis method*, World Scientific Press, Shanghai, 1–33, doi: 10.1142/9789814551250_0001.

Lee, S., Lee, J., Kang, J. (2017). A Genetic Algorithm based form-finding of tensegrity structures with multiple self-stress states, *Journal of Asian Architecture and Building Engineering* 16(1), 155–162, doi: 10.3130/jaabe.16.155.

Lee, H.P., Tan, T.H., Leng, G.S.B. (1998). Parametric instability of spinning pretwisted beams subjected to sinusoidal compressive axial loads, *Computers & Structures* 66, 745–764.

Lefschetz, S., La Salle, J. (1966). *Zarys Lapunov stability theory and its direct method (in Polish)*, PWN, Warsaw, Poland.

Li, Y., Feng Xi-Q. Cao, Y.-P., Gao, H. (2010). A monte carlo form-finding method for large scale regular and irregular tensegrity structures, *International Journal of Solids and Structures* 47(14–15), 1888–1898.

Linkwitz, K. (1999). Form-finding by the "direct approach" and pertinent strategies for the conceptual design of prestressed and hanging structures, *International Journal of Space Structures* 14(2), 73–87.

Long, C. (1983). Visualization of matrix singular value decomposition, *Mathematics Magazine* 56(3), 161–167.

Luo, Y., Lu, J. (2006). Geometrically non-linear force method for assemblies with infinitesimal mechanisms, *Computer and Structures* 84(31), 2194–2199.

Lyapunov, A.M. (1892). *The general problem of the stability of motion*, PhD thesis, University of Kharkov, Kharkiv, Ukraine.

Ma, S., Yuan, X.-F., Xie, S.-D. (2019). A new genetic algorithm-based topology optimization method of tensegrity tori, *KSCE Journal of Civil Engineering* 23(5), 2136–2147.

Mascolo, I. (2019). Recent developments in the dynamic stability of elastic *Frontiers in AppliMathematics and Statistics* 5, 51, doi: 10.3389/fams.2019.00051.

Masic M., Skelton R.E., Gill P.E. (2005), Algebraic tensegrity form-finding, *International Journal of Solids and Structures* 42, 4833–4858.

Mathieu, É. (1868). Memoir on the vibratory movement of an elliptical membrane, *Journal de Mathématiques Pures et Appliquées* 13, 137–203.

Micheletti, A., Williams, W.O. (2007). A marching procedure for form-finding for tensegrity structures, *Journal of Mechanics of Materials and Structures* 2(5), 857–882.

Misiak, J., Stachura, S. (2010). *Selected issues of static and dynamic stability of rod and shell structures (in Polish)*, Publising House WSEiZ, Warsaw, Poland.

Motro, R. (1984). *Forms and forces in tensegrity systems*, H. Nooshin (ed.), Proceedings of Third International Conference on Space Structures, Elsevier, 180–185.

Murakami, H. (2001a). Static and dynamic analyses of tensegrity structures. Part 1. Nonlinear equations of motion, *International Journal of Solids and Structures* 38, 3599–3613.

Murakami, H. (2001b). Static and dynamic analyses of tensegrity structures. Part 2. Quasi-static analysis, *International Journal of Solids and Structures* 38, 3615–3629.

Murakami, H. Nishimura, Y. (2001a). Static and dynamic characterization of regular truncated icosahedral and dodecahedral tensegrity modules, *International Journal of Solids and Structures* 38, 9359–9381.

Murakami, H., Nashimura, Y. (2001b). Initial shape finding and modal analyses of cyclic right-cylindrical tensegrity modules, *Computers & Structures* 79(9), 891–917.

Obara, P. (2019). *Dynamic and dynamic stability of tensegrity structures (in Polish)*, Publishing House of the Kielce University of Technology, Kielce, Poland.

Obara, P., Gilewski, W. (2016). Dynamic stability of moderately thick beams and frames with the use of harmonic balance and perturbation methods, *Bulletin of the Polish Academy of Sciences Technical Sciences* 64(4), 739–750.

Obara, P., Solovei, M., Tomasik, J. (2023). Genetic algorithm via other methods for determination self-stress states of tensegrity domesf-stress states of tensegrity domes, s*Applied Sciences* 13(9), 5267, doi: 10.3390/app13095267.

Obara, P., Tomasik, J. (2020). Parametric analysis of tensegrity plate-like structures: Part 1 —qualitative analysis, Applied f-stress states of tensegrity domesf-stress states of tensegrity domes, s*Applied Sciences* 13(9), 5267, doi: 10.3390/app13095267.

Obara, P., Tomasik, J. (2020). Parametric analysis of tensegrity plate-like structures: Part 1 —qualitative analysis, *Applied Sciences* 10(20), 7042, doi: 10.3390/app10207042.

Obara, P., Tomasik, J. (2021). Active control of stiffness of tensegrity plate-like structures built with simplex modules, *Materials* 14(24), 7888, doi: 10.3390/ma14247888.

Pagitz, M., Tur, J.M. (2009). Finite element based form finding algorithm, *International Journal of Solids and Structures* 46(17), 3235–3240.

Paul, C., Lipson, H., Cuevas, F.V. (2005). *Evolutionary form-finding of tensegrity structures*, Proceedings of the 2005 Conference: Genetic & Evolutionary Computation, Washington.

Pellegrino, S. (1986). *Mechanics of kinematically indeterminate structures*, Ph.D. Thesis, University of Cambridge, UK.

Pellegrino, S. (1990). Analysis of prestressed mechanisms, *International Journal of Solids and Structures* 26, 1329–1350.

Pellegrino, S. (1993). Structural computations with the singular value decomposition of the equilibrium matrix, *International Journal of Solids and Structures* 30, 3025–3035.

Pellegrino, S., Calladine, C.R. (1986). Matrix analysis of statically and kinematically indeterminate frameworks, *International Journal of Solids and Structures* 22(4), 409–428.

Pomaro, B., Majorana, C.E. (2021). Parametric resonance of fractional multiple-degree-of-freedom damped beam systems, *Acta Mechanica* 232, 4897–4918, doi: 10.1007/s00707-021-03087–1.

Rahami, H., Kaveh, A., Ardalan, Asl, M., Mirghaderi, S.R. (2013). Analysis of near-regular structures with node irregularity using SVD of equilibrium matrix, *International Journal of Civil Engineering* 11(4), 226–239.

Rakowski, G., Kasprzyk, Z. (2005), *Finite element method in structural mechanics (in Polish)*, Publishing House of the Warsaw University of Technology, Warsaw, Poland.

Rimoli, J.J. (2018). A reduced-order model for the dynamic and post-buckling behavior of tensegrity structures, *Mechanics of Materials* 116, 146–157.

Safaei, S.D., Eriksson, A., Micheletti, A., Tibert, G. (2013). Study of various tensegrity modules as building blocks for slender booms, *International Journal of Space Structures* 2(5), 41–52.

Schek, H. (1974). The force density method for form finding and computation of general networks, *Computer Methods in Applied Mechanics and Engineering* 3(1), 115–134.

Simitses, G.J. (1990). *Dynamic stability of suddenly loaded structures*, New York, Springer-Verlag.

Skelton, R.E., Adhikari, R., Pinaud, J.P., Chan, W., Helton, J.W. (2001). *An introduction to the mechanics of tensegrity structures*, Proceedings of the 40th IEEE Conference on Decision and Control, Orlando, FL, December, 4254–4258.

Skelton, R.E., de Oliveira, M.C. (2009). *Tensegrity systems*, Springer, London, UK.

Skelton, R.E., Helton, J.W., Adhikari , R., Pinaud, J.P., Chan W. (2002). An introduction to the mechanics of tensegrity structures. In *The Mechanical Systems Design Handbook*, (Chapter 17), CRC press, Boca Raton, US.

Song, Z., Chen, Z., Li, W., Chai, Y. (2016). Dynamic stability analysis of beams with shear deformation and rotary inertia subjected to periodic axial forces by using discrete singular convolution method, *Journal of Engineering Mechanics* 142, 04015099, doi: 10.1061/(ASCE)EM.1943–7889.0001023.

Stewart, G.W. (1998). *Matrix algorithms: Basic decompositions*, Philadelphia.

Strang, G. (1993). *Introduction to linear algebra*, Wellesley-Cambridge Press, Wellesley.

Sultan, C. (2009). Tensegrity: 60 years of art, science and engineering, *Advances in Applied Mechanics* 43, 69–145.

Sultan, C., Corless, M., Skelton, R.E. (1999). *Reduced prestressability conditions for tensegrity systems*, Conference: 40th Structures, Structural Dynamics, and Materials Conference, 2300–2308.

Sun, Z., Zhao, L., Liu, K., Jin, L., Yu, J., Li, C. (2022). *An advanced form-finding of tensegrity structures aided with noise-tolerant zeroing neural network*, *Neural Computing and Applications* 34, 6053–6066, doi: 10.1007/s00521-021-06745–6.

Szmelter, J. (1980). *Computer methods in mechanics (in Polish)*, PWN, Warsaw, Poland.

Tibert, A.G., Pellegrino, S. (2003). Review of form-finding methods for tensegrity structures, *International Journal of Space Structures* 18(4), 209–223.

Tomasik, J. (2023*). Parametric analysis of double-layer tensegrity girds – discrete and continual model (in Polish)*, Ph. D. Thesis, Publishing House of the Kielce University of Technology, Kielce, Poland.

Tran, H.C., Lee, J. (2007). Advanced form finding for cable-strut structures, *International Journal of Solids and Structures* 47, 1785–1794.

Tran, H.C., Lee, J. (2010a). Advanced form-finding of tensegrity structures, *Computers & Structures* 88, 237–246.

Tran, H.C., Lee, J. (2010b). Initial self-stress design of tensegrity grid structures, *Computers & Structures* 88, 558–566.

Tran, H.C., Lee, J. (2011). Form-finding of tensegrity structures using double singular value decomposition, *Engineering with Computers* 29, 71–86.

Uzun, F. (2016). Form-finding of free-form tensegrity structures by genetic algorithm-based total potential energy optimization, *Advanced Civil Engineering* 20(5), 784–796, doi: 10.1177/1369433216664739.

Veenendaal, D., Block, P. (2012). An overview and comparison of structural form finding methods for general networks, *International Journal of Solids and Structures* 49(26), 3741–3753.

Volmir,A.C. (1963). *Stability of elastic systems*, Science, Moscow, Russia.

Wang, K., Cai, J., Sang-hoon Lee, D., Xu, Y., Feng, J. (2021)**.** Numerical form-finding of multi-order tensegrity structures by grouping elements, *Steel and Composite Structures* 41(2), 267–277, doi: 10.12989/scs.2021.41.2.267.

Wang, Y., Xian, X., Luo, Y. (2021). Form-finding of tensegrity structures via rank minimization of force density matrix, *Engineering Structures* 227, 111419, doi: 10.1016/j.engstruct.2020.111419.

Wei-Chau, X. (2006). *Dynamic stability of structures*, Cambridge, Cambridge University Press.

Xu, X., Luo, Y. (2010). Form-finding of nonregular tensegrities using a genetic algorithm, *Mechanics Research Communications* 37(1), 85–91.

Xu, X., Wang, Y., Luo, Y. (2018). Finding member connectivities and nodal positions of tensegrity structures based on force density method and mixed integer nonlinear programming, *Engineering Structures* 166, 240–250.

Yamamoto, M., Gan, B.S., Fujita, K., Kurokawa, J.A. (2011)**.** Genetic algorithm based form-finding for tensegrity structure, *Proceedia Engineering* 14, 2949–2956, doi: 10.1016/j.proeng.2011.07.371.

Yang, X.D., Tang, Y.Q., Chen, L.Q., Lim, C.W. (2010). Dynamic stability of axially accelerating timoshenko beam: Averaging method, *European Journal of Mechanics – Asolids 29*, 81–90, doi: 10.1016/j.euromechsol.2009.07.003.

Zhang, J.Y., Ohsaki, M. (2006). Adaptive force density method for form-finding problem of tensegrity structures, *International Journal of Solids and Structures* 43, 5658–5673.

Zhang, J.Y., Ohsaki, M. (2015). *Tensegrity structures: Form, stability, and symmetry*, Springer, Japan.

Zhang, L.Y., Zhu, S.-X., Li, S.-X., Xu, G.-K. (2018). Analytical form-finding of tensegrities using determinant of force-density matrix, *Composite Structures* 189, 87–98.

Zhang, P., Zhou, J., Chen, J. (2021). Form-finding of complex tensegrity structures using constrained optimization method, *Composite Structure* 268, 113971, doi: 10.1016/j.compstruct.2021.113971.

Zhang, Q., Wang, X., Cai, J., Yang, R., Feng, J. (2021). Prestress design for cable-strut structures by grouping elements, *Engineering Structures* 244, 112010, doi: 10.1016/j.engstruct.2021.112010.

Zhang, Q., Wang, X., Cai, J., Zhang, J., Feng, J. (2020). Closed-form solutions for the form-finding of regular tensegrity structures by group elements, *Symmetry* 12, 374, doi: 10.3390/sym12030374.

Zhang, Q.C., Cui, S.Y., Fu, Z., Han, J.X. (2021). Modal interaction-induced parametric resonance of stayed cable: A combined theoretical and experimental investigation, *Mathematical Problems in Engineering*, 1–18, doi:10.1155/2021/5797761.

Ziemba, S. (1959). *Analysis of vibrations (in Polish*, PWN, Warsaw, Poland.

Zienkiewicz, O.C., Taylor, R.L. (2000). *The finite element method: The basis*, London.

4 Assessment of Tensegrity Structures – Examples

NOTE

1. Names introduced by the author are italicized.
2. The equations are based on theoretical background presented in Chapter 3.
3. In the considered examples, the literature analyzing similar structures is presented.

4.1 INTRODUCTION

Literature analysis (see Section 1.6) shows that the vast majority of works and monographs look at tensegrity design, search for stable forms, optimization algorithms, and methods of controlling the shape of tensegrity structures under the influence of external loads and then discuss the use of these structures. Against this background, the parametric analysis that assesses the impact of the initial prestress on the static and dynamic properties of tensegrity structures is the subject of incomparably less works. In addition, these works relate to specific solutions. There are several monographs on tensegrity in world literature, but they present the issue in a completely different way than this book.

Generally, tensegrity is understood in many ways. This term is often improperly used for structures that have some, but not necessarily key tensegrity properties. The concept of this book leads to a proper understanding of the unique nature of tensegrity structures characterized by specific mechanical and mathematical properties. Based on the theoretical background presented in Chapter 3, a broad spectrum of different planar and spatial design solutions is considered. This monographic study describes in a compact manner the behavior of the structures.

Section 4.2 is intended for beginners interested in tensegrity systems. The chapter is written step-by-step, referring to the theoretical considerations presented in Chapter 3. This approach makes it easier to understand both the mathematical description and the behavior of the structures. The following chapters contain examples, from the simplest to the most advanced tensegrity structures or structures with tensegrity features. Each example poses one or more questions for a better understanding of the properties of tensegrity. A qualitative and quantitative assessment is carried out for each structure. The analysis consisted of four stages:

- qualitative analysis;
- quantitative analysis:

    - static analysis;
    - dynamic analysis;
    - dynamic stability analysis.

Qualitative analysis determines the characteristic features of tensegrity structures. This assessment leads to a correct classification into one of the four groups (Table 3.1). Such systematization facilitates the analysis and design because it is a consequence of the

different behavior of tensegrity structures under the influence of external loads. The immanent features, like the infinitesimal mechanisms and self-equilibrated systems of longitudinal forces that stabilize mechanisms, are identified. In this process, singular value decomposition of the elongation matrix (3.7) and spectral analysis of the stiffness matrix, considering the effect of self-equilibrated forces (3.17) are employed. For selected two-dimensional (2D) n-element structures with m degrees of freedom, considerations are presented in detail; the following matrices are determined:

- $B \in \mathbb{R}^{n \times m}$ (3.3) – non-dimensional elongation matrix;
- $Y \in \mathbb{R}^{n \times n}$ (3.11), $Z \in \mathbb{R}^{n \times m}$, $X \in \mathbb{R}^{m \times m}$ (3.15) – matrices of singular value decomposition of the elongation matrix; dependence between the matrices Y, Z, X (3.16);
- $H \in \mathbb{R}^{n \times n}$ (3.10) – eigenvalues of the matrix BB^{T};
- $y_S \in \mathbb{R}^{n \times 1}$ – eigenvector of BB^{T} corresponding to the zero eigenvalue $\mu_i = 0$ in the matrix H, which is responsible for the existence of the self-stress state;
- $L \in \mathbb{R}^{m \times m}$ (3.14) – eigenvalues of matrix $B^{\mathrm{T}}B$;
- $x_S \in \mathbb{R}^{m \times 1}$ – eigenvector of $B^{\mathrm{T}}B$ corresponding to the zero eigenvalue $\gamma_i = 0$ in the matrix L, which is responsible for the existence of the mechanism;
- $K_L \in \mathbb{R}^{m \times m}$ – linear stiffness matrix;
- $S = y_S S \in \mathbb{R}^{n \times 1}$ (3.18) – self-equilibrated longitudinal forces, where S is the initial prestress level;
- $K_G(S) \in \mathbb{R}^{m \times m}$ – geometric stiffness matrix depending on the self-equilibrated longitudinal forces S;
- $O \in \mathbb{R}^{m \times 1}$ (3.20) – eigenvalues of the stiffness matrix with the self-equilibrated longitudinal forces $[K_L + K_G(S)]$ (3.19).

In other cases, the number of identified mechanisms and self-stress states and the values of the self-stress state are shown. These values are normalized in such a way that the minimum compressed force in struts is equal to $N = -1$. In the figures, struts are marked with thick lines, while cables with thin lines. These normalized values are included in the quantitative assessment, which contains a static, dynamic, and dynamic stability analysis.

The existence of self-stress states and mechanisms does not depend on geometric and material properties; however, the spectral analysis of the stiffness matrix (3.17) does. Moreover, the quantitative assessment also depends. In order to be able to evaluate the behavior of different structures and make a comparative analysis, calculations are made assuming specific material and geometric constants. It is assumed that the structures are made of steel with the Young modulus $E = 210\mathrm{GPa}$ and the density $\rho = 7860\mathrm{kg/m^3}$. The Halfen DETAN Rod System is used. The material and geometric characteristics are presented in Table 4.1. The load-bearing capacity is calculated by taking into account a partial factor for structural resistance. In the case of struts (made of cold-finished circular hollow section), it depends on the length l (Table 4.2).

TABLE 4.1 Material and Geometric Characteristics of Elements

Elements	Steel	Diameter ϕ (mm)	Thickness t (mm)	Cross-sectional area A (m²)	Moment of inertia I (m⁴)	Load-bearing capacity N_{Rd} (kN)
Cables	S460N	20.0	–	$3.14 \cdot 10^{-4}$	$7.85 \cdot 10^{-9}$	110.2
Struts	S355J2	76.1	2.9	$6.67 \cdot 10^{-4}$	$4.47 \cdot 10^{-7}$	$N_{b,Rd}(l)$

TABLE 4.2 Load-Bearing Capacity of Struts $N_{b,Rd}$ (l)

l (m)	0.6	1.0	1.333	1.4	1.5	1.645	2.3	4.2
$N_{b,Rd}$ (l) (kN)	224	198.9	175.4	170.5	163.0	152.1	107.1	41.9

Static analysis leads to study the behavior of structures under time-independent external load $P = P(t = 0)$. The assessment of the influence of initial prestress level S on static parameters is analyzed, i.e.:

- q_i – displacements;
- N_{cable} – longitudinal forces in cables;
- N_{strut} – longitudinal forces in struts;
- W_{max} (3.22) – effort of the structure;
- GSP (3.32) – global stiffness parameter.

The calculations are carried out using the second-order theory (3.e) and third-order theory (3.23). The first and very important aspect of the analysis is the determination of the prestress range:

- S_{min} – minimum prestress level is related to the appropriate distribution of longitudinal forces in the elements of the structure caused by external loads; assuming a minimum prestress level of $S_{min} = 0$ means that the external load causes an appropriate distribution of longitudinal forces in the elements of the structure, i.e., the cables are tensioned and the struts are compressed;
- S_{max} – maximum prestress level is related to the load-bearing capacity of the most stressed elements; in the study, a value of S_{max} is estimated with the effort of the structure at $W_{max} < 1$.

Dynamic analysis leads to the determination of the influence of initial prestress level S on vibration frequencies (3.38), i.e.:

- $f_i(0) = f_i(P = 0)$ – natural frequencies calculated using the modal analysis (3.36);
- $f_i(P)$ – free frequencies depend on the time-independent external loads $P = P(t = 0)$ and calculated using the modal analysis (3.37).

Dynamic stability analysis leads to study the behavior of structures under *periodic force* $P(t) = P + P_t \cos(\theta t)$, where P is the constant component, P_t is the amplitude, and θ is the frequency of the periodic force. The pulsatility index $v = P_t/P$ varying within the following limits $v \in \langle 0; 0.75P \rangle$ is taken into account. Based on Equation (3.53) or (3.74), the influence of initial prestress S on the following parameters is analyzed:

- η_i – resonance frequency depends on the pulsatility index v;
- $A_{\eta i}$ – main unstable regions in the plane of a resonance frequency η and pulsatility index v;
- λ (3.75) – dimensionless parameter, which measures changes in the area of the unstable regions, i.e., the effect of the initial prestress level S.

4.2 SIMPLEST TWO-ELEMENT STRUCTURE

The simplest possible structure is considered first (Gilewski et al., 2015; Kasprzak, 2014; Luo and Lu, 2006; Obara, 2019; Obara and Tomasik, 2023c, 2023d; Motro, 1992; Tibert, 2002; Volokh et al., 2003; Zhang, 2007). It is a truss consisting of two elements $(n = 2)$ with length l and stiffness EA. It is characterized by two degrees of freedom $(m = 2)$ (Figure 4.1a). The displacement vector (3.1) and elasticity matrix (3.6) are as follows:
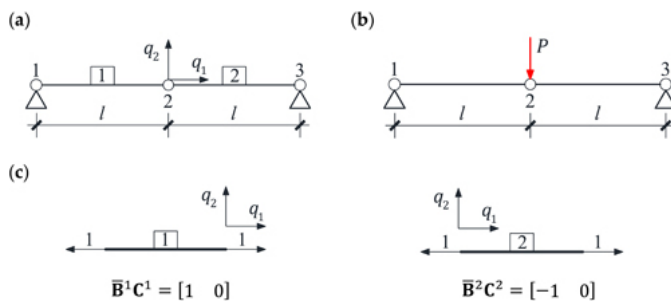

FIGURE 4.1 Two-element structure: (a) geometry, (b) scheme of loading regime, and (c) elongation row matrices for elements.

$$q = \begin{bmatrix} q_1 \\ q_2 \end{bmatrix} \in \mathbb{R}^{2\times 1}, E = \frac{EA}{l} \begin{bmatrix} 1 & 0 \\ 0 & 1 \end{bmatrix} \in \mathbb{R}^{2\times 2}.$$

Both qualitative and quantitative analyses are presented in detail. In the quantitative considerations, the behavior under external load is considered. A force P applied to the second node in the vertical direction is taken into account (Figure 4.1b). Three values of load are considered, i.e., $P = \{1\text{kN}, 3\text{kN}, 5\text{kN}\}$. Material and geometric characteristics are assumed according to Table 4.1. The length of elements $l = 1\text{m}$ is assumed. In this case, the minimum level of initial prestress does not depend on external loads, so $S_{min} = 0$ is assumed. In turn, the maximum level of initial prestress for such data equals $S_{max} = 70\text{kN}$ and corresponds to the effort of the structure (3.22) equal to $\text{W}_{\max} = 0.85$. Assuming geometric and mechanical characteristics, the values of prestressing forces S are much lower than the longitudinal stiffness EA: (4.1)

$$S_{max} = 0.07\text{MN} \ll EA = 66\text{MN}.$$

Purpose of the Consideration

Determination of the influence of the initial prestress level S on static and dynamic parameters, including the influence on unstable regions, in an explicit manner.

4.2.1 QUALITATIVE ANALYSIS

The elongation matrix of structure (3.3) $B \in \mathbb{R}^{2\times 2}$ depends on the elongation row matrices for elements (Figure 4.1c):

$$B = \begin{bmatrix} \overline{B}^1 C^1 \\ \overline{B}^2 C^2 \end{bmatrix} = \begin{bmatrix} 1 & 0 \\ -1 & 0 \end{bmatrix}.$$

The singular value decomposition (3.7) of the matrix (4.2) leads do obtain the following matrices $Y \in \mathbb{R}^{2\times 2}$, $Z \in \mathbb{R}^{2\times 2}$, $X \in \mathbb{R}^{2\times 2}$: (4.2)

$$Y = \begin{bmatrix} \frac{\sqrt{2}}{2} & \frac{\sqrt{2}}{2} \\ -\frac{\sqrt{2}}{2} & \frac{\sqrt{2}}{2} \end{bmatrix}, Z = \begin{bmatrix} \sqrt{2} & 0 \\ 0 & 0 \end{bmatrix}, X = \begin{bmatrix} 1 & 0 \\ 0 & 1 \end{bmatrix}.$$

Because the matrix Z (4.2)$_2$ is square, according to dependence (3.16), the matrices $H \in \mathbb{R}^{2\times 2}$ and $L \in \mathbb{R}^{2\times 2}$ are the same: (4.3)

$$H = \text{diag}[2 \quad 0], \qquad L = \text{diag}[2 \quad 0].$$

The zero eigenvalue in the matrix H (4.4)$_1$ ($\mu_2 = 0$) is related to the existence of one self-stress state considered as an eigenvector related to the zero eigenvalue – the second column of the matrix Y (4.3)$_1$: (4.4)

$$y_S = y_2(\mu_2 = 0) = \begin{bmatrix} \frac{\sqrt{2}}{2} \\ \frac{\sqrt{2}}{2} \end{bmatrix} \xrightarrow{normalized} y_S = \begin{bmatrix} 1 \\ 1 \end{bmatrix}.$$

(4.5)

In turn, the zero eigenvalue in the matrix L (4.4)$_2$ $(\gamma_2 = 0)$ is related to the existence of one mechanism (Figure 4.2a) considered as an eigenvector related to the zero eigenvalue – the second column of the matrix X (4.3)$_3$ (Figure 4.2a):
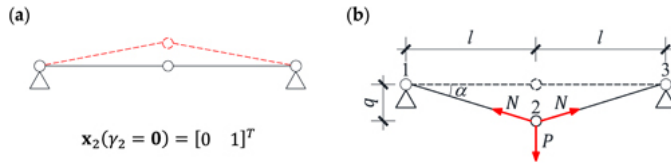

FIGURE 4.2 Two-element structure: (a) infinitesimal mechanism and (b) actual configuration.↵

$$x_S = x_2(\gamma_2 = 0) = \begin{bmatrix} 0 \\ 1 \end{bmatrix}.$$ (4.6)

In order to identify whether the mechanism (4.6) is infinitesimal or finite, the spectral analysis of the stiffness matrix (3.17) should be carried out.

In non-linear analysis, the stiffness matrix consists of the linear K_L, geometric $K_G(S)$, and non-linear $K_{N,NL}(q)$ parts. All matrices are built in accordance with finite element method rules (3.4). It should be noted that the geometric stiffness matrix depends on the self-equilibrated forces S (3.18), which are defined due to the existence of the self-stress state vector (4.5) – $S = [S \quad S]^T$. Therefore, the stiffness matrices take the following form:

$$K_L = \frac{2EA}{l} \begin{bmatrix} 1 & 0 \\ 0 & 0 \end{bmatrix}, K_G(S) = \frac{2S}{l} \begin{bmatrix} 1 & 0 \\ 0 & 1 \end{bmatrix}, K_{N,NL}(q) = \frac{EA}{l^3} \begin{bmatrix} q_1^2 & q_1 q_2 \\ q_1 q_2 & q_2^2 \end{bmatrix}.$$

However, in the spectral analysis (3.17), the stiffness matrix consists of two parts, i.e., the linear stiffness matrix (4.7)$_1$ and geometric stiffness matrix (4.7)$_2$. The eigenvalues of this matrix are as follows: (4.7)

$$o_1 = \frac{2(EA + S)}{l}, \qquad o_2 = \frac{2S}{l}.$$

The first value (4.8)$_1$ depends on both the longitudinal stiffnessEA and the prestressing forces S. The longitudinal stiffness is always positive; however, the prestressing forces S can be any number. Due to this, from the mathematical point of view, three cases would be occurred: (4.8)

- if $(EA + S) < 0$ – the eigenvalue (4.8)$_1$ is negative;
- if $(EA + S) = 0$ – the eigenvalue (4.8)$_1$ is equal to zero;
- if $(EA + S) > 0$ – the eigenvalue (4.8)$_1$ is positive.

For real structures, the values of prestressing forces S are much lower than the longitudinal stiffness ($S \ll EA$), thus the first value (4.8)$_1$ is always a positive number. However, this proves the spectral analysis of the stiffness matrix (3.19) needs to be performed including material and geometric characteristics.

In turn the second value (4.8)$_2$ depends only on the value of force S:

- if $S < 0$ (elements are compressed) – the eigenvalue (4.8)$_2$ is negative and the structure is unstable;

- if $S = 0$ – the eigenvalue $(4.8)_2$ is equal to zero, which corresponds to the finite mechanism;
- if $S > 0$ (elements are tensioned) – the eigenvalue $(4.8)_2$ is positive and the structure is stable; it means the self-stress states stabilize the mechanism, i.e., the mechanism is infinitesimal.

The stable structure $(S > 0)$ is characterized by four tensegrity features. It is a truss (TT) with tensile elements that have no rigidity in compression (TC) and in which there is one self-stress state (SS) that stabilizes one infinitesimal mechanism (IM). The features ($IN-$ the set of struts is contained within the continuous net of cables) and $(DS -$ the struts form a discontinuous set$)$ cannot be met because there are no struts. According to the tensegrity classification (Table 3.1), this is a *structure with tensegrity features of class 1*.

Despite the fact that this structure is not tensegrity, its behavior fully reflects the behavior of *ideal tensegrity* and *pure tensegrity* structures. A common feature of these three classes of structures is the infinitesimal mechanism stabilized by the self-stress state. In the following considerations, the behavior under external load is considered, which is responsible for displacements consistent with an infinitesimal mechanism.

4.2.2 STATIC ANALYSIS

The non-linear equation of a static equilibrium (3.23) for a considered truss is as follows:

$$\left\{ \frac{2EA}{l} \begin{bmatrix} 1 & 0 \\ 0 & 0 \end{bmatrix} + \frac{2S}{l} \begin{bmatrix} 1 & 0 \\ 0 & 1 \end{bmatrix} + \frac{EA}{l^3} \begin{bmatrix} q_1^2 & q_1 q_2 \\ q_1 q_2 & q_2^2 \end{bmatrix} \right\} \begin{bmatrix} q_1 \\ q_2 \end{bmatrix} = \begin{bmatrix} 0 \\ -P \end{bmatrix}.$$

Due to the symmetry of the structure and load, the displacement q_1 is zero. Taking to(4.9) simplify the notation $q = -q_2$, the equation (4.9) takes the following form:

$$[S + N(P)]q = \frac{Pl}{2},$$

where $\hspace{12cm}$ (4.10)

$$N(P) = \frac{EA}{2} \left(\frac{q}{l} \right)^2$$

is a longitudinal force caused by the load P. For a considered structure, it is possible(4.11) to obtain the formula for longitudinal forces $N(P + S)$ generated jointly by the external load P and prestress forces S. It can be simply determined by the static equilibrium of second node in the actual configuration (Figure 4.2b):

$$N(P + S) = \frac{P}{2 \sin \alpha}; \sin\alpha = \frac{q}{\sqrt{l^2 + q^2}}.$$

The application of non-linear theory (third-order theory) takes into account the(4.12) stiffening of the structure under the influence of an external load. The considered force stabilizes the mechanism. In the absence of initial prestress $(S = 0\text{kN})$, Equation (4.10) results in the calculation of the displacement

$$q(S = 0) = \sqrt[3]{\frac{P}{EA}} l.$$

In turn, if the influence of non-linear is neglected $(N(P) = 0)$, the solution of(4.13) Equation (4.10) results in the calculation of the displacement

$$q = \frac{Pl}{2S},$$

which increase to infinity in the absence of initial prestress $(S = 0)$. (4.14)

The influence of the initial prestress level S on the displacement q is shown in Figure 4.3a. The displacement is calculated using the second-order theory (4.14) and third-order theory (4.10), marked as II and III, respectively. The stiffness of the considered structure is not only conditioned on the geometry and material characteristics, but also on the initial prestress level S, which stabilizes the infinitesimal mechanisms, and on the external load P. With the increase of prestressing forces, the differences between the calculations made according to the second-order (II) and third-order (III) theories are decreasing. The influence of non-linearity is most significant at low values of initial prestress forces. Thereby, with lower values of the load, the initial prestress has a higher impact on the total rigidity of the structure, and the differences between the displacements obtained using the second- and third-order theory at $P = 1\text{kN}$ are smaller than those at $P = 5\text{kN}$.
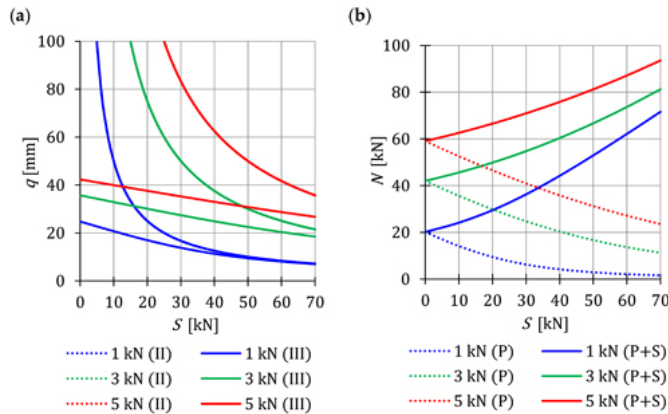
FIGURE 4.3 Influence of the initial prestress level S on the: (a) displacement q and (b) longitudinal force N. ⏎

In turn, Figure 4.3b shows the change in the value of longitudinal forces caused by loads (4.11) and the longitudinal forces generated jointly by the load and prestress forces (4.12), marked as (P) and $(P + S)$, respectively. The external load prestresses the structure; additional tensile forces are generated in the cables. However, after introducing the initial prestress, the longitudinal forces from the external load $N(P)$ successively decrease and thus its influence on the displacement decreases.

In considered structure, there is only one non-zero displacement, so the assessment of the behavior of this displacement (local assessment) is also an assessment of the behavior of the entire structure (global assessment). In the case of structures with many degrees of freedom, it is not possible to trace all displacements for objective reasons. Therefore, a *global stiffness parameter* GSP (3.32) that helps to assess the influence of the initial prestress on the total rigidity of the structure at a given load is proposed. In the case of the analyzed structure, the nature of changes in the GSP can be expressed explicitly as

$$GSP = \frac{q(0)}{q(S_i)}.$$

The influence of initial prestress level S on the GSP parameter is presented in Figure 4.4a. At the maximum level $S_{max} = 70$kN for the value of external force $P = 1$kN, the GSP parameter is 2.2 times higher than for the value $P = 5$kN. This confirms the previous conclusions. With lower external load, the initial prestress values have a higher impact on the overall stiffness of the structure. Additionally, due to the effect of the initial prestress on the longitudinal forces, the effort of structure W_{max} (3.22) is also monitored (Figure 4.4b). In this case, as in the case of the stiffness, the influence of the initial prestress decreases as the load increases.
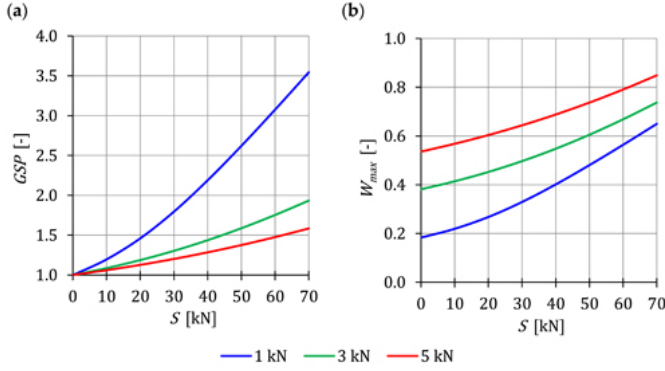
FIGURE 4.4 Influence of the initial prestress level *S* on the: (a) *global stiffness parameter GSP* and (b) effort of structure *W*$_{max}$. ⏎

4.2.3 DYNAMIC ANALYSIS

The dynamic response is studied by modal analysis (3.37). The mass matrix in the considered case takes the following form:

$$M = \frac{2\rho A l}{3} \begin{bmatrix} 1 & 0 \\ 0 & 1 \end{bmatrix}.$$

Taking into account, as before, the simplification $q = -q_2$ (the considered force P(4.15) makes the displacement q_1 equal to zero) and the dependence (4.11), the equation of motion (3.37) takes the following form:

$$\left\{ \frac{2EA}{l} \begin{bmatrix} 1 & 0 \\ 0 & 0 \end{bmatrix} + \frac{2S}{l} \begin{bmatrix} 1 & 0 \\ 0 & 1 \end{bmatrix} + \frac{N(P)}{l} \begin{bmatrix} 0 & 0 \\ 0 & 1 \end{bmatrix} - \Omega^2 \frac{2\rho A l}{3} \begin{bmatrix} 1 & 0 \\ 0 & 1 \end{bmatrix} \right\} \begin{bmatrix} q_1 \\ q_2 \end{bmatrix} = \begin{bmatrix} 0 \\ 0 \end{bmatrix}.$$

The non–trivial solution of equation (4.16) leads to the determination of the two (4.16) frequencies

$$f_1 = \frac{1}{2\pi} \sqrt{\frac{3[S + N(P)]}{\rho A l^2}}, f_2 = \frac{1}{2\pi} \sqrt{\frac{3(EA + S)}{\rho A l^2}},$$

and corresponding to them the vibration modes (Figure 4.5a, b): (4.17)

FIGURE 4.5 Vibration modes: (a) first mode $(4.18)_1$, and (b) second mode $(4.18)_2$. Influence of the initial prestress level S on the: (c) first frequency $(4.17)_1$ and (d) second frequency $(4.17)_2$.

$$a_1(f_1) = \begin{bmatrix} 0 \\ 1 \end{bmatrix}, a_2(f_2) = \begin{bmatrix} 1 \\ 0 \end{bmatrix}$$

(4.18)

> **NOTE**
>
> The first vibration mode $(4.18)_1$ describes the infinitesimal mechanism (4.6).

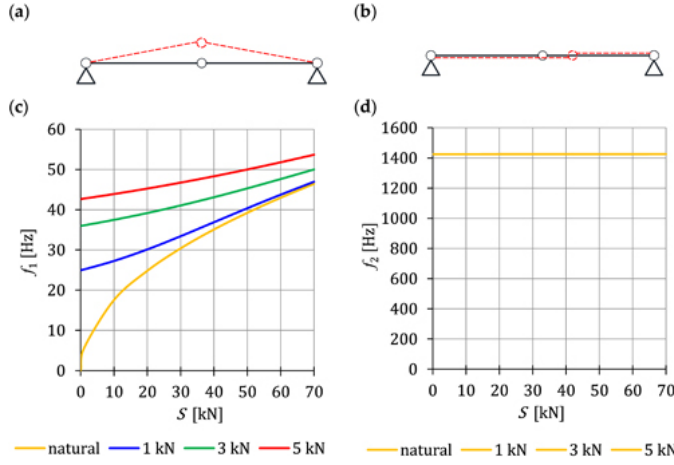The first frequency $(4.17)_1$ depends on both the initial prestress level S and the longitudinal force caused by the load $N(P)$ (4.11). However, the influence of the prestress diminishes with the rise in the load value. The external load P prestresses the structure. Additional tensile forces are generated in the cables and the initial dynamic response at $S = 0$ corresponds to the values of the natural frequency $f_1(0)$ at the following prestress levels: $S(P = 1\text{kN}) = 20.20\text{kN}$, $S(P = 3\text{kN}) = 42.11\text{kN}$, and $S(P = 5\text{kN}) = 59.12\text{kN}$. In turn, considering the natural frequency obtained from $(4.17)_1$ for $P = 0$

$$f_1(0) = \frac{1}{2\pi}\sqrt{\frac{3S}{\rho A l^2}},$$

it can be seen that it is highly dependent on the initial prestress level S: (4.19)

- if $S < 0$ (elements are compressed) – the frequency (4.19) is an imaginary number, which means the structure is unstable;
- if $S = 0$ – the frequency (4.19) is equal to zero which corresponds to the infinitesimal mechanism, described by the vibration mode $(4.18)_1$;
- if $S > 0$ (elements are tensioned) – the frequency (4.19) is positive and increases proportionally to the square root of the prestressing amplitude.

The influence of initial prestress level S on the first frequency is shown in Figure 4.5c.

The second frequency $(4.17)_2$ behaves quite differently. First, this frequency does not depend on the longitudinal force caused by the load $N(P)$. This means that the second

natural frequency and the free frequency are the same: $f_2 = f_2(0) = f_2(P)$. Second, the influence of initial prestress S is negligible because the values of prestress forces S are much lower than the longitudinal stiffness $(S_{max} \ll EA)$. In the absence of prestress $(S = 0)$, it is $f_2 = 1424.9\,\text{Hz}$, and at $S_{max} = 70\text{kN}$, it is $f_2 = 1425.6\text{Hz}$; the relative difference is equal $0.05\,\%$. In summary, the second vibration frequency does not depend on both changes in the level of prestress and the impact of external loads (Figure 4.5d).

4.2.4 DYNAMIC STABILITY ANALYSIS

In dynamic stability analysis a periodic character of force is taken into account. Resonance frequencies are determined using the harmonic balance method (3.53) and the small parameter method (3.74).

4.2.4.1 Harmonic Balance Method

Due to that, the displacement q_1 is zero and taking into account the simplification $q = -q_2$, Equation (3.53) takes the following form:

$$det\left\{ \frac{2EA}{l}\begin{bmatrix} 1 & 0 \\ 0 & 0 \end{bmatrix} + \frac{2S}{l}\begin{bmatrix} 1 & 0 \\ 0 & 1 \end{bmatrix} + \left(1 \pm \frac{1}{2}v\right)\frac{N(P)}{l}\begin{bmatrix} 0 & 0 \\ 0 & 1 \end{bmatrix} - \eta^2\frac{2\pi^2\rho Al}{3}\begin{bmatrix} 1 & 0 \\ 0 & 1 \end{bmatrix} \right\} = 0.$$

Solution of Equation (4.20) leads to obtain two resonance frequencies: (4.20)

$$\eta_1 = \frac{1}{\pi}\sqrt{\frac{3\left[S + \left(1 \pm \frac{1}{2}v\right)N(P)\right]}{\rho Al^2}}, \eta_2 = \frac{1}{\pi}\sqrt{\frac{3(EA + S)}{\rho Al^2}}.$$

The first resonant frequency $(4.21)_1$ depend on both the initial prestress level S and (4.21) the longitudinal force caused by the load $N(P)$ (4.11). Taking into account the time-independent load $(P_t = 0 \rightarrow v = 0)$, this frequency is twice the free frequency $(4.17)_1$ – $\eta_1 = 2f_1$. In turn, the second-resonant frequency $(4.21)_2$, as the free second frequency $(4.17)_2$, does not depend on longitudinal force caused by the load $N(P)$ and the initial prestress S $(S \ll EA)$. Additionally, it is twice the free second frequency – $\eta_2 = 2f_2$.

4.2.4.2 Small Parameter Method

Using the small parameter method, according to the algorithm, first the normalized dimensionless parameters (3.56) are calculated

$$\alpha_1 = \alpha_2 = \sqrt{\frac{3m_0}{2\rho Al}},$$

and the modal transformation matrix composed of M-orthonormal eigenvectors (4.22) (3.55) is build

$$V = \begin{bmatrix} 0 & \alpha_2 \\ \alpha_1 & 0 \end{bmatrix}.$$

Next, the geometric stiffness matrix (3.58) is formulated (4.23)

$$K_{GN} = \frac{N(P)}{l}\begin{bmatrix} 0 & 0 \\ 0 & 1 \end{bmatrix} \xrightarrow{\overset{*}{K}_{GN}=V^T K_{GN} V} \overset{*}{K}_{GN} = \begin{bmatrix} \frac{3m_0}{\rho Al^2}N(P) & 0 \\ 0 & 0 \end{bmatrix}.$$

Generally, the geometric stiffness matrix $\overset{*}{K}_{GN}$ is not a diagonal matrix. However, in this case it is. The pulsatility index (3.63) takes the following form:

$$v_G = \frac{3}{2}\frac{vN(P)}{\rho Al^2 \Omega_0^2}$$

and based on the formula (3.74), taking into account the first free vibration frequency including static component of periodic force P $(4.17)_1 \rightarrow \Omega_0 = 2\pi f_1$, the formula on first resonance frequency is obtained:

$$\eta_1 = \frac{1}{\pi}\sqrt{\frac{3\left[S + \left(1 \pm \frac{1}{2}v\right)N(P)\right]}{\rho Al^2}}.$$

It should be noted that both methods, i.e., HBM and SPM, result in the same formula for the first resonance frequency: $(4.21)_1 \equiv (4.26)$. Based on this, the boundaries of the first unstable region in the plane of parameters η and v can be determined. Using the HBM method, the independence of the second frequency from the load and the initial prestress was proven $(4.21)_2$. It means that only one main unstable region can be identified. This is because the structure is characterized by one infinitesimal mechanism.

The influence of the initial prestress level S and load on the main unstable region is shown. Three values of the constant part of periodic force are taken into account, i.e., $P = \{1\text{kN}, 3\text{kN}, 5\text{kN}\}$. For example, Figure 4.6 shows the boundaries for three cases of initial prestress level, i.e., $S_{min} = 0\text{kN}$, $S = 30\text{kN}$, and $S_{max} = 70\text{kN}$. These boundary values are between the dynamic stability and instability zones. As can be seen, independent of the value of prestress, the range of regions mostly depends on the load. The greater the load, the greater the region. At the same time, the higher the load, the higher the frequency. The introduction of prestress (Figure 4.6b, c) causes a decrease in the range of unstable regions and an increase in resonant frequencies. The initial prestress level has a greater influence on the range of the unstable regions when lower loads are applied. For example, in the case of $P = 1\text{kN}$, introducing the $S_{max} = 70\text{kN}$ results in an overlapping of the boundaries of unstable region (Figure 4.6c).
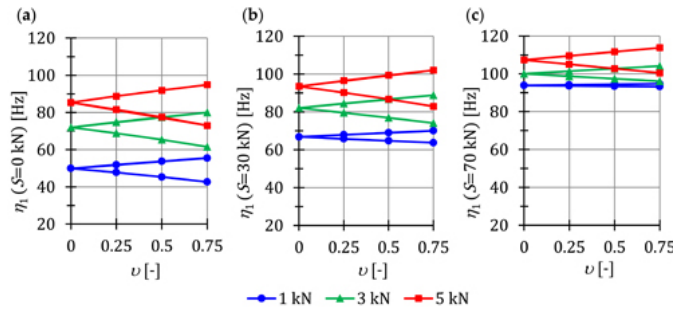

FIGURE 4.6 Limits of the main unstable region: (**a**) S = 0 kN, (**b**) S = kN, and (**c**) S = 70 kN.

To better compare the influence of the initial prestress level S and the load, Figure 4.7a shows the areas of unstable regions $A_\eta(S)$. Different behavior is observed depending on the value of the load. In the case of $P = 1\text{kN}$, the chart is almost an exponential function. In turn, in the cases of $P = 3\text{kN}$ and $P = 5\text{kN}$, the charts behave similarly. Comparing the load $P = 5\text{kN}$ with $P = 1\text{kN}$, the area of the unstable regions is larger by 1.7 (at $S = 0\text{kN}$), 3.0 (at $S = 30\text{kN}$), and 8.9 (at $S = 70\text{kN}$) times. In turn, comparing the load $P = 5\text{kN}$ with $P = 3\text{kN}$, the area of the unstable regions is larger by 1.2 (at $S = 0\text{kN}$), 1.3 (at $S = 30\text{kN}$), and 1.7 (at $S = 70\text{kN}$) times.
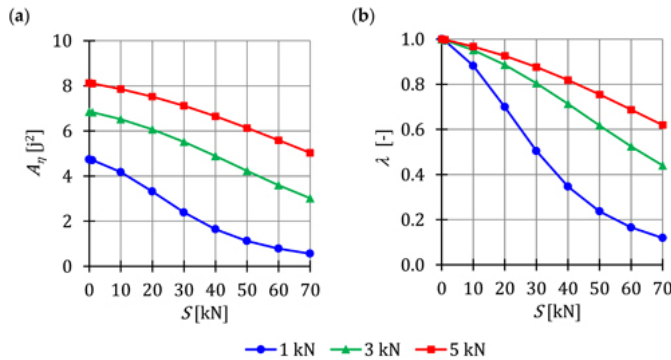

FIGURE 4.7 Influence of the initial prestress level S on the: (**a**) area of unstable regions $A_\eta(S)$ and (**b**) range of unstable regions λ. ↵

To measure the changes in the area of the unstable regions, the dimensionless parameter λ (3.75) is calculated (Figure 4.7b). In the case of the load $P = 1\text{kN}$, the parameter λ is equal: $\lambda = 0.88$ (at $S = 10\text{kN}$), $\lambda = 0.7$ (at $S = 30\text{kN}$), and $\lambda = 0.12$ (at $S = 70\text{kN}$), which means that the unstable regions are, respectively, 12%, 30%, and 88% smaller than those at the absence of the initial prestress $(S = 0\text{kN})$. In turn, in the case of the load $P = 5\text{kN}$, the unstable regions for the prestress levels assumed as previous is lower by 3% $(\lambda = 0.97)$, 8% $(\lambda = 0.92)$, and 38% $(\lambda = 0.62)$, respectively. As can be seen, load causes a different character of change in the parameter λ with a growth in the initial prestress level. For $P = 1\text{kN}$, the parameter λ decreases almost exponentially; in turn, for $P = 5\text{kN}$, it is a polynomial of second degree.

4.2.5 CHAPTER SUMMARY

The chapter is intended for beginners interested in tensegrity systems. Despite the fact that the analyzed two-element truss is not a tensegrity (this is only a *structure with tensegrity features of class 1*), its behavior fully reflects the behavior of tensegrity structures. This is because the structure is characterized by two immanent features of tensegrity systems, i.e., self-stress state and infinitesimal mechanism. This example makes it easier to understand the behavior of tensegrity structures due to its simplicity. For such a simple structure, it is possible to determine the impact of the initial prestress level S on the static and dynamic parameters in explicit forms. The considerations serve as an explanation of the use of the non-linear analysis of tensegrity systems that stiffen under the application of the external load.

In addition, it is easily proven that both the harmonic balance method and the small parameter method give the same results.

4.3 SIX-ELEMENT TRUSS (X-TRUSS)

The concept of tensegrity is understood in many ways. This term is often improperly used for structures that have some, but not necessarily the key tensegrity properties. This idea is misused in reference to both mathematical models and completed engineering structures. To explain the sense of the proposed classification (Table 3.1), the behavior of a truss with six elements $(n = 6)$ (Figure 4.8a) is considered. For this truss, the self-stress state can be simply determined by the static equilibrium of nodes (Figure 4.8b):
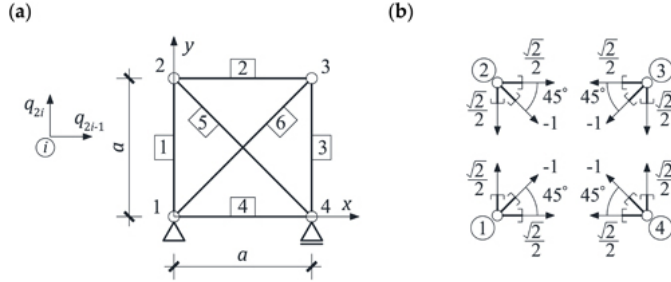

FIGURE 4.8 Six-element truss: (a) geometry and (b) static equilibrium of nodes (the self-stress state).

$$y_S = \left[\begin{array}{cccccc} \frac{\sqrt{2}}{2} & \frac{\sqrt{2}}{2} & \frac{\sqrt{2}}{2} & \frac{\sqrt{2}}{2} & -1 & -1 \end{array} \right]^T.$$

It can be seen that static equilibrium also exists for forces opposite to (4.27). For this reason, two variants of the type of element are taken into account: (4.27)

- the structure with two struts (*X-truss*) (Figure 4.9a);
- the structure with four struts (Figure 4.9b).
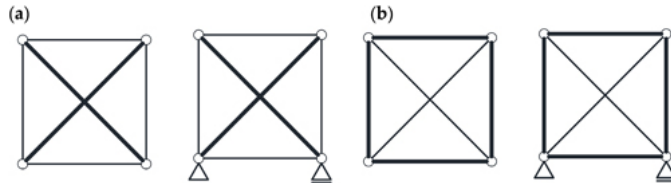
FIGURE 4.9 Six-element truss with: (**a**) two struts (*X-truss*) and (**b**) four struts.

The qualitative analysis is performed for unsupported and supported trusses. The considerations are presented in detail. In turn, the quantitative analysis includes the behavior of the supported *X-truss* (Figure 4.9a). The values of the self-stress state are taken according to the vector (4.27). Material and geometric characteristics are assumed according to Table 4.1. Taken into account the dimension $a = 1m$ means the length of the struts is $l = 1.4m$ with a load-bearing capacity of $N_{b,Rd} = 170.5kN$ (Table 4.2). The truss is loaded by one force applied to second node. Two cases of direction are considered, i.e., the vertical $P_y = P$ and horizontal $P_x = P$ (Figure 4.10a). In order to illustrate the influence of external loads on the behavior of a structure, three values of load are taken into account, i.e., $P = \{1 \text{ kN}, 5 \text{ kN}, 10 \text{ kN}\}$. For both cases of load, the maximum prestress level is assumed to be $S_{max} = 130kN$, and corresponds to the effort of the structure (3.16) equal to $W_{max} = 0.91$. In turn, the minimum prestress level depends on the load. For vertical load P_y, it is equal to $S_{min} = 0$, which means an external load causes an appropriate distribution of longitudinal forces (Figure 4.10b). In the case of the

horizontal load P_x, it does not (Figure 4.10c). In order to obtain a proper distribution of longitudinal forces, the structure must be compressed with a minimum prestress level $S_{\min} > 0.3535\ P_x$.
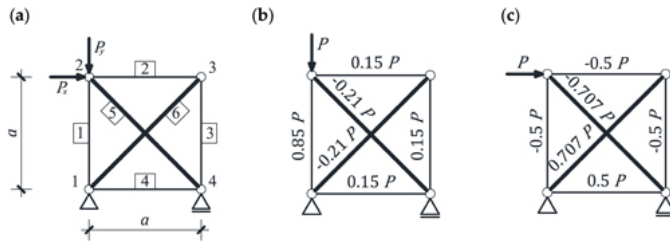
FIGURE 4.10*X-truss*: (a) scheme of loading regime; longitudinal forces caused by the load: (b) $P_y = P$, and (c) $P_x = P$.↵

Purpose of Consideration
Answer the following questions:

1. What is the difference between a finite and an infinitesimal mechanism?
2. Does the self-stress state depend on support?
3. How does the structure behave without the infinitesimal mechanism?
4. Is the term 'tensegrity' always used justifiably?

4.3.1 QUALITATIVE ANALYSIS

4.3.1.1 Unsupported Six-Element Truss

An unsupported truss is characterized by eight degrees of freedom $(m = 8)$ $q = [q_1\ \ q_2\ \ q_3\ \ q_4\ \ q_5\ \ q_6\ \ q_7\ \ q_8]^T$. The elongation matrix of structures (3.3) $B \in \mathbb{R}^{6\times 8}$ takes the form:

$$B = \begin{bmatrix} 0 & -1 & 0 & 1 & 0 & 0 & 0 & 0 \\ 0 & 0 & -1 & 0 & 1 & 0 & 0 & 0 \\ 0 & 0 & 0 & 0 & 0 & 1 & 0 & -1 \\ -1 & 0 & 0 & 0 & 0 & 0 & 1 & 0 \\ 0 & 0 & -0.707 & 0.707 & 0 & 0 & 0.707 & -0.707 \\ -0.707 & -0.707 & 0 & 0 & 0.707 & 0.707 & 0 & 0 \end{bmatrix}.$$

The singular value decomposition (3.7) of the matrix (4.28) leads to obtain the(4.28) following matrices $Y \in \mathbb{R}^{6\times 6}$, $Z \in \mathbb{R}^{6\times 8}$, $X \in \mathbb{R}^{8\times 8}$:

$$Y = \begin{bmatrix} 0.35 & 0 & 0.87 & 0 & 0 & 0.3535 \\ 0.35 & 0.3 & -0.29 & -0.76 & -0.07 & 0.3535 \\ 0.35 & -0.78 & -0.29 & 0.15 & -0.21 & 0.3535 \\ 0.35 & 0.47 & -0.29 & 0.60 & 0.28 & 0.3535 \\ 0.5 & -0.21 & 0 & -0.14 & 0.66 & -0.5 \\ 0.5 & 0.21 & 0 & 0.14 & -0.66 & -0.5 \end{bmatrix},$$

$$
Z = \begin{bmatrix}
2 & 0 & 0 & 0 & 0 & 0 & 0 & 0 \\
0 & 1.41 & 0 & 0 & 0 & 0 & 0 & 0 \\
0 & 0 & 1.41 & 0 & 0 & 0 & 0 & 0 \\
0 & 0 & 0 & 1.41 & 0 & 0 & 0 & 0 \\
0 & 0 & 0 & 0 & 1.41 & 0 & 0 & 0 \\
0 & 0 & 0 & 0 & 0 & 0 & 0 & 0
\end{bmatrix},
$$

$$
X = \begin{bmatrix}
-0.35 & -0.44 & 0.2 & -0.5 & 0.13 & 0.51 & -0.33 & 0.04 \\
-0.35 & -0.1 & -0.61 & -0.07 & 0.33 & 0.11 & 0.57 & 0.18 \\
-0.35 & -0.11 & 0.2 & 0.61 & -0.28 & 0.43 & 0.25 & -0.36 \\
0.35 & -0.1 & 0.61 & -0.07 & 0.33 & 0.11 & 0.57 & 0.18 \\
0.35 & 0.31 & -0.2 & -0.46 & -0.38 & 0.43 & 0.25 & -0.36 \\
0.35 & -0.44 & -0.2 & 0.18 & -0.48 & 0.19 & -0.01 & 0.58 \\
0.35 & 0.23 & -0.2 & 0.35 & 0.53 & 0.51 & -0.33 & 0.04 \\
-0.35 & 0.65 & 0.2 & -0.04 & -0.18 & 0.19 & -0.01 & 0.58
\end{bmatrix}.
$$

According to dependence (3.16), the matrices $H \in \mathbb{R}^{6 \times 6}$ and $L \in \mathbb{R}^{8 \times 8}$ are as (4.31) follows:

$$
H = \mathrm{diag}[4 \quad 2 \quad 2 \quad 2 \quad 2 \quad 0], L = \mathrm{diag}[4 \quad 2 \quad 2 \quad 2 \quad 2 \quad 0 \quad 0 \quad 0]
$$

The zero eigenvalue in the matrix H $(4.32)_1$ $(\mu_6 = 0)$ is related to the existence of (4.32) one self-stress state considered as an eigenvector related to the zero eigenvalue – the sixth column of the matrix Y (4.29):

$$
y_6(\mu_6 = 0) = [0.3535 \quad 0.3535 \quad 0.3535 \quad 0.3535 \quad -0.5 \quad -0.5]^T.
$$

The vector (4.33) is a normalized vector (4.27) determined by the static equilibrium (4.33) of nodes (Figure 4.8b).

In turn, there are three zero eigenvalues in the matrix $L (4.32)_2$ $(\gamma_6 = \gamma_7 = \gamma_8 = 0)$, which means three mechanisms are identified. These mechanisms are considered as eigenvectors related to the zero eigenvalues – the sixth, seventh, and eighth columns of matrix X (4.31):

$$
x_6(\gamma_6 = 0) = [0.51 \quad 0.11 \quad 0.43 \quad 0.11 \quad 0.43 \quad 0.19 \quad 0.51 \quad 0.19]^T
$$

$$
x_7(\gamma_7 = 0) = [-0.33 \quad 0.57 \quad 0.25 \quad 0.57 \quad 0.25 \quad -0.01 \quad -0.33 \quad -0.01]^T
$$

$$
x_8(\gamma_8 = 0) = [0.04 \quad 0.18 \quad -0.36 \quad 0.18 \quad -0.36 \quad 0.58 \quad 0.04 \quad 0.58]^T \quad (4.34)
$$

In order to identify whether the mechanisms (4.34) are infinitesimal or finite, the spectral analysis of the stiffness matrix (3.17) should be applied. The linear stiffness matrix with the unit elasticity matrix $E \equiv I$ is considered. In turn, the geometric stiffness matrix can be built due to the existence of the self-stress state vector (4.27), and the spectral analysis leads to obtaining the following eigenvalues:

$$O = \mathrm{diag}[3.41 \quad 3.41 \quad 3.41 \quad 2.83 \quad 0.59 \quad 0 \quad 0 \quad 0 \;].$$

Three zero eigenvalues in (4.35) mean the mechanisms are finite; a distance (4.35) between any pair of nodes does no change (Figure 4.11).
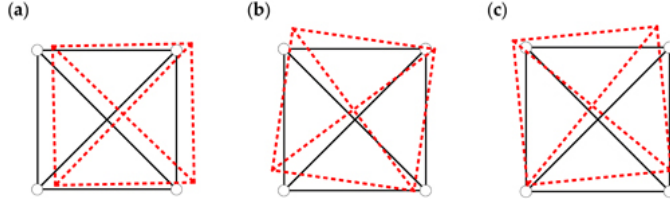
FIGURE 4.11 Finite mechanisms of unsupported six-element truss (4.34): (a) $\mathbf{x}_6$, (b) $\mathbf{x}_7$, and (c) $\mathbf{x}_8$.↵

4.3.1.2 Supported Six-Element Truss

A supported truss is characterized by five degrees of freedom $(m = 5)$ $q = [q_3 \; q_4 \; q_5 \; q_6 \; q_7]^T$. The elongation matrix of structures (3.3) takes the form $B \in \mathbb{R}^{6 \times 5}$:

$$B = \begin{bmatrix} 0 & 1 & 0 & 0 & 0 \\ -1 & 0 & 1 & 0 & 0 \\ 0 & 0 & 0 & 1 & 0 \\ 0 & 0 & 0 & 0 & 1 \\ -0.707 & 0.707 & 0 & 0 & 0.707 \\ 0 & 0 & 0.707 & 0.707 & 0 \end{bmatrix}$$

The singular value decomposition (3.7) of the matrix (4.36) leads to obtain the (4.36) following matrices $Y \in \mathbb{R}^{6 \times 6}$, $Z \in \mathbb{R}^{6 \times 5}$, $X \in \mathbb{R}^{5 \times 5}$:

$$Y = \begin{bmatrix} -0.21 & 0.35 & -0.25 & -0.71 & -0.38 & -0.3535 \\ -0.69 & -0.35 & 0.52 & 0 & 0.05 & -0.3535 \\ -0.11 & -0.35 & -0.69 & 0 & 0.51 & -0.3535 \\ -0.21 & 0.35 & -0.25 & 0.71 & -0.38 & -0.3535 \\ -0.57 & 0.5 & -0.12 & 0 & 0.4 & 0.5 \\ -0.30 & -0.5 & -0.35 & 0 & -0.54 & 0.5 \end{bmatrix},$$

(4.37)

$$Z = \begin{bmatrix} 1.7 & 0 & 0 & 0 & 0 \\ 0 & 1.41 & 0 & 0 & 0 \\ 0 & 0 & 1.16 & 0 & 0 \\ 0 & 0 & 0 & 1 & 0 \\ 0 & 0 & 0 & 0 & 0.51 \\ 0 & 0 & 0 & 0 & 0 \end{bmatrix},$$

$$X = \begin{bmatrix} 0.64 & 0 & -0.37 & 0 & -0.67 \\ -0.35 & 0.5 & -0.29 & -0.71 & -0.19 \\ -0.53 & -0.5 & 0.23 & 0 & -0.64 \\ -0.19 & -0.5 & -0.8 & 0 & 0.26 \\ -0.36 & 0.5 & -0.28 & 0.71 & -0.19 \end{bmatrix}.$$

According to dependence (3.16), the matrices $H \in \mathbb{R}^{6 \times 6}$ and $L \in \mathbb{R}^{5 \times 5}$ are, (4.39) respectively,

$$H = \mathrm{diag}[2.89 \quad 2 \quad 1.35 \quad 1 \quad 0.25 \quad 0 \;], \quad L = \mathrm{diag}[2.89 \quad 2 \quad 1.35 \quad 1 \quad 0.25]$$

The zero eigenvalue in the matrix H (4.40)$_1$ ($\mu_6 = 0$) is related to the existence of (4.40) one self-stress state considered as an eigenvector related to the zero eigenvalue – the sixth column of the matrix Y (4.37):

$$y_6(\mu_6 = 0) = [-0.3535 \quad -0.3535 \quad -0.3535 \quad -0.3535 \quad 0.5 \quad 0.5 \;]^T.$$

At this point, it should be noted that the vector (4.41) is opposite to the vector (4.41) (4.33). From the mathematical point of view, it does not matter. Equilibrium occurs, and the self-stress state does not depend on the support. However, from the physical point of view, the truss can be built with two struts and four cables (4.33) (Figure 4.9a) or with four struts and two cables (4.41) (Figure 4.9b).

In turn, the absence of a zero eigenvalue in the matrix L (4.40)$_2$ means that no mechanism has been identified. Despite the fact that there is no mechanism, the stability of structures should be checked. As before, the linear stiffness matrix with the unit elasticity matrix $E \equiv I$ is considered. The spectral analysis of the stiffness matrix (3.17) leads to obtain two different solutions depending on the self-stress vector:

$$y_6(4.33) \xrightarrow{\text{yields}} O = \mathrm{diag}[3.17 \quad 2.87 \quad 1.71 \quad 0.54 \quad 0.25],$$

$$y_6(4.41) \xrightarrow{\text{yields}} O = \mathrm{diag}[2.62 \quad 1.71 \quad 0.38 \quad 0.29 \quad 0 \;].$$

The obtained results mean that in the case of a truss with four struts (4.42)$_1$, (4.42) prestressing forces are balanced with stiffness (see the qualitative analysis for two-element structure, Equation (4.8)$_1$, the case – $(EA + S) = 0$). It is not true. Assuming the unit elasticity matrix $E \equiv I$ does not include the correct stiffness of the structure. If the material and geometric characteristics are included, the spectral analysis (3.17) leads to obtaining positive eigenvalues:

$$y_6(4.32) \xrightarrow{\text{yields}} O = \mathrm{diag}[2.3 \quad 1.6 \quad 0.9 \quad 0.6 \quad 0.2]*10^5,$$

$$y_6(4.41) \xrightarrow{\text{yields}} O = \mathrm{diag}[3.1 \quad 1.9 \quad 1.6 \quad 1.4 \quad 0.2]*10^5,$$

which means that a supported truss is stable independently of the number of struts. (4.42a)

4.3.1.3 Conclusion

The structure with two struts (Figure 4.9a) is characterized by four tensegrity features. It is a truss (TT) with a set of struts contained within the continuous net of tensile elements (IN) that have no rigidity in compression (TC) and in which there is one self-stress state (SS). According to the tensegrity classification (Table 3.1), due to a lack of mechanism, it is a *structure with tensegrity features of class 2*. This truss is the most popular structure in the literature, usually referred to as 'the simplest 2D tensegrity structure', called Snelson's X tensegrity module (Ashwear and Eriksson, 2014; Ashwear et al., 2016; Cai et al., 2018; Connelly and Back, 1998; Lee, 2012; Masic and Skelton, 2002; Moored and Bart–Smith, 2009; Moored et al., 2011; Pełczyński and Gilewski, 2018; Pagitz and Tur, 2009; Pugh, 1976; Skelton and de Oliveira, 2009, 2010; Skelton et al., 2001a, 2001b, 2002; Tibert, 2002; Tibert and Pellegrino, 2003; Tran and Lee, 2010a, 2010b, 2010c; Williamson et al., 2003a, 2003b; Xu et al., 2018; Zhang, 2007; Zhang and Ohsaki, 2007; Zhang L.Y. et al., 2014).

In turn, the structure with four struts (Figure 4.9b) is characterized only by three tensegrity features. It is the truss (TT) with tensile elements that have no rigidity in compression (TC) and in which there is one self-stress state (SS). This means that it cannot be classified into any group. It is a non-tensegrity structure.

4.3.2 STATIC ANALYSIS

The *X-truss* is a *structure with tensegrity features of class 2*, it means that it is devoid of mechanisms. The global stiffness parameter (3.32) is equal to $GSP = 1$, independent of the value and direction of the load and the initial prestress level S. In this case, the second-order theory is sufficient for the calculation. The load-bearing characteristics are shown in Tables 4.3 and 4.4, respectively for the load P_y and P_x. The displacements are insensitive to the change in the prestress level (e.g., the displacements according to the direction of load are shown). Only longitudinal forces N and the effort of the structure W_{max} are changed. These quantities are linearly dependent on the initial prestress level, because the longitudinal forces caused by load P are independent of the value of prestress. In Figure 4.12, the value of longitudinal forces arising from loads (marked as (P)) and the longitudinal forces generated jointly by the load and prestress forces (marked as (P+S)) are shown.

TABLE 4.3 Strength Characteristics of the *X-truss* Loaded by the Force P_y ↵

S(kN)	Type of Element	P_y = 1k		P_y = 5kN		P_y = 10 kN	
		W_{max} (-)	q_y (mm)	W_{max} (-)	q_y (mm)	W_{max} (-)	q_y (mm)
0	Cables	0.01	–0.13	0.04	–0.06	0.08	–0.128
	Struts	0.00		0.01		0.01	
70	Cables	0.46	–0.13	0.49	–0.06	0.53	–0.128
	Struts	0.41		0.42		0.42	
130	Cables	0.84	–0.13	0.87	–0.06	0.91	–0.128
	Struts	0.76		0.77		0.77	

TABLE 4.4 Strength Characteristics of the *X-truss* Loaded by the Force P_x ↵

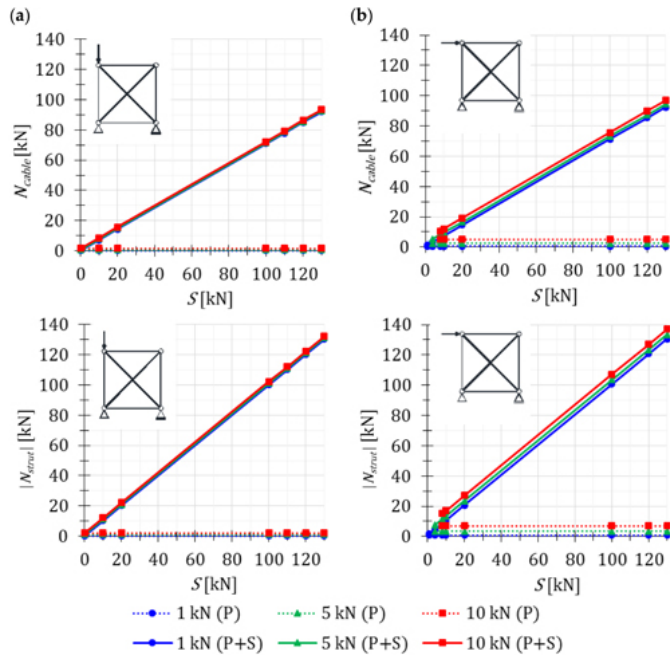| S(kN)	Type of element	P_x = 1 kN(S_{min} = 1 kN)		P_x = 5 kN(S_{min} = 4 kN)		P_x = 10 kN(S_{min} = 8 kN)	
		W_{max} (-)	q_x (mm)	W_{max} (-)	q_x (mm)	W_{max} (-)	q_x (mm)
S_{min}	Cables	0.01	0.025	0.05	0.125	0.10	0.249
	Struts	0.00		0.04		0.09	
70	Cables	0.45	0.025	0.47	0.125	0.49	0.249
	Struts	0.41		0.43		0.45	
130	Cables	0.84	0.025	0.86	0.125	0.88	0.249
	Struts	0.77		0.78		0.80	

FIGURE 4.12 Influence of the initial prestress level *S* on the longitudinal force *N*: (a) caused by the force P_y and (**b**) caused by the force P_x.

4.3.3 DYNAMIC ANALYSIS

The static assessment showed insensitivity to a change in the level of initial prestress S. The same is true in the dynamic assessment (Table 4.5). Independent of the initial prestress level, the natural frequency $f(0)$ and free frequency $f(P)$ are constant; the relative increase is 0.06% for all frequencies. Additionally, the free frequencies do not depend on the load. This means that the natural frequency and the free frequency are the same.

TABLE 4.5 Natural and Free Frequency of the *X-Truss*

S(kN)	f_1 (0)(Hz)	f_2 (0)(Hz)	P = 1 kN		P = 5 kN		P = 10 kN	
			f_1 (Hz)	f_2 (Hz)	f_1 (Hz)	f_2 (Hz)	f_1 (Hz)	f_2 (Hz)
S_{min}	317.0	644.3	317.0	644.3	317.0	644.3	317.0	644.3
130	317.2	644.7	317.2	644.7	317.2	644.7	317.2	644.7

Since the *X-truss* does not have a mechanism (is geometrically invariant), it is possible to perform modal analyze in the Autodesk Robot Structural Analysis. This example allows us to verify the calculation procedure written in the Mathematica environment. Assuming comparable geometric characteristics of the struts (the Halfen DETAN Rod System is not included in the program), i.e., the diameter $\phi = 70[\text{mm}]$ and thickness $t = 3.2[\text{mm}]$, the following frequencies were obtained: $f_1 = 318.14[\text{Hz}]$ and $f_2 = 649.04[\text{Hz}]$. The maximum relative difference of 0.7% results from the difference in cross-sectional areas. In the case of the assumed struts, it is equal to $A = 6.72 \cdot 10^{-4}[\text{m}^2]$ and is 0.7% smaller.

4.3.4 DYNAMIC STABILITY ANALYSIS

As previous analysis, the dynamic stability assessment showed insensitivity to the change in the level of initial prestress S (Table 4.6). Independent of the initial prestress level, the

resonance frequency $f(0)$ and free frequency $f(P)$ are constant; the relative increase is 0.08% for all frequencies. Additionally, the resonance frequencies do not depend on the load.

TABLE 4.6 First- and Second-Resonance Frequencies of the *X-Truss* ↵

S(kN)	P = 1 kN		P = 5 kN		P = 10 kN	
	η_1 (Hz)	η_2 (Hz)	η_1 (Hz)	η_2 (Hz)	η_1 (Hz)	η_2 (Hz)
S_{min}	634.0	1288.5	634.0	1288.5	634.0	1288.5
130	634.5	1289.5	634.5	1289.5	634.5	1289.5

4.3.5 CHAPTER SUMMARY

The chapter considers a simple and very popular example in the literature, the so-called Snelson's X tensegrity module. The behavior of structures characterized by only one of the two immanent features of tensegrity systems, i.e., the self-stress state, is shown. These considerations explain the proposed classification, in particular, the differences between a *structure with tensegrity features of class 2* and a *structure with tensegrity features of class 1* (see 4.2). Additionally, the differences between a finite and an infinitesimal mechanism are explained. For clarity, the summary is presented as the answers to the questions posed at the beginning of the consideration.

1. What is the difference between a finite and an infinitesimal mechanism?

The occurrence of a mechanism characterizes a geometrically variable structure. It means that the occurrence of displacements is not necessarily associated with the appearance of the generation of internal forces. Mechanisms can be finite (rigid body movements) or infinitely small (infinitesimal). Finite mechanisms refer to movements that do not change the distance between any pair of nodes (Figure 4.9). Infinitesimal mechanisms, on the other hand, describe local geometric variation in the range of small displacements (Figure 4.1c). These mechanisms are stabilized by introducing the initial prestress. It should be noted that a mechanism is an eigenvalue of a structure.

2. Does the self-stress state depend on support?

In the case of *X-truss*, the self-stress state does not depend on support. However, sometimes struts have been replaced by the supports (see Sections 4.2.1, 4.4.1, and 4.6.1).

3. How does the structure behave without the infinitesimal mechanism?

In the case of a structure without the infinitesimal mechanism, the initial prestress has no effect on displacements, stiffness (GSP), natural, free, and resonance frequencies. Only longitudinal forces linearly changed according to the initial prestress introduced. Due to this, the effort of the structure W_{max} has also changed. Therefore, the question arises: what is the point of introducing an initial prestress in a structure without the infinitesimal mechanism? In these cases, it is necessary to obtain a proper distribution of the longitudinal forces. This means that for structures without mechanisms, the minimum prestress level S_{min} should be introduced.

4. Is the term 'tensegrity' always used justifiably?

In general, the term 'tensegrity' is often misused in the literature, and these structures are not related to true tensegrity, which is characterized by special features distinguishing

them from conventional systems (Obara et al., 2019). From the architectural aspect, the possibility of creating new forms of '*islands of compression in a sea of tension*' is the most important. This means that the most important thing is to find a self-balancing configuration of systems (form-finding). However, from a mechanical point of view, the most interesting are structures characterized by the occurrence of infinitesimal mechanisms. Of course, these systems have to be additionally characterized by the self-equilibrated systems of longitudinal forces (self-stress states), which stabilize mechanisms. When teaching structural mechanics, it is said that building structures cannot be geometrically variable. The uniqueness of tensegrity structures is that geometric variability is their great advantage. Mechanisms in tensegrity structures allow control of their static and dynamic properties. This control is achieved by changing the level of initial prestress, i.e., the system of self-balancing internal forces.

The proposed classification systematizes and precisely defines tensegrity structures, minimizing the misuse of the term to refer to structures that are not them. Additionally, in engineering practice, such systematization facilitates the analysis and design of tensegrities. It is a consequence of the different behavior of structures under the influence of external loads.

Some examples of two-dimensional structures, which in the literature are referred to as tensegrity structures, are shown in Figure 4.13. The analysis, based on the tensegrity classification (Table 3.1), showed that in some cases, the term 'tensegrity' is used unjustifiably. The structure shown in Figure 4.13a (Zhang J.Y. et al., 2009, 2010) has only one characteristic feature, which is that it is a truss (TT). Three next trusses are characterized additionally by the existence of the self-stress state (SS), i.e., Figure 4.13b (Lee, 2012), Figure 4.13c (Lee, 2012; Michelettand and Cadoni, 2011; Paul et al., 2005; Pugh, 1976), and Figure 4.13d (Paul et al., 2005; Pugh, 1976; Zhang, 2007). However, none of these trusses can be referred to as tensegrity due to the absence of the other characteristic features.
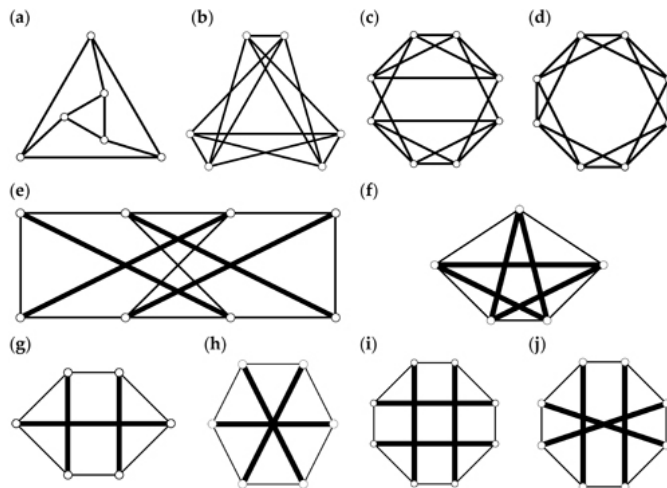
FIGURE 4.13 Truss: (a)–(d) non-tensegrity structures, (e)–(f) *structures with tensegrity features of class 2*, and (**j**) *ideal tensegrity*. ⏎

The structures shown in Figure 4.13e (De Jager and Skelton, 2006; Masic and Skelton, 2002, 2006; Masic et al., 2005, 2006; Zhang J.Y. et al., 2010) and in Figure 4.13f (Micheletti, 2008) have four characteristic features: they are trusses (TT) with a self-stress state (SS), built with cables (TC), and the set of struts is contained within the continuous net of cables (IN). It means they are *structures with tensegrity features of class 2*.

Ideal tensegrity structures, characterized by all characteristic features occurring, are shown in Figures 4.13g–j: Figure 4.13g (Cai et al., 2018; Estrada et al., 2006; Lee, 2012; Micheletti, 2008; Pugh, 1976; Tibert, 2002; Tibert and Pellegrino, 2003; Tran and Lee, 2010a, 2011a, 2011b, 2011c; Volokh, 2003; Xu et al., 2018; Zhang J.Y. et al., 2006; Zhang L.Y. et al., 2014, 2018), Figure 4.13h (Michelettand and Cadoni, 2011; Pugh, 1976; Paul et al., 2005; Zhang, 2007; Zhang L.Y. et al., 2014), Figure 4.13i (Lee, 2012; Zhang L.Y. et al., 2018), and Figure 4.13j (Kasprzak, 2014; Koohestani and Guest, 2013; Motro, 2003; Zhang L.Y. et al., 2014, 2018).

4.4 BASIC 2D TENSEGRITY MODELS

The basic two-dimensional (2D) models contain trusses, which can be used to create tensegrity *Geiger domes*. Two variants of connecting in the center of the span are considered, i.e., girders connected by a strut (*type A*) and by cables (*type B*). The qualitative analysis is performed for two basic models (*A-0* and *B-0*) and their extensions. The extended models are created by adding repetitive levels consisting of two struts and five cables. The number after a letter means a number of additional levels, i.e., *A-1* and *B-1* – one additional level is added, *A-2* and *B-2* – two additional levels. Six models are analyzed, i.e.:

- *Geiger truss type A-0* (Figure 4.14a);
- *Geiger truss type B-0* (Figure 4.14b);
- *Geiger truss type A-1* (Figure 4.15a);
- *Geiger truss type A-2* (Figure 4.15c);
- *Geiger truss type B-1* (Figure 4.15b);
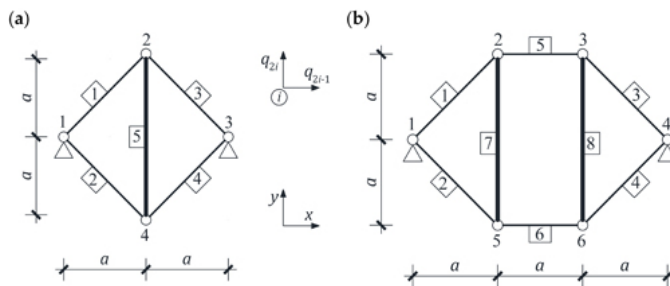- *Geiger truss type B-2* (Figure 4.15d).

FIGURE 4.14 Basic two-dimensional models: (**a**) *Geiger truss type A-0* and (**b**) *Geiger truss type B-0.* ↵
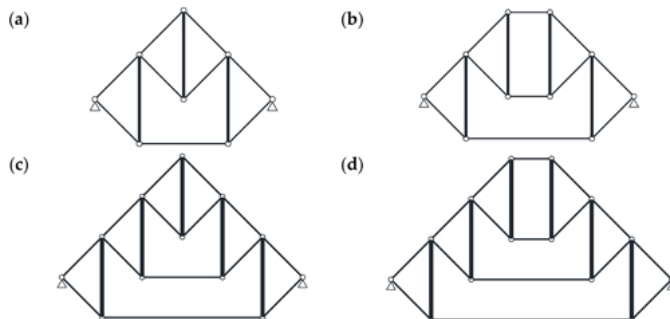

FIGURE 4.15 Extended *Geiger truss type:* (a) *A-1*, (b) *B-1*, (c) *A-2*, and (d) *B-2.* ↵

For the *Geiger truss type A-0* and *type B-0*, the considerations are presented in detail. In turn, for the extended *Geiger truss* only the results of the analysis are presented. The formulas for longitudinal self-stress forces are derived. In turn, the quantitative analysis includes the behavior of the *Geiger truss type B-0*. Material and geometric characteristics are assumed according to Table 4.1. In this case, an attempt is made to analyze the behavior of the structure, in which the load-bearing capacity of the struts is much lower than that of the cables. For this purpose, the dimension $a = 2.1\text{m}$ is assumed (the length of the struts is $l = 4.2\text{m}$, and their load-bearing capacity is $N_{b,Rd} = 41.9$ kN (Table 4.2). In order to illustrate the influence of external loads on the behavior of a structure, two types of load are considered, i.e., symmetrical load (two forces applied to the second and third nodes) and asymmetrical load (one force applied to the second node). Three values of load are taken into account, i.e., $P = \{1\text{kN}, 5\text{kN}, 10\text{kN}\}$. The range of initial prestress depends on the case of the load:

- in the case of symmetrical load, the maximum prestress level is assumed to be $S_{max} = 35\text{kN}$, and corresponds to the effort of the structure (3.22) equal to $\text{W}_{max} = 0.94$, whereas the minimum level depends on the value of load; in order to obtain a proper distribution of longitudinal forces, the structure must be compressed with a minimum prestress level $S_{min} > 0.56\ P$;
- in the case of asymmetrical load, the maximum prestress level is assumed to be $S_{max} = 20\text{kN}$, and corresponds to the effort of the structure (3.22) equal to $\text{W}_{max} = 0.96$, whereas the minimum level is equal to $S_{min} = 0$, which means an external load causes an appropriate distribution of longitudinal forces.

Purpose of the Consideration

This section presents basic tensegrity trusses that can be used to create Geiger domes, addressing the following questions:

1. Is it possible to derive formulas for self-equilibrium forces (self-stress state)?
2. How does the structure behave when the load causes the displacements that are incompatible with an infinitesimal mechanism?
3. How does the structure behave when the load causes the displacements that are comapatibble with an infinitesimal mechanism?
4. How does the structure behave when the load capacity of the struts is much smaller than the load capacity of the cables?

4.4.1 QUALITATIVE ANALYSIS

4.4.1.1Geiger Truss Type A-0

The *Geiger truss type A-0* (Figure 4.14a) is a truss with five elements $(n = 5)$ and with four degrees of freedom $(m = 4)$ $q = [q_3 \quad q_4 \quad q_7 \quad q_8]^T \in \mathbb{R}^{4 \times 1}$ (Chan and Skelton, 2002; Ohsaki and Zhang, 2006; Malerba et al., 2012). In this case, the elongation matrix is rectangular $B \in \mathbb{R}^{5 \times 4}$; hence, the matrices $H \in \mathbb{R}^{5 \times 5}$ and $L \in \mathbb{R}^{4 \times 4}$ are, respectively

$$H = \text{diag}[3 \quad 1 \quad 1 \quad 1 \quad 0], L = \text{diag}[3 \quad 1 \quad 1 \quad 1]$$

The zero eigenvalue in the matrix H (4.43)$_1$ $(\mu_5 = 0)$ is related to the existence of one self-stress state (4.43)

$$y_5(\mu_5 = 0) = \left[\frac{\sqrt{2}}{2} \quad \frac{\sqrt{2}}{2} \quad \frac{\sqrt{2}}{2} \quad \frac{\sqrt{2}}{2} \quad -1\right]^T.$$

The absence of a zero value in the matrix L (4.43)2 means that there is no mechanism. The eigenvalues of the stiffness matrix (3.19) (4.44)

$$O = \text{diag}[\ 2 \quad 1 \quad 1 \quad 0.42]$$

are positive, which means, the structure is stable. (4.45)

The *Geiger truss type A-0* is characterized by five tensegrity features. It is a truss (TT) with a set of discontinuous set of struts (DS) contained within the continuous net of tensile elements (IN) that have no rigidity in compression (TC) and in which there is one self-stress state (SS). According to the tensegrity classification (Table 3.1), due to a lack of mechanism, it is a *structure with tensegrity features of class 2*.

4.4.1.2 Geiger Truss Type B-0

The *Geiger truss type B-0* (Figure 4.14b) is a truss with eight elements $(n = 8)$ and with eight degrees of freedom $(m = 8)$ $q = \begin{bmatrix} q_3 & q_4 & q_5 & q_6 & q_9 & q_{10} & q_{11} & q_{12} \end{bmatrix}^T \in \mathbb{R}^{8 \times 1}$ (Zhang, 2007; Zhang et al., 2006; Chen and Feng, 2012a; Xu et al., 2018). In this case, the elongation matrix is square $B \in \mathbb{R}^{8 \times 8}$ and the matrices $H \in \mathbb{R}^{8 \times 8}$ and $L \in \mathbb{R}^{8 \times 8}$ are the same

$$H \equiv L = \text{diag}[\ 3 \quad 2.62 \quad 2.61 \quad 2 \quad 1 \quad 0.38 \quad 0.38 \quad 0\ ]$$

The zero eigenvalue in the matrix (4.46) is related to the existence of one self-stress (4.46) state

$$y_8(\mu_8 = 0) = \begin{bmatrix} \sqrt{2} & \sqrt{2} & \sqrt{2} & \sqrt{2} & 1 & 1 & -1 & -1 \end{bmatrix}^T$$

and one mechanism (4.47)

$$x_8(\gamma_8 = 0) = \frac{\sqrt{2}}{4}[\ 1 \quad -1 \quad 1 \quad 1 \quad -1 \quad -1 \quad -1 \quad 1\ ]^T$$

The eigenvalues of the stiffness matrix (3.19) are positive: (4.48)

$$O = \text{diag}[2.54 \quad 2.23 \quad 2.10 \quad 1.45 \quad 1.12 \quad 0.47 \quad 0.47 \quad 0.16],$$

it means the structure is stable, and that, in turn, means the self-stress state (4.49) stabilizes the mechanism, i.e., the mechanism is infinitesimal (describes the local geometrical variability).

The *Geiger truss type B-0* is characterized by all six tensegrity features. It is a truss (TT) with a set of discontinuous set of struts (DS) contained within the continuous net of tensile elements (IN) that have no rigidity in compression (TC). In this structure, there is one self-stress state (SS) that stabilizes one infinitesimal mechanism (IM). According to the tensegrity classification (Table 3.1), this is an *ideal tensegrity.* It is worth noting at this point the similarity between the *Geiger truss type B-0* (Figure 4.14b) and the tensegrity structure shown in Figure 4.13g. In the case of the *Geiger truss*, the horizontal strut has been replaced by the supports.

4.4.1.3 Extended Geiger Trusses

For extended *Geiger trusses* (Figures 4.15), the results of the qualitative analysis are shown in Table 4.7. Generally, the number of mechanisms can be determined by Maxwell's formula (Maxwell, 1864). However, due to repeatability of *Geiger trusses*, it is possible to determine the number of mechanisms (nm) as a function of the number of struts (ns). In turn, regardless of the type of models, there is one self-stress state. All eigenvalues of the stiffness matrix (3.19) are positive. This means the self-stress state identifies the

appropriate normal forces in the structural elements and stabilizes mechanisms, i.e., the mechanisms are infinitesimal. It should be noted that results obtained can be used for models with any additional levels i ($i \in N$), i.e., *Geiger trusses types A-3, B-3, A-4, B-5,* etc.

TABLE 4.7 Results of the Qualitative Analysis of the *Geiger Trusses* ⏎

Type of Truss	No. of						Classification
	Nodes	Elements	d.o.f	Struts	Mechanisms	Self-Stress States	
	(nn)	(n)	(m)	(ns)	(nm)	(nss)	
Geiger trusses type A							
A-0	4	5	4	1	0	1	structure with tensegrity features of class 2
A-1	8	12	12	3	1	1	ideal tensegrity
A-2	12	19	20	5	2	1	
A-3	16	26	28	7	3	1	
A-i				$2i + 1$	$\frac{ns-1}{2}$	1	
Geiger trusses type B							
B-0	6	8	8	2	1	1	ideal tensegrity
B-1	10	15	16	4	2	1	
B-2	14	22	24	6	3	1	
B-3	18	29	32	8	4	1	
B-i				$2i + 2$	$\frac{ns}{2}$	1	

Extended Geiger trusses exhibit all six tensegrity features. They are trusses (TT) with a set of discontinuous struts (DS) contained within the continuous net of tensile elements (IN) that have no rigidity in compression (TC). In these structures, there is one self-stress state (SS) that stabilizes all infinitesimal mechanisms (IM), ensuring their stability. According to the tensegrity classification (Table 3.1), these structures represent *ideal tensegrity.*

4.4.1.4 Formulas for Self-Equilibrium Forces (Self-Stress State) for *Geiger Trusses*

In the case of basic 2D tensegrity models, the self-stress states (4.44) and (4.47) can be simply determined by the static equilibrium of nodes. Furthermore, it is also possible for all extended models, since they are feature by one self-stress state. In Figure 4.16, the geometry of the models with two additional levels is presented. Struts are marked as S_1, S_2, and S_3, whereas the cables are separated on diagonally (1, 2, 3, 4, 5, 6) and horizontally (C_1, C_2, C_4, C_6). Various angles of diagonal cables are taken into account. These models can be extended by adding additional repeatable elements. The formulas for longitudinal self-stress forces are presented in Table 4.8. These formulas depend on the type of model and the angle of inclination of the diagonal cables of truss.
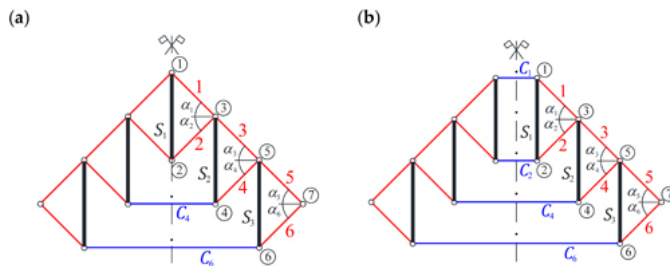

FIGURE 4.16 *Geiger truss type*: (**a**) *A-2* and (**b**) *B-2.* ⏎

TABLE 4.8 Formulas for Self-Equilibrium Forces (Self-Stress State) for the *Geiger Trusses* ⏎

Geiger Trusses Type A	Geiger Trusses Type B

$$N_1 = \text{const.} \, ; \quad i \in N_+$$

struts:

$$N_{S_1} = -2N_1 \sin(\alpha_1) \qquad N_{S_1} = -N_1 \sin(\alpha_1)$$

$$N_{S_{i+1}} = -N_{2(i+1)} \sin\left(\alpha_{2(i+1)}\right)$$

diagonal cables:

$$N_{2i} = N_{2i-1} \frac{\sin(\alpha_{2i-1})}{\sin(\alpha_{2i})} \qquad N_{2i+1} = \frac{N_{2i-1}\cos(\alpha_{2i-1}) + N_{2i}\cos(\alpha_{2i})}{\cos(\alpha_{2i+1})}$$

horizontal cables:

$$N_{C_{2(i+1)}} = N_{2(i+1)} \cos\left(\alpha_{2(i+1)}\right)$$

$$N_{C_1} = N_1 \cos(\alpha_1) N_{C_2} = N_2 \cos(\alpha_2)$$

Geiger trusses types A-2 and *B-2* will be used to create small-scale *Geiger domes* (Section 4.6). Due to this, sample coordinates (Table 4.9) and angles of diagonal cables (Table 4.10) are adopted. The trusses' span is 12 m, and their height is 3.25 m. Next, based on these formulas shown in Table 4.8, the self-stress state states are calculated (Table 4.11). In addition, Table 4.11 shows the self-stress state states for all the models considered in this chapter (the coordinates shown in Table 4.9 are taken into account). For *Geiger trusses type A-2* and *type B-2*, the infinitesimal mechanisms are shown in Figure 4.17.

TABLE 4.9 Coordinates of *Geiger Trusses Types A-2* and *B-2* ⏎

No. of Node		1	2	3	4	5	6	7
type A-2	x (m)	0.0	0.0	2.0	2.0	4.0	4.0	6.0
type B-2		0.5	0.5					
type A-2, B-2	z (m)	2.1	1.5	1.85	0.45	1.15	–1.15	0.0

TABLE 4.10 Angles of Diagonal Cables α_i of *Geiger Trusses Types A-2* and *B-2* ⏎

		α_1	α_2	α_3	α_4	α_5	α_6
type A-2	$\sin(\alpha_i)$	0.1240	0.1724	0.3303	0.4985		
type B-2		0.1644	0.2272				
type A-2	$\cos(\alpha_i)$	0.9923	0.9850	0.9438	0.8669		
type B-2		0.9864	0.9738				

TABLE 4.11 Values of Self-stress State $\mathbf{y}_s$ for the *Geiger Trusses* ⏎

	Geiger Trusses Type A			Geiger Trusses Type B		
	A-0	A-1	A-2	B-0	B-1	B-2
	y_s(-)			y_s(-)		
S_1	–1.0000	–0.4167	–0.1268	–1.0000	–0.2778	–0.0845
S_2	–	–1.0000	–0.3043	–	–1.0000	–0.3043
S_3	–	–	–1.0000	–	–	–1.0000
1	4.0311	1.6796	0.5112	6.0827	1.6896	0.5142
2	2.9006	1.2086	0.3678	4.4014	1.2226	0.3721
3	–	3.0271	0.9213	–	3.0271	0.9213

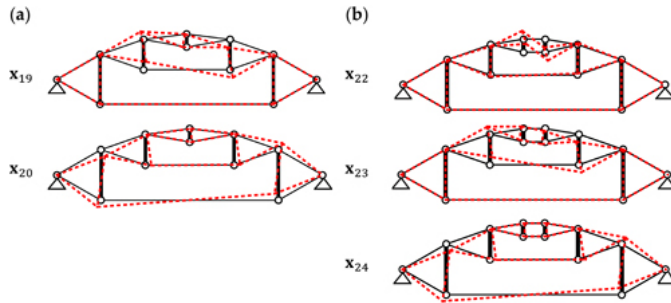|	Geiger Trusses Type A			Geiger Trusses Type B		
	A-0	A-1	A-2	B-0	B-1	B-2
	y_s(-)			y_s(-)		
4	–	3.0271	0.9213	–	3.0271	0.9213
5	–	–	2.0061	–	–	2.0061
6	–	–	2.0061	–	–	2.0061
C_1	–			0.5072	0.5072	0.5072
C_2	–			0.3623	0.3623	0.3623
C_4	–	2.8571	0.8696	–	2.8571	0.8696
C_6	–	–	1.7391	–	–	1.7391

FIGURE 4.17 Infinitesimal mechanisms for the *Geiger truss type:* (**a**) *A-2* and (**b**) *B-2.*

4.4.2 STATIC ANALYSIS

The static analysis includes the behavior of the *Geiger truss type B-0*. The values of the self-stress state are assumed according to the vector (4.47) (Figure 4.18a). A considered truss is a *structure with tensegrity features of class 1* with one infinitesimal mechanism (4.48) (Figure 4.18b). However, the behavior of this truss depends mainly on the load. More precisely, on whether the load causes displacements that are compatible or incompatible with the mechanism. To explain, the displacements q_3 and q_4 are calculated. In the case of the mechanism, the corresponding components of the eigenvector describing the deformation $x_8(\gamma_8 = 0)$ (4.48) are opposite and equal: $x_3 = \sqrt{2}/4$ and $x_4 = -\sqrt{2}/4$. In the case of the symmetric load, the displacements are incompatible with the mechanism (Table 4.12) they have the same sign and differ in value. In turn, in the case of the asymmetric load, the displacements are compatible with the infinitesimal mechanisms (slight differences in values are due to numerical approximations) (Table 4.13).
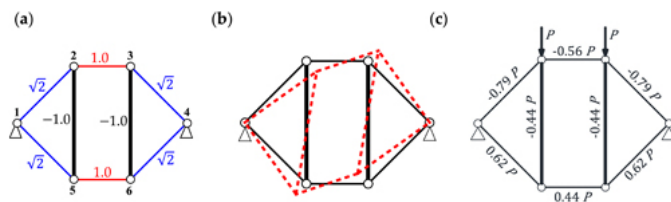

FIGURE 4.18 *Geiger truss type B:* (**a**) self-stress state (4.47), (**b**) infinitesimal mechanism (4.48), and (**c**) longitudinal forces caused by symmetrical load.

TABLE 4.12 Strength Characteristics of the Symmetrically Loaded *Geiger Truss Type B-0*

S(kN)	Type of Element	P = 1 kN(S_min = 1 kN)			P = 5 kN(S_min = 3 kN)			P = 10 kN(S_min = 6 kN)		
		W_{max} (–)	q_3(mm)	q_4(mm)	W_{max} (–)	q_3(mm)	q_4(mm)	W_{max} (–)	q_3(mm)	q_4(mm)
S_{min}	Cables	0.01	–0.01	–0.06	0.07	–0.05	–0.30	0.13	–0.09	–0.59
	Struts	0.03			0.12			0.25		
20	Cables	0.26	–0.01	–0.06	0.28	–0.05	–0.30	0.31	–0.09	–0.59
	Struts	0.49			0.53			0.58		
35	Cables	0.45	–0.01	–0.06	0.48	–0.05	–0.30	0.50	–0.09	–0.59
	Struts	0.84			0.89			0.94		

TABLE 4.13 Strength Characteristics of the Asymmetrically Loaded *Geiger Truss Type B-0* ⏎

S(kN)	Type of Element	P = 1 kN			P = 5 kN			P = 10 kN		
		W_{max} (–)	q_3(mm)	q_4(mm)	W_{max} (–)	q_3(mm)	q_4(mm)	W_{max} (–)	q_3(mm)	q_4(mm)
0	Cables	0.08	31.45	–31.43	0.23	54.50	–54.51	0.37	69.22	–69.31
	Struts	0.15			0.46			0.76		
10	Cables	0.15	15.57	–15.53	0.28	43.66	–43.71	0.42	60.45	–60.57
	Struts	0.28			0.56			0.85		
20	Cables	0.26	8.76	–8.78	0.36	33.98	–34.05	0.48	52.04	–52.18
	Struts	0.50			0.69			0.96		

Note that the symmetrical load does not result in the correct distribution of longitudinal forces in elements (Figure 4.18c). Only the introduction of the initial prestress above $S_{\min} > 0.56\,P$ leads to the correct distribution. This type of load causes displacements that are incompatible with the mechanism.

The behavior of a symmetrically loaded structure is the same as the behavior of the *X-truss* (see Section 4.3.2). The displacements and stiffness are insensitive to the change in the level of initial prestress. The *global stiffness parameter* (3.32) is constant and equal to $GSP = 1$. The effort of the structure W_{max} is linearly dependent on the prestress, just like longitudinal forces caused jointly by the load and prestress forces N(P+S) (Figure 4.19), and the longitudinal forces caused by the load N(P) are independent of the value of the initial prestress.
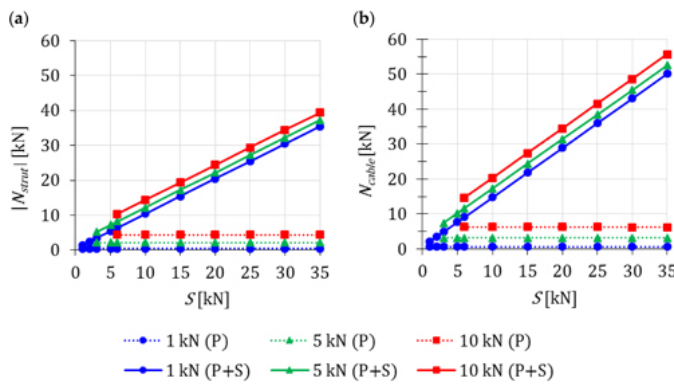

FIGURE 4.19 Symmetrical load. Influence of the initial prestress level *S* on the longitudinal force *N*: (**a**) in struts and (**b**) in cables.⏎

The behavior of an asymmetrically loaded structure is completely different and similar to that of the simplest two-element structure (see Section 4.2.2). The influence on the longitudinal forces N is shown in Figure 4.20. Displacement values calculated using second-order theory (II) in the absence of prestress increase to infinity (Figure 4.21), which is due to the singularity of the stiffness matrix. In this case, the effect of non-linearity (III) on displacements is significant. This is due to the possibility of maximum prestress, which,

due to the bearing capacity, is at a low level. Additionally, the others static parameters mostly depend on the initial prestress level, i.e., the *global stiffness parameter* GSP (Figure 4.22a), the effort of structure W_{max} (Figure 4.22b). The influence of the initial prestress level on stiffness, as in the case of two-element structure, is greater at lower loads. At the maximum of the initial prestress level $S_{max} = 20\text{kN}$ for the value of external force $P = 1\text{kN}$, parameter GSP is 2.7 times higher than for the value $P = 10\text{kN}$. In the case of effort of structure, as in the case of the stiffness, the influence of the initial prestress decreases as the load increases.
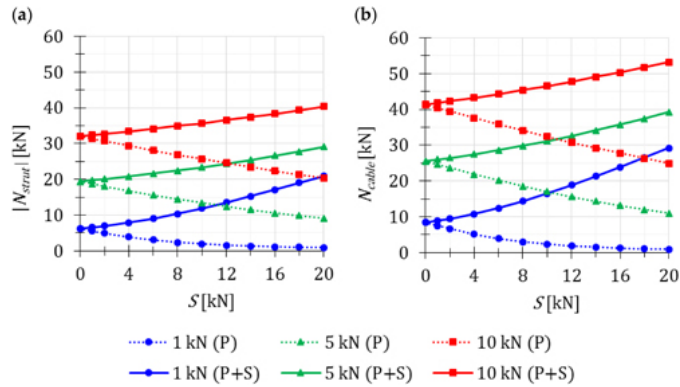

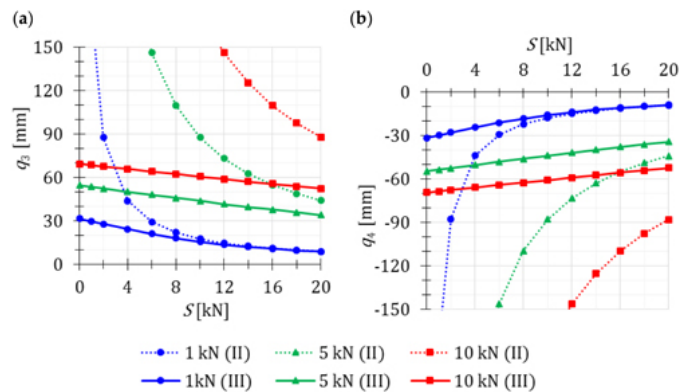**FIGURE 4.20** Asymmetrical load. Influence of the initial prestress level S on the longitudinal force: (**a**) in struts and (**b**) in cables.

FIGURE 4.21 Asymmetrical load. Influence of the initial prestress level S on the: (**a**) displacement q_3 and (**b**) displacement q_4.
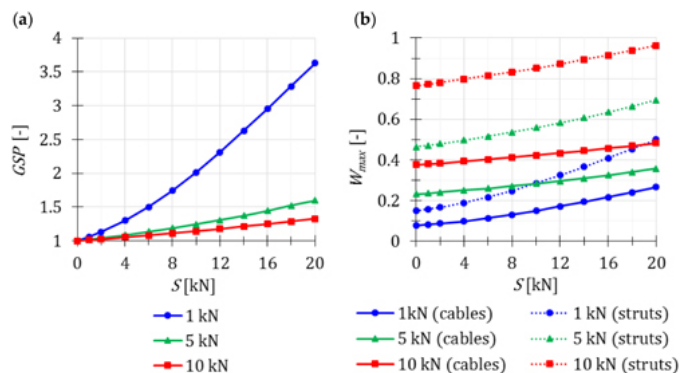
FIGURE 4.22 Asymmetrical load. Influence of the initial prestress level S on the: (**a**) *global stiffness parameter GSP* and (**b**) effort of structure W_{max}. ⏎

4.4.3 DYNAMIC ANALYSIS

The dynamic analysis included calculations of the natural vibrations $f(0)$ and the free vibrations of structure loaded with time-independent force $f(P)$. The maximum prestress level is assumed as $S = 20\text{kN}$ to compare behavior of structure under different load. Since a one infinitesimal mechanism has been identified, only the first natural frequency depends on the initial prestress level (Figure 4.23). The influence is significant. In the absence of prestress ($S = 0$), this frequency is zero, and after the introduction of prestress it increases, e.g., for $S = 20\text{kN}$, it is $f_1(0) = 5.55$ Hz. In turn, the free frequency depends on the type of load:
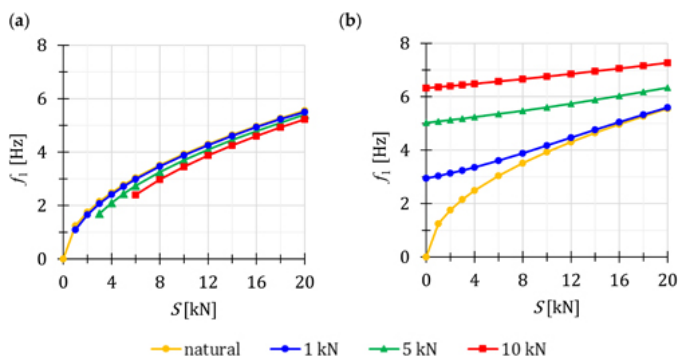

FIGURE 4.23 Influence of the initial prestress level S on the first frequency: (**a**) symmetrical load and (**b**) asymmetrical load.⏎

- in the case of symmetrical load (Figure 4.23a), the free frequencies are lower than the natural about 2%, 10%, and 21% for $S = 6\text{kN}$ and 0.5%, 3%, and 6% for $S = 20\text{kN}$, respectively, for the cases $P = 1\text{kN}$, $P = 5\text{kN}$, and $P = 10\text{kN}$,
- in the case of asymmetrical load (Figure 4.23b), the free frequencies are higher than the natural about 19%, 76%, and 116% for $S = 6\text{kN}$ and 0.9%, 14%, and 31% for $S = 20\text{kN}$, respectively for the cases $P = 1\text{kN}$, $P = 5\text{kN}$, and $P = 10\text{kN}$; the external load prestresses the structure; additional forces are generated in the elements and the initial dynamic response at $S = 0$ corresponds to the values of the natural frequency at the following prestress levels: $S(P = 1\text{kN}) \approx 6\text{kN}$, $S(P = 5\text{kN}) \approx 16\text{kN}$, and $S(P = 10\text{kN}) \approx 26\text{kN}$.

The second frequency f_2 is practically insensitive to both changes in the level of prestress and the effects of external loads (Table 4.14). The maximum relative difference is equal 0.08%.

TABLE 4.14 Second Natural and Free Frequencies of the *Geiger Truss Type B-0* ⏎

S(kN)	Type of Load	$f_2(P = 0)$(Hz)	P = 1 kN	P = 5 kN	P = 10 kN
			$f_2(P)$(Hz)		
6	Symm.	120.16	120.17	120.16	120.16
35		120.21	120.26	120.21	120.20
6	Asym.	120.16	120.17	120.21	120.24
20		120.21	120.21	120.23	120.26

4.4.4 DYNAMIC STABILITY ANALYSIS

The influence of the initial prestress level S and load on the main unstable region is shown. Three values of constant part of periodic force are taken into account, i.e., $P = \{1\text{kN}, 5\text{kN}, 10\text{kN}\}$. The symmetrical and asymmetrical loads are considered. Resonance frequencies are determined using the harmonic balance method. *The Geiger truss type B-0* is characterized by one infinitesimal mechanism. Due to this, one main unstable region is obtained.

The main unstable region is shown in Figures 4.24 and 4.25. To compare the behavior of truss under different loads, the boundaries for three cases of initial prestress level are presented, i.e., S_{min}, $S \approx 0.5 S_{max}$, and S_{max}. In the case of symmetrical load (Figure 4.24), only for $P = 10\text{kN}$ resonance frequency depends on the prestress. However, an increase in prestress reduces the unstable region. The behavior of the truss under asymmetrical load (Figure 4.25) is completely different and resembles that of the simplest two-element structure (see Section 4.2.4). The same conclusions can be drawn. Independently on the value of prestress, the range of regions mostly depends on the load. The greater the load, the greater the region. The introduction of prestress (Figures 4.25b and 4.25c) causes decreasing the range of unstable regions decreases, and resonant frequencies increase. The initial prestress level has a greater influence on the range of the unstable regions when lower loads are applied. For example, in the case of $P = 1\text{kN}$ introducing the $S_{max} = 20\text{kN}$ results in an overlapping of the boundaries of unstable region (Figure 4.25c).
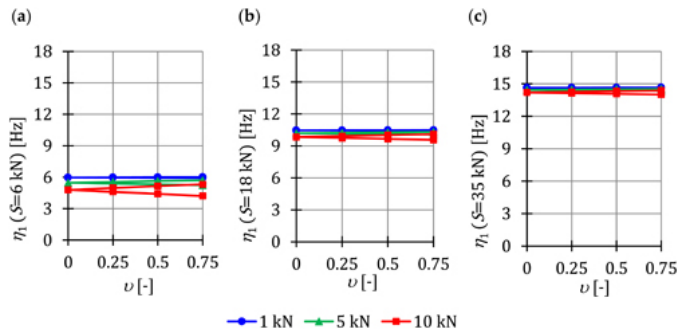

FIGURE 4.24 Limits of the main unstable regions for the case of symmetrical load: (**a**) S = 6 kN, (**b**) S = 18 kN, and (**c**) S = 35 kN.
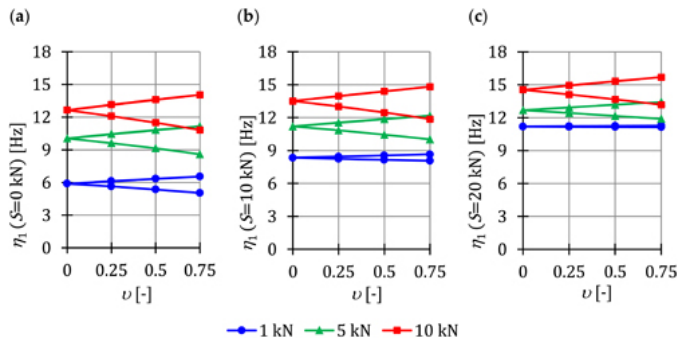

FIGURE 4.25 Limits of the main unstable regions for the case of asymmetrical load: (**a**) S = 0 kN, (**b**) S = 10 kN, and (**c**) S = 20 kN.

To better compare the influence of the initial prestress level and the load, Figures 4.26a and 4.27a show the areas of unstable regions $A_\eta(S)$. In turn, to measure the changes in the area of the unstable regions, the dimensionless parameter λ (3.75) is calculated

(Figures 4.26b and 4.27b). In the case of the symmetrical load (Figure 4.26), the areas of unstable regions are small, and changes in the area practically do not depend on the load. At the maximum initial prestress level, the unstable regions are about 60% less than at the minimum prestress level. In the case of the asymmetrical load (Figure 4.27), on the other hand, changes in the area depend on the load. At the maximum initial prestress level, the unstable regions are 90%, 40%, and 20% smaller than at the minimum prestress level, respectively, for $P = 1\text{kN}$, $P = 5\text{kN}$, and $P = 10\text{kN}$. As can be seen, the load causes a different character of change in the parameter λ with growth the initial prestress level. For $P = 1\text{kN}$, the parameter λ decreases almost exponentially; in turn, for $P = 5\text{kN}$ and $P = 10\text{kN}$, it is a polynomial of second degree.
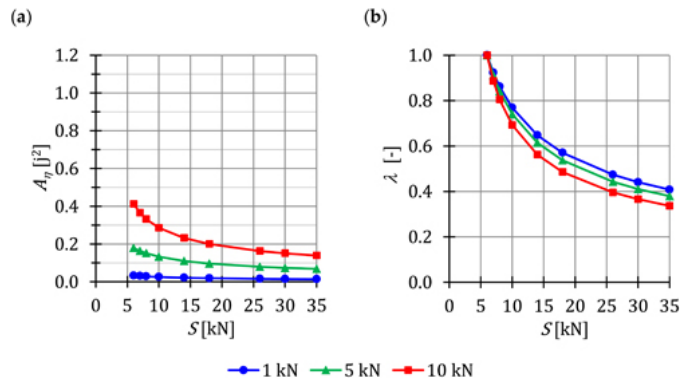

FIGURE 4.26 Symmetrical load. Influence of the initial prestress level S on the: (**a**) area of unstable regions $A_\eta(S)$ and (**b**) range of unstable regions λ.

FIGURE 4.27 Asymmetrical load. Influence of the initial prestress level S on the: (**a**) area of unstable regions $A_\eta(S)$ and (**b**) range of unstable regions λ.
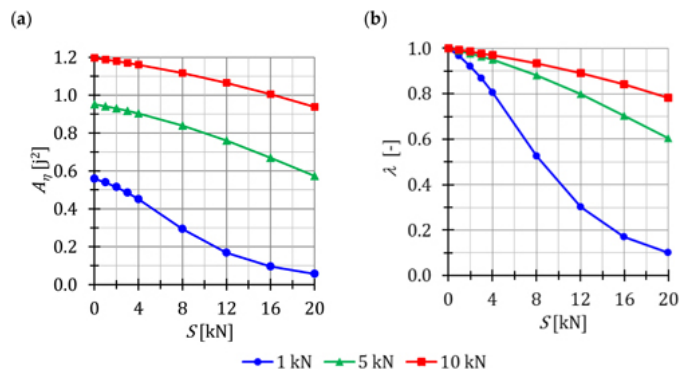
The second-resonance frequency η_2 does not depend on both changes in the level of prestress and external loads (Table 4.15). Additionally, it is twice the free second frequency - $\eta_2 = 2f_2$.

TABLE 4.15 Second-Resonance Frequency of the *Geiger Truss Type B-0*

S(kN)	Type of Load	P = 10 kN	P = 20 kN	P = 30 kN
		η_2 (Hz) ($\nu = 0 \div 0.75$)		
6	Symm.	240.33	240.33	240.33
35		240.51	240.51	240.51
6	Asym.	240.33	240.40	240.46
20		240.42	240.48	240.55

4.4.5 CHAPTER SUMMARY

This chapter discusses two-dimensional structures, which can be used to create tensegrity *Geiger domes*. For clarity, the summary is presented as the answers to the questions posed at the beginning of the consideration

1. Is it possible to derive formulas for self-equilibrium forces (self-stress state)?

In the case of basic 2D tensegrity models, the self-stress states can be simply determined by the static equilibrium of nodes. Due to the repetitive nature of the models, the considerations can be generalized to any extended versions of these models.

2. How does the structure behave when the load causes the displacements that are incompatible with an infinitesimal mechanism?

The behavior of structure under load, which causes displacements incompatible with an infinitesimal mechanism, is similar to the behavior of the *X-truss (*see Sections 4.3.2–4.3.4). The displacements and unaffected by changes in the of initial prestress level. The *global stiffness parameter* is constant and the effort of the structure is linearly dependent on the prestress. The dynamic parameters, i.e., natural, free, and resonance frequencies, are also independent of the value of the initial prestress.

3. How does the structure behave when the load causes the displacements that are compatible with an infinitesimal mechanism?

The behavior of a structure under load, which causes displacements incompatible with an infinitesimal mechanism, is similar to that of the simplest two-element structure (see Sections 4.2.2–4.2.4). All static parameters are dependent on the initial prestress. In the case of dynamic parameters, the number of frequencies depending on prestress is equal to the number of infinitesimal mechanisms. The influence of the initial prestress level on behavior, as in the case of two-element structure, is greater at lower loads.

4. How does the structure behave when the load capacity of the struts is much smaller than the load capacity of the cables?

In the case where the load capacity of the struts is much lower than that of the cables, the effect of non-linearity is significant. This means a greater influence of the load value on the behavior of the structure. This is due to the possibility of maximum prestressing, which is at a low level due to the load-bearing capacity of the struts. In such cases, the parameter λ does not approach zero. This, in turn, results in the occurrence of unstable motion, which is independent of the initial prestress level.

4.5 BASIC 3D TENSEGRITY MODULES

The simplest diamond-pattern systems with three and four struts are considered. Two versions of the modules are taken into account, i.e., *regular* and *modified* (see Section

1.5.2). This means four basic 3D tensegrity modules are analyzed, i.e.:

- *regular Simplex module* (Figure 4.28a);
- *modified Simplex module* (Figure 4.28b);
- *regular Quartex module* (Figure 4.29a);
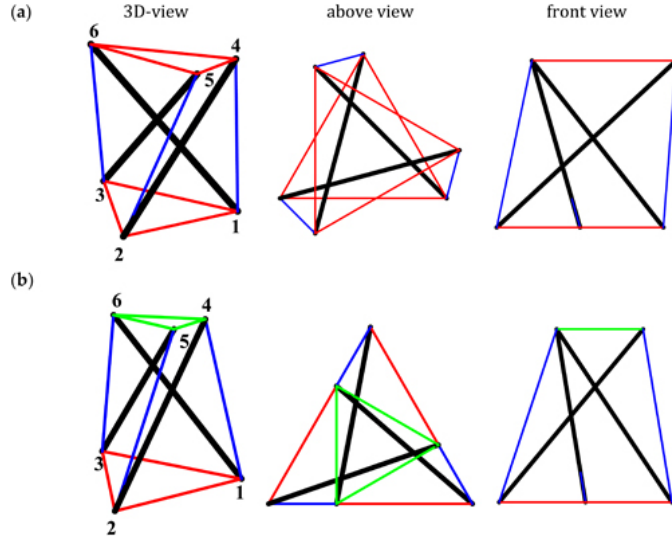- *modified Quartex module* (Figure 4.29b).

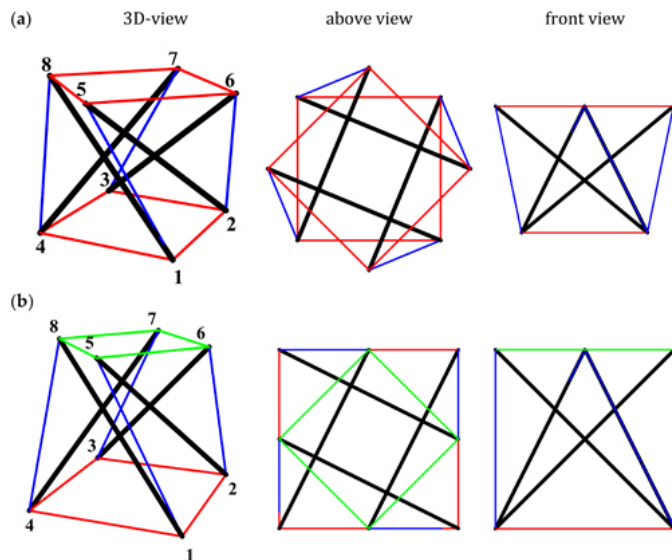

FIGURE 4.28 *Simplex module*: (**a**) *regular* and (**b**) *modified.* ↵

FIGURE 4.29 *Quartex module*: (**a**) *regular* and (**b**) *modified.* ↵

The coordinates of the nodes are shown in Tables 4.16 and 4.17. The qualitative analysis is performed for unsupported and supported modules. Only the results of the analysis are presented. In turn, the quantitative analysis includes the behavior of supported modules. Material and geometric characteristics are assumed according to Table 4.1. The dimension $a = 1\mathrm{m}$ is taken into account. The length of the struts and the load-bearing capacity $N_{b,Rd}$ (Table 4.2) depend on the type of module:

TABLE 4.16 Coordinates of the *Simplex Module* Nodes

No. of Node		1	2	3	4	5	6
regular	x	0.5a	–0.5a	0	0.5774a	–0.2887a	–0.2887a
modified					0.3333a	–0.1667a	–0.1667a
regular	y	–0.2887a	–0.2887a	0.5774a	0	–0.5a	0.5a
modified						–0.2887a	0.2887a
regular	z	0	0	0	a	a	a
modified							

TABLE 4.17 Coordinates of the *Quartex Module* Nodes

No. of Node		1	2	3	4	5	6	7	8
regular	x	–0.5a	0.5a	0.5a	–0.5a	–0.7071a	0	0.7071a	0
modified						–0.5a		0.5a	
regular	y	–0.5a	–0.5a	0.5a	0.5a	0	–0.7071a	0	0.7071a
modified							–0.5a		0.5a
regular	z	0	0	0	a	a	a	a	a
modified									

- regular *Simplex module*: $l = 1.5$m, $N_{b,Rd} = 163.0$kN;
- modified *Simplex module*: $l = 1.333$m, $N_{b,Rd} = 175.4$kN;
- regular *Quartex module*: $l = 1.645$m, $N_{b,Rd} = 152.1$kN;
- modified *Quartex module*: $l = 1.5$m, $N_{b,Rd} = 163.0$kN.

The modules are loaded by one force applied to fifth node in z-direction. In order to illustrate the influence of external loads on the behavior of modules, three values of load are taken into account, i.e., $P = \{10\text{kN}, 20\text{kN}, 30\text{kN}\}$. The minimum prestress level is equal to $S_{min} = 0$, which means an external load causes an appropriate distribution of longitudinal forces. In turn, the maximum prestress level is assumed to be $S_{max} = 110$kN and corresponds to the effort of the structure (3.22) equal to $W_{max} = 0.91$.

Purpose of Consideration

Presentation of the basic tensegrity modules, which can be used to create towers and double-layered grids. Additionally, the analysis is comparative in nature. It leads to answers to the following questions:

1. How does the modification affect the behavior of modules?
2. Which type of module is more sensitive to the risk of excitation vibrations?

4.5.1 QUALITATIVE ANALYSIS

The results of the qualitative analysis are shown in Table 4.18. Unsupported *Simplex* and *Quartex modules* are characterized by 18 ($m = 18$) and 24 ($m = 24$) degrees of freedom, respectively. One self-stress state was identified for the modules. The values of eigenvectors y_S are shown in Figures 4.30 and 4.31. The cables are marked in red, green, and blue, whereas the struts are black. The different colors of cables correspond to the different values of the self-stress state. The *Simplex module* features seven mechanisms, while the *Quartex module* features nine. The spectral analysis of the stiffness matrix (3.17) leads to obtaining six zero eigenvalues independently of the type of module. It means the six identified mechanisms are finite (rigid movements). In order to eliminate rigid movements, support conditions have been added. The six and eight blocked degrees of freedom are considered, i.e., q_1, q_3, q_5, q_6, q_8, q_9, and q_1, q_3, q_5, q_6, q_7, q_9, q_{11}, q_{12}, for the *Simplex* and *Quartex modules*, respectively. Supported modules were characterized by one self-stress state (the same as for the

unsupported modules) and one mechanism realized by the displacements of the top nodes (Figures 4.32 and 4.33). All eigenvalues of the stiffness matrix (3.19) are positive. This means the self-stress state identifies the appropriate normal forces in the structural elements and stabilizes mechanisms, i.e., the mechanisms are infinitesimal.

TABLE 4.18 Results of the Qualitative Analysis of the Basic 3D Tensegrity Modules

Type of Module	No. of Nodes (nn)	Elements (n)	d.o.f (m)	Mechanisms (nm)	Self-Stress States (nss)	Classification
Unsupported						
Simplex	6	12	18	7	1	6 rigid movements
Quartex	8	16	24	9	1	
Supported						
Simplex	6	12	12	1	1	ideal tensegrity
Quartex	8	16	16	1	1	
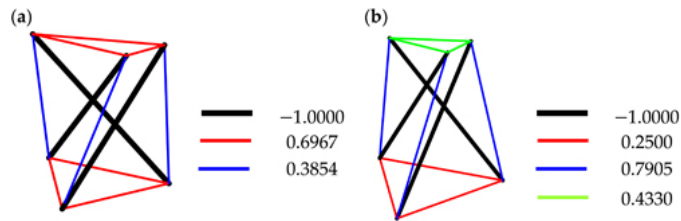
FIGURE 4.30 Normalized self-stress state $\mathbf{y}_s$(–) of the *Simplex modules*: (**a**) *regular* and (**b**) *modified.*
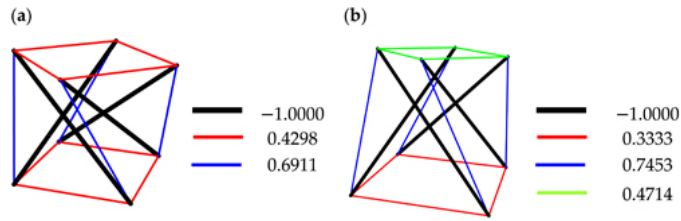
FIGURE 4.31 Normalized self-stress state $\mathbf{y}_s$(–) of the *Quartex modules*: (**a**) *regular* and (**b**) *modified.*
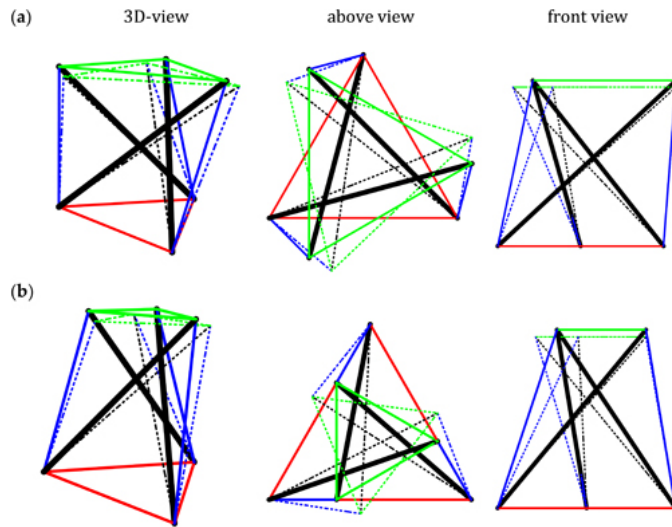
FIGURE 4.32 Infinitesimal mechanism of the supported *Simplex modules*: (**a**) *regular* and (**b**) *modified.* ↵
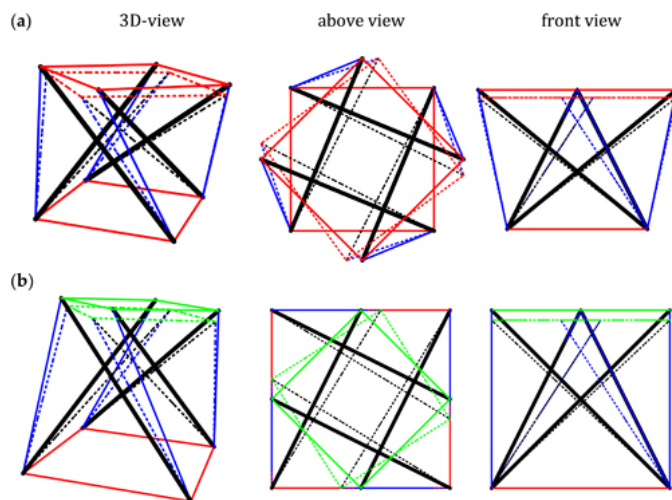

FIGURE 4.33 Infinitesimal mechanism of the supported *Quartex modules:* (**a**) *regular* and (**b**) *modified.*↵

The supported basic 3D tensegrity modules are characterized by all six tensegrity features. They are trusses (TT) with a set of discontinuous set of struts (DS) contained within the continuous net of tensile elements (IN) that have no rigidity in compression (TC). In these structures, there is one self-stress state (SS) that stabilizes one infinitesimal mechanism (IM). According to the tensegrity classification (Table 3.1), the supported basic 3D tensegrity modules are *ideal tensegrity*.

4.5.2 STATIC ANALYSIS

4.5.2.1 Simplex Modules

The values of the self-stress state y_S are assumed according to Figure 4.30. Comparing the behavior of the *Simplex regular* and *modified modules,* it can be said that better results are obtained in the second case. The displacements of the loaded node obtained for the

regular module (Figure 4.34a) are about 63% for $S = 0$ and 90% for $S = 110\text{kN}$ higher than for the *modified module* (Figure 4.34b). However, the difference between the displacements obtained for two different values of load is the same for both modules. For example, in the case of the minimal level of prestress, the difference for $P = 10\text{kN}$ and $P = 20\text{kN}$ is about 21%, while the difference for $P = 20\text{kN}$ and $P = 30\text{kN}$ is about 13%. In turn, in the case of the maximum level of prestress, the differences are about 97% and 46%, respectively. With the increase in initial prestress, the displacements become lower for both models.
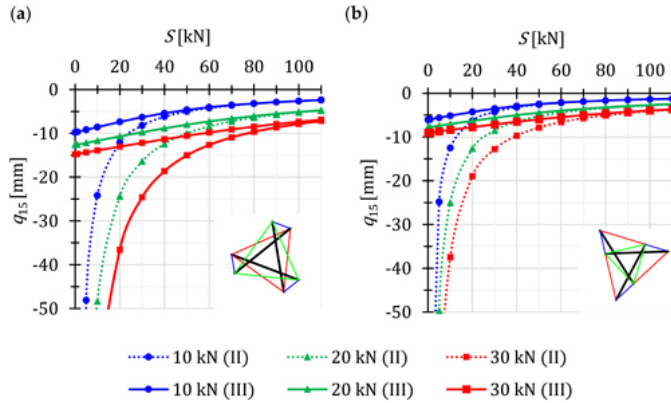

FIGURE 4.34 Influence of the initial prestress level *S* on the displacement q_{15}: (**a**) *regular Simplex module* and (**b**) *modified Simplex module*.↵

   Additionally, differences between the calculations made according to the second-order (II) and third-order (III) order theory are higher for the *regular module*. The influence of non-linearity is most significant at low values of initial prestress forces for both modules. Thereby, with lower values of the load, the initial prestress has a higher impact on the total rigidity of the structure, and the differences between the displacements obtained using the second and third-order theory at $P = 10\text{kN}$ are smaller than at $P = 20\text{kN}$ and $P = 30\text{kN}$. The external load prestresses the structure; however, after introducing the initial prestress, the longitudinal forces from the external load $N(\text{P})$ successively decrease (Figure 4.35), and thus its influence on the displacement decreases. In the case of the *modified module*, at a higher initial prestress level, the load values have less significance.
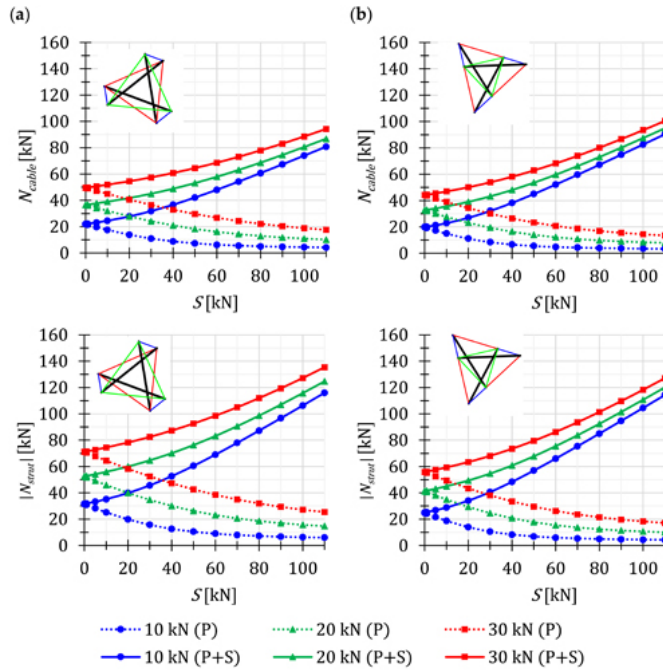
FIGURE 4.35 Influence of the initial prestress level *S* on the longitudinal force *N*: (**a**) *regular Simplex module* and (**b**) *modified Simplex module.*⏎

It can also be observed that with the increment of the initial prestress, the *modified module* becomes slightly more susceptible to the increase in load level. With the increase in load, the impact of the prestress initial level on the stiffness of the structure is more significant (Figure 4.36**)**. More beneficial values of the parameter GSP are obtained for the *modified module*. At the maximum level of initial prestress, the parameter GSP for the *modified module* is 1.1, 0.8, and 0.6 times higher than for the *regular module*, respectively, for $P = 10\text{kN}$, $P = 20\text{kN}$, and $P = 30\text{kN}$.
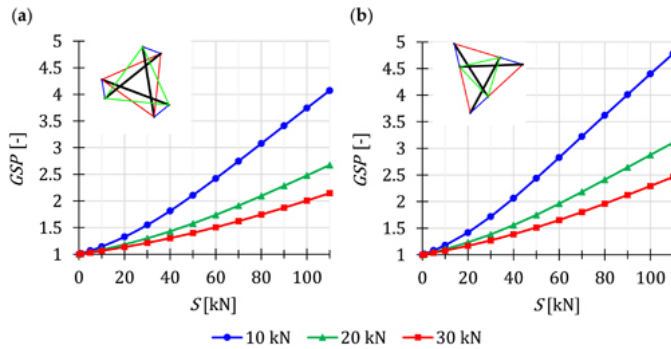

FIGURE 4.36 Influence of the initial prestress level *S* on the *global stiffness parameter GSP*: (**a**) *regular Simplex module* and (**b**) *modified Simplex module.*⏎

On the other hand, the effort of struts and cables in the case of *regular module* (Figure 4.37a**)** behaves in the same way. In the case of the *modified module* (Figure 4.37b**)**, the effort of the cables is on average about 26% higher than the effort of the struts. The

difference between the efforts increases with the increment of the prestress level and the rise of the load level.
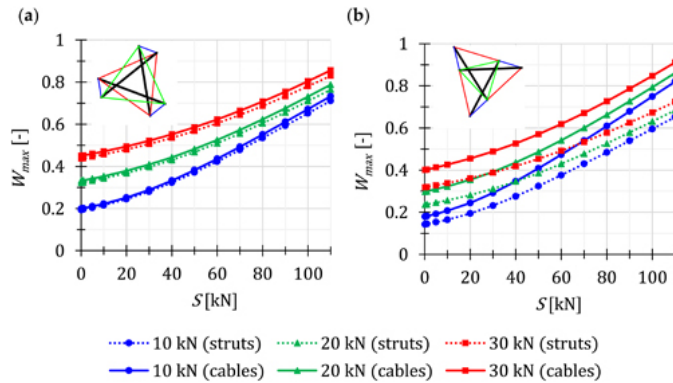

FIGURE 4.37 Influence of the initial prestress level S on the effort of structure W_{max}: (**a**) *regular Simplex module* and (**b**) *modified Simplex module.* ⏎

4.5.2.2 Quartex Modules

The values of the self-stress state y_S are assumed according to Figure 4.31. Comparing the behavior of the *Quartex regular* and *modified modules*, the same conclusions can be drawn as for the *Simplex modules*. However, the differences are smaller. The displacements of the loaded node, obtained for the *regular module* (Figure 4.38a) are about 39% for $S = 0$ and 50% for $S = 110$ kN higher than for the *modified module* (Figure 4.38b). The difference between the displacements obtained for two different values of load in the case of the minimal level of prestress is about 30% for $P = 10$ kN and $P = 20$ kN and 17% for $P = 20$ kN and $P = 30$ kN. In turn, in the case of the maximum level of prestress, the differences are about 93% and 43%, respectively. With the increase in initial prestress, the displacements become lower for both models. Differences between the calculations made according to the second-order (II) and third-order (III) theories are also higher for the *regular module*. However, unlike the *Simplex module*, both solutions of the *Quartex module* are sensitive to load values independently of the initial prestress level.
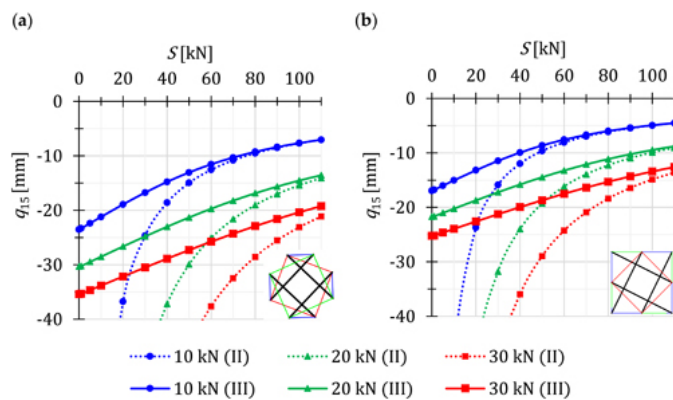

FIGURE 4.38 Influence of the initial prestress level S on the displacement q_{15}: (**a**) *regular Quartex module* and (**b**) *modified Quartex module.* ⏎

The influence of initial prestress level on longitudinal forces (Figure 4.39) is the same as in *Simplex modules*. However, the values are higher, and moreover, so are the displacement values. The stiffness of the *Quartex modules* (Figure 4.40**)** is lower than that of the *Simplex modules*. More beneficial values of the parameter GSP are obtained for the *modified module*. This parameter is 1.1 times higher than that of the *regular module*, regardless of the initial prestress level, as well as the value of the load.
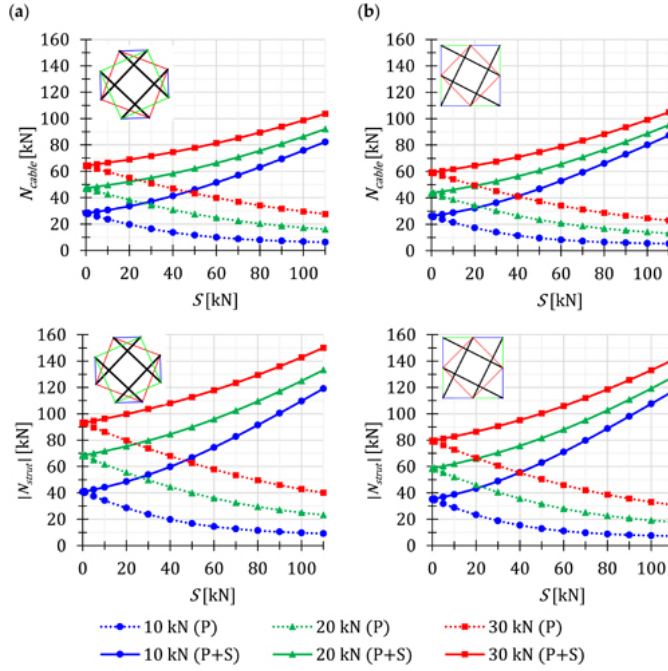

FIGURE 4.39 Influence of the initial prestress level *S* on the longitudinal force *N*: (**a**) *regular Quartex module* and (**b**) *modified Quartex module.* ⏎
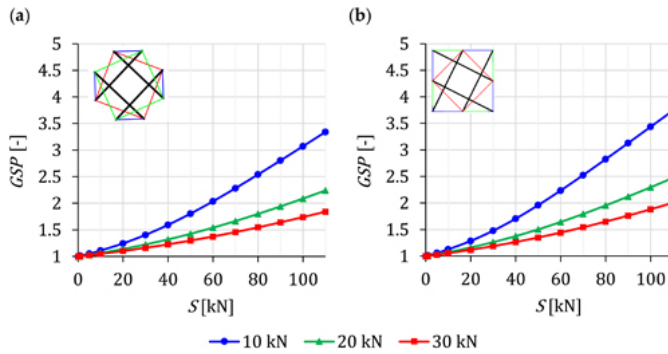
FIGURE 4.40 Influence of the initial prestress level *S* on the global stiffness parameter *GSP*: (**a**) *regular Quartex module* and (**b**) *modified Quartex module.* ⏎

A different behavior, compared to *Simplex modules*, can be observed in the case of the effort of structures. The most strained are the struts for *regular Quartex modules* (Figure 4.41a**).** This is due to the lowest load-bearing capacity of these struts $\left(N_{b,Rd} = 152.1 \text{ kN}\right)$. In the case of the *modified module (* Figure 4.41b**),** the effort of the cables is on average

about 10% higher than the effort of the struts. The difference between the efforts is practically independent of the initial prestress level and load.
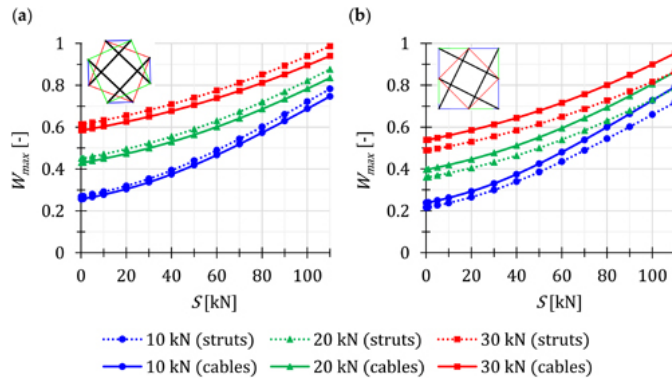
FIGURE 4.41 Influence of the initial prestress level S on the effort of structure W_{max}: (**a**) *regular Quartex module* and (**b**) *modified Quartex module.* ↵

4.5.3 DYNAMIC ANALYSIS

The dynamic analysis included calculations of the natural vibrations $f(0)$ and the free vibrations of structure loaded with time-independent force $f(P)$. Since a one infinitesimal mechanism has been identified for all modules, only the first natural frequency depends on the initial prestress level. The influence is significant. In the absence of prestress ($S = 0$), this frequency is zero, and after the introduction of prestress it increases to:

- $24.8\ \mathrm{Hz}$ for *regular Simplex module* (Figure 4.42a);
- $37.8\ \mathrm{Hz}$ for *modified Simplex module* (Figure 4.42b);
- $18.5\ \mathrm{Hz}$ for *regular Quartex module* (Figure 4.43a);
- $24.8\ \mathrm{Hz}$ for *modified Quartex module* (Figure 4.43b).

FIGURE 4.42 Influence of initial prestress level S on the first frequency: (**a**) *regular Simplex module* and (**b**) *modified Simplex module.* ↵

FIGURE 4.43 Influence of initial prestress level *S* on the first frequency: (**a**) *regular Quartex module* and (**b**) *modified Quartex module.*
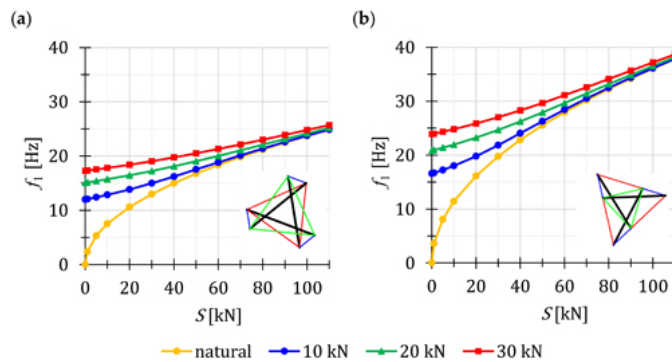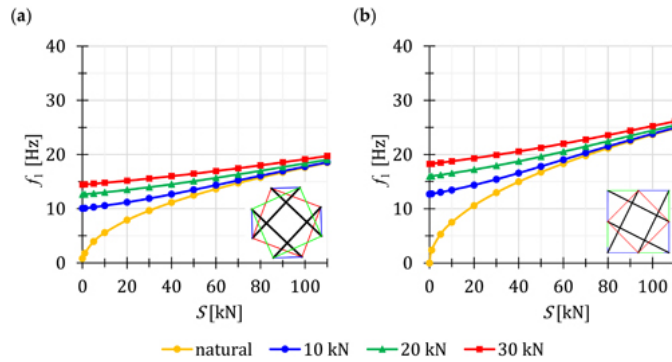
It is very interesting that the first natural frequency for the *regular Simplex module* is almost the same as for the *modified Quartex module.* Slight differences exist in the case of the first free frequency. For the *modified Quartex module* this frequency is higher about $6\% - 2\%$ in depending on the initial prestress level – from $S_{min} = 0$ to $S_{max} = 110\text{kN}$.

As in the case of the two-element structure (see Section 4.2.3) and the *Geiger truss type B-0* (see Section 4.4.3), the first free frequency depends on the type of load (Figures 4.42 and 4.43). Due to the load prestresses the structure, this frequency in the absence of prestress ($S = 0$) is not zero. The higher the load, the higher the frequency. With increase of the initial prestress level, the first free frequency values converge to the first natural frequency. The second frequency f_2 is practically insensitive to both changes in the level of prestress and the effects of external loads (Table 4.19). The maximum relative difference is equal 0.2% (*modified Quartex module*).

TABLE 4.19 Second Natural and Free Frequencies of the Basic 3D Tensegrity Modules

S(kN)	Type of Module	f_2 (0) (Hz)	P = 10 kN	P = 20 kN	P = 30 kN
			f_2 (P) (Hz)		
Simplex modules					
0	*regular*	128.61	128.64	128.66	128.67
110		128.85	128.83	128.82	128.82
0	*modified*	152.61	152.63	152.64	152.65
110		152.78	152.78	152.77	152.76
Quartex modules					
0	*regular*	136.61	136.65	136.66	136.67
110		136.89	136.85	136.83	136.82
0	*modified*	193.74	193.81	193.84	193.85
110		194.14	194.11	194.09	194.08

4.5.4 DYNAMIC STABILITY ANALYSIS

The influence of the initial prestress level *S* and load on the main unstable region is shown. Three values of constant part of periodic force are taken into account, i.e., $P = \{10\text{kN}, 20\text{kN}, 30\text{kN}\}$. *The all modules are* characterized by one infinitesimal mechanism. Due to this, one main unstable region is obtained. The boundaries for three cases of initial prestress level are shown, i.e., $S_{min} = 0$, $S = 50\text{kN}$, and $S_{max} = 110\text{kN}$.

4.5.4.1 Simplex Modules

The main unstable regions are shown in Figures 4.44 and 4.45. In brief, the behavior of *regular module* (Figure 4.44) is comparable with the *modified module* (Figure 4.45). First,

the higher the load, the larger the region. Second, the introduction of prestress reduces the range of unstable regions and increases resonant frequencies. However, to better compare the influence of the initial prestress level and the load, the areas of unstable regions $A_\eta(S)$ (Figure 4.46a) and the dimensionless parameter λ (3.75) (Figure 4.46b) are shown. As can be seen, the areas of unstable regions are larger for the *modified module.* However, for this type of module, reducing unstable regions is faster. For example, at $S = 50\text{kN}$ the unstable regions are smaller than at the minimum prestress level about:

FIGURE 4.44 Limits of the main unstable regions for the *regular Simplex module*: (**a**) S = 0 kN, (**b**) S = 50 kN, and (**c**) S = 110 kN.

FIGURE 4.45 Limits of the main unstable regions for the *modified Simplex module*: (**a**) S = 0 kN, (**b**) S = 50 kN, and (**c**) S = 110 kN.

FIGURE 4.46*Simplex modules.* Influence of the initial prestress level S on the: (**a**) area of unstable regions $A_\eta(S)$ and (**b**) range of unstable regions λ.

- 66%, 40%, and 28% for the *regular Simplex module*;
- 75%, 50%, and 37% for the *modified Simplex module*,

respectively, for $P = 10\text{kN}$, $P = 20\text{kN}$, and $P = 30\text{kN}$.

4.5.4.2 Quartex Modules

The main unstable regions for *regular module* are shown in Figure 4.47, in turn for the *modified module* in Figure 4.48. The conclusions are the same as in the case of *Simplex modules*. The higher the load, the larger the region, and the higher the initial prestress level, the smaller the unstable regions. The areas of unstable regions $A_\eta(S)$ are larger for the *modified module* (Figure 4.49a) and for this type of module, reducing unstable regions is faster (Figure 4.49b). For example, at $S = 50\text{kN}$ the unstable regions are smaller than at the minimum prestress level about:
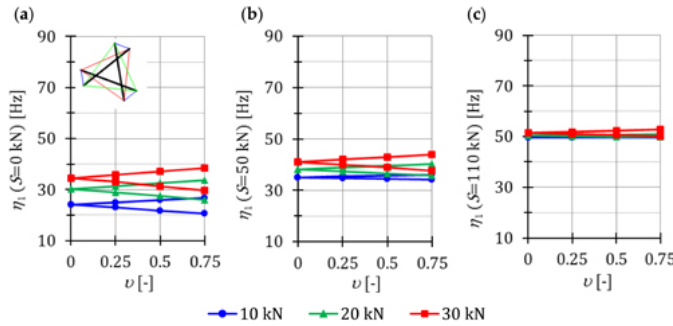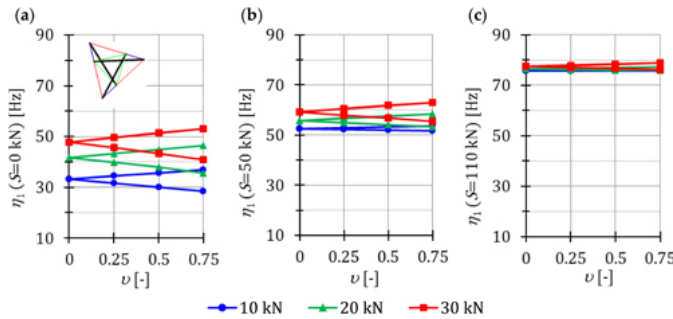

FIGURE 4.47 Limits of the main unstable regions for the *regular Quartex module*: (**a**) $S = 0$ kN, (**b**) $S = 50$ kN, and (**c**) $S = 110$ kN.

FIGURE 4.48 Limits of the main unstable regions for the *modified Quartex module*: (**a**) $S = 0$ kN, (**b**) $S = 50$ kN, and (**c**) $S = 110$ kN.
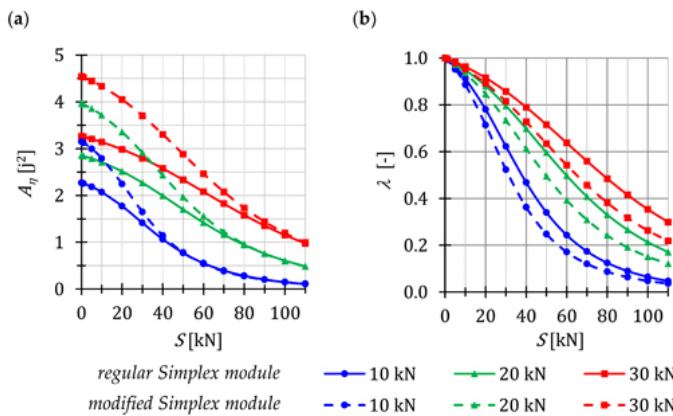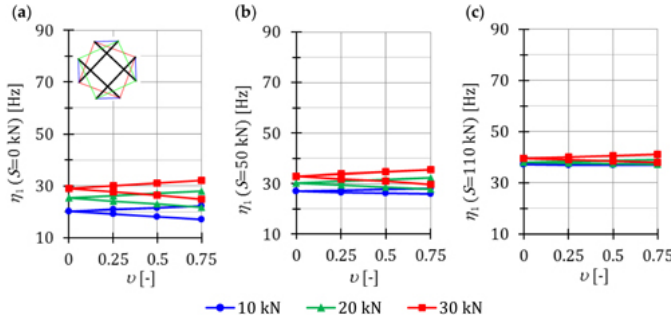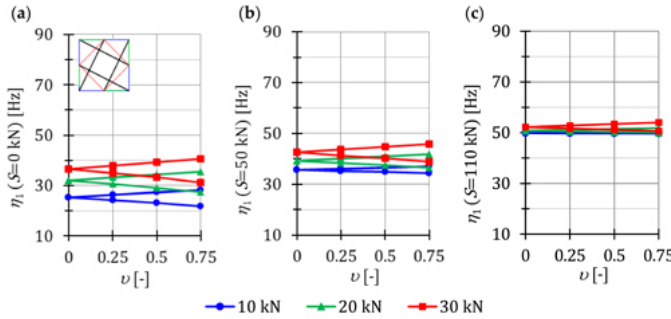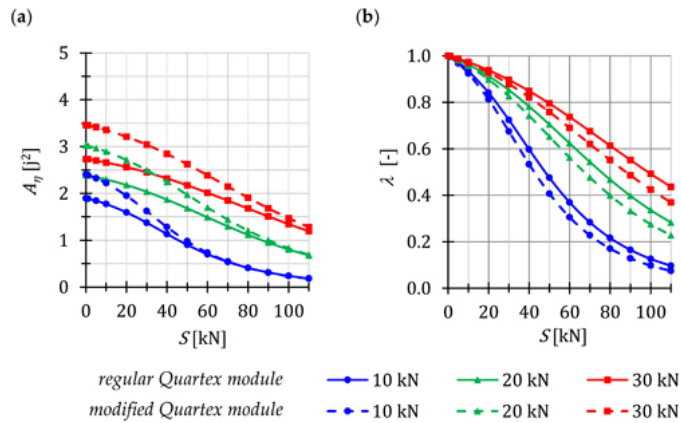
FIGURE 4.49 *Quartex modules.* Influence of the initial prestress level *S* on the: (**a**) area of unstable regions $A_\eta(S)$ and (**b**) range of unstable regions λ.

- 52%, 30%, and 21% for the *regular Quartex module*;
- 59%, 35%, and 24% for the *modified Quartex module*,

respectively, for $P = 10\text{kN}$, $P = 20\text{kN}$, and $P = 30\text{kN}$.

Comparing *Quartex modules* with *Simplex modules*, it can be seen that the modification in the case of *Simplex modules* has a greater influence on the range of unstable regions.

The second-resonance frequency η_2 does not depend on both changes in the level of prestress and external loads (Table 4.20). Additionally, it is twice the free second frequency – $\eta_2 = 2f_2$ (see Table 4.19). The maximum relative difference is equal 0.2% (*modified Quartex module*).

TABLE 4.20 Second-Resonant Frequency of the Basic 3D Tensegrity Modules

S(kN)	Type of Module	P = 10 kN	P = 20 kN	P = 30 kN
		η_2 (Hz) ($v = 0 \div 0.75$)		
Simplex modules				
0	*regular*	257.29	257.32	257.34
110		257.67	257.65	257.64
0	*modified*	305.27	305.28	305.30
110		305.56	305.54	305.53
Quartex modules				
0	*regular*	273.31	273.33	273.33
110		273.71	273.67	273.64
0	*modified*	387.63	387.68	387.71
110		388.22	388.19	388.17

4.5.5 CHAPTER SUMMARY

This chapter discusses two basic three-dimensional modules in two versions, i.e., *regular* and *modified*. These modules can be used to create two types of structures, depending on how they are connected. A linear connection leads to the creation of towers and booms (beam-like structures), while a planar connection leads to double-layer tensegrity grids (plate-like structures). *Modified* modules are easier to combine into multi-module structures. Comparative nature of analysis leads to answers to the questions posed at the beginning of the consideration.

1. How does the modification affect the behavior of modules?

Qualitatively, the modification makes no difference. However, quantitatively, there is a difference. Static analysis shows that *modified* modules are stiffer than *regular* ones. This would suggest that this solution is better, but the dynamic stability analysis leads to the opposite conclusion.

It should be noted that the first natural frequency of the *regular Simplex module* is almost identical to that of the *modified Quartex module.*

2. Which type of module is more sensitive to the risk of excitation vibrations?

Modified modules are sensitive to the risk of excitation vibrations. The modification in the case of *Simplex modules* has a greater influence on the range of unstable regions than in the case of Quartex modules.

NOTE

1. The circumferential cables C_3 and C_5 are only in the *modified Geiger domes.*↵

4.6 TENSEGRITY DOMES

The two most well-known and completely different cable-strut domes are considered, i.e., *Geiger dome* and *Levy dome*. The differences are in both geometry and tensegrity classification. The domes are built with load-bearing girders distributed radially, rotated by angle γ with respect to the axis z in the center of the span. The girders base on *Geiger truss types A-2* and *B-2*. This means two variants of connecting in the center of the span are considered, i.e., girders connected by a strut (*type A*) (Figure 4.50a) and by a ring (*type B*) (Figure 4.50b). Element designations are the same as in 2D models (see Section 4.4). Struts are marked as S_1, S_2, and S_3, whereas the cables are separated on diagonally (1, 2, 3, 4, 5, 6) and circumferential (C_1, C_2, C_3, C_4, C_5,C_6) [1] . In the case of *Geiger domes*, the load-bearing girder is flat, which results in all struts being in a line. In contrast, in the case of Levy domes, the girder is spatial, which results in the relocation of strut S_3. The small-scale steel domes are analyzed. The domes' diameter is 12 m, and their height is 3.25 m. The coordinates of the leading load-bearing girders are given in Table 4.21. The coordinates of the subsequent girders are determined according to the variables polar as: $x = r_i \cos\gamma$ and $y = r_i \sin\gamma$ ($i = 0, 1, 2, 3$). The following radii are assumed: $r_0 = 0.5$ m, $r_1 = 2.0$ m, $r_2 = 4.0$ m, and $r_3 = 6.0$ m.
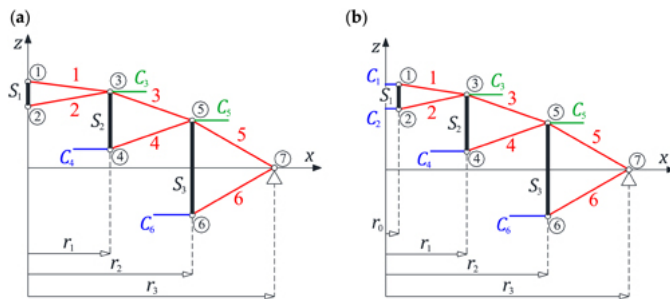
FIGURE 4.50 Load-bearing girders: (**a**) *type A-2* and (**b**) *type B-2.*

TABLE 4.21 Coordinates of the Load-Bearing Girder Nodes

No. of Node		1	2	3	4	5	6	7
Geiger girders								
type A-2	x (m)	0.0	0.0	2.0	2.0	4.0	4.0	6.0
type B-2		0.5	0.5					
type A-2, B-2	y (m)	0.0	0.0	0.0	0.0	0.0	0.0	0.0
type A-2, B-2	z (m)	2.1	1.5	1.85	0.45	1.15	−1.15	0.0
Levy girders								
type A-2	x (m)	0.0	0.0	2.0	2.0	$4\cos\frac{\gamma}{2}$	$4\cos\frac{\gamma}{2}$	6.0
type B-2		0.5	0.5					
type A-2, B-2	y (m)	0.0	0.0	0.0	0.0	$4\sin\frac{\gamma}{2}$	$4\sin\frac{\gamma}{2}$	0.0
type A-2, B-2	z (m)	2.1	1.5	1.85	0.45	1.15	−1.15	0.0

The number of load-bearing girders (ng) used in the construction of the domes can be arbitrary. In addition, two design solutions are being considered for the *Geiger domes*, i.e., a dome according to Geiger's patent (*regular dome*) and a modification of the Geiger patent by adding additional circumferential cables (C_3 and C_5) connecting the top nodes (*modified dome*). Consequently, all design solutions known from the literature (see Section 1.5.1) are analyzed:

- *regular Geiger dome type A-2* (Figure 4.51a);
- *regular Geiger dome type B-2* (Figure 4.51b);
- *modified Geiger dome type A-2* (Figure 4.52a);
- *modified Geiger dome type B*-2 (Figure 4.52b);
- *Levy dome type A-2* (Figure 4.53a);
- *Levy dome type B-2* (Figure 4.53b).
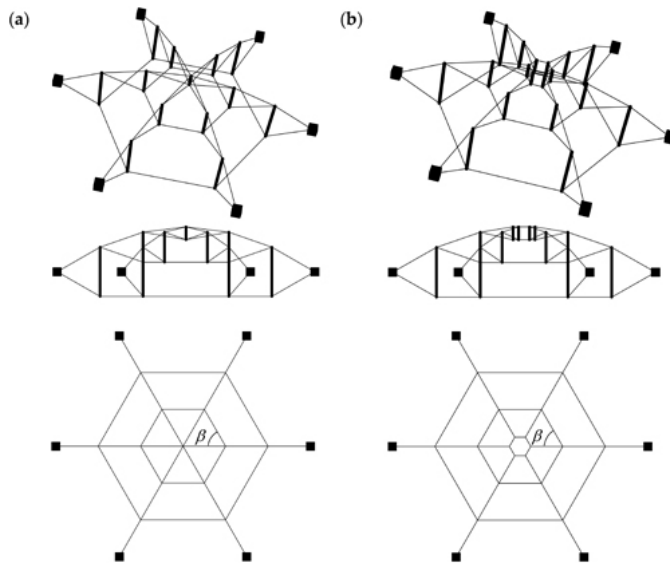
FIGURE 4.51 *Regular Geiger dome* with six load-bearing girders: (**a**) *type A-2* and (**b**) *type B-2.*
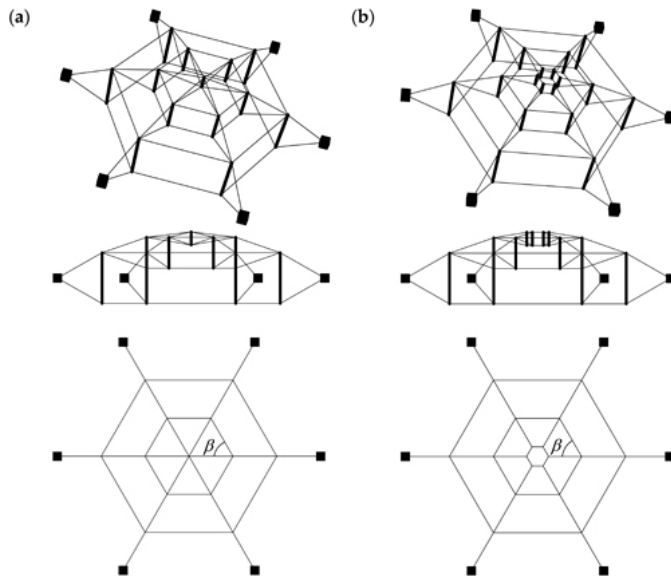
FIGURE 4.52 *Modified Geiger dome* with six load-bearing girders: (**a**) *type A-2* and (**b**) *type B-2.*
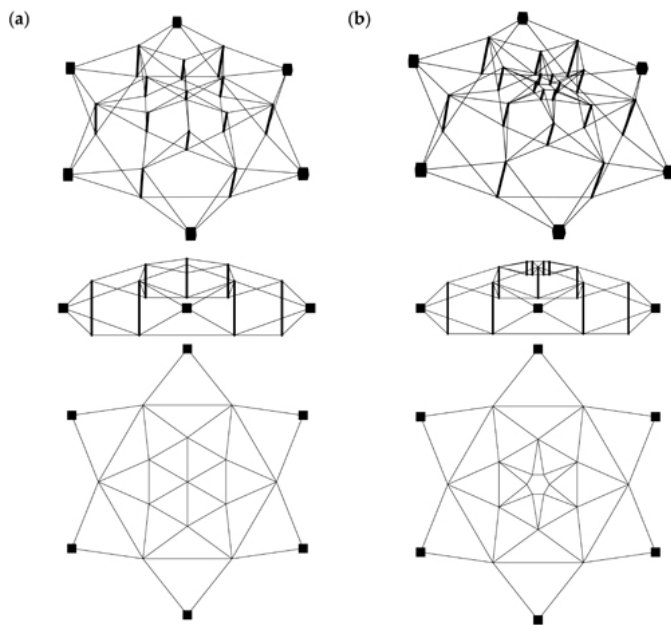
FIGURE 4.53 *Levy dome* with six load-bearing girders: (**a**) *type A-2* and (**b**) *type B-2.*

The domes are supported at each external node of the lower section. Three translational degrees of freedom have been taken away (in figures marked by a cuboid). This type of support corresponds to a circumferential clamping ring.

The qualitative analysis is performed for domes with different numbers of load-bearing girders (ng). The 6, 8, 10, and 12 girders are taken into account ($ng = \{6, 8, 10, 12\}$). Only the results of the analysis are presented. In turn, the quantitative analysis includes the behavior of domes with six load-bearing girders ($ng = 6$). Material and geometric

characteristics are assumed according to Table 4.1. The struts were divided into three groups according to length l and load-bearing capacity N_{Rd} (Table 4.2):

- S_1 group: $l = 0.6$m and $N_{Rd} = 224.3$kN;
- S_2 group: $l = 1.4$ m and $N_{Rd} = 170.5$kN;
- S_3 group: $l = 2.3$ m and $N_{Rd} = 107.1$kN.

The domes are loaded by force $P = 5$kN applied to one node in z-direction. The analysis is cognitive in nature. The assumed load is sufficient to evaluate the behavior of domes under exceptional loads. To compare the response to an external disturbance, load is applied successively in the first, third, and fifth nodes (see Figure 4.50). The minimum prestress level S_{min} is calculated individually for each dome for each variant of load applications (Table 4.22). In turn, the same maximum prestress level $S_{max} = 50$kN was adopted to compare the behavior of all domes. This value corresponds to the maximum effort of the structure (3.22) equal to $W_{max} = 0.93$ (for *Geiger domes*). As can be seen, in the case of the *Levy dome type B-2* with load applied in the first and third nodes, the minimum prestress level is equal to the maximum one, $S_{min} = S_{max}$.

TABLE 4.22 Values of the Minimum Prestress Level S_{min} for Domes⏎

Type of Dome	Force P = 5 kN applied to:		
	First node	Third node	Fifth node
	S_{min} (kN)		
regular Geiger dome type A-2	8	22	24
regular Geiger dome type B-2	2		
modified Geiger dome type A-2	11	34	36
modified Geiger dome type B-2	41	26	2
Levy dome type A-2	18	42	5
Levy dome type B-2	50	50	12

Purpose of the Consideration

In the previous chapters the simple structures have been described in detail. Based on the results and conclusions obtained, several questions about the domes under consideration arise:

1. Is it possible to derive formulas for self-equilibrium forces (self-stress state)?
2. How does the modification of Geiger patent (*regular Geiger dome type B-2*) affect the behavior of *Geiger domes*?
3. Which solution of *Geiger domes* is best in terms of its ability to control static and dynamic parameters?
4. Whether the number of infinitesimal mechanisms affects the behavior of *Geiger domes*?
5. Whether the upper section type matter in the case of *Levy dome*?
6. The behavior of which type of *Levy dome* is possible to control?
7. Is it possible to controlling the occurrence of infinitesimal mechanisms by changing the number of load-bearing girders?
8. How does the initial prestress level influence the natural frequencies correlated with the infinitesimal mechanisms?
9. Is the number of natural frequencies depending on the prestressing equal to the number of infinitesimal mechanisms?
10. Whether the number of load-bearing girders impacts the natural frequencies corresponding to the infinitesimal mechanisms?

4.6.1 QUALITATIVE ANALYSIS

4.6.1.1 Regular Geiger Domes

The results of the qualitative analysis of *regular Geiger domes* are shown in Table 4.23. The number of mechanisms depends on type of load-bearing girder. In the case of girder *type A-2*, it is possible to determine the number of mechanisms (nm) as a function of the number of struts (ns). For the case of girder *type B-2*, on the other hand, as a function of the number of cables $(n - ns)$. In turn, only one self-stress state is identified independently on type of girder. All eigenvalues of the stiffness matrix (3.19) are positive. This means the self-stress state identifies the appropriate normal forces in the structural elements and stabilizes mechanisms, i.e., the mechanisms are infinitesimal.

TABLE 4.23 Results of the Qualitative Analysis of the *Regular Geiger Domes* ↵

No. of Girders (ng)	Nodes (nn)	Elements (n)	d.o.f (m)	Struts (ns)	Mechanisms (nm)	Self-stress states (nss)	Classification
regular Geiger domes type A-2							
6	32	61	78	13	18	1	*ideal tensegrity*
8	42	81	102	17	22	1	
10	52	101	126	21	26	1	
12	62	121	150	25	30	1	
$\frac{ns-1}{2}$					$ns + 5$	1	
regular Geiger domes type B-2							
6	42	78	108	18	31	1	*ideal tensegrity*
8	56	104	144	24	41	1	
10	70	130	180	30	51	1	
12	84	156	216	36	61	1	
$\frac{ns}{3}$					$\frac{n-ns}{2} + 1$	1	

The *regular Geiger domes* are characterized by all six tensegrity features. They are trusses (TT) with a set of discontinuous set of struts (DS) contained within the continuous net of tensile elements (IN) that have no rigidity in compression (TC). In these structures, there is one self-stress state (SS) that stabilizes all infinitesimal mechanisms (IM). According to the tensegrity classification (Table 3.1), the *regular Geiger domes* are *ideal tensegrity.*

It should be noted that, due to the *regular Geiger domes* consist of basic 2D tensegrity models (see Section 4.4.1), the formulas for self-equilibrium forces are possible to derive (Table 4.24). These formulas depend on the type of load-bearing girders, the angle of inclination of the diagonal cables of gird α_i (see Figure 4.16), and additionally on the angle β (2β is the angle between *circumferential* cables). Taking into account the coordinates of the *Geiger girders* (Table 4.21), the values on the self-stress forces y_S are shown in Tables 4.25.

TABLE 4.24 Formulas for Self-Equilibrium Forces (Self-Stress State) for the *Regular Geiger Domes* ↵

Regular Geiger Domes Type A-2	Regular Geiger Domes Type B-2
$N_1 = \mathrm{const.};\quad i \in N_+$	
struts:	
$N_{S_1} = -ng \cdot N_1 \sin(\alpha_1)$	$N_{S_1} = -N_1 \sin(\alpha_1)$
$N_{S_{i+1}} = -N_{2(i+1)} \sin\left(\alpha_{2(i+1)}\right)$	
diagonal cables:	

Regular Geiger Domes Type A-2	Regular Geiger Domes Type B-2
$N_{2i} = N_{2i-1}\frac{\sin(\alpha_{2i-1})}{\sin(\alpha_{2i})}$	$N_{2i+1} = \frac{N_{2i-1}\cos(\alpha_{2i-1})+N_{2i}\cos(\alpha_{2i})}{\cos(\alpha_{2i+1})}$
circumferential cables:	
$N_{C_{2(i+1)}} = 0.5N_{2(i+1)}\frac{\cos(\alpha_{2(i+1)})}{\cos(\beta)}$	$N_{C_1} = 0.5N_1\frac{\cos(\alpha_1)}{\cos(\beta)}$ $N_{C_2} = 0.5N_2\frac{\cos(\alpha_2)}{\cos(\beta)}$

TABLE 4.25 Values of Self-Stress State $\mathbf{y}_s$ of the
Regular Geiger Domes ⏎

el.	Regular Geiger Domes Type A-2				Regular Geiger Domes Type B-2			
	ng = 6	ng = 8	ng = 10	ng = 12	ng = 6	ng = 8	ng = 10	ng = 12
	y_s(–)				y_s(–)			
S_1	–0.3804	–0.5072	–0.6341	–0.7609	–0.0845			
S_2	–0.3043				–0.3043			
S_3	–1.0000				–1.0000			
1	0.5112				0.5142			
2	0.3678				0.3721			
3	0.9213				0.9213			
4								
5	2.0061				2.0061			
6								
C_1	–				0.5072	0.6627	0.8207	0.9799
C_2	–				0.3623	0.4734	0.5862	0.6999
C_4	0.8696	1.1361	1.4070	1.6799	0.8696	1.1361	1.4070	1.6799
C_6	1.7391	2.2723	2.8140	3.3597	1.7391	2.2723	2.8140	3.3597

4.6.1.2 Modified Geiger Domes

The results of the qualitative analysis of *modified Geiger domes* are shown in Table 4.26. Generally, the modification leads to the reduction of the number of infinitesimal mechanisms. In the case of *domes type A*, independently on the type and on the number of load-bearing girders, eight mechanisms are identified, whereas for *domes type B,* the number of mechanisms depends on the number of struts. In turn, the number of self-stress states does not depend on the number of load-bearing girders and on type, it always equals three. Since neither of the three states correctly identifies the type of elements, a superimposed self-stress state is necessary (Table 4.27). If the superposed self-stress state is taken into account, all eigenvalues of the stiffness matrix (3.19) are positive. This means the self-stress state identifies the appropriate normal forces in the structural elements and stabilizes mechanisms, i.e., the mechanisms are infinitesimal.

TABLE 4.26 Results of the Qualitative Analysis of the *Modified Geiger Domes* ⏎

No. of							Classification
Girders	Nodes	Elements	d.o.f	Struts	Mechanisms	Self-Stress States	
(ng)	(nn)	(n)	(m)	(ns)	(nm)	(nss)	
modified Geiger domes type A-2							
6	32	73	78	13	8	3	*structures with tensegrity features of class 1*
8	42	97	102	17	8	3	
10	52	121	126	21	8	3	
12	62	145	150	25	8	3	
$\frac{ns-1}{2}$					8	3	
modified Geiger domes type B-2							

No. of Girders (ng)	Nodes (nn)	Elements (n)	d.o.f (m)	Struts (ns)	Mechanisms (nm)	Self-Stress States (nss)	Classification
6	42	90	108	18	21	3	*structures with tensegrity features of class 1*
8	56	120	144	24	27	3	
10	70	150	180	30	33	3	
12	84	180	216	36	39	3	
$\frac{ns}{3}$					$ns + 3$	3	

TABLE 4.27 Values of Self-Stress State $\mathbf{y}_s$ of the *Modified Geiger Dome* ⏎

el.	Modified Geiger Domes Type A-2				Modified Geiger Domes Type B-2			
	ng = 6	ng = 8	ng = 10	ng = 12	ng = 6	ng = 8	ng = 10	ng = 12
	y_s(–)				y_s(–)			
S_1	–0.2277	–0.3036	–0.3795	–0.4554	–0.0506			
S_2	–0.2646				–0.2646			
S_3	–1.0000				–1.0000			
1	0.3060				0.3076			
2	0.2201				0.2225			
3	0.8010				0.8010			
4								
5	2.0061				2.0061			
6								
C_1	–				0.3034	0.3964	0.4909	0.5862
C_2	–				0.2167	0.2830	0.3505	0.4185
C_3	0.2356	0.3078	0.3812	0.4551	0.2356	0.3078	0.3812	0.4551
C_4	0.7560	0.9877	1.2233	1.4606	0.7560	0.9877	1.2233	1.4606
C_5	0.2270	0.2968	0.3676	0.4389	0.2270	0.2968	0.3676	0.4389
C_6	1.7391	2.2720	2.8139	3.3597	1.7391	2.2720	2.8139	3.3597

The *modified Geiger domes* are characterized by all six tensegrity features. They are trusses (TT) with a set of discontinuous set of struts (DS) contained within the continuous net of tensile elements (IN) that have no rigidity in compression (TC). In these structures, there is superposed self-stress state (SS) that stabilizes all infinitesimal mechanisms (IM). According to the tensegrity classification (Table 3.1), although the *modified domes* meet all tensegrity features, the necessity of superposition of the self-stress states classified them into *structures with tensegrity of class 1*.

4.6.1.3 Levy Domes

The results of the qualitative analysis of *Levy domes* are shown in Tables 4.28. These structures completely differ from *Geiger domes*. In the case of *domes type A-2,* there are no mechanisms and in the case of *domes type B-2*, there is only one mechanism, regardless of the number of load-bearing girders. In turn, there are a lot of self-stress states for all domes. In the case of grids *type A-2*, the number of self-stress states is a function of the number of struts (ns). In turn, in the case of *type B-2*, is a function of the number of struts (ns) and the number of girders (ng). Since neither of the states correctly identifies the type of elements, a superimposed self-stress state is necessary (Table 4.29). If the superposed self-stress state is taken into account, all eigenvalues of the stiffness matrix (3.19) are positive. This means the self-stress state identifies the appropriate normal forces in the structural elements and, in the case of *Levy domes type B-2*, stabilizes mechanism, i.e., the mechanism is infinitesimal.

TABLE 4.28 Results of the Qualitative Analysis of the *Levy Domes* ⏎

No. of							Classification
Girders (ng)	Nodes (nn)	Elements (n)	d.o.f (m)	Struts (ns)	Mechanisms (nm)	Self-Stress States (nss)	
Levy domes type A-2							
6	32	85	78	13	0	7	structures with tensegrity features of class 2
8	42	113	102	17	0	11	
10	52	141	126	21	0	15	
12	62	169	150	25	0	19	
$\frac{ns-1}{2}$						0	$ns - 6$
Levy domes type B-2							
6	42	114	108	18	1	7	structures with tensegrity features of class 1
8	56	152	144	24	1	9	
10	70	190	180	30	1	11	
12	84	228	216	36	1	13	
$\frac{ns}{3}$						1	$ns - 2ng + 1$

TABLE 4.29 Values of Self-Stress State $\mathbf{y}_s$ of the Levy Domes ↵

el.	Levy Domes Type A-2				Levy Domes Type B-2			
	ng = 6	ng = 8	ng = 10	ng = 12	ng = 6	ng = 8	ng = 10	ng = 12
	$y_s(-)$				$y_s(-)$			
S_1	–0.147	–0.308	–0.465	–0.616	–0.031	–0.050	–0.061	–0.068
S_2	–0.161	–0.218	–0.248	–0.264	–0.161	–0.218	–0.248	–0.264
S_3	–1.000				–1.000			
1	0.197	0.311	0.375	0.414	0.100	0.157	0.189	0.209
2	0.142	0.224	0.270	0.298	0.073	0.114	0.137	0.151
3	0.295	0.372	0.406	0.424	0.295	0.372	0.406	0.424
4								
5	1.491	1.303	1.204	1.147	1.491	1.303	1.204	1.147
6								
C_1	–				0.154	0.353	0.554	0.748
C_2	–				0.109	0.252	0.396	0.534
C_4	0.336	0.691	1.032	1.359	0.336	0.691	1.032	1.359
C_6	1.040	1.753	2.401	3.016	1.040	1.753	2.401	3.016

The *Levy domes type A-2* are characterized by four tensegrity features. They are trusses (TT) with the discontinuous system of compression elements (DS) included inside the set of elements in tension (IN), that have no rigidity in compression (TC). According to the tensegrity classification (Table 3.1), due to the lack of mechanisms, these domes are *structures with tensegrity features of class 2.* In turn, although the *Levy domes type B-2* meet all tensegrity features, the necessity of superposition of the self-stress states classified them into *structures with tensegrity of class 1*.

It should be noted that the mechanism of *Levy domes type B-2* is related only to the upper open section (Figure 4.54). The type of mechanism differs from in the case of the *Geiger domes* which are related to the entire structure. For example, in Figure 4.55, the infinitesimal mechanisms for *modified Geiger dome type A-2* with six load-bearing girders are shown.

(a)   (b)   (c)   (d)
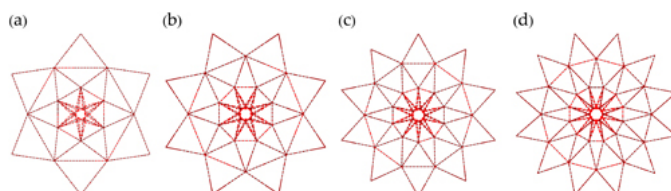
FIGURE 4.54 Infinitesimal mechanisms for the *Levy dome type B-2:* (**a**) *ng* = 6, (**b**) *ng* = 8, (**c**) *ng* = 10, and (**d**) *ng* = 12.↵
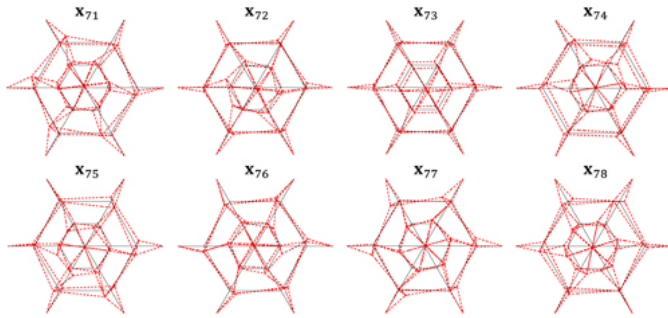

FIGURE 4.55 Infinitesimal mechanisms for the *modified Geiger dome type A-2.* ↵

4.6.2 STATIC ANALYSIS

4.6.2.1 Geiger Domes

The static analysis includes the behavior of the *Geiger domes with* six load-bearing girders ($ng = 6$). The values of the self-stress state y_S are assumed according to Tables 4.25 and 4.27 for *regular* and *modified* domes, respectively. To compare the behavior of different solutions, the *global stiffness parameter* GSP and the effort of structure W_{max} (for cables) are shown in Figure 4.56. As can be seen, the behavior mostly depend on type of solution and on the point of application of the load.
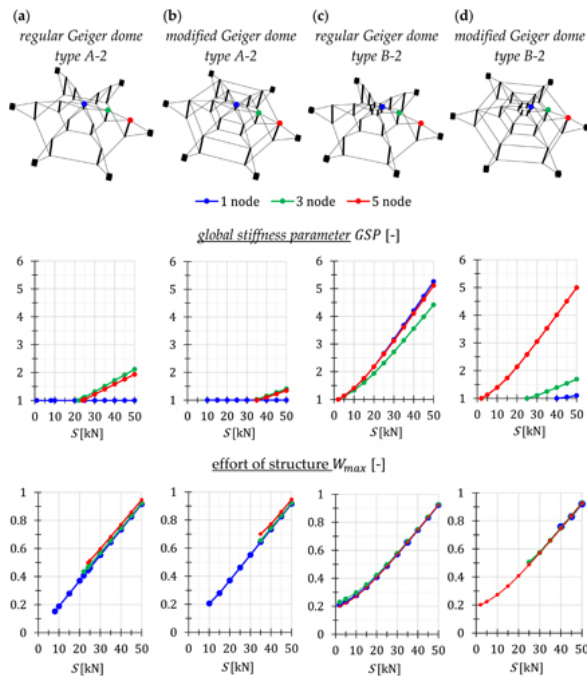
FIGURE 4.56 Results of static analysis for the *Geiger domes.*↵

In the case of *domes type A-2* (Figures 4.56a, 4.56b), a load applied to the first node (blue color) causes displacements that are incompatible with the mechanism. The behavior

of domes is the same as the behavior of the *X-truss* (see Section 4.3.2). The *global stiffness parameter* (3.32) is constant and equal to $GSP = 1$, in turn the effort of the structure W_{max} is linearly dependent on the prestress. When the exceptional load is applied in the third (green color) and fifth (red color) nodes, there is an increase in stiffness, but it is small compared to Geiger's patent (Figure 4.56c). The linear nature of changes in the effort of the structure W_{max} means a negligible influence of prestress on the behavior of domes. This is due to the value of the minimum prestress level and, more specifically, the small range of prestress changes.

In the case of *regular Geiger dome type B-2* (Geiger patent) (Figure 4.56c), the minimum prestress level does not depend on the type of load application. In addition, the value of them is small $(S_{min} = 2\text{kN})$. As can be seen, this dome behave completely different than the *domes type A-2*. The influence of initial prestress is large. At the maximum level of initial prestress, the parameter GSP for the *regular Geiger dome type B-2* is 2.1 and 2.6 times higher than for the *regular Geiger dome type A-2,* for the load applied in the third and fifth nodes, respectively. On the other hand, when compared with the *modified Geiger dome type A-2,* the differences are larger, and the parameter GSP is 3.1 and 3.8 times higher, respectively.

In turn, the modification of Geiger patent by added additional circumferential cables (Figure 4.56d) leads to an increase the value of the minimum prestress level and to decrease the influence of prestress on behavior of dome. Only, in the case of load applied in the fifth node, the *modified Geiger dome type B-2* behave as the *regular Geiger dome type B-2.*

4.6.2.2 Levy Domes

The static analysis includes the behavior of the domes with six load-bearing girders ($ng = 6$). The values of the self-stress state y_S are assumed according to Table 4.29. The results of analysis for are shown in Table 4.30. In the case of the *Levy dome type B-2*, the analysis is notable only for the load applied to the fifth node. This is due to the fact that the level of the minimum prestress level is equal to the maximum one, $S_{min} = S_{max}$. However, in all cases, the influence of the initial prestress on the static parameters is negligible, even for dome with infinitesimal mechanism (*dome type B-2*). The mechanism has a local character, related only to the upper open section.

TABLE 4.30 Results of Static Analysis for the *Levy Domes* ⏎

S(kN)	Typeof Element	Force P = 5 kN applied to:							
		First node		Third node		Fifth node		Fifth node	
		W_{max}(–)	GSP(–)	W_{max}(–)	GSP(–)	W_{max}(–)	GSP(–)	W_{max}(–)	GSP(–)
		dome type A-2						dome type B-2	
		S_{min} = 18 kN		S_{min} = 42 kN		S_{min} = 5 kN		S_{min} = 12 kN	
S_{min}	Cables	0.25	1.0	0.61	1.0	0.10	1.0	0.18	1.0
	Struts	0.16		0.41		0.05		0.11	
50	Cables	0.68	1.0	0.72	1.0	0.71	1.0	0.69	1.0
	Struts	0.46		0.49		0.47		0.47	

4.6.3 DYNAMIC ANALYSIS

4.6.3.1 Geiger Domes

Static analysis has shown that, from the point of view of the ability to control static parameters, the best solution is the *regular Geiger dome type B-2*. In order to check the dynamic behavior of domes, the natural frequencies are calculated. First, the behavior of the *Geiger domes* with six load-bearing girders ($ng = 6$) is analyzed. Next, the influence of the number of girders on the behavior is considered.

4.6.3.2 Geiger Domes with Six Load-Bearing Girders

Figure 4.57 presents the results of the analysis for the *Geiger domes* with six load-bearing girders. The influence of the initial prestress level on the first f_1 and last natural frequency f_{nm}, correlated with infinitesimal mechanisms, is shown. In the absence of prestress, these frequencies are zero, and the corresponding vibration modes implement the mechanisms. For example, Figure 4.58 shows the *modified Geiger dome type A-2* is showed (compare with Figure 4.55). Interestingly, there are eight different forms of vibration but six different frequencies ($f_2 = f_3$ and $f_5 = f_6$). In the case of other domes, it is the same.
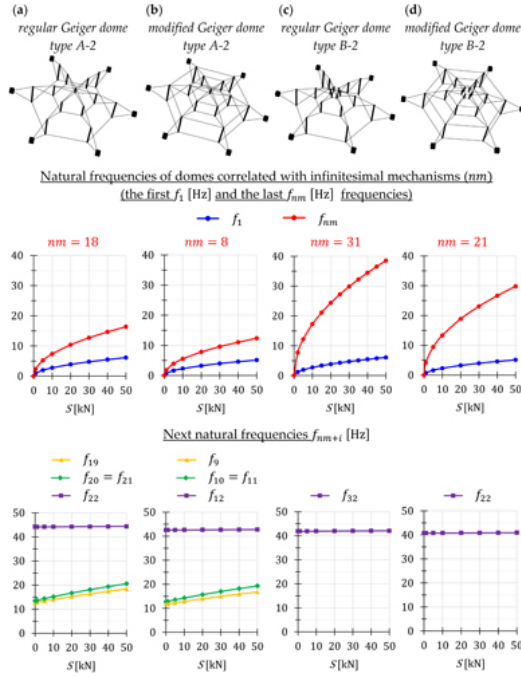
FIGURE 4.57 Influence of the initial prestress *S* on the natural frequencies for *Geiger domes.*
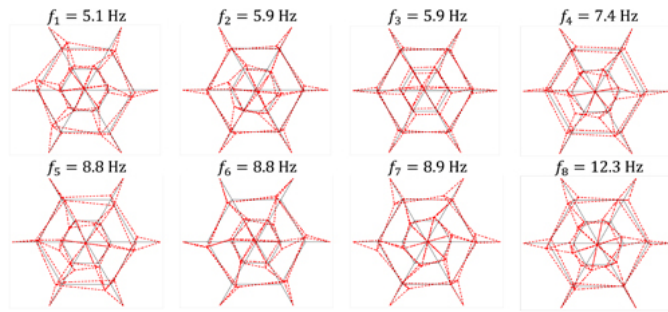
FIGURE 4.58 Forms of vibration for the *modified Geiger dome type A-2* (values of frequencies for $S_{\max}$).

After the introduction of prestress, the considered frequencies increase nonlinearly. The range of changes mainly depends on the kind of dome, which means, on the number of infinitesimal mechanisms. The level of the first frequency f_1 is similar for each considered dome $f_1 = 5.1\,\mathrm{Hz} \div 6.5\,\mathrm{Hz}$ for S_{max}, while differs for the frequency f_{nm}. It should be

noted that between frequencies f_1 and f_{nm} there are several, a dozen, or several dozen frequencies depending on prestress. The number of them are equal to the number of infinitesimal mechanisms. For this reason, the *regular Geiger dome type B-2* is the most sensitive to dynamic parameter control.

A study of the next frequencies f_{nm+i} showed that in the case of *dome type B-2*, they do not depend on the prestress (Figure 4.57c, d). They are equal to $f_{32} = 42\mathrm{Hz}$ and $f_{22} = 41\mathrm{Hz}$ for *regular* and *modified* domes, respectively. Nevertheless, it is different for the *Geiger domes type A-2*. In this case, three additional frequencies depend on prestress (Figure 4.57a, b). In the absence of prestress, they are non-zero, and the dependence on prestress is almost linear. The additional natural frequencies characterized by a little sensitivity to the change in the initial prestress level, comparing to the natural frequencies correlated to the infinitesimal mechanisms. Independent of prestress is the fourth next frequency, i.e., $f_{22} = 44\mathrm{Hz}$ and $f_{12} = 43\mathrm{Hz}$ for *regular* and *modified domes*, respectively. As can be seen, the values of frequencies independent on prestress for all domes are at the same level.

4.6.3.3 Geiger Domes with Different Numbers of Load-Bearing Girders

Figure 4.59 presents the results of dynamic analysis for domes with a different number of load-bearing girders (ng), i.e., $ng = \{6, 8, 10, 12\}$. The influence of the initial prestress level on the first f_1 (dotted line) and the last correlated with infinitesimal mechanisms f_{nm} (continuous line) natural frequencies is shown. The level of frequency f_1 is similar for each considered dome, independently of the number of girders. In turn, frequency f_{nm} depends on the type of dome and is more sensitive to the changes in prestressing.

(a) regular Geiger dome type A-2		(b) modified Geiger dome type A-2		(c) regular Geiger dome type B-2		(d) modified Geiger dome type B-2	
No. of							
ng	*nm*	*ng*	*nm*	*ng*	*nm*	*ng*	*nm*
6	18	6	8	6	31	6	21
8	22	8	8	8	41	8	27
10	26	10	8	10	51	10	33
12	30	12	8	12	61	12	39
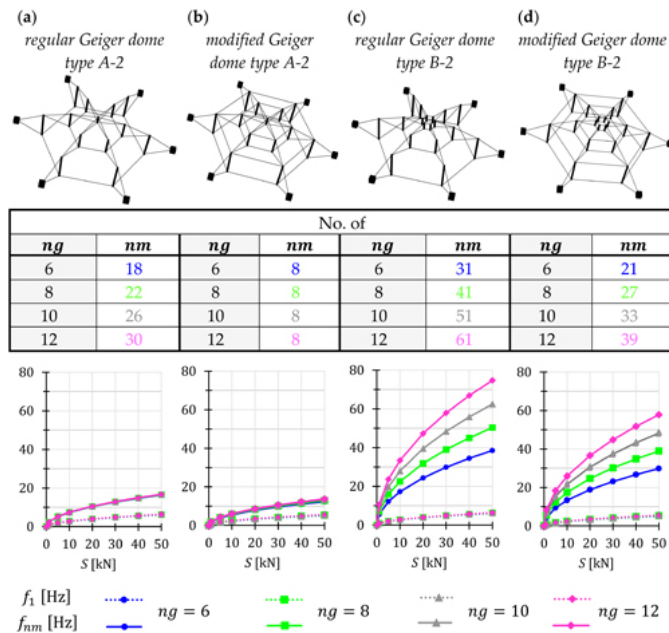
FIGURE 4.59 The first f_1 and last f_{nm} natural frequencies correlated with infinitesimal mechanisms (*nm*) for domes with different numbers of load-bearing girders (*ng*).

In the case of *regular Geiger dome type A-2* (Figure 4.59a), the increasing number of load-bearing girders is not affecting the frequencies f_{nm}. There is the same range of changes, despite the number of mechanisms is differ. It means that frequency f_{18} for a

dome with 6 girders is equal to frequency f_{30} for a dome with 12 girders. The same is true for the *modified Geiger dome type A-2* (Figure 4.59b), however, in this case, the number of mechanisms is constant and equal to $nm = 8$. It is a completely different for the *domes type B-2* (Figures 4.59c, 4.59d). An increase in the number of load-bearing girders results in the increase in the value of the frequency f_{nm}.

In addition, it should be noted that the *Geiger domes type A-2* are the specific structures. A study of the next frequencies f_{nm+i} showed that for these structures, there are additional frequencies depending on prestress (f_{add}). The number of them depends on the number of load-bearing girders (ng). Thus the total frequencies depending on prestress (f_{total}) is equal:

$$f_{total} = f_{nm} + f_{add}; f_{add} = (ng - 3)$$

In the absence of prestress, the frequencies f_{add} are non-zero and linearly (4.50) dependent on prestress. However, they are characterized by a low sensitivity to the change in the initial prestress level compared to the natural frequencies correlated with the infinitesimal mechanisms. The next frequencies ($f_{total+1}$) are independent of the prestress for all domes, and they are at the same level (Table 4.31). In the case of the *Geiger domes type B-2,* the number of frequencies depending on prestress is equal to the number of infinitesimal mechanisms ($f_{total} = f_{nm}$).

TABLE 4.31 First Natural Frequencies of the *Geiger Domes* Independent on the Initial Prestress Level S ($f_{total\,+\,1}$)↵

No. of Girders(ng)	Regular Geiger Domes				Modified Geiger Domes			
	nm	i	S		nm	i	S	
			0	50 kN			0	50 kN
			f_i (Hz)				f_i (Hz)	
type A-2								
6	18	(22)	44.2	44.4	8	(12)	42.6	42.7
8	22	(28)	44.4	44.7		(14)	43.1	43.3
10	26	(34)	44.5	44.7		(16)	43.4	43.6
12	30	(40)	44.4	44.7		(18)	43.5	43.7
type B-2								
6	31	(32)	41.9	42.1	21	(22)	40.7	40.9
8	41	(42)	42.0	42.2	27	(28)	41.2	41.4
10	51	(52)	41.9	42.1	33	(34)	41.3	41.5
12	61	(62)	41.6	41.8	39	(40)	41.3	41.5

4.6.3.4 *Levy Domes* with Different Numbers of Load-Bearing Girders

Static analysis has shown, that the initial prestress level S does not influence on the behavior of the *Levy domes*. In order to check the dynamic response of domes, the influence of the number of girders ($ng = \{6, 8, 10, 12\}$) on the behavior is considered.

Figure 4.60 presents the results of dynamic analysis for the domes without infinitesimal mechanisms, i.e., *Levy domes type A-2*. Three first frequencies are shown. Independently on the number of load-bearing girders, the dependences are linear and almost constant, especially for domes with a small number of girders. In the case of the first frequency, with the growth of the prestress from S_{min} to S_{max}, it increased by 6.4% ($ng = 6$), 6% ($ng = 8$), 7% ($ng = 10$), and 8.3% ($ng = 12$). In turn, the third frequency increased only by 0.4% ($ng = 6$), 3.5% ($ng = 8$), 5.1% ($ng = 10$), and 6.4% ($ng = 12$). Comparing all results, we can say that due to the lack of mechanisms, the natural frequencies are practically not affected by the initial prestress level, independent of the number of load-bearing girders.
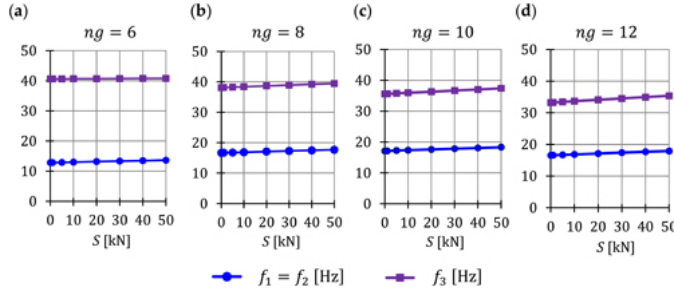
FIGURE 4.60 Influence of the initial prestress level *S* on the natural frequency for the *Levy domes type A-2:* (**a**) *ng* = 6, (**b**) *ng* = 8, (**c**) *ng* = 10, and (**d**) *ng* = 12.

Figure 4.61 presents the results of dynamic analysis for the domes with one infinitesimal mechanism, independently on the number of load-bearing girders, i.e., *Levy domes type B-2*. In the absence of prestress, the first natural frequency f_1 is zero, and the corresponding mode of vibration implements the mechanism. After the introduction of prestress, this frequency increase non-linearly. The range of changes mainly depends on the number of load-bearing girders. Additionally, as in the case of the *Geiger domes type A-2,* for these domes, there are additional frequencies depending on prestress (f_{add}). The number of them depends on the number of load-bearing girder (ng). Thus the total frequencies depending on prestress (f_{total}) is equal:
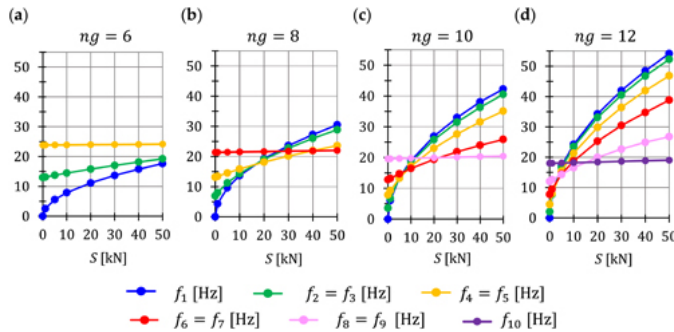
FIGURE 4.61 Influence of the initial prestress *S* on the natural frequencies for the *Levy domes type B-2:* (**a**) *ng* = 6, (**b**) *ng* = 8, (**c**) *ng* = 10, and (**d**) *ng* = 12.

$$f_{total} = 1 + f_{add}; f_{add} = (ng - 4)$$

The first frequency corresponding to the infinitesimal mechanism f_1, the additional(4.51) dependent of prestress f_{add}, and the first independent of prestress $f_{total+1}$ones are shown. In the absence of prestress, the additional frequencies, unlike to frequency corresponding to the mechanism, are not zero and the character of dependence on the prestress depends on the number of girders. Increasing the number of girders results in a greater sensitivity to a change in prestress. For example, the second frequency, with the growth of the prestress fromS_{min} to S_{max}, varies from $12.95\,\mathrm{Hz}$ to $19.24\,\mathrm{Hz}$ ($ng = 6$), $6.93\,\mathrm{Hz}$ to $28.88\,\mathrm{Hz}$ ($ng = 8$), $3.58\,\mathrm{Hz}$ to $40.55\,\mathrm{Hz}$ ($ng = 10$), and $2.07\,\mathrm{Hz}$ to $52.29\,\mathrm{Hz}$ ($ng = 12$). This means, the frequency value increased by 0.5% ($ng = 6$), 3% ($ng = 8$), 10% ($ng = 10$

), and 24% ($ng = 12$). In turn, the value of the first independent frequency is on the similar level $f_{total+1} = 18.4\,\mathrm{Hz} \div 23.9\,\mathrm{Hz}$.

4.6.4 Dynamic Stability Analysis

The static and dynamic analysis showed that the *Geiger domes type B-2* are the most sensitive to the influence of the initial prestress level. Due to this the unstable regions are determined for two variants of these domes, i.e., *regular* and *modified.* Domes with six load-bearing girders are considered.

The *regular Geiger dome type B-2* is characterized by 31 infinitesimal mechanisms. Due to this, 31 main unstable regions should be determined, however only four selected regions are shown. These regions correspond to the following resonance frequencies:η_1, η_{10}, η_{20}, and η_{31} (Figure 4.62). Three cases of initial prestress, i.e., $S_{min} = 2\mathrm{kN}$, $S = 10\mathrm{kN}$, and $S = 25\mathrm{kN}$, are considered. The area of unstable regions is larger at higher frequencies. The increasing of prestress reduces the range of unstable regions and increases resonant frequencies.
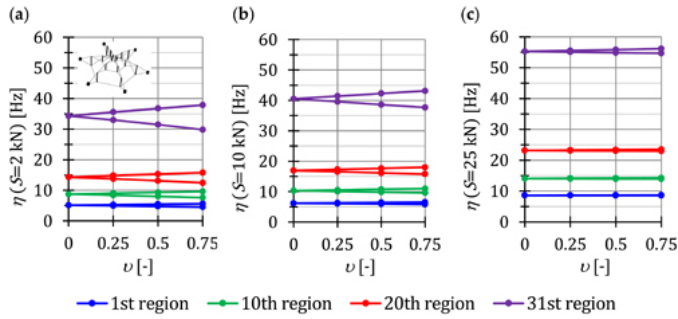
FIGURE 4.62 Limits of the selected four main unstable regions of the *regular Geiger dome type B-2*: (a) S_{min} = 2 kN, (b) S = 10 kN, and (c) S = 25 kN.↵

The *modified Geiger dome type B-2* behaves the same way. This dome characterizes by 21 infinitesimal mechanisms, therefore 21 main unstable regions should be determined. To comparison the behavior of both domes, Figure 4.63 presents the regions correspond to the following resonance frequencies:η_1, η_7, η_{14}, and η_{21}. The same levels of initial prestress are considered. In the case of a *modified dome* resonance frequencies η are lower, and unstable regions for the same level of initial prestress S are smaller than for the *regular dome.*
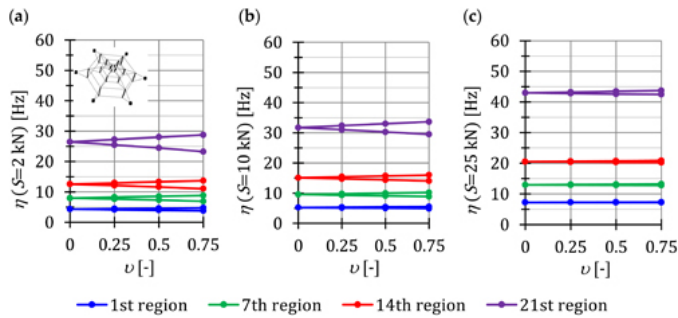
FIGURE 4.63 Limits of the selected four main unstable regions of the *modified Geiger dome type B-2*: (a) S_{min} = 2 kN, (b) S = 10 kN, and (c) S

= 25 kN.

To better compare the behavior of domes, the influence of initial prestress S on the area of unstable regions $A_\eta(S)$ is shown in Figure 4.64a. As can be seen, at low values of initial prestress forces ($S \in \langle 2\text{kN}; 25\text{kN} \rangle$), the area of the unstable regions for the *regular dome* (continuous line) is greater than those for the *modified dome* (dashed line). For example, for the minimum prestress level $S_{min} = 2\text{kN}$, the areas of the unstable region corresponding to the first and last resonance frequencies are larger by 14% and 47%, respectively. However, further compression significantly narrows the unstable areas, and the area sizes are similar for both domes.
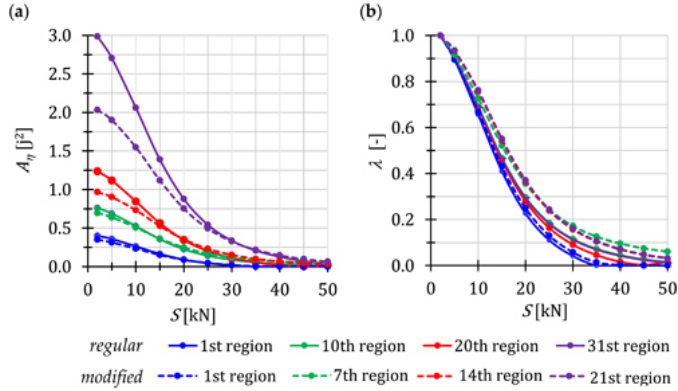
FIGURE 4.64 Influence of the initial prestress level *S* on the: (**a**) area of unstable regions A_η and (**b**) range of unstable regions λ.

The influence of the initial prestress level S on the distribution and range of unstable regions is measured by the nondimensional parameter λ (3.29) (Figure 4.64b). In the case of the *regular dome* (continuous line), as the initial prestress level increases, the changes in the range of areas are greater. For example, for $S = 15\text{kN}$, the areas are smaller by about 53% than the areas at the minimum prestress level, while in the case of the *modified dome* (dashed line), they are about 45% smaller. As can be seen, the changes in the range of unstable regions corresponding to almost all resonance frequencies are comparable for both domes, except for the first region (this region corresponds to the first resonance frequency η_1). In this case, the parameter λ decreases as the initial prestress level increases for both domes, and at the maximum level is $\lambda = 0.02$ and $\lambda = 0.04$, respectively (the unstable region decreases by 98% and 96%).

As has been noted, the unstable regions are the greatest for the minimum prestress level $S_{min} = 2\text{kN}$. In this case, if all the main unstable regions were determined, i.e., 31 for the *regular* and 21 for the *modified dome*, the regions would overlap. For example, in Figure 4.65, the limits of all the main unstable regions of the regular and modified domes in the case of minimal prestress level are shown (the black line marks the rest of the regions, except for those selected: η_1, η_{10}, η_{20}, and η_{31} for the *regular dome* and η_1, η_7, η_{14}, η_{21} for the *modified dome*).
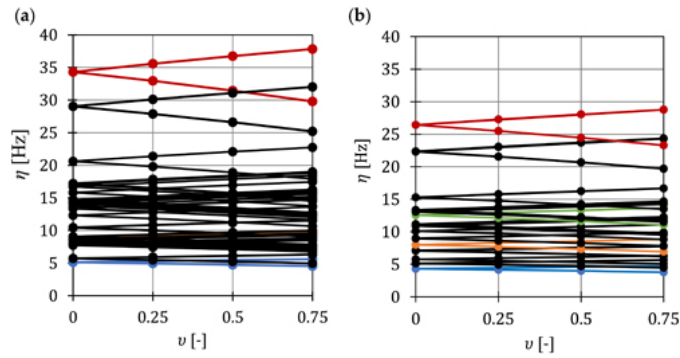
FIGURE 4.65 Limits of all main unstable regions in the case of minimal prestress level S_{min} = 2 kN: (**a**) *regular Geiger dome type B-2* and (**b**) *modified Geiger dome type B-2.*↵

It should be noted that the next resonance frequencies (like natural frequencies), i.e., $\eta > \eta_{31}$ and $\eta > \eta_{21}$, for *regular* and *modified domes*, respectively, are independent of pulsatility index v $(\eta(v = 0 \div 0.75) = \text{const.})$ and on the initial prestress level S (Table 4.32). The relative increase is less than 3% for all frequencies. These resonance frequencies are twice as high as the free frequencies.

TABLE 4.32 Next Resonance Frequencies of the *Geiger Domes Type B-2* ↵

	Regular Dome				Modified Dome			
	η_i (Hz) ($v = 0 \div 0.75$)							
	η_{32}	η_{33}	η_{34}	η_{35}	η_{22}	η_{23}	η_{24}	η_{25}
S_{min} = 2 kN	83.8	180.4	180.9	180.9	81.5	143.9	144.0	169.3
S_{max} = 50 kN	84.2	181.3	181.3	181.3	81.8	144.4	144.4	170.0

4.6.5 CHAPTER SUMMARY

This chapter discusses the two most popular tensegrity domes, i.e., *Geiger* and *Levy domes.* These structures are very different in their behavior. Comparative nature of analysis leads to answers to the questions posed at the beginning of the consideration.

1. Is it possible to derive formulas for self-equilibrium forces (self-stress state)?

Only formulas for self-equilibrium forces have been derived for *regular Geiger domes*. This is due to the fact that these domes consist of basic 2D tensegrity models. These formulas can be used for any number of load-bearing girders.

2. How does the modification of Geiger patent (*regular Geiger dome type B-2*) affect the behavior of *Geiger domes*?

From both qualitative and quantitative points of view, the modification of Geiger patent matters. The influence of the modification on the number of immanent features of tensegrity structures. Additionally, for *modified Geiger domes*, it is impossible to obtain formulas for self-stress state. In turn, assessing the behavior of the domes, each modification result in an increase in the minimum prestress level. As a result, the range of prestress is reduced.

3. Which solution of *Geiger domes* is best in terms of its ability to control static and dynamic parameters?

The Geiger patent (*regular Geiger dome type B-2*) is the best solution in terms of its ability to control static and dynamic parameters. Any modification leads to reduced controllability.

4. Whether the number of infinitesimal mechanisms affects the behavior of *Geiger domes*?

The number of infinitesimal mechanisms affects the behavior of Geiger domes. More mechanisms mean more parameters to control. The number of mechanisms depends on the design solutions.

5. Whether the upper section type matter in the case of *Levy dome*?

In the case of the Levy dome, the type of upper section is important in the qualitative analysis. In the case of domes with a strut in the upper section (*dome type A-2*), there are no mechanisms. On the other hand, in the case of domes with a ring in the upper section (*domes type B-2*), there is only one mechanism, regardless of the number of load-bearing girders. In the quantitative analysis, however, the type of upper section is virtually irrelevant. The mechanism in the *domes type B-2* has a local character, related only to the open upper section. Irrespective of the type of the upper section, the influence of the initial prestress on the static and dynamic parameters is negligible.

6. The behavior of which type of *Levy dome* is possible to control?

Control of static parameters is impossible regardless of the type of *Levy dome*. On the other hand, dynamic parameters can be controlled on *domes type B-2.*

7. Is it possible to controlling the occurrence of infinitesimal mechanisms by changing the number of load-bearing girders?

It is possible to control the occurrence of mechanisms by changing the number of load-bearing girders is possible for some domes. The number of load-bearing girders affects the number of infinitesimal mechanisms in the cases of *regular Geiger domes* and *modified Geiger domes type B-2.* In the cases of *modified Geiger dome type A-2* and *Levy domes type B-2*, the number of infinitesimal mechanisms is constant, independent of the number of load-bearing girders.

8. How does the initial prestress level influence the natural frequencies correlated with the infinitesimal mechanisms?

In the case of $S = 0$ the natural frequencies correlated with the infinitesimal mechanisms are zero, and after introducing an initial prestress they increase in a nonlinear way. The impact is greater with a lower level of prestress.
   In the case of *Geiger domes*, the initial prestress level has a large influence on the natural frequencies correlated with the infinitesimal mechanisms. The range of changes depends mainly on the type of dome and the number of load-bearing girders. The greater the number of load-bearing girders, the greater the number of infinitesimal mechanisms (except for the *modified dome type A-2*, which has a constant number of infinitesimal mechanisms regardless of the number of load-bearing girders). The greater the number of infinitesimal mechanisms, the greater the influence of the initial prestress level on the natural frequencies.

On the other hand, in the case of *Levy domes*, the initial prestress level has an influence only on the *domes type B-2* with one mechanism, regardless of the number of load-bearing girders. The range of changes mainly depends on the number of girders. The greater the number of girders, the greater the influence of the initial prestress level on the first natural frequency.

9. Is the number of natural frequencies depending on the prestressing equal to the number of infinitesimal mechanisms?

For the *Geiger domes type B-2*, the number of natural frequencies depending on the prestressing equals to the number of infinitesimal mechanisms. On the other hand, in the case of *Geiger domes type A-2* and *Levy domes type B-2*, not only the frequencies correlated with the infinitesimal mechanisms depend on the prestress. There are additional frequencies that depend on prestress. The number of them, and the sensitivity on the initial prestress changes, depends on the number of load-bearing girders.

10. Whether the number of load-bearing girders impacts the natural frequencies corresponding to the infinitesimal mechanisms?

The number of load-bearing girders impacts the natural frequencies corresponding to the infinitesimal mechanisms in the case of *Geiger domes type B.*

More results of the parametric analysis of *Geiger and Levy domes* are available in the following publications (Obara and Solovei, 2023, 2024; Obara et al., 2023a, 2023b, 2024).

4.7 TENSEGRITY TOWERS

Tensegrity towers built with the modified basic three-dimensional tensegrity modules (units) considered in Section 4.5 are analyzed, i.e., *modified Simplex module* and *modified Quartex module*. The units are connected node-to-node. The *Simplex modules* could only be connected in one way, whereas the *Quartex modules* could be connected in two ways. This means three types of towers are analyzed. In Figure 4.66, the four-unit towers are shown:
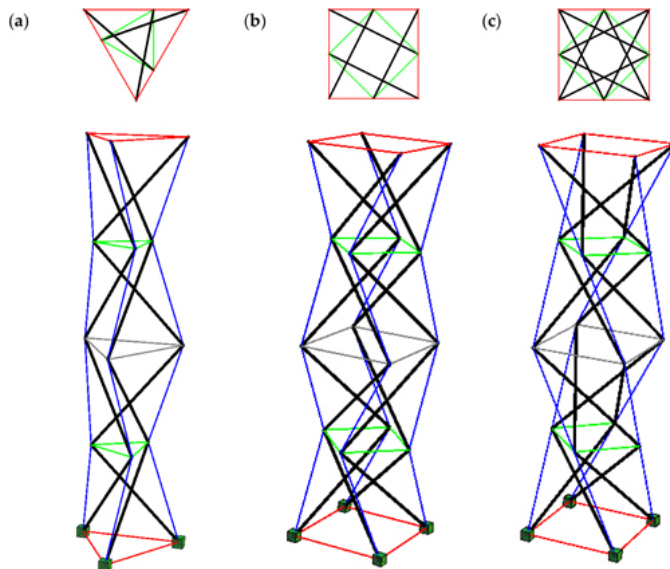
FIGURE 4.66 Tensegrity towers built with four modules: (**a**) *Simplex tower*, (**b**) *Quartex tower type A*, and (**c**) *Quartex tower type B.* ↵

- *Simplex tower* (Figure 4.66a);
- *Quartex tower type A – the struts overlap in a plan view* (Figure 4.66b);
- *Quartex tower type B – the struts form a star* (Figure 4.66c).

Towers built with u-units $(u = \{2, 3, 4, 5, 6\})$ are considered. The bottom units are supported. The support eliminates rigid movements, which means six and eight blocked degrees of freedom are considered for *the Simplex* and *Quartex modules*, respectively (see Section 4.5). The towers are loaded with a force $P = 5\text{kN}$ applied to one top node in z-direction. The minimum prestress level depends on the number of units. The value $S_{min} = 5\text{kN}$ is taken into account to compare the behavior of towers. In turn, the maximum prestress level is assumed to be $S_{max} = 110\text{kN}$, and corresponds to the effort of the structure (3.22) equal to $W_{max} = 0.91$.

Purpose of the Consideration

The analysis is comparative in nature, leading to answers to the following questions:

1. Is it possible to control the occurrence of mechanisms by changing the number of modules?
2. How the number of modules affects *global stiffness parameter GSP*?
3. Does the method of connecting the *Quartex modules* matter?
4. Which towers are more sensitive to the changes in the initial prestress level?
5. How does the initial prestress level influence the natural frequencies correlated with the infinitesimal mechanisms?
6. Is the number of natural frequencies depending on the prestressing equal to the number of infinitesimal mechanisms?
7. Whether the number of units impacts the natural frequencies corresponding to the infinitesimal mechanisms?

4.7.1 QUALITATIVE ANALYSIS

The results of the qualitative analysis are shown in Table 4.33. Regardless of the type of modules, the structures behave in the same way. The number of self-stress states and infinitesimal mechanisms equal the number of units. None of the self-stress states correctly identify the type of element (i.e., which is a strut and what is a cable). In all cases, the superposition of self-stress states leads to obtaining the self-stress states for the single modules (Figures 4.30b and 4.31b), including common elements. If the superposed self-stress state is taken into account, all eigenvalues of the stiffness matrix (3.19) are positive. This means the self-stress state identifies the appropriate normal forces in the structural elements and stabilizes the mechanisms, i.e., the mechanisms are infinitesimal.

TABLE 4.33 Results of the Qualitative Analysis of Tensegrity Towers↵

No. of							Classification
Units	Nodes	Elements	d.o.f	Struts	Mechanisms	Self-Stress States	
(u)	(nn)	(n)	(m)	(ns)	(nm)	(nss)	
Simplex towers							
2	9	21	21	6	2	2	*structures with tensegrity features of class 1*
3	12	30	30	9	3	3	
4	15	39	39	12	4	4	
5	18	48	48	15	5	5	
6	21	57	57	18	6	6	
u					u	u	
Quartex towers							

No. of							Classification
Units	Nodes	Elements	d.o.f	Struts	Mechanisms	Self-Stress States	
(u)	(nn)	(n)	(m)	(ns)	(nm)	(nss)	
2	12	28	28	8	2	2	*structures with tensegrity features of class 1*
3	16	40	40	12	3	3	
4	20	52	52	16	4	4	
5	24	64	64	20	5	5	
6	28	76	76	24	6	6	
u				u	u		

The towers are characterized by four tensegrity features. They are trusses (TT) with tensile elements that have no rigidity in compression (TC) and in which there is one superposed self-stress state (SS) that stabilizes all infinitesimal mechanisms (IM). The features (IN—the set of struts is contained within the continuous net of cables) and (DS − the struts form a discontinuous set) cannot be met because of the method of connecting modules. According to the tensegrity classification (Table 3.1), the towers are *structures with tensegrity features of class 1.*

4.7.2 STATIC ANALYSIS

The static analysis includes the influence of the initial prestress level and external load on the rigidity of the structures. Additionally, the influence of the number of units is considered. To compare the behavior of different solutions, the *global stiffness parameter* GSP and the effort of structure W_{max} (for cables) are shown in Figure 4.67. The continuous line describes the behavior of towers built with an odd number of units, while the dashed line describes towers built with an even number of units.
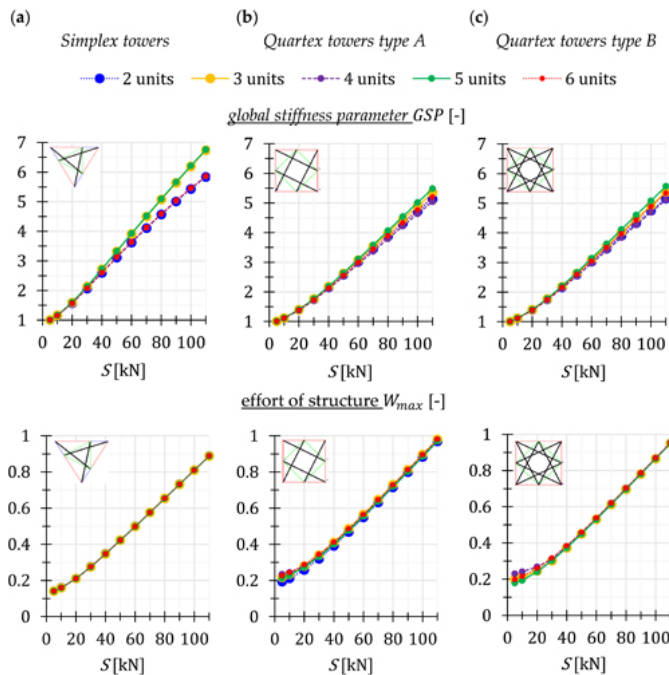
FIGURE 4.67 Results of static analysis for the tensegrity towers.

The *Simplex towers* built with odd numbers of units are the stiffest of all (Figure 4.67a). Interestingly, the stiffness does not depend on the number of units. At the maximum level of initial prestress, the parameter GSP is average 1.3 times higher than for *Quartex*

towers. In the case of towers built with an even number of units, the stiffness also does not depend on the number of units but is smaller. It is equal to 0.87 of the stiffness of towers built with an odd number of units. In turn, the stiffness of *Quartex towers* (Figures 4.67b and 4.67c) depends on the number of units. *Quartex towers type B* are more sensitive. For both types of *Quartex towers,* the stiffest is the tower built with five units, while the weakest the tower built with four units.

Like in the previous examples, the influence of non-linearity is most significant at low values of initial prestress forces. The non-linear nature of the stiffness function is for initial prestress forces in the range of $S \in \langle 5\mathrm{kN}; 25\mathrm{kN} \rangle$ for the *Simplex towers* and $S \in \langle 5\mathrm{kN}; 40\mathrm{kN} \rangle$ for the *Quartex towers.*

The number of units has practically no influence on the effort of structure. At the same initial prestress level, the *Quartex towers type A* are the most stressed.

4.7.3 DYNAMIC ANALYSIS

In order to check the dynamic behavior of towers, the natural $f = f(0)$ and free $f(P)$ frequencies are calculated. The impact of the number of units (u) is taken into account. First, the natural frequencies correlated with infinitesimal mechanisms $f_{nm} = f_{nm}(P = 0)$ are determined. Next, the additional prestress-dependent frequencies are presented. At the end, the dynamic response of towers affected by external loads is considered. The free frequencies of structures loaded with time-independent force are measured. The three-unit towers are considered.

4.7.3.1 Natural Frequencies of Towers Correlated with Infinitesimal Mechanisms

The first example concerns the influence of the initial prestress level S and the number of units (u) on natural frequencies f_i correlated with infinitesimal mechanisms ($i = \{1, 2, \ldots, nm\}$). It should be noted that the number of infinitesimal mechanisms equals the number of units $(nm = u)$. Considered frequencies are zero in the absence of prestress and increase when the initial prestress is applied. Figure 4.68 presents the first f_1 (dashed line) and the last f_{nm} (continuous line) frequencies correlated with the infinitesimal mechanisms are presented. The range of changes mainly depends on the number and type of units used to create the towers.
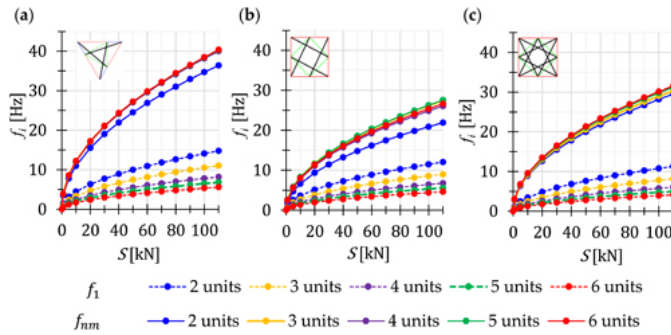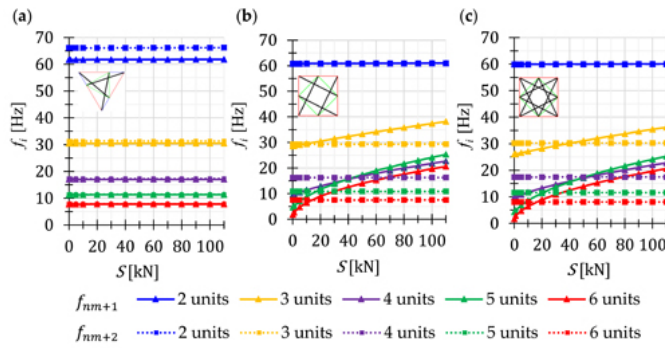

FIGURE 4.68 Natural frequencies f_1 and f_{nm}: (**a**) *Simplex towers*, (**b**) *Quartex towers type A*, and (**c**) *Quartex towers type B.* ⏎

The first frequency f_1 is the most sensitive to the change in the number of units. Its value decreases by 25%, 45%, 54%, and 62% as the number of units increases for *Simplex towers* (Figure 4.68a) and *Quartex towers type A* (Figure 4.68b). In the case of *Quartex towers type B* (Figure 4.68c), differences are higher by two percentage points.

Comparing the behavior of the way of connecting the *Quartex modules,* the first frequencies f_1 *of towers type B* are lower by about 10% then those *of towers type A.*

In turn, the last frequency f_{nm} is less sensitive. For *Simplex towers* built with 3–6 units, the frequency f_{nm} does not depend on the number of units at all. This means that the third frequency of three-unit towers is the same as the fourth, fifth, and sixth frequencies of towers built with four, five, and six units. Only the second frequency of a two-unit tower differs. It is lower, and the difference increases as the initial prestress level S increases. For example, at the maximum level, the difference equals $3.86\,\mathrm{Hz}$. The *Quartex towers* behave differently. The number of units influences the values of the frequency f_{nm}, but to a much lesser extent than in the case of the frequency f_1. Additionally, the obtained results confirm that the way of connecting the *Quartex modules* is important. For the towers with star-forming struts (*Quartex towers type B*), the frequencies f_{nm} for S_{max} are about 1.3 times higher than for the towers with struts overlapping in a plan view (*Quartex towers type A*).

Summary: (1) the frequency f_{nm} is more sensitive to prestress than the frequency f_1. For example, the value of the sixth frequency of a six-unit tower varies from 0 to $40.35\,\mathrm{Hz}$ for a *Simplex tower*, from 0 to $26.61\,\mathrm{Hz}$ for *Quartex tower type A*, and from 0 to $31.60\,\mathrm{Hz}$ for *Quartex tower type B.* (2) the natural frequencies of *Simplex towers* are higher than those of *Quartex towers*. At the maximum level of initial prestress, the first frequencies f_1 of *Simplex towers* are 1.3 times higher than for *Quartex towers type B* and 1.2 times higher than for *Quartex towers type A*, while the frequencies f_{nm} are 1.5 and 1.3 times higher, respectively.

4.7.3.2 Additional Prestress-Dependent Natural Frequencies of Towers

Considerations of tensegrity domes showed a typical behavior with additional frequencies depending on prestress were determined. The same is true for tensegrity towers. The rule stating that 'the number of natural frequencies, depending on the prestressing, is equal to the number of infinitesimal mechanisms' holds true only for all *Simplex towers* and *Quartex towers* built with two units.

In Figure 4.69, the next two frequencies, i.e., f_{nm+1} (continuous line) and f_{nm+2} (dotted line), are shown. For *Simplex towers* (Figure 4.69a), these frequencies are constant independently of the number of units. It should also be noted that these frequencies are the same for towers built with 3–6 units. Only for two-unit tower the frequency f_{nm+2} is 7% times higher than f_{nm+1}. In turn, for *Quartex towers* (Figures 4.69b and 4.69c), these frequencies do not depend on prestress only in the case of two-unit towers. For towers built with 3–6 units, there is one additional prestress-dependent frequency f_{nm+1}. In the absence of initial prestress $(S = 0)$, the frequency f_{nm+1} is not zero, and its values vary with the change in prestress. Interesting is a frequency function, which is changed from linear for three-unit towers to non-linear for towers built with 4–6 units. The sensitivity grows with the number of units. For example, for six-unit towers, the frequency, with the growth of the prestress from $S_{\min}$ to $S_{\max}$, varies from $1.81\,\mathrm{Hz}$ to $20.62\,\mathrm{Hz}$ for *Quartex towers type A and* $1.68\,\mathrm{Hz}$ to $20.61\,\mathrm{Hz}$ for *Quartex towers type B.* As can be seen, the differences between towers are not significant.

FIGURE 4.69 Natural frequencies f_{nm+1} and f_{nm+2}: (**a**) *Simplex towers*, (**b**) *Quartex towers type A*, and (**c**) *Quartex towers type B.* ↵

On the other hand, the frequency f_{nm+2}, like the next ones, does not depend on the initial prestress level S. The relative increase between $f(S_{min})$ and $f(S_{max})$ is less than 1%. In Table 4.34, the frequencies f_{nm+3} and f_{nm+4} are shown. The frequencies are not sensitive to prestressing, except for the two-unit *Quartex towers*. In this case, the frequency f_{nm+3} is not constant, but the relative increase is equal to only 3.7% and 4.5% for *towers types A* and *B,* respectively. However, the next frequencies f_{nm+4} do not depend on the initial prestress level.

TABLE 4.34 Natural Frequencies f_{nm+3} and f_{nm+4} of Tensegrity Towers↵

No. of Units(u)	Simplex Towers		Quartex Towers Type A		Quartex Towers Type B	
	S = 0	S = 110 kN	S = 0	S = 110 kN	S = 0	S = 110 kN
	f_{nm+3} **(Hz)**					
2	167.7	167.9	75.3	78.1	66.3	69.4
3	136.5	136.7	29.3	29.4	30.2	30.4
4	95.7	95.9	16.3	16.3	17.4	17.5
5	65.8	65.9	10.8	10.9	11.6	11.6
6	46.4	46.5	7.5	7.5	8.1	8.1
	f_{nm+4} (Hz)					
2	249.8	250.1	219.1	219.5	223.5	223.8
3	185.2	185.4	156.1	156.4	162.3	162.5
4	105.9	106.1	89.6	89.8	101.5	101.7
5	69.2	69.3	62.9	63.1	68.6	68.7
6	47.9	48.0	44.5	44.6	48.6	48.7

4.7.3.3 Free Frequencies of Three-Unit Towers

Three-unit towers are characterized by three infinitesimal mechanisms. However, taking into account the conclusions from the previous considerations, five successive frequencies are shown in Figure 4.70. The external load prestresses the structures, and the free frequencies at $S_{min} = 5\text{kN}$ are higher than natural frequencies. The impact of loads is greater at lower levels of initial prestress, and as the prestress increases, the free frequencies approach to the natural frequencies. Convergence depends on the frequency; the higher the frequency, the slower the convergence, while at $S = 60\text{kN}$ ($W_{max} \approx 0.5$), regardless of frequency number, the impact of loads is negligible.
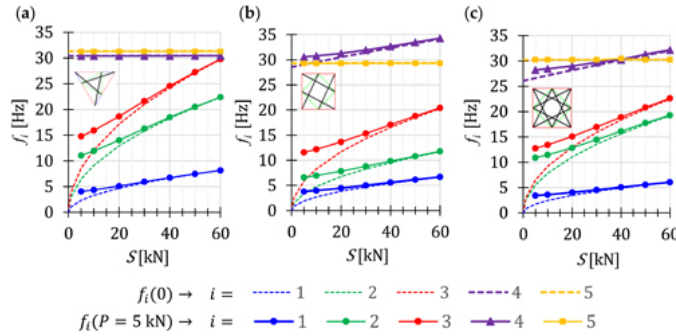
FIGURE 4.70 Free frequencies of three-unit towers: (**a**) *Simplex tower*, (**b**) *Quartex tower type A*, (**c**) *Quartex tower type B*. ↵

The *Quartex tower type B* (Figure 4.70c) behaves similarly to the *Simplex tower* (Figure 4.70a); for these structures, the second frequency ($i = 2$) is closer to the third frequency ($i = 3$) than to the first frequency. While while for the *Quartex tower type A* (Figure 4.70b), the second frequency is closer to the first frequency ($i = 1$). As with of natural frequencies, in the case of *Quartex towers* the fourth frequency ($i = 4$) is additionally dependent on prestress. In turn, the fifth frequency ($i = 5$) is not sensitive to prestress, and is almost identical to that of the *Simplex tower*. As in the case of natural frequencies, in the case of *Quartex towers* the fourth frequency ($i = 4$) is additionally dependent on the prestress.

4.7.4 DYNAMIC STABILITY ANALYSIS

The static and dynamic analyses showed that the *Simplex towers* are more sensitive to the changes in the level of prestress than the *Quartex towers*. Additionally, results confirm that the way of connecting the *Quartex modules* is important. However, the influence of prestressing is most significant at low values of initial prestress forces. The same conclusions can be drawn for resonance frequencies. To illustrate this, the dynamic response of towers affected by external periodical loads is considered. The unstable regions are determined for the three-unit towers. In Figures 4.71–4.73, the limits of the main unstable regions are shown. The results for three cases of initial prestress are presented, i.e., $S_{min} = 5\text{kN}$ ($W_{max} \approx 0.14 \div 0.22$), $S = 20\text{kN}$ ($W_{max} \approx 0.21 \div 0.28$) and $S = 50\text{kN}$ ($W_{max} \approx 0.42 \div 0.48$).

In the case of the *Simplex tower*, three main unstable regions are determined, corresponding to three resonant load frequencies: η_1 (first region), η_2 (second region), and η_3 (third region) (Figure 4.71). As can be seen, the area of unstable regions increase with an increase in the pulsatility index v, and it is larger at higher frequencies. Additionally, it should be noted that in the case of minimum prestress level $S_{min} = 5\text{kN}$, the second and third regions are located close. This is related to the fact that the second free frequency is closer to the third frequency. As in the previous examples, as the level of initial prestress S increases, the resonant frequencies increase and the range of instability areas decreases.
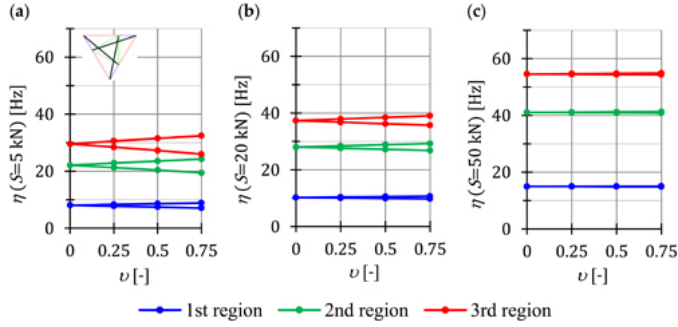
FIGURE 4.71 Limits of the main unstable regions for the *Simplex tower*: (**a**) $S = 5$ kN, (**b**) $S = 20$ kN, and (**c**) $S = 50$ kN.

In the case of *Quartex towers* (Figures 4.72 and 4.73), as there are four prestress-dependent frequencies, four main unstable regions are determined. The behavior is similar to behavior of the *Simplex tower*. The resonant frequencies share the greatest similarity between the *Quartex tower type B* (Figure 4.73) and the *Simplex tower* (as for free frequencies). Comparing the locations of the unstable regions, the second and the third regions are placed close to each other and partially overlap for lower levels of the initial prestress. This behavior poses a risk for the structure. It increases the probability that the resonant frequency will occur. For the *Quartex tower type A* (Figure 4.72), regions do not coincide. This means that this solution is safer.
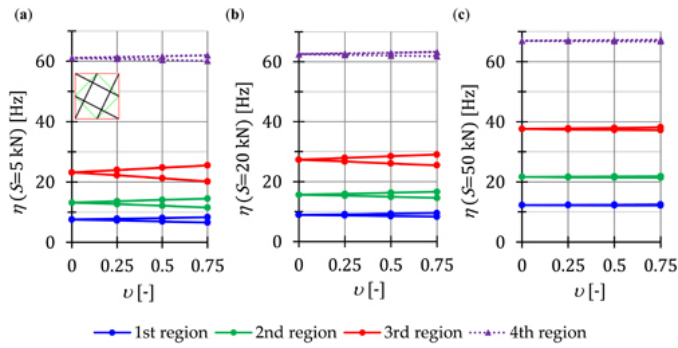
FIGURE 4.72 Limits of the main unstable regions for the *Quartex tower type A*: (**a**) $S = 5$ kN, (**b**) $S = 20$ kN, and (**c**) $S = 50$ kN.
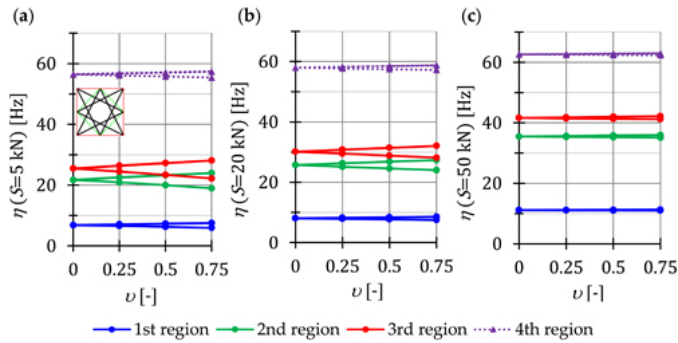
FIGURE 4.73 Limits of the main unstable regions for the *Quartex tower type B* : (**a**) $S = 5$ kN, (**b**) $S = 20$ kN, and (**c**) $S = 50$ kN.

To compare the behavior of towers, the influence of initial prestress S on the area of unstable regions A_η is shown in Figure 4.74. The areas are similar for the *Simplex tower* (Figure 4.74a) and *Quartex tower type B* (Figure 4.74c). To measure the changes in the area of the unstable regions, the nondimensional parameter λ (3.75) is also calculated (Figure 4.75). The change in the range of areas in the unstable regions correlated to infinitesimal mechanisms (the first, second, and third regions) is comparable in all cases (graphs overlap). At low values of initial prestress forces, the range of the three main unstable regions changes only slightly for example, at $S = 10\text{kN}$, the parameter λ is equal to $\lambda = 0.85$ for the *Simplex tower* and $\lambda = 0.91$ for the *Quartex towers*. This means that the unstable regions are 15% and 9% smaller than the regions at the minimum level of initial prestress $(S_{min} = 5\text{kN})$. However, further prestress significantly narrows the unstable regions. At $S = 60\text{kN}$, the regions decrease by 95% and 99% ($\lambda = 0.05$ and $\lambda = 0.1$). This means that the boundaries of instability practically coincide, and the risk of the excitation of motion with increasing amplitudes decreases.
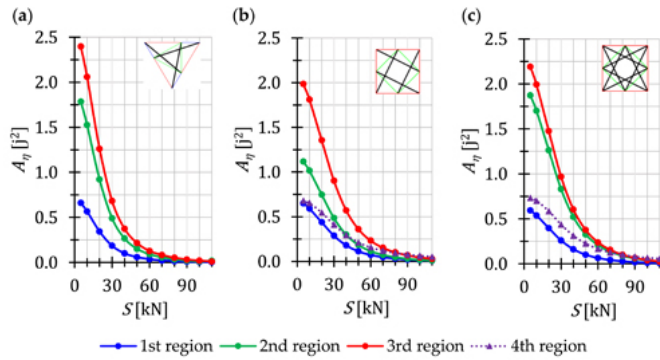
FIGURE 4.74 Influence of the initial prestress level *S* on the area of unstable regions *A$_\eta$*(*S*): (**a**) *Simplex tower*, (**b**) *Quartex tower type A*, and (**c**) *Quartex tower type B.*
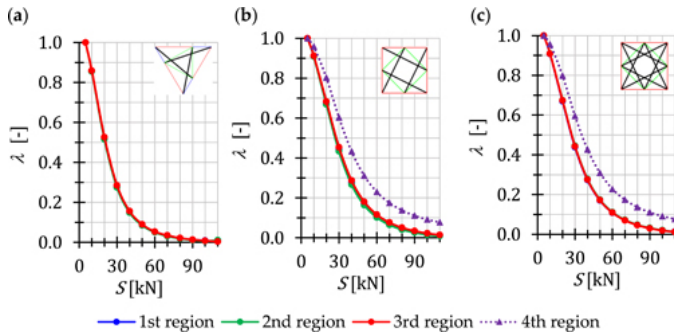
FIGURE 4.75 Influence of the initial prestress level *S* on the range of unstable regions *λ*: (**a**) *Simplex tower*, (**b**) *Quartex tower type A*, and (**c**) *Quartex tower type B.*

In turn, the unstable region correlated with the additional prestress-dependent natural frequency (the fourth region) behaves differently. On the one hand, the area is smaller (Figures 4.74c and 4.74d) than the second and third regions. On the other hand, the magnitude of the change is slower than in the previous regions (Figures 4.75c and 4.75d). At $S = 10\text{kN}$, the parameter λ is equal to $\lambda = 0.95$, and at $S = 60\text{kN}$, it is equal to $\lambda = 0.22$.

The next resonance frequencies (like natural frequencies), i.e., $\eta > \eta_3$ and $\eta > \eta_4$, for the *Simplex tower* and for the *Quartex towers*, respectively, are independent of pulsatility index v $(\eta(v = 0 \div 0.75) = \mathrm{const.})$ and on the initial prestress level S (Table 4.35). The relative increase is less than 3% for all frequencies. These resonance frequencies are twice as high as the free frequencies.

TABLE 4.35 Next Resonance Frequencies of the
Tensegrity Towers↵

	Simplex Tower	Quartex Tower Type A	Quartex Tower Type B
	η_i (Hz) (v = 0 ÷ 0.75)		
	η_4	η_5	η_5
S_{min} = 5 kN	60.85	58.60	60.46
S_{max} = 110 kN	62.69	58.73	60.78

4.7.5 CHAPTER SUMMARY

This chapter discusses tensegrity towers constructed using the *modified Simplex* and *Quartex modules*. The influence of the type of support on the behavior is considered. The comparative nature of analysis leads to answers to the questions posed at the beginning of the discussion.

1. Is it possible to control the occurrence of infinitesimal mechanisms by changing the number of modules?

The occurrence of infinitesimal mechanisms can be controlled by changing the number of modules. The number of mechanisms equals the number of modules.

2. How the number of modules affects *global stiffness parameter* GSP?

The influence of the number of modules on the stiffness (GSP) depends on the type of modules. Generally, towers built with an odd numbers of modules are the stiffest of all. Comparing towers, the stiffest is the *Simplex towers.*

3. Does the method of connecting the *Quartex modules* matter?

The method of connecting the *Quartex modules* is very important. Towers with star-forming struts (*Quartex towers type B*) are stiffer than the towers with overlapping struts in the plan view (*Quartex towers type A*). The frequencies are higher (except for the first frequency, which are almost the same). Furthermore, the dynamic stability analysis shows that the probability of the resonance frequency occurring is higher for *Quartex towers type B.*

4. Which towers are more sensitive to the changes in the initial prestress level?

More sensitive to the changes in the initial prestress level are the *Simplex tower*. However, *Quartex tower type B* behaves similarly to the *Simplex tower.*

5. How does the initial prestress level influence the natural frequencies correlated with the infinitesimal mechanisms?

In the case of $S = 0$, the natural frequencies correlated with the infinitesimal mechanisms are zero, and after introducing an initial prestress, they increase in a nonlinear way. The

impact is greater at lower level of prestress. If several mechanisms are identified, higher frequencies are more susceptible to changes in the initial prestress.

6. Is the number of natural frequencies depending on the prestressing equal to the number of infinitesimal mechanisms?

For the *Simplex towers*, the number of natural frequencies depending on the prestressing equals the number of infinitesimal mechanisms. This is also true in the case of *Quartex towers* constructed with two units. In other cases, there is one additional prestress-dependent frequency. In the absence of initial prestress, this frequency is non-zero, and its values vary with change in prestress. The sensitivity to the prestress grows with the number of units.

7. Whether the number of units impacts the natural frequencies corresponding to the infinitesimal mechanisms?

The number of modules impacts the natural frequencies corresponding to the infinitesimal mechanisms in of towers cases.

Additional results of the parametric analysis of tensegrity towers built with *Simplex* and *Quartex modules* are available in the following publications (Mochocki and Obara, 2021; Obara, 2019a; Obara and Tomasik, 2023c, 2023d).

4.8 DOUBLE-LAYERED TENSEGRITY GRIDS

Double-layered tensegrity grids (plates) constructed with the modified basic three-dimensional tensegrity modules (units) considered in Section 4.5 are analyzed, namely, the *modified Simplex module* and the *modified Quartex module*. Two small-sized plates are taken considered, namely, small-sized plates:

- *six-unit Simplex plate (MS-6)* (Figure 4.76a);
- *four-unit Quartex plate (MQ-4)* (Figure 4.77a).
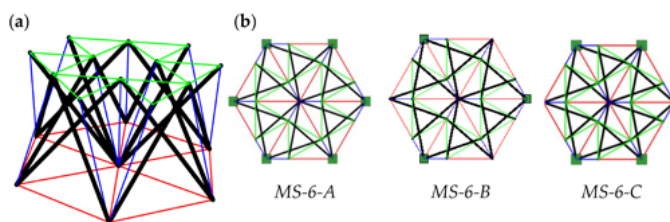
FIGURE 4.76 Six-unit *Simplex plate*: (**a**) 3D view and (**b**) scheme of support.
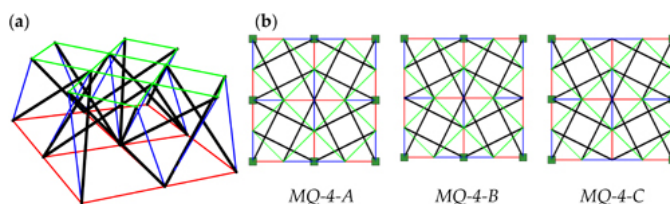
FIGURE 4.77 Four-unit *Quartex plate*: (**a**) 3D view and (**b**) scheme of support.

The plates are supported at the bottom nodes of the structure. The influence of the type of support on the behavior is considered. Three static schemes are considered (Figures 4.76b and 4.77b).

The considered models are subjected by concentrated forces $P = 1\text{kN}$ applied to all top nodes in z-direction. The minimum prestress level, $S_{min} = 2\text{kN}$, is considered to compare the behavior of plates. In turn, the maximum prestress level is assumed to be $S_{max} = 60\text{kN}$, which corresponds to the effort of the structure (3.22), equal to $W_{max} = 0.91$.

Purpose of the Consideration

The analysis is of a comparative in nature, leading to answers to the following questions:

1. Is it possible to control the occurrence of mechanisms by changing the support conditions of the tensegrity plate?
2. Which plate model is the stiffest?
3. Which plate is more sensitive to changes in the initial prestress level?
4. Is the number of natural frequencies depending on the prestressing equal to the number of infinitesimal mechanisms?

4.8.1 QUALITATIVE ANALYSIS

The results of the qualitative analysis are shown in Table 4.36. In the case of the *six-unit Simplex plate*, there is one infinitesimal mechanism, regardless of the model (Figure 4.78). The forms of mechanism are different depending on the model. However, in all cases, the mechanisms are realized by in-plane displacements of the top nodes. Out-of-plane displacements of the upper nodes are significantly smaller (almost negligible). Only the bottom unsupported node moves significantly out-of-plane relative to the lower nodes. In turn, for the *four-unit Quartex plate*, the number of mechanisms depends on the model. Thus, the *MQ-4-A* model is characterized by one mechanism, the *MQ-4-B* by two mechanisms, and the *MQ-4-C* model by three mechanisms (Figure 4.79). The forms of the mechanisms vary from model to model, but both in-plane and out-of-plane displacements of the top nodes are comparable.

TABLE 4.36 Results of the Qualitative Analysis of the Tensegrity Plates↵

Name of Plate	No. of						Classification
	Units	Nodes	Elem.	d.o.f	Mechanisms	Self-Stress States	
	(u)	(nn)	(n)	(m)	(nm)	(nss)	
Simplex plates							
MS-6-A	6	19	60	39	1	22	structures with tensegrity features of class 1
MS-6-B				48	1	13	
MS-6-C				45	1	16	
Quartex plates							
MQ-4-A	4	21	56	39	1	18	structures with tensegrity features of class 1
MQ-4-B				45	2	13	
MQ-4-C				45	3	14	
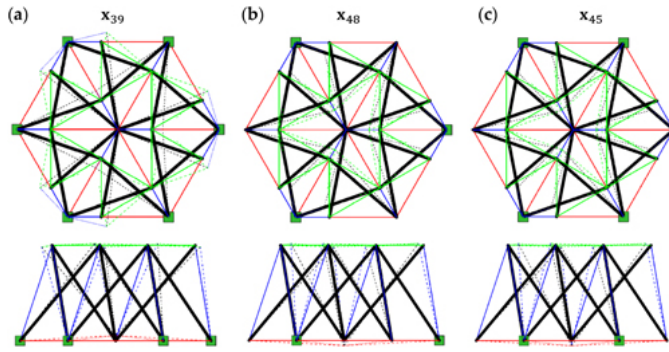
FIGURE 4.78 Infinitesimal mechanisms of the *six-unit Simplex plates*: (**a**) *MS-6-A*, (**b**) *MS-6-B*, and (**c**) *MS-6-C*. ⏎
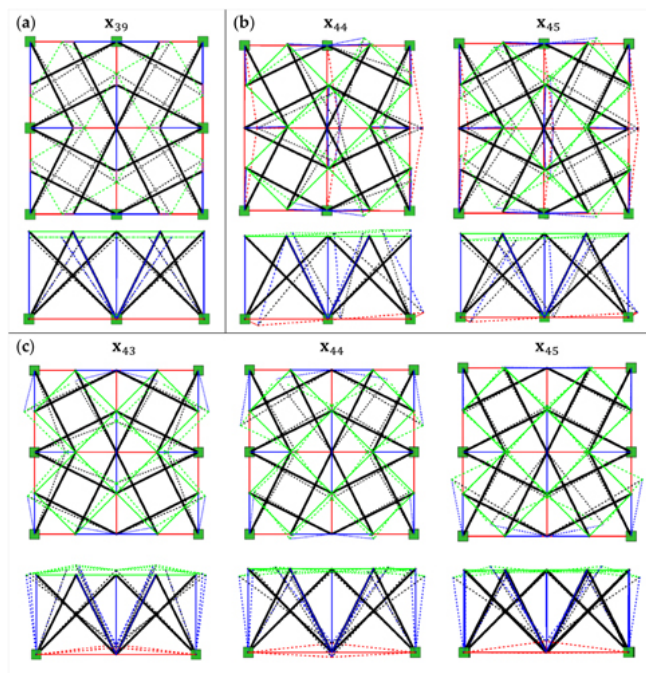
FIGURE 4.79 Infinitesimal mechanisms of the *four-unit Quartex plates*: (**a**) *MQ-4-A*, (**b**) *MQ-4-B*, and (**c**) *MQ-4-C4* ⏎

The number of a second immanent feature of tensegrity, i.e., the self-stress states, depends significantly on the model considered. There are dozen or more self-stress states. However, none of the self-stress states correctly identify the type of element (i.e., what is a strut and what is a cable). In all cases, the superposition of self-stress states leads to obtaining the self-stress states for the single modules (Figures 4.30b and 4.31b), including common elements. If the superposed self-stress state is taken into account, all eigenvalues of the stiffness matrix (3.19) are positive. This means the self-stress state identifies the appropriate normal forces in the structural elements and stabilizes mechanisms, i.e., the mechanisms are infinitesimal.

The plates exhibit four tensegrity features. They are trusses (TT) with tensile elements that have no rigidity in compression (TC) and in which there is one superposed self-stress state (SS) that stabilizes all infinitesimal mechanisms (IM). The features $(IN$—the set of struts is contained within the continuous net of cables) and $(DS$ — the struts form a

discontinuous set) cannot be met because of the method of connecting modules. According to the tensegrity classification (Table 3.1), plates are *structures with tensegrity features of class 1.*

4.8.2 STATIC ANALYSIS

The static analysis concerns the influence of the initial prestress level and external load on structural rigidity. To compare the behavior of different solutions, the *global stiffness parameter* GSP and the effort of structure W_{max} (for cables) are shown in Figure 4.80.
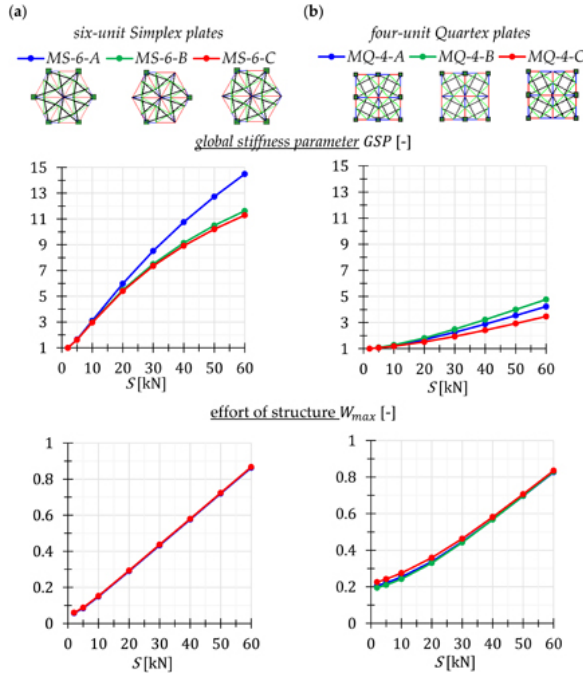
FIGURE 4.80 Results of static analysis for the tensegrity plates.↵

The plates built with *Simplex modules* are stiffer than plates built with *Quartex modules*. At the maximum level of initial prestress, the GSP parameter is on average three times higher. The simply supported model (*MS-6-A*) is the stiffest one. However, it should be noted that for *Simplex plates,* the GSP parameter exhibits a different functional behavior. In "normal' cases, that is, when the behavior of the structure depends on the initial prestress level, it should be an exponential function. The large values of the GSP parameter are due to the fact that the denominator of this parameter is close to zero $\left([q(S_i)]^T K_S(S_i)q(S_i) \approx 0\right)$. This means that the *Simplex plates* are not sensitive to the prestress. Consequently, this means that the load causes displacements that are incompatible with an infinitesimal mechanism. This conclusion confirms the effort of the structure W_{max}, which is linearly dependent on the prestress.

In the case of *Quartex plates*, the stiffest is model supported on two opposite edges (*MQ-4-B*), while the direction of support is important. The parameter GSP is 1.4 times higher for the *MQ-4-B* model than for the *MQ-4-C* model. The *Quartex plates* are sensitive to the prestress. The influence of the initial prestress level depends on the model.

4.8.3 DYNAMIC ANALYSIS

In order to check the dynamic behavior of tensegrity plates, the natural $f(0)$ and free $f(P)$ frequencies are calculated. The *Simplex plates* are characterized by one infinitesimal mechanism, and only the first natural frequency depends on the initial prestress level (Figure 4.81). This frequency (continuous line) is the same for all models. The way of support does not influence the value of frequency but influences the vibrations. The forms of vibration realize mechanisms (Figure 4.78). In the case of free frequencies (dotted line), the first also depends on the prestress, while it is almost equal to the natural ones. This is further evidence that the load causes displacements that are incompatible with an infinitesimal mechanism (see Figure 4.23a).
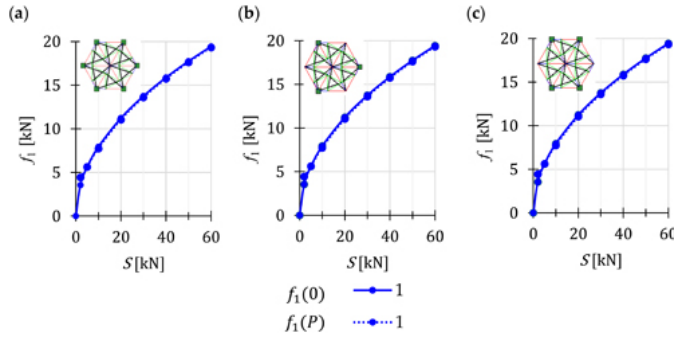
FIGURE 4.81 Influence the initial prestress level S on frequencies of the *six-unit Simplex plates*: (**a**) *MS-6-A,* (**b**) *MS-6-B,* and (**c**) *MS-6-C.*

In the case of *Quartex plates*, both the value of frequencies (Figure 4.82) and form of vibrations (Figure 4.79) depend on the way of support. The *MQ-4-A* plate is characterized by one infinitesimal mechanism and only the first natural and free frequencies depend on the initial prestress level (Figure 4.82a). In turn, the *MQ-4-B* plate is characterized by two infinitesimal mechanisms, thus, the first and second natural and free frequencies depend on prestress (Figure 4.82b). Consequently, in the case of *MQ-4-C* plate with three mechanisms, three frequencies depend on prestress (Figure 4.82c). As can be seen, the last frequencies correlated with mechanisms are the same for all models. In turn, free frequencies behave as in the case of single modules. For a small value of the initial prestress level, they are much higher than the natural frequencies. With an increase in the initial prestress level, the free frequency values converge to the first natural frequency. There is one exception. The first free frequency of the *MQ-4-B* plate behaves as the frequency for the *Simplex plates*.
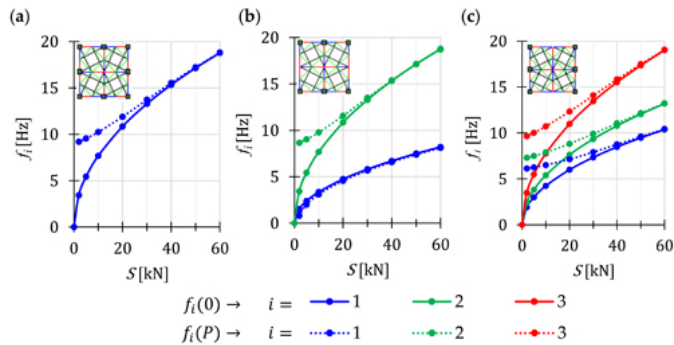
FIGURE 4.82 Influence the initial prestress level S on frequencies of the *four-unit Quartex plates*: (**a**) *MQ-4-A,* (**b**) *MQ-4-B,* and (**c**) *MQ-4-C.*

The tensegrity plates built with *modified Simplex* and *Quartex modules* behave like single modules, i.e., the number of natural frequencies, depending on the prestressing, is equal to the number of infinitesimal mechanisms. Next natural and free frequencies ($f_{nm+i} = f_{nm+i}(0) = f_{nm+i} = (P))$) are independent on the initial prestress level S. In Table 4.37 the frequencies f_{nm+1} are shown. The relative increase between $f(S_{min})$ and $f(S_{max})$ is less than 1%.

TABLE 4.37 First Natural Frequencies of Tensegrity (f_{nm+1}) Plates Independent on the Initial Prestress Level S ↵

Simplex Plates				Quartex Plates			
Model	nm	S		Model	nm	S	
		2 kN	60 kN			2 kN	60 kN
		f_{nm+1} (Hz)				f_{nm+1} (Hz)	
MS-6-A	1	150.48	151.94	MQ-4-A	1	171.09	171.77
MS-6-B	1	137.42	138.60	MQ-4-B	2	162.63	163.11
MS-6-C	1	131.37	132.21	MQ-4-C	3	88.52	89.04

4.8.4 DYNAMIC STABILITY ANALYSIS

The influence of the initial prestress level *S* and load on the main unstable region is shown. The values of constant part of periodic force are taken into account as $P = 1\text{kN}$. The forces are applied to all top nodes in z-direction. The boundaries for one case of initial prestress level are shown, i.e., $S_{min} = 2\text{kN}$.

In the case of *Simplex plates,* one main unstable region is obtained (Figure 4.83). However, the unstable region does not depend on the mode, and they are not large. Taking into account the changes of the initial prestress level, the areas of unstable regions $A_\eta(S)$ and the dimensionless parameter λ (3.75) are shown in Figure 4.84. The dynamic stability analysis confirms the previous conclusions, the initial prestress level does not influence the behavior of the Si*mplex plates.*
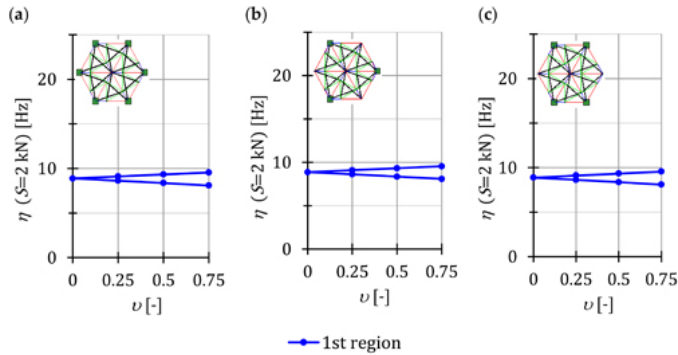
FIGURE 4.83 Limits of the main unstable regions of the *six-unit Simplex plates* for S_{min} = 2 kN: (**a**) *MS-6-A,* (**b**) *MS-6-B,* and *(**c**) MS-6-C.* ↵
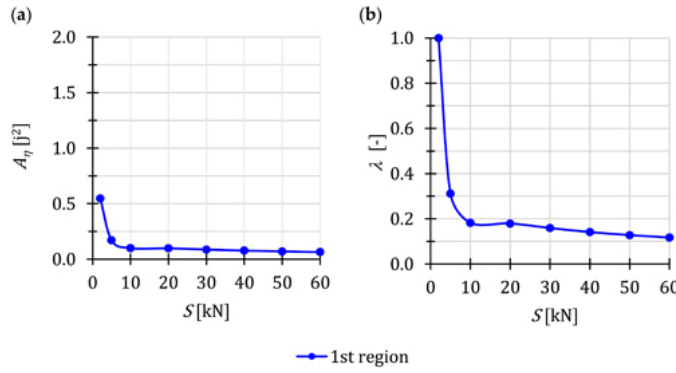
FIGURE 4.84 Influence of the initial prestress level S on the *six-unit Simplex plates*: (**a**) area of unstable regions A_η and (**b**) range of unstable regions λ. ↵

In the case of *Quartex plates*, the number of main unstable region depends on type of model. For plate characterized by one infinitesimal mechanism (*MQ-4-A*), one main unstable region is obtained (Figure 4.85a). Consequently for plate characterized by two mechanisms (*MQ-4-B*) and by three mechanisms (*MQ-4-C*), two (Figure 4.85b) and three (Figure 4.85c) main unstable regions are obtained, respectively. As can be see, the higher risk of occurring excitation vibrations is in the case of *MQ-4-C* model. To better compare the behavior of models, the influence of initial prestress S on the area of unstable regions $A_\eta(S)$ is shown in Figure 4.86. Taking into account fact that fist unstable region (first region) for the *MQ-4-B* model is practically insensitive on the prestress, this is the best solution of support. This is also confirmed by parameter λ (3.75), which measures the range of unstable regions (Figure 4.87).
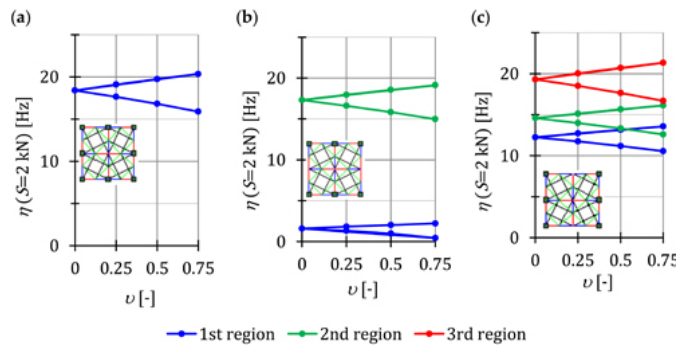
FIGURE 4.85 Limits of the main unstable regions of the *four-unit Quartex plates* for S_{min} = 2 kN: (**a**) *MQ-4-A*, (**b**) *MQ-4-B*, and (**c**) *MQ-4-C*. ↵
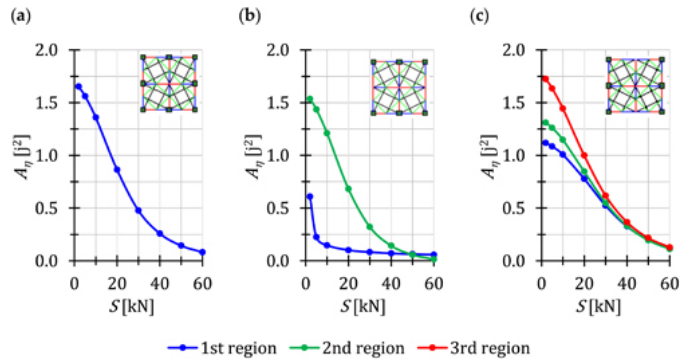
FIGURE 4.86 Influence of the initial prestress level S on the area of unstable regions $A_\eta(S)$ for the *four-unit Quartex plates*: (**a**) *MQ-4-A*, (**b**) *MQ-4-B*, and (**c**) *MQ-4-C*. ↵
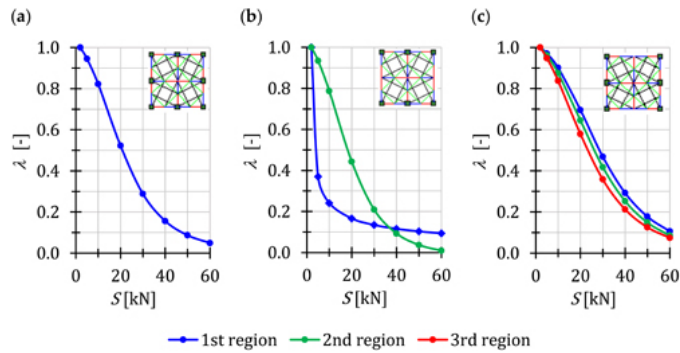
FIGURE 4.87 Influence of the initial prestress level S on the range of unstable regions λ for the *four-unit Quartex plates*: (**a**) *MQ-4-A*, (**b**) *MQ-4-B*, and (**c**) *MQ-4-.C* ↵

The next resonance frequencies (like natural frequencies), i.e., $\eta > \eta_{nm}$ are independent of pulsatility index υ ($\eta(\upsilon = 0 \div 0.75) = \mathrm{const.}$) and on the initial prestress level S (Table 4.38). The relative increase is less than 1% for all frequencies. These resonance frequencies are twice as high as the free frequencies.

TABLE 4.38 Next Resonance Frequencies of the Tensegrity Plates ↵

Simplex Plates				*Quartex Plates*			
Model	*nm*	*S*		*Model*	*nm*	*S*	
		2 kN	*60 kN*			*2 kN*	*60 kN*
		η_{nm+1} *(Hz)* $(\upsilon = 0 \div 0.75)$				η_{nm+1} *(Hz)* $(\upsilon = 0 \div 0.75)$	
MS-6-A	1	301.02	303.85	MQ-4-A	1	342.45	343.53
MS-6-B	1	274.86	277.16	MQ-4-B	2	325.39	326.22
MS-6-C	1	262.75	264.39	MQ-4-C	3	177.50	178.14

4.8.5 CHAPTER SUMMARY

This chapter discusses double-layer tensegrity grids (plates) built with the *modified Simplex* and *Quartex modules*. The influence of the way of support on the behavior is considered. Comparative nature of analysis leads to answers to the questions posed at the beginning of the consideration.

1. Is it possible to control the occurrence of mechanisms by changing the support conditions of the tensegrity plate?

Controlling the occurrence of mechanisms is possible by changing the support conditions of the tensegrity plate.

2. Which plate model is the stiffest?

The *Simplex plate*, which supports all external bottom nodes, is the stiffest.

3. Which plate is more sensitive to changes in the initial prestress level?

The *Simplex plates* are not sensitive to the prestress. This is because the load causes displacements that are incompatible with infinitesimal mechanisms. The *Quartex plates*, on the other hand, are sensitive to the prestress. The *MQ-4-C* model characterized by the three infinitesimal mechanisms, is more sensitive to the changes.

4. Is the number of natural frequencies depending on the prestressing equal to the number of infinitesimal mechanisms?

The tensegrity plates built with *modified Simplex* and *Quartex modules* behave independently, like single modules, i.e., the number of natural frequencies, depending on the prestressing, is equal to the number of infinitesimal mechanisms.

More results of the parametric analysis of double-layered tensegrity grids built with *Simplex* and *Quartex modules* are available in the following publications (Obara 2019a, 2019b, 2019c; Obara and Tomasik, 2020, 2021a, 2021b, 2023a, 2023b).

REFERENCES

Ashwear, N., Eriksson, A. (2014). Natural frequencies describe the pre-stress in tensegrity structures, *Computer and Structures* 138(1), 162–171.

Ashwear, N., Tamadapu, G., Eriksson, A. (2016). Optimization of modular tensegrity structures for high stiffness and frequency separation requirements, *International Journal of Solids and Structures* 80, 297–309.

Cai, J., Wang, X., Deng, X., Feng, J. (2018). Form-finding method for multi-mode tensegrity structures using extended force density method by grouping elements, *Composite Structures* 187, 1–9.

Chan, W.L., Skelton, R.E. (2002). *Equilibria and stiffness of planar tensegrity structures*, AAS/AIAA Space Flight Mechanics Meeting, San Antonio, Texas, USA.

Chen, Y., Feng, J. (2012a). Generalized eigenvalue analysis of symmetric prestressed structures using group theory, *Journal of Computing in Civil Engineering* 26(4), 488–497.

Connelly, R., Back, A. (1998). Mathematics and tensegrity, *American Sciences* 86, 142–151.

De Jager, B., Skelton, R.E. (2006). Stiffness of planar tensegrity truss topologies, *International Journal of Solids and Structures* 43, 1308–1330.

Estrada, G., Bungartz, H.J., Mohrdieck, C. (2006). Numerical form-finding of tensegrity structures, *International Journal of Solids and Structures* 43, 6855–6868.

Gilewski, W., Kłosowska, J., Obara, P. (2015). Applications of tensegrity structures in civil engineering, *Procedia Engineering* 111, 242–248.

Kasprzak, A. (2014). *Assessing the feasibility of using tensegrity structures in bridge construction (in Polish)*, Ph. D. Thesis, Publishing House of the Warsaw University of Technology, Warsaw, Poland.

Koohestani, K., Guest, S.D. (2013). A new approach to the analytical and numerical form–finding of tensegrity structures, *International Journal of Solids and Structures* 50(19), 2995–3007

Lee, S.J. (2012), A form–finding of planar tensegrity structures, *Architectural Research* 14(4), 143–152.

Luo Y., Lu J. (2006). Geometrically non-linear force method for assemblies with infinitesimal mechanisms, *Computer and Structures* 84(31), 2194–2199.

Malerba, P.G., Patelli, M., Quagliaroli, M. (2012). An extended force density method for the form finding of cable systems with new forms, *Structural Engineering and Mechanics* 42(2), 191–210.

Masic, M., Skelton, R.E. (2002). Deployable plates made from stable-element class 1 tensegrity, smart structures and mechanics 2002: Industrial and commercial applications of smart structures technologies, A.M.R. McGowan, ed., *Proceedings of SPIE*, 220–230.

Masic, M., Skelton, R.E. (2006). Selection of prestress for optimal dynamic/control performance of tensegrity structures, *International Journal of Solids and Structures* 43, 2110–2125.

Masic, M., Skelton, R.E., de Oliveira, M.C. (2005). *Integrated structure and control design of modular tensegrities*, Proceedings 44th IEEE Conference on Decision and Control, and the European Control Conference, Seville, Spain.

Masic, M., Skelton, R.E., Gill, P.E. (2006). Optimization of tensegrity structures, *International Journal of Solids and Structures* 42, 4687–4703.

Maxwell, J.C. (1864). On the calculation of equilibrium and stiffness of frames, *Philosophical Magazine* 27, 250.

Micheletti, A. (2008). On generalized reciprocal diagrams for self-stressed frameworks, *International Journal of Space Structures* 23(3), 153–166.

Micheletti, A., Cadoni, D. (2011). *Design of single-layer floating–compression tensegrities* Giens, France.

Mochocki, W., Obara, P. (2021). *Reliability analysis of tensegrity towers in a system approach*, Modern Trends in Research on Steel, Aluminium and Composite Structures, Routledge, ISBN: 978-0-367-67637-7.

Moored, K.W., Bart–Smith, H. (2009). Investigation of clustered actuation in tensegrity structures, *International Journal of Solids and Structures* 46, 3272–3281.

Moored, K.W., Kemp, T.H., Bart–Smith, H. (2011). Analytical prediction, optimization, and design of a tensegrity–based artificial pectoral fin, *International Journal of Solids and Structures* 48, 3142–3159.

Motro, R. (1992). Tensegrity systems: The state of the art, *International Journal of Space Structures* 7(2), 75–83.

Motro R. (2003), *Tensegrity: Structural systems for the future*, Kogan Page, London, UK.

Obara, P. (2019a). *Dynamic and dynamic stability of tensegrity structures (in Polish)*, Publishing House of the Kielce University of Technology, Kielce, Poland.

Obara, P. (2019b). Analysis of orthotropic tensegrity plate strips using a continuum two-dimensional model, *MATEC Web of Conferences* 262, 10010, doi: 10.1051/matecconf/201926210010.

Obara, P. (2019c). Application of linear six-parameter shell theory to the analysis of orthotropic tensegrity plate-like structures, *Journal of Theoretical and Applied Mechanics* 57(1), 167–178, doi: 10.15632/jtam-pl.57.1.167.

Obara, P., Kłosowska, J., Gilewski, W. (2019). Truth and myths about 2D tensegrity trusses, *Applied Sciences* 9(1), 179, doi: 10.3390/app9010179.

Obara, P., Solovei, M. (2023). Assessment of the impact of the number of girders on the dynamic behaviour of Geiger dome, *Archives of Civil Engineering* 69(3), 597–611, doi: 10.24425/ace.2023.146100.

Obara, P., Solovei, M. (2024). Influence of the initial prestress level on the distribution of regions of dynamic instability of geiger domes, *Applied Sciences* 14(17), 7512, doi: 10.3390/app14177512.

Obara, P., Solovei, M., Tomasik, J. (2023a). Qualitative and quantitative analysis of tensegrity steel domes, *Bulletin of Polish Academy of Sciences* 71(1), 1–8, doi: 10.24425/bpasts.2023.144574.

Obara, P., Solovei, M., Tomasik, J. (2023b). Genetic algorithm via other methods for determination self-stress states of tensegrity domes, *Applied Sciences* 13(9), 5267, doi: 10.3390/app13095267.

Obara, P., Tomasik, J. (2020). Parametric analysis of tensegrity plate-like structures: Part 1—qualitative analysis, *Applied Sciences* 10(20), 7042, doi: 10.3390/app10207042.

Obara, P., Tomasik, J. (2021a). Parametric analysis of tensegrity plate-like structures: Part 2—quantitative analysis, *Applied Sciences* 11(2), 602, doi: 10.3390/app11020602.

Obara, P., Tomasik, J. (2021b). Active control of stiffness of tensegrity plate-like structures built with simplex modules, *Materials* 14(24), 7888, doi: 10.3390/ma14247888.

Obara, P., Tomasik, J. (2023a). Influence of the support conditions on dynamic response of tensegrity grids built with Quartex modules, *Archives of Civil Engineering* 69(3), 629–644, doi: 10.24425/ace.2023.146102.

Obara, P., Tomasik, J. (2023b). Validation of the continuum orthotropic model of tensegrity beam-like and plate-like structures, *Archives of Mechanics* 75(3), 249–269, doi: 10.24423/aom.4182.

Obara, P., Tomasik, J. (2023c). Dynamic stability of tensegrity structures – Part I: The time-independent external load, *Materials* 16(2), 580, doi: 10.3390/ma16020580.

Obara, P., Tomasik, J. (2023d). Dynamic stability of tensegrity structures – Part II: The periodic external load, *Materials* 16(13), 4564, doi: 10.3390/ma16134564.

Obara, P., Tomasik, J., Solovei, M. (2024). Parametric dynamic analysis of tensegrity cable-strut domes, *Journal of Theoretical and Applied Mechanics* 62(2), 253–267 doi: 10.15632/jtam-pl/183833.

Ohsaki, M., Zhang J.Y. (2006), Stability conditions of prestressed pin-joint structures, *International Journal of Non-Linear Mechanics* 41, 1109–1117.

Pagitz, M., Tur, J.M. (2009). Finite element based form finding algorithm, *International Journal of Solids and Structures* 46(17), 3235–3240.

Paul, C., Lipson, H., Cuevas, F.V. (2005). *Evolutionary Form–Finding of Tensegrity Structures*, Proceedings of the 2005 Conference: Genetic & Evolutionary Computation, Washington.

Pełczynski, J., Gilewski, W. (2018). *An extension of algebraic equations of elastic trusses with self-equilibrated system of Forces*, 6th European Conference on Computational Mechanics (Eccm 6), 7th European Conference on Computational Fluid Dynamics (Ecfd 7) 1115, June 2018, Glasgow, UK.

Pugh, A. (1976). *An introduction to tensegrity*, University of California Press, Berkeley.

Skelton, R.E., Adhikari, R., Pinaud, J.P., Chan, W., Helton, J.W. (2001b). *An introduction to the mechanics of tensegrity structures*, Proceedings of the 40th IEEE Conference on Decision and Control, Orlando, Florida, December, 4254–4258.

Skelton, R.E., Helton, J.W., Adhikari, R., Pinaud, J.P., Chan, W. (2002). An introduction to the mechanics of tensegrity structures. In *T* (Chapter 17), CRC Press, Boca Raton, US.

Skelton, R.E., de Oliveira, M.C. (2009). *Tensegrity systems*, Springer, London, UK.

Skelton, R.E., de Oliveira, M.C. (2010). Optimal complexity of deployable compressive structures, *Journal of the Franklin Institute* 347, 228–256.

Skelton, R.E., Pinaud, J.P., Mingori, D.L. (2001a). Dynamics of the shell class of tensegrity structures, *Journal of the Franklin Institute* 338, 255–320.

Tibert, A.G. (2002). *Deployable tensegrity structures for space applications*, Ph. D. Thesis, Royal Institute of Technology, Stockholm, Sweden.

Index